ENGINEERING DOCTORATE

EXECUTIVE SUMMARY

AUGUST 2008

ACHIEVING AEROSPACE STANDARD POROSITY LEVELS WHEN WELDING THIN AND THICK-SECTION ALUMINIUM USING FIBRE-DELIVERED LASERS

Author: Ing G Verhaeghe

CONTENTS

LIST OF FIGURES

LIST OF TABLES

ABSTRACT

Environmental and commercial pressures have forced the aerospace industry to look at alternatives to riveting for the manufacture of aluminium aircraft structures. This resulted, at the end of last century, in an extensive study by Airbus into the possiblities of using CO_2 lasers, which led to the process being implemented for a (small) number of stringer-to-skin fuselage panels in the newer Airbus models. Since this initial commercial success, new laser sources have become available that are more suitable for the welding of aluminium than CO_2 lasers, in the form of Nd:YAG and Yb-fibre lasers. Both produce a wavelength that is absorbed more efficiently by aluminium alloys than the CO_2 laser wavelength, resulting in an improved keyhole stability, as demonstrated in the late nineties for Nd:YAG lasers. In addition, Yb-fibre lasers have become available at output powers higher than available for Nd:YAG lasers, allowing thicker sections of aluminium to be welded in a single pass. However, despite their claimed advantages, no efforts were made to demonstrate the potential of these lasers for (aluminium) aircraft manufacture. For this reason, the author initiated a series of studies in 2001, with the overall aim to develop procedures to laser weld both thin (3.2mm) and thick-section (12.7mm) aerospace aluminium alloys using these fibre-delivered lasers to a weld quality, in particular related to weld metal porosity, suitable for aerospace service. The focus in this research was on weld metal porosity, because this is a particular problem when laser welding aluminium, either in the form of fine (hydrogen) porosity or larger porosity associated with an unstable keyhole behaviour. The benchmark weld metal porosity for this study was obtained from the stringent weld quality classes defined in BS EN 13919-2 and AWS D17.1. The approach to this research was in three parts, with work in the first aimed at demonstrating that a 3kW Nd:YAG laser was capable of producing low-porosity welds in 3.2mm thickness 2024 aluminium alloy, and thus can be considered for replacing the CO_2 laser currently used for the stringer-to-skin fuselage application. Prior to the final part of the research, in which a 7kW Yb-fibre laser was used to demonstrate that these benchmark porosity levels could also be achieved in thicker section (aerospace-grade) aluminium, a comparison study was carried out to quantify the difference in welding performance between the Nd:YAG and the Yb-fibre laser. At an output power of 4kW focused in a 0.4mm diameter spot, the Yb-fibre laser was capable of a 30% higher welding speeds in 4mm (5083) aluminium alloy, or a 20% increase in depth of penetration for welding speeds between 1 and 15m/min, compared with the Nd:YAG laser. This improvement in welding performance, together with an output power of 7W, produced full penetration in 12.7mm thickness (aerospace-grade) Al-Zn-Mg-Cu aluminium alloy using the Yb-fibre laser autogenously, or in a hybrid configuration with a MIG arc. Both the autogenous laser and hybrid laser-MIG process were capable of producing welds with a weld metal porosity in line with the BS EN 13919-2 and AWS D17.1 benchmark conditions, at welding speeds of 0.55 and 0.75m/min, respectively. At these production rates, the 248 metres of stringer incorporated in a typical aluminium wing structure can be welded in 7.5 and 5.5 hours, in case of autogenous laser and hybrid laser-MIG, respectively, compared with 37.6 hours currently needed for the riveting process.

ACKNOWLEDGEMENTS

The more I study, the more I know.
The more I know, the more I forget.
The more I forget, the more I have to study.
So why study?

Unknown author

Despite this dilemma, so often recited by students, I undertook this Engineering Doctorate in the autumn of 2000, while in full-time employment at TWI. This seems like a long time ago now. At the end of 2003, I interrupted my EngD work briefly to fully concentrate on the installation and commissioning of TWI's 7kW Yb-fibre laser, for which I relocated from Cambridge to Sheffield. In retrospect, this one-year period has shaped my business insight and was instrumental in focusing my research, led to some of the findings reported in this EngD and brought me some of the reputation I now enjoy in the field of laser processing.

In all, it has taken me six years to complete my EngD and this would not have been possible without the support and regular words of encouragement from my wife, Mary. A great thank you also goes to my parents, Walter and Christiane, my sisters An, and her family, and Els, and to all my friends for their continued support.

I would also like to acknowledge my employer, TWI, for granting me the opportunity to do this EngD, and am indebted to the EPSRC for their grant, which paid all EngD course fees. A special thanks also to all the partner companies with whom I have worked over the years, on some of the projects related to this research, in particular the partners in CEMWAM and DEFUSE, and to TWI's member companies for funding some of the research, through TWI's Core Research Programme.

Thanks also to my industrial mentor, Geoff Booth, and to all my colleagues at TWI who have supported me through these years, either technically, or simply for taking pity on me for having to work after hours on my EngD.

Last, but certainly not least, a very big thank you to my academic supervisor, Stuart Barnes. Your advice, guidance and constructive criticism has been invaluable to me and I thank you especially.

Geert Verhaeghe
August 2007

1. INTRODUCTION

At the end of the 20th century, riveting had been used in aircraft manufacture for over 70 years for the joining of thin-sheet structures. The process is considered mature, but slow, absorbing as much as 40% of the total manufacturing time (1). For an aluminium stringer-to-skin fuselage structure, the current productivity is 4.5 rivets per minute, with on average one million rivets used in the fuselage structure of a typical passenger jet (2-3). Over the years, the rivet and the process have been perfected to yield the lowest weight and maximum production performance, such that further improvements in terms of weight savings and productivity are not anticipated (2-3). A review carried out in 2000, looking back at the use of aluminium alloys for aerospace applications over the past century, concluded that aluminium remained the foremost material used in the commercial aircraft construction for non-temperature critical applications (4). At that time, aluminium remained the preferred material for civil aircraft fuselage structures, with, by weight, 80% of civilian aircraft structures made of aluminium (5).

Environmental and commercial pressures at the start of the 21st century have encouraged aerospace companies to investigate new approaches to aircraft design and manufacturing methods, with, similar to the automotive industry, economising through weight-savings and improved productivity some of the key drivers empowering changes in aircraft manufacture (6). Reducing the weight of an aircraft results in reduced fuel-consumption, a higher payload capacity or better agility in case of military aircraft (4-8). In terms of productivity, the focus is on the cost of manufacture, with any reduction in manufacturing cost significantly impacting on the final cost of the aircraft. This is because at the turn of the century, manufacturing represented 95% of the cost of a civil airframe structure, with the airframe in turn representing about one fifth of the total aircraft cost (4). In case of military aircraft, about one third of the aircraft cost was for the airframe, of which 60% was contained in the manufacture of load-bearing structures (8). Welding is one such alternative manufacturing route, with TIG, plasma, friction stir, electron beam and laser welding all under investigation (1,9-10). The schematic in Fig.1 shows which parts of the aircraft structure are currently being considered for welding.

It is estimated that laser welding, the subject of this report, is capable of production rates that are thirty to one hundred times higher than conventional riveting (2,11). In addition to a higher productivity, laser welding reduces the weight of the structure, because of eliminating the rivet itself, as well as the overlap joint. The latter is required for riveting, but not for laser welding. The weight of one aluminium rivet depends on the rivet diameter and grip length, which in turn depend on the material thicknesses used. With an average of 1 million rivets used in the manufacture of a standard passenger jet (2) and assuming an average weight of one gram per rivet, the total weight of all rivets used would be 1000 kg.

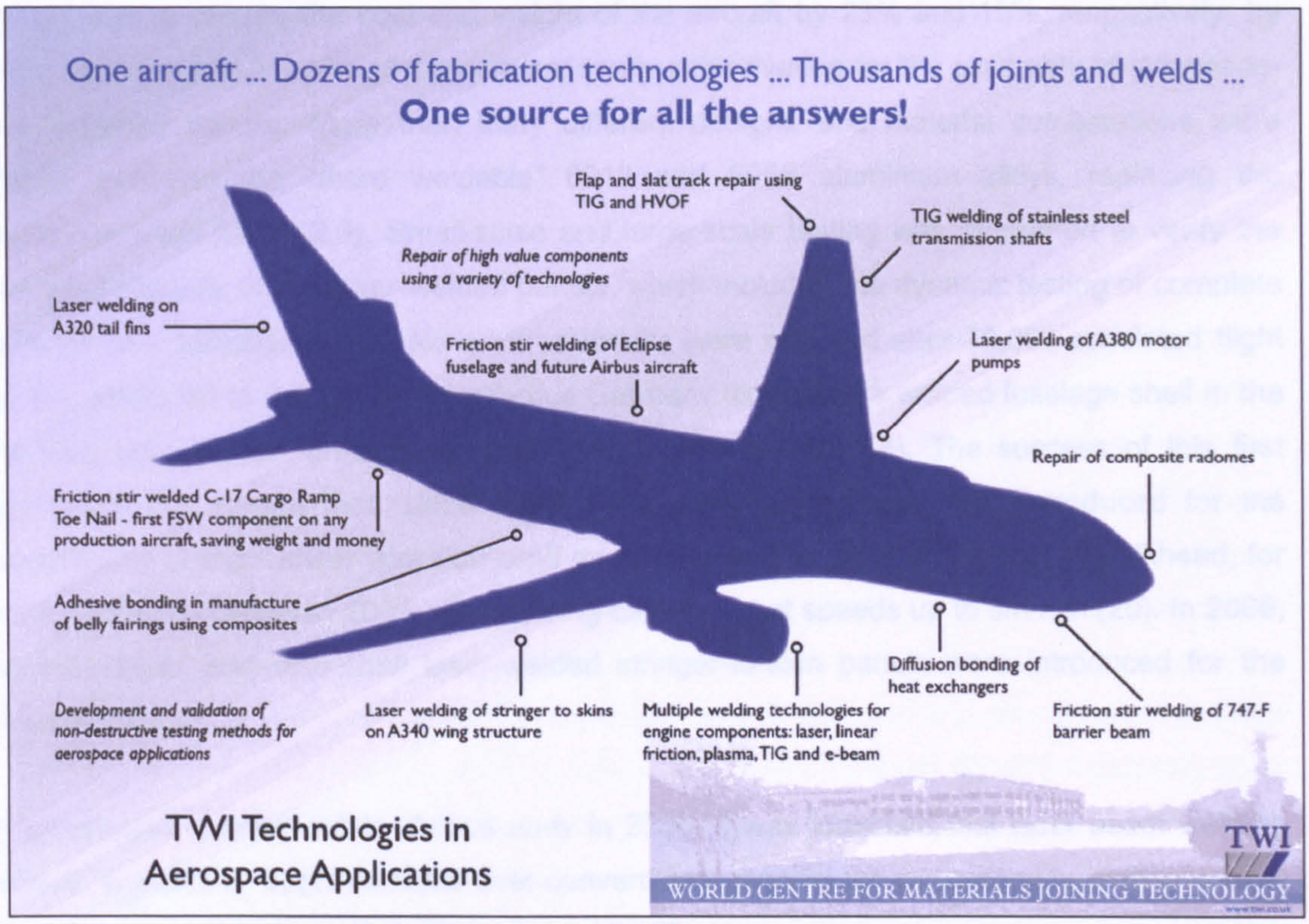

Fig.1 Alternative joining technologies under investigation for the manufacture of aircraft structures and components

When lasers were first applied for the welding of aluminium in the 1970s and 1980s, deep-penetration keyhole welding proved difficult because of the initial high surface reflectivity and high thermal conductivity of the material (12). This was subsequently overcome by the availability of laser sources with higher average output powers and improved focussing systems, producing a power density high enough to produce a stable keyhole for welding (12). Particularly since the end of the 1990s, the automotive industry has been a pioneer in demonstrating the capabilities of the laser as a production tool for the welding of aluminium, with the Audi A2 aluminium spaceframe as the most quoted example of a production application of laser-welded aluminium (13-14). Contrary to this, little has been published on the subject of laser welding for the manufacture of aluminium aircraft structures. This is partly because of confidentiality, which prevents much of research in the aerospace industry from being published, at least not until the results have been fully tested and demonstrated in production. Of those published, most report on investigations using CO_2 lasers and on laser welding of thin-section structures comprising typical aerospace alloys, such as 2024 (15-16) and 6013 (8,17) in thicknesses ranging from 2 to 3mm, with welding carried out from one side (15) or from both sides simultaneously (8,16,17). The industry's Audi A2 equivalent is undoubtedly the Airbus A318 model. The A318 was launched at the end of 1999 with two CO_2 laser-welded aluminium stringer-to-skin shells, positioned in the lower fuselage structure of the aircraft (2,18,19). The inclusion of the laser-welded panels was the culmination of a pioneering study, co-ordinated by Airbus Germany and involving German, French and Dutch materials producers, institutes and universities (2,3). The overall objective of this extensive

project was to reduce the cost and weight of the aircraft by 25% and 15%, respectively, by using laser welding instead of the conventionally used riveting for the assembly of stringer-to-skin fuselage panels. More than thirty different designs and material combinations were tested, including the "more weldable" 6013 and 6056 aluminium alloys, replacing the commonly used 2024 (2,3). Small-scale and large-scale testing was performed to verify the structural integrity of the laser-welded panels, which included the dynamic testing of complete sections of a fuselage *barrel*. No adverse results were reported after 70,000 simulated flight cycles, which led to the decision by Airbus Germany to include a welded fuselage shell in the 5m long (aft) section towards the back of the Airbus A318 (2). The success of this first application has meant that, since 1999, laser welding has also been introduced for the manufacture of eight lower and side-shell panels, as well as parts of the cockpit bulkhead, for the Airbus A380 model in 2005, with welding carried out at speeds up to 8m/min (20). In 2006, fourteen lower and side-shell laser-welded stringer-to-skin panels were introduced for the A340 model (19).

In an analysis carried out by Airbus early in 2006, it was identified that laser beam welding offered "significant" improvements over conventional riveting for the assembly of (aluminium) aircraft fuselage structure (21). These were identified as:

- *weight reduction* through reduced material consumption, absence of sealants and improved design (no overlap joint needed, contrary to riveting);
- *cost reduction* through reduced material consumption, higher processing speeds and fewer processing steps;
- *improved corrosion behaviour* and *improved aerodynamics* because there are no holes and no rivets present in the structure.

In terms of weight savings over conventionally riveted structures, Airbus carried out a study, published internally early in 2006, comparing the weight of two conventionally riveted aircraft structures with that of two similar structures in which "several" riveted panels in the forward fuselage section were replaced with laser-welded panels. This required the structure design to be modified locally, but according to Airbus, this in itself did not impact on the overall weight of the structure. Both conventionally riveted structures were in weight between 500 and 650kg, with their laser-welded counterparts offering a weight saving of 9 and 11%, respectively (21). In terms of cost savings, Airbus considered a laser welding machine to have an investment cost "similar" to that of a riveting machine, but capable of processing ten times faster. The forecast by Airbus was that through further process development, cost savings of between 20 and 25% could be achieved for laser welding of fuselage structure, although at the time of reporting (early in 2006) , this had not been achieved (21).

2. THE NEED FOR RESEARCH INTO LASER WELDING FOR ALUMINIUM AIRCRAFT STRUCTURES

Notwithstanding the commercial success, as discussed in Section 1, further uptake of lasers for the welding of aluminium aircraft structures outside Airbus has been limited. This is despite a whole new range of laser sources that have become available since the late 1990s, which are at least as suitable as, if not better suited than, the CO_2 laser for this welding application. The first example of such a source is the Nd:YAG laser, which emits laser light with a wavelength of 1.06μm, ten times shorter than that of a CO_2 laser. The shorter wavelength is better absorbed by aluminium (allowing higher processing speeds) and also allows the laser power to be transmitted through a fibre-optic cable, eliminating the need for mirrors as used in case of CO_2 lasers (22-25). At an output power of 2.2kW, the Nd:YAG laser was demonstrated, in the late 1990s, to offer improved process (keyhole) stability compared with a CO_2 laser for the welding of aluminium, resulting in welds of a "better overall quality" and with a higher weld *aspect ratio*, i.e., ratio between weld depth and width (26-27). However, apart from a limited number of publications on the performance of a 2kW pulsed Nd:YAG laser for the welding of 2219, 2024, 7020 and 7075 aerospace aluminium alloy (28), and on the use of 3kW Nd:YAG lasers for the welding of 3mm thickness 2024 (29-30), little has been published on the capabilities of these lasers for welding aerospace aluminium alloys. At the start of the work reported here, in 2001, no publications were found on the laser welding of aerospace aluminium alloys thicker than 4mm, despite the fact that Nd:YAG lasers, available at that time with output powers up to 4kW and in 2006 up to 6kW, were capable of keyhole welding aluminium as thick as 8mm. For thicker sections of aluminium alloy, CO_2 lasers remained the preferred choice, because of their availability (commercially) at output powers up to 15kW (31). For example, 10kW of CO_2 laser power was demonstrated to penetrate 10mm thickness 2014 aluminium alloy in a single pass (32). This situation remained largely unchanged until 2003, when high-power Yb-fibre lasers were introduced, which, in 2006, were available (commercially) at output powers even exceeding those offered for CO_2 lasers (31). With the capability of these new laser sources to emit a wavelength similar to that of the Nd:YAG laser, i.e., 1.07μm, meaning fibre-delivery and good absorption in aluminium, interest in this technology has been growing rapidly. Particular interest from the aerospace industry arose from the availability of output powers exceeding those of Nd:YAG lasers, thereby extending the range of aluminium thicknesses which could be welded in a single pass beyond 8mm.

However, to allow these new laser sources, the Nd:YAG laser and the Yb-fibre laser, to be used for the welding of aluminium aircraft structures, a considerable amount of performance data is required for laser welds in the heat-treatable, high-strength aluminium alloys typically used for these applications. Moreover, building on the successes achieved for the laser-welded stringer-to-skin fuselage structure, the industry also requires such data to be available for thicker-section aluminium, to be used, for instance, in the manufacture of aluminium wing structures of future aircraft models. In order for CO_2 laser welding to replace the conventional

riveting operation for stringer-to-skin fuselage structures, Airbus undertook an extensive study to demonstrate its capabilities, as detailed in Section 1. Similar studies are therefore now required for the industry to accept the newer laser sources, i.e., Nd:YAG and Yb-fibre laser, as viable production tools for the manufacture of aluminium aircraft structures.

It is essential that such studies demonstrate joint properties that approach those of the base materials used, including static and dynamic strength, toughness, fracture toughness and corrosion resistance. To achieve this, further optimisation of the aluminium laser weld quality in particular, is needed. Whereas the Nd:YAG laser has been demonstrated to offer a weld quality acceptable to automotive standards, these requirements are considerably less stringent than those applicable to an aluminium joint in the fuselage or wing structure of a passenger jet. To be of a suitable weld quality, welds must contain a minimum of imperfections, including pores (33). Weld metal porosity is a particular concern when laser welding aluminium. By applying similar techniques as those developed for the arc welding of aluminium, such as parent material cleaning prior to welding and minimising the moisture-content of the shielding gas, laser welding had been demonstrated to produce a weld quality in aluminium that was acceptable to automotive standards. However, at the onset of the research work described in this document, no such data was available for Nd:YAG laser welds in aerospace aluminium. Differing views exist in the literature on how weld metal porosity affects the mechanical properties of laser-welded aluminium. Research in Japan on CO_2 laser welds in 5182 aluminium alloy, revealed no "discernible decrease" in strength or elongation when a "few" pores smaller than 0.5mm in diameter were present in the welds (33). However, other research in Japan and elsewhere showed that weld metal porosity reduced the cross-sectional area of the weld, which "adversely" impacted on the strength of the joint (34-37). Unless proven otherwise, the aerospace industry sector shares the latter view and, ultimately, would like to develop a zero-porosity process for the welding of aluminium aircraft structures. Although a difficult task for a fusion process, measures can be taken to minimise weld metal porosity, as mentioned above. However, for a safety-critical structure, such as an aircraft, it is vital for any joining process to demonstrate that a minimum level of weld metal porosity can be obtained, consistently. This was addressed in the first part of the work detailed here, for the Nd:YAG laser welding of stringer-to-skin structures comprising thin-section aerospace aluminium.

As discussed above, the newer Yb-fibre lasers offer the potential of extending the thickness range of aluminium that can be welded in a single pass using a wavelength similar to that of Nd:YAG. However, because these particular laser sources were new at the time of this research, no information was available on the performance of these high-power Yb-fibre lasers for the welding of materials, including aluminium. A study was therefore carried out comparing the performance of this new laser source with that of the Nd:YAG laser, at an output level of 4kW, for the welding of aluminium. An output power of 4kW was chosen, because this was the most commonly used (maximum) output power of the Nd:YAG laser at

the time of the research. Using this baseline performance data of a 4kW Yb-fibre laser for the welding of aluminium, further work was carried out by increasing the output power of the Yb-fibre laser used for this research to its maximum of 7kW, to assess its performance for the welding of aluminium sections in thicknesses up to 12.7mm. In these thicknesses of aluminium, the likelihood of the laser keyhole collapsing increases, with these keyhole instabilities manifesting themselves as large voids in the weld. In order for these new lasers to be capable of welding thick-section aluminium, it was therefore essential to investigate how these keyhole instabilities could be eliminated consistently, and how the overall level of weld metal porosity could be reduced to a level acceptable to aerospace standards. At the onset of the research described in this report, no such data was available for aluminium sections thicker than 4mm, which is why an investigation to that effect was carried out in the final part of this work on thick-section aerospace aluminium to be used for aircraft wing structures.

Currently, wing structures comprise stringers that are fastened to the wing skin, Fig.2, in a similar way as stringer-to-skin fuselage structures (21). The differences are that fasteners (bolts) are used instead of rivets, that the materials used are thicker in section, typically 8mm for the stringer, and that fasteners are positioned on either side of the stringers, as shown in Fig.2. A sealant material is also applied at the interface and in the pre-drilled holes. Airbus reported that savings are expected in terms of cost and weight (see Section 1), but also in terms of improved structural behaviour. This is because of the absence of holes, which can leak or act as crack initiators. However, it is expected that for the fastened structure, the damage tolerance, i.e., how fast a crack or failure grows to critical size, will be better than that of a welded structure. To investigate all of this, an extensive test programme is currently underway at Airbus (21).

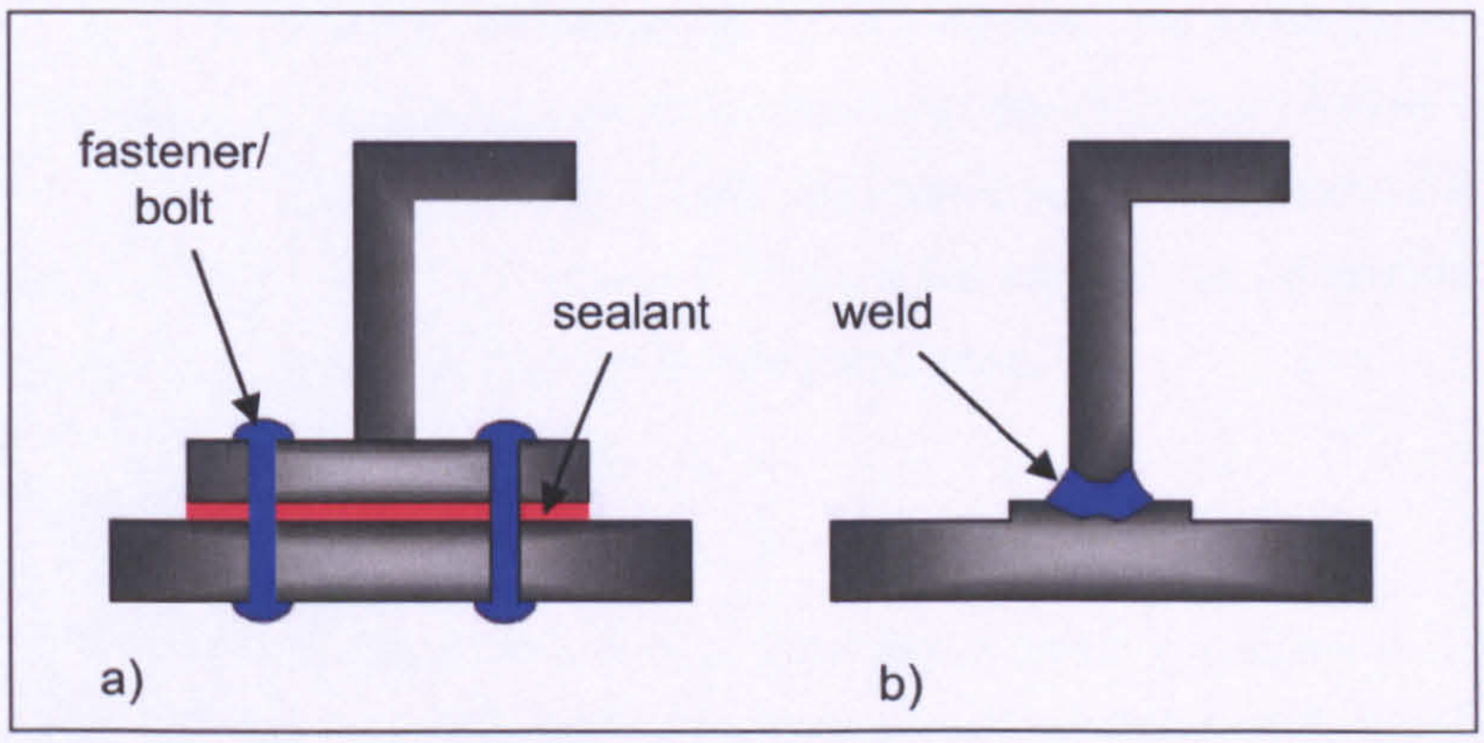

Fig.2 Fastened/bolted joint (a); welded joint (b)

The following example demonstrates the magnitude of productivity improvement Airbus expects to achieve by changing to a laser-welded design (21). The structure of a typical aircraft wing geometry (of an unspecified Airbus model) is shown in Fig.3. Considering 8mm thick stringers, a *pitch*, i.e., distance between the stringers, of 160 mm and the approximated dimensions as shown in Fig.3, the total length of stringers for one wing structure is 248m. Currently, 6.5 fasteners are assembled per minute, with 2 rows of fasteners per stringer and

62 fasteners per metre of stringer. This means that the current process takes 9.5 minutes per metre of stringer, i.e., a processing speed of 0.11m/min. From this can be calculated that it currently takes Airbus staff 37.6 hours to assemble the 248m length of stringers. In contrast, Airbus anticipates that laser welding will be capable, in a single pass, of welding speeds of to 1m/min. Or, that the same length of stringers can be completed in just over 4 hours, i.e., nearly 10 times faster.

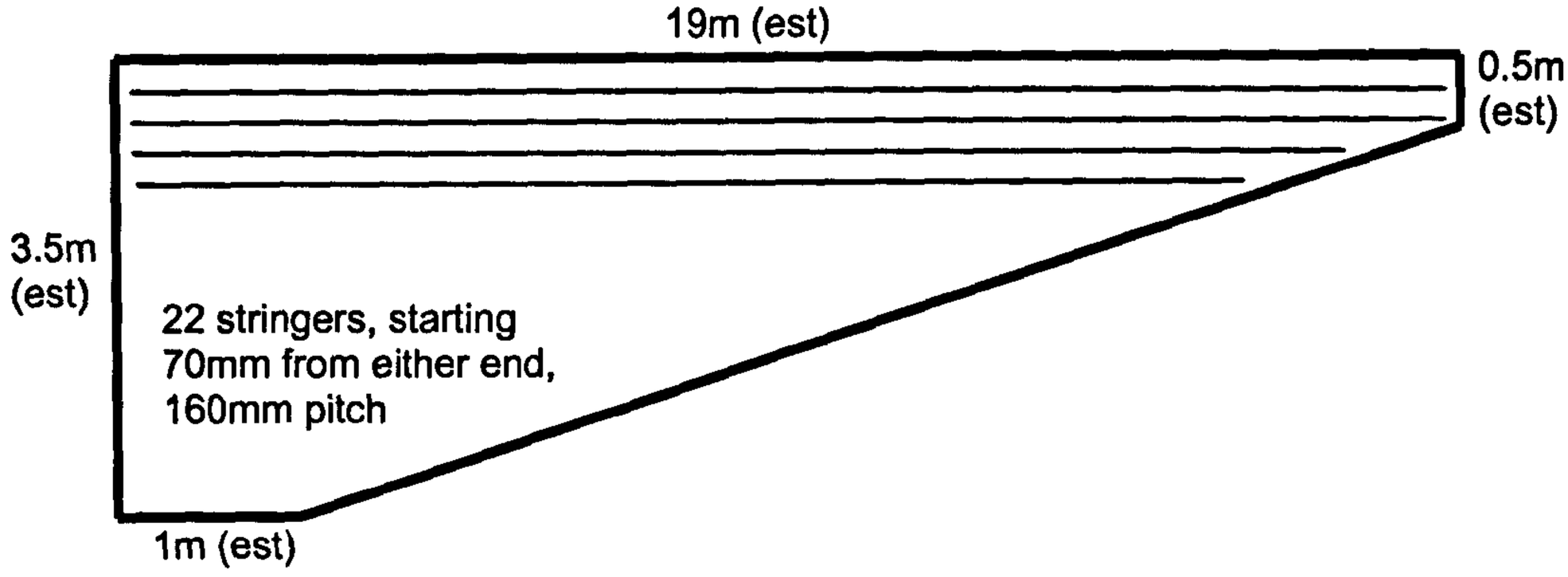

Fig.3 Schematic of a stringer-to-skin wing structure, with typical dimensions for an (unspecified) Airbus aircraft

3. OBJECTIVES AND APPROACH OF THE RESEARCH

With the requirements of the aerospace industry in mind, as discussed in Section 2, the author has undertaken several studies since 2001, whilst employed by TWI Ltd, which formed the basis of his Engineering Doctorate (EngD) work. These were all carried out using commercially available fibre-delivered lasers, including lamp-pumped (LP) Nd:YAG lasers and a Yb-fibre laser, to weld both thin-section, i.e., 3.2mm, and thick-section, i.e., up to 12.7mm, aluminium alloys typically used in aircraft manufacture. The overall objective of these investigations was *to develop laser welding procedures using fibre-delivered lasers to weld both thin and thick-section aerospace aluminium alloys of a weld quality, in particular related to weld metal porosity, suitable for aerospace service*. In the absence of a universally recognised aerospace standard for the laser welding of aluminium for aircraft structures, the benchmark weld quality in terms of porosity for this study was obtained from the European standard BS EN 13919-2 (38), on laser welding of aluminium, the American standard AWS D17.1 (39), on fusion welding for aerospace applications, and a confidential standard, ABP 2-4102 (40), currently in use at a UK aerospace company for the laser welding of aluminium.

The approach to this EngD work is schematically represented in Fig.4. At the start of the work, a review of the literature was undertaken, to identify the origin(s) of weld metal porosity in laser welded aluminium and the proposed measures to minimise it. This literature review is described in EngD Submission 1 (41) and summarised below in Section 4. To achieve the main objective, as described above, a series of research projects were then undertaken in three distinct areas, as shown in Fig.4, each with their own objective. These areas were related to the welding of thin-section aerospace aluminium, the performance assessment of an Yb-fibre laser for the welding of aluminium and the welding of thick-section aerospace aluminium. Each of these, further referred to as the *thin-section*, the *performance comparison* and the *thick-section* trials, and their respective objectives are discussed further below. These individual studies were the subject of EngD Submissions 2 to 8 (31,42-47), and are summarised below in the Sections 5, 6 and 7. They were carried out consecutively, with the experience gained in one study used in the subsequent ones.

3.1. THIN-SECTION TRIALS

The objective of the thin-section trials was *to develop a welding procedure using a lamp-pumped Nd:YAG laser to produce fully penetrating butt welds in thin-section aerospace aluminium alloy, containing a level of weld metal porosity acceptable to those specified for the stringent weld quality classes in BS EN 13919-2 (38), AWS D17.1 (39) and ABP 2-4102 (40)*. The welding trials, detailed in EngD Submission 2 (42) and summarised below in Section 5, were carried out with the aim to establish practical laser processing conditions, in terms of material cleaning, shielding gas and laser energy distribution, capable of producing a minimum level of hydrogen-induced weld metal porosity.

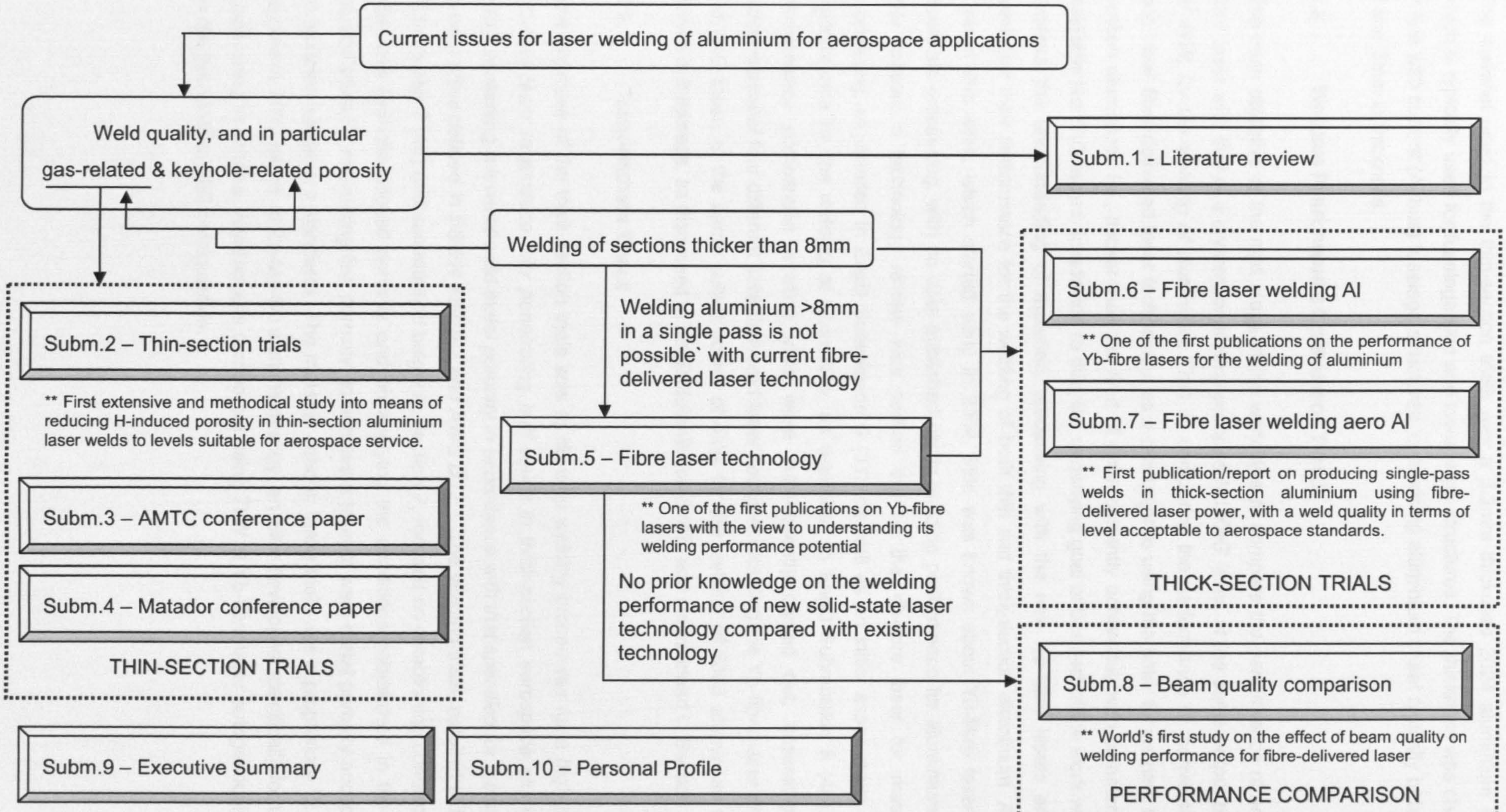

Fig.4 Approach taken for this Engineering Doctorate (EngD) work

The material used in the thin-section trials was a 3.2mm thickness 2024 aluminium alloy, which is typically used for fuselage skin and lower wing structures. The thickness was chosen in line with current (Airbus) fuselage structures, comprising aluminium sheet typically between 2 and 3mm in thickness.

3.2. WELDING PERFORMANCE COMPARISON TRIALS

The main objective of the next stage of the work was *to compare the performance of an Yb-fibre laser with that of a conventional lamp-pumped Nd:YAG laser, at the same output power of 4kW, for the welding of aluminium*. That is, comparing the performance of 'conventional' and 'new' fibre-delivered laser technology, as a precursor to using the latter for welding thick-section aluminium, i.e., thicker than the limit of 8mm currently achievable with commercially available Nd:YAG lasers. In addition to this, the underlying goal of this part of the work was to improve the understanding of materials processing with the new Yb-fibre lasers and in particular their performance for the welding of both thin and thick-section aluminium. At the time of this work, which started early in 2004, little was known about Yb-fibre lasers for materials processing, with no data published on its welding performance for aluminium. For that reason, a technology review was carried out on the Yb-fibre laser for materials processing, as detailed in EngD Submission 5 (31), as well as an initial assessment of its performance for the welding of aluminium, as described in EngD Submission 6 (45). The performance comparison welding trials were subsequently carried out, assessing the performance of four different fibre-delivered laser sources, including the Yb-fibre laser and LP Nd:YAG laser, at the same output power of 4kW for the welding of 5083 aluminium up to 10mm in thickness, as discussed in EngD Submission 8 (47) and summarised in Section 6.

3.3. THICK-SECTION TRIALS

The objective of the thick-section trials was *to develop welding procedures for a high-power Yb-fibre laser to produce fully penetrating butt welds in thick-section aerospace aluminium alloy, containing a level of weld metal porosity in accordance with that specified for a stringent quality class defined in BS EN 13919-2 and AWS D17.1.* The welding trials, detailed in EngD Submission 7 (46) and summarised below in Section 7, focused on establishing conditions to eliminate keyhole-induced porosity and on applying the conditions established in the thin-section trials for minimising fine porosity, to achieve a level of weld metal porosity acceptable to selected aerospace standards. The material used in these trials was a proprietary 12.7mm thickness 7000-series Al-Zn-Mg-Cu aluminium alloy, an alloy developed specifically for use in upper wing structures. Welding was carried out using 7kW of Yb-fibre laser autogenously and in the hybrid laser-MIG configuration.

4. LITERATURE REVIEW

What follows is a summary of a more detailed review of published work on the subject of weld metal porosity in laser-welded aluminium, presented in EngD Submission 1 (41). The summary considers the origins and mechanisms involved with the formation of weld metal porosity, preceded by an introduction into the type of alloys typically used in aluminium aircraft manufacture, the basic principles of laser keyhole welding and some of the technical challenges to be overcome when laser welding aluminium. In conclusion, an overview is given of the measures that can be taken to minimise weld metal porosity in laser-welded aluminium, as suggested in the literature.

4.1. ALUMINIUM ALLOYS FOR AEROSPACE APPLICATIONS

It is essential for an aerospace alloy to perform, at all times, safely under its designed static and dynamic in-service conditions. Therefore, an aluminium aerospace alloy must be of high strength and toughness, resistant to fatigue crack growth, referred to as *damage tolerance*, and resistant to corrosion and stress corrosion cracking (4). Historically, the most commonly used aluminium alloys for aircraft structures originate from the 2000 and 7000-series alloys (4-7). Both these series comprise high-strength aluminium alloys that have obtained their high strength through a controlled thermal treatment, which consists of a solution treatment, followed by a quenching operation and precipitation or age-hardening (48). The alloys are referred to as *heat-treatable* aluminium alloys. The 2000-series alloys, with copper (Cu) as the principal alloying element along with some additions of magnesium (Mg) (48), are typically used in fatigue-critical structures, such as the fuselage and lower wing surfaces, because of their high strength, corrosion resistance and damage tolerance (1). Alloys from the 7000-series alloys, with zinc (Zn) as the principal alloying element along with some additions of magnesium (Mg) (48), offer even higher strengths compared with the 2000-series alloys, but at the expense of damage tolerance (1). This restricts the main use of 7000-series aluminium alloys to upper wing structures, where fatigue cracks and their growth are less critical as, in flight, the upper wing is in compression (1).

Of the 2000-series alloys, the 2024 aluminium alloy has been used for fuselage skin and lower wing structures since the 1930s (49). This alloy, of which the nominal chemical composition and salient mechanical properties are given in Table 1, was used in the thin-section trials (Section 5). The proprietary 7000-series Al-Mg-Zn-Cu alloy used in the thick-section trials (Section 7) had a lower level of alloying elements, but a higher strength, compared with the 7075 aluminium alloy. The 7075 alloy, of which the nominal chemical composition and salient mechanical properties are given in Table 1, is the 2024 'equivalent' for the 7000-series alloys, and has been used for upper wing structures since the 1940s (4-8).

Table 1 Nominal compositions (wt%) and basic mechanical properties for some of the typically used aerospace aluminium alloys (www.matweb.com, September 2006)

	Cu	Si	Mn	Mg	Zn	$R_{p,0.2}$, MPa	R_m MPa	El, %	HB
2014-T0	3.9-5	0.5-1.2	0.4-1.2	0.2-0.8	<0.25	96.5	186	18	45
2024-T0	3.8-4.9	<0.5	0.3-0.9	1.2-1.8	<0.25	75.8	186	22	47
2024-T3	3.8-4.9	<0.5	0.3-0.9	1.2-1.8	<0.25	345	483	18	120
2219-T0	5.8-6.8	<0.2	0.2-0.4	<0.02	<0.1	75.8	172	18	46
2519	5.3-6.4	<0.25	0.1-0.5	0.05-0.4	<0.1				
5052-T0	0.15-0.35	<0.25	<0.1	2.2-2.8	<0.05	89.6	193	25	47
5083-T0	0.05-0.25	<0.4	0.4-1	4-4.9	<0.25	145	290	22	77
5182-T0	<0.15	<0.2	0.2-0.5	4-5	<0.25	130	275	25	77
6013	0.6-1.1	0.6-1	0.2-0.8	0.8-1.2	<0.25				
6056	0.5-1.1	0.7-1.3	0.4-1	0.6-1.2	0.1-0.7				
6061-T4	0.15-0.4	0.4-0.8	<0.15	0.8-1.2	<0.25	55.2	124	25	30
6082-T0	<0.1	0.7-1.3	0.4-1	0.6-1.2	<0.2	110	205	14	57
7020	<0.2	<0.35	0.05-0.5	1-1.4	4.0-5.0				
7075-T0	1.2-2	<0.4	<0.3	2.1-2.9	5.1-6.1	103	228	16	60
7150	1.9-2.5	<0.12	<0.1	2-2.7	5.9-6.9				

$R_{p,0.2}$ = 0.2% proof strength, R_m = tensile stress, El = amount of elongation before fracture (as % of original length)
HB = Brunel hardness, measured with a 10mm diameter ball and a 500kg load.

However, most of the 2000 and 7000-series aluminium alloys used for the manufacture of aircraft structures, are considered to have 'poor weldability', with some categorised as 'unweldable' by the Aluminum Association (48), because of their high solute content, resulting in a wide freezing range, and solidification and liquation cracking during conventional fusion welding. Since the industry has been considering fusion welding as an alternative manufacturing route for aircraft structures, the interest in both existing and newly formulated high-strength alternatives from the 6000-series aluminium alloys has grown (2). These alloys, with magnesium (Mg) and silicon (Si) as the principal alloying elements, are also heat-treatable, but typically offer lower strengths compared with both the 2000 and 7000 series alloys (48). They are 'readily weldable', with some risk of hot cracking, but a reduced crack-sensitivity compared with the 2000 and 7000-series alloys, according to the Aluminium Association (48). The 6013 and the 6056 aluminium alloy are examples of two such alloys, with the nominal chemical composition and salient mechanical properties given in Table 1. The manufacturer of the 6013 aluminium alloy, Alcoa, describes the alloy as "weldable", whilst exhibiting properties similar to 2024-T3, with improved formability (4). Because these alloys exhibit a lower strength, the aerospace industry accepts that thicker sections will have to be used to maintain the strength and stiffness of structures currently manufactured using the 2000 and/or 7000-series alloys (1,21). Thicker sections add more weight to the aircraft,

impacting on fuel-efficiency, which is why a balance between strength/stiffness and thickness is sought, whilst maintaining properties such as damage tolerance and corrosion resistance.

In addition to these typical aerospace aluminium alloys, reference is also made, in what follows, to 5000-series aluminium alloys, in particular 5083 and 5182. This is because, based on the literature review carried out by the author, EngD Submission 1 (41), over 80% of the research into weld metal porosity in laser-welded aluminium has been carried out on these alloys. The 5000-series aluminium alloys, with magnesium (Mg) as the principal alloying element, are classed as *non heat-treatable*, meaning that they obtain their strength through cold-work (48). Out of the non heat-treatable alloys, the 5000-series alloys have the highest strength, making them particularly useful for structural applications, including automotive and railroad (rolling stock) structures. However, no reports exist of their use for aircraft assemblies. The nominal chemical composition and salient mechanical properties of some of these non-aerospace aluminium alloys referred to in the report below, are given in Table 1.

4.2. LASER WELDING OF ALUMINIUM – NOT A BLACK ART

Laser welding is a fusion welding process. It is, in contrast with the more conventional fusion welding processes, such as TIG, MIG or plasma, a fast, high energy-density, low heat-input welding process. The process delivers narrow welds with a high aspect ratio and has rapid heating and cooling cycles. This minimises thermal distortion and loss in strength, which is common for any fusion welding process used on aluminium (50). However, the tolerance to fit-up is small and the tendency for weld imperfections, such as hot cracking, is high because of the rapid cooling rates (50). The particular concerns when laser welding of aluminium are further discussed in Section 4.3.

The main differences with conventional fusion welding originate from the *keyhole welding* technique typically used with lasers for deep-penetration welding. A fusion weld, such as that produced by TIG welding, is formed through heat conduction into the material, resulting in a wide but shallow weld with a low *aspect ratio*, typically in the order of 1:2 (51). Contrary to a diffuse TIG arc, the laser is a high-energy heat source, which when focused into a small area, creates an energy density capable of locally evaporating the material, forming a keyhole deep into the material (as further described on page 15). Although the laser is also capable of welding in the conduction-limited mode, like a TIG arc, deep-penetration keyhole welding is most commonly used. Only keyhole-mode welding was considered for this review and used for the welding trials described in this report. This typical keyhole welding mode produces welds with a high aspect ratio, which depends on a range of factors, including material composition, power density and laser beam divergence at the point of welding. The cross-section in Fig.5 is of a two-pass (double-sided) laser weld produced through an 11-pass weld completed using manual metal arc welding, demonstrating the difference in aspect ratio between a laser weld and a conventional arc weld (51).

The laser beam is a quasi-parallel, single-wavelength beam of light (51). It propagates mainly in one direction, with the measure of how much the beam expands along its propagation direction referred to as the *beam divergence* (52). For material processing, including welding, the beam is focussed into a *laser spot*, also referred to as *beam waist*, of a small diameter, typically smaller than 0.6mm. The imprint in Fig.6 was produced by traversing a 4kW laser beam focused into a 0.4mm spot size at high speed (5m/min) through photographic paper.

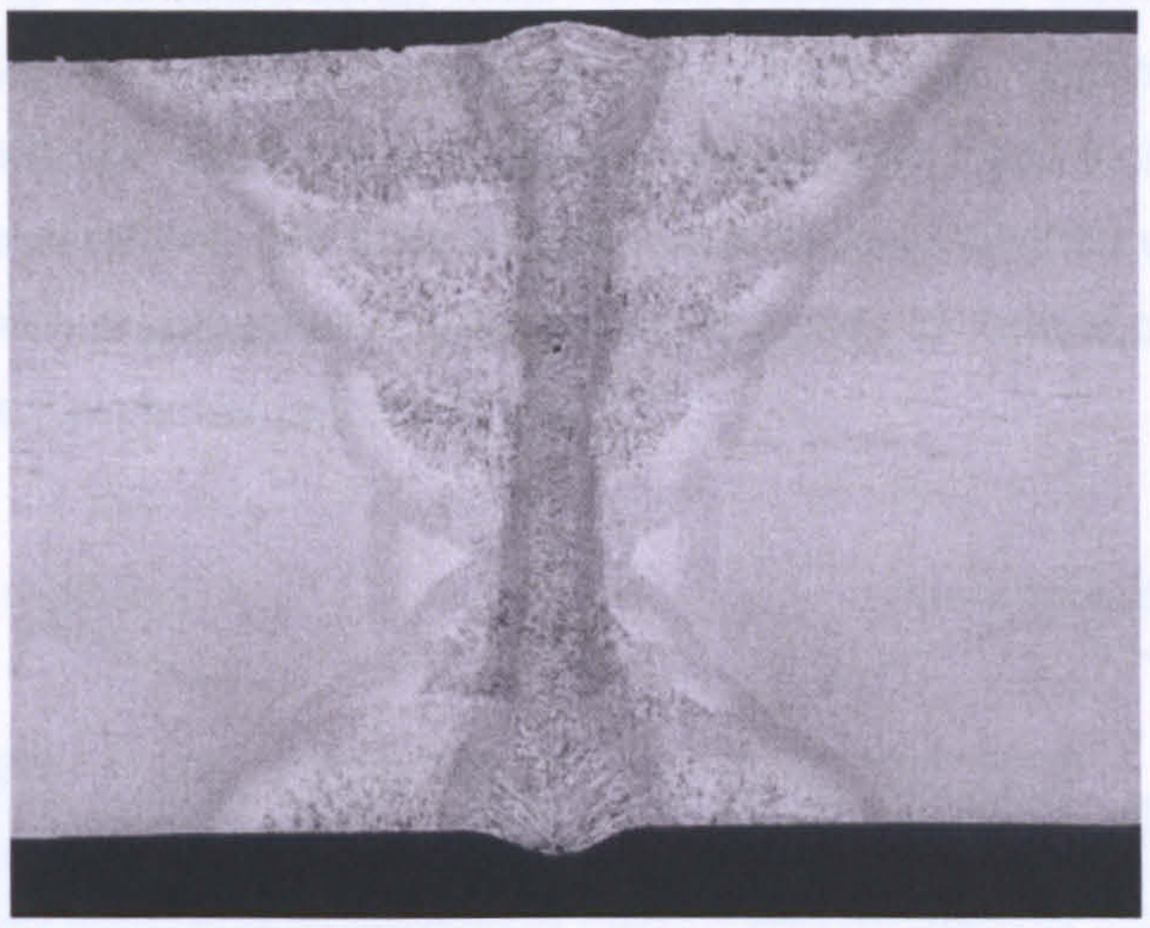

Fig.5 A double-sided CO_2 laser weld in 25mm thickness C-Mn steel produced through an 11-pass manual metal arc welded joint, demonstrating the high aspect ratio of a laser weld compared with conventional arc welding (51)

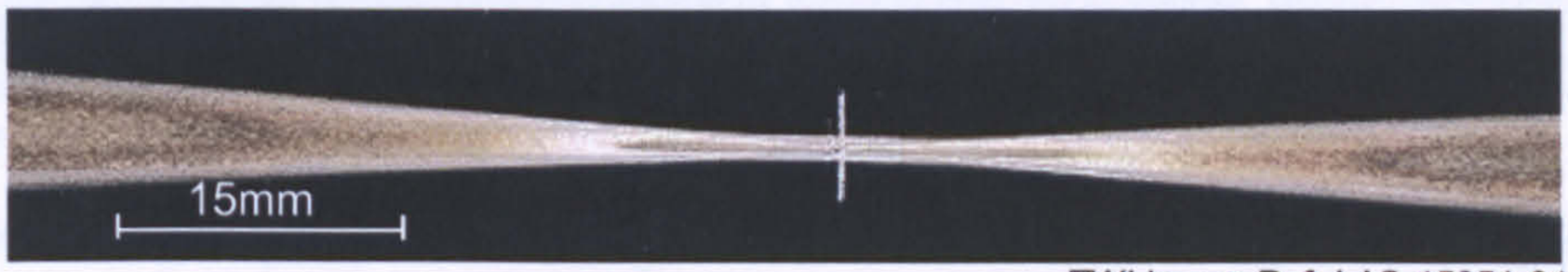

TWI Image Ref: LAS-15851-01

Fig.6 Beam print on photographic paper of 4kW of Yb-fibre laser power focused into a 0.4mm spot diameter

Focusing the laser beam in this way creates power densities high enough to locally heat, melt and evaporate the material (51), which are the different stages of keyhole formation, as shown schematically in Fig.7 and detailed further in EngD Submission 1 (41). With power densities between 10^6 and 10^7 W/cm^2, local melting occurs in less than a microsecond (50), with a keyhole established in less than one millisecond, as observed by high-speed images during Nd:YAG spot welding of 5083 aluminium (53). With today's laser systems, power densities as high as 10^8 W/cm^2 are readily achieved (54).

Prior to the keyhole being established, up to 97% of the incident laser energy is reflected back from an aluminium surface (55). Because of this initial high reflectivity of aluminium, it is customary to angle the laser (at least 5°) away from the perpendicular direction to the aluminium surface to avoid the reflected laser light damaging the optics or the laser (55). This *back-reflection* drops as a *hot spot* is created at the laser impingement point, which gradually absorbs more energy, forming a *weld pool*. When a melt is created, the reflectivity drops and

the absorption increases to 50%, with heat transfer occurring through both conduction and convection (50,55). As the material continues to absorb more laser power, the temperature increases, with metal vapour created when reaching the boiling temperature. The initial evaporation of the material in these early stages of keyhole formation creates metal atoms in the atmosphere above the melt, some of which ionise as a function of temperature, as further explained in Section 4.3.5. The incident laser power reacts with this metal vapour by a process called *inverse Bremsstrahlung*, which is the absorption of electromagnetic radiation (photons) by free electrons, thereby increasing their kinetic energy (and temperature) (56-58). As the vapour temperature rises, more ionisation occurs, and more incident laser energy is absorbed. The pressure of both the laser radiation and the vaporisation creates a depression in the weld pool, which progressively deepens into the melt to form a cylindrical shape, the *keyhole* (51,55), as shown schematically in Fig.7.

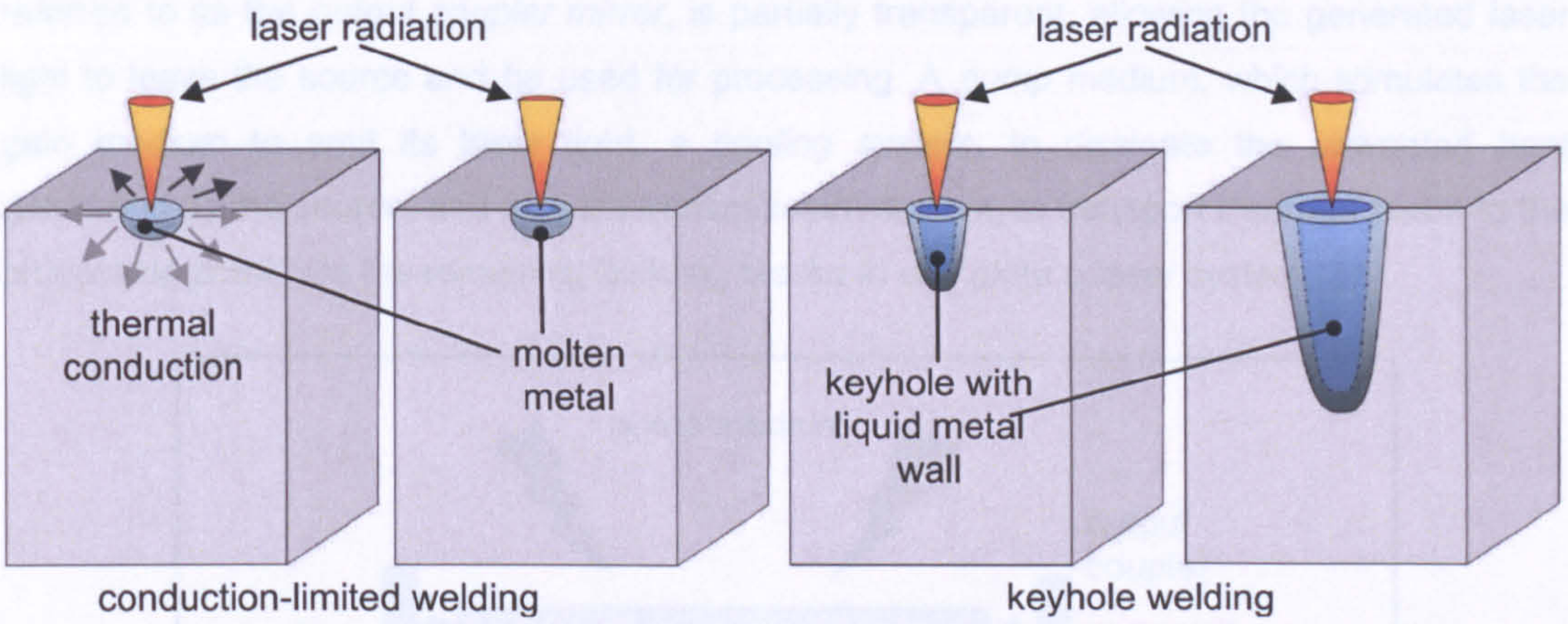

Fig.7 The principle of laser welding, from conduction-limited to keyhole welding (51)

Once established, the keyhole becomes the medium responsible for *coupling* the laser energy into the material, i.e., converting the incident laser energy into heat for melting the material (50). The keyhole is surrounded by a thin liquid film and is filled with metal vapour, with the vapour pressure keeping the keyhole open during laser welding, preventing the thin sheath liquid keyhole walls from collapsing under the surface tension pressure (50,51,59). The keyhole acts like an optical black body absorbing up to 98% of the incident laser energy in case of aluminium (55). Absorption inside the keyhole occurs through multiple reflections inside the keyhole, i.e., *Fresnel absorption*, with energy absorbed by the material at each reflection off the surface. This means that the vapour channel traps the incident laser beam, thereby minimising loss of energy by reflection, and forms a cylindrical heat source which transfers its heat to the surrounding material through convection, which is dominant in the weld pool, and conduction through the thickness of the material (50,59). As the keyhole moves through the material, the thin sheath of liquid metal surrounding it, flows from the front of the keyhole to the back, forming the weld pool. This flow is the result of a reflected wave caused by the forward beam movement itself, a temperature gradient-induced *Marangoni flow* (which is a fluid flow caused by a difference in surface tension), or a pulsing wave motion

caused by the keyhole itself through an instability, or a combination of some or all of these (41,50-51,59).

At the start of this EngD work, at the end of 2000, the CO_2 laser and the LP Nd:YAG laser were the only two established, high-power, industrial laser sources in use for deep-penetration keyhole welding of aluminium and its alloys. What follows is a summary of their salient features relevant for the laser welding of aluminium. For more detailed information on laser sources and their use for welding, the reader is referred to other publications, such as, for instance (50), (51), (52), (55) and (59).

In its most basic form, as shown in Fig.8, a laser consists of a *resonator*, or *optical cavity*, in which the generated laser light is circulated between two *end mirrors*, and a *gain medium* within this cavity which generates the laser light and amplifies it (59). One of the mirrors, referred to as the *output coupler mirror*, is partially transparent, allowing the generated laser light to leave the source and be used for processing. A *pump* medium, which stimulates the gain medium to emit its laser light, a *cooling system*, to dissipate the unwanted heat generated by the source, and a *beam transmission medium*, to transport the laser beam to the processing point, are the remaining building blocks to complete a laser system (31).

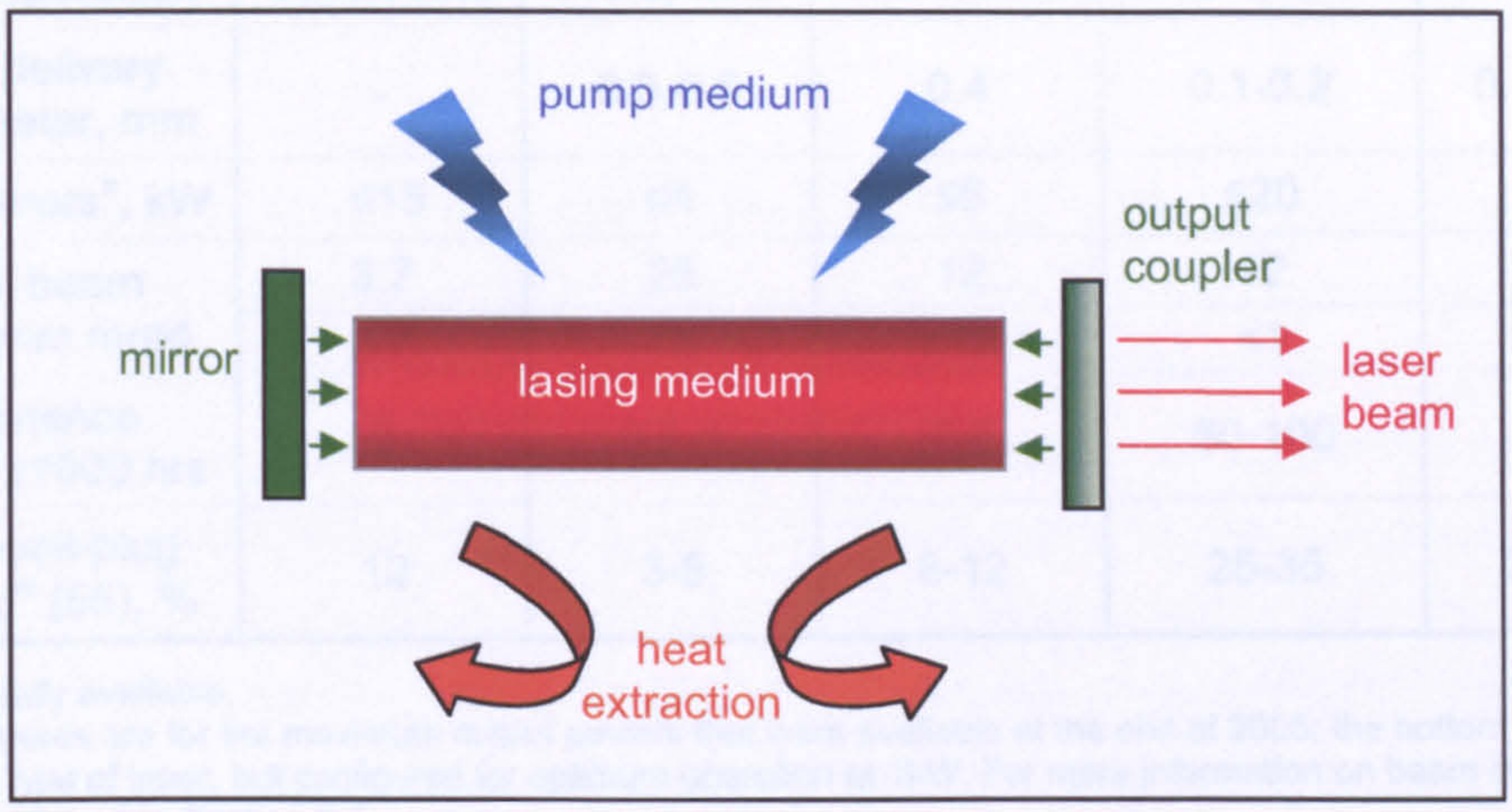

Fig.8 Building blocks of a laser source

A CO_2 laser is a *gas* laser, using a three-part gas mixture of CO_2, He and N_2, as the gain medium, which is electrically stimulated (pumped) to produce a laser wavelength of 10.6μm. The Nd:YAG laser is a *solid-state* laser, in which an Yttrium Aluminium Garnet (YAG) crystal rod doped with traces of Neodymium (Nd) as the gain medium, is pumped using visible light emitted from either flash lamps or laser diodes, to produce a laser wavelength of 1.06μm. The practical consequence of this 10-fold difference in wavelength is that mirrors are required to transmit the CO_2 laser power to the workpiece, whereas flexible optical fibres can be used in case of the Nd:YAG lasers. Optical fibres are easier to use than mirrors particularly when welding complex 3D components. Another consequence, which is particularly relevant for the laser welding of aluminium, is that the absorption of incident laser power is higher for the

shorter Nd:YAG wavelength (22-25). For that reason, the *threshold power density*, defined as the minimum power density required to initiate a keyhole in aluminium, is higher for the CO_2 laser wavelength than for the shorter Nd:YAG wavelength. Although dependent on material composition, temperature and joint geometry, an accepted approximation in the laser welding industry is that a power density of at least $4x10^6$ W/cm^2 and $1.5x10^6$ W/cm^2 is needed to initiate a keyhole in aluminium using a CO_2 and a Nd:YAG laser, respectively (12,22-27,55,60). In practice, this difference in threshold power density means that, for a given output power, an Nd:YAG laser is often preferred over the CO_2 laser for the welding of aluminium (61). However, once the keyhole is established, there is little, if any, difference between the two wavelengths in terms of absorption by the aluminium alloy (55). A review of the salient features of both the CO_2 and the Nd:YAG laser is given in Table 2.

Table 2 Available laser sources capable of keyhole welding of aluminium (31)

	CO_2	Lamp-pumped Nd:YAG	Diode-pumped Nd:YAG	Yb-fibre (multi-mode)	Yb-YAG disc
Lasing medium	Gas mixture	Crystalline rod	Crystalline rod	Doped fibre	Crystalline disk
Typical wavelength, µm	10.6	1.06	1.06	1.07	1.03
Beam transmission	Mirror, lens	Fibre, lens	Fibre, lens	Fibre, lens	Fibre, lens
Typical delivery fibre diameter, mm	-	0.3-0.6	0.4	0.1-0.2	0.15-0.2
Output powers[a], kW	≤15	≤4	≤6	≤20	≤8
Typical beam quality[b], mm.mrad	3.7	25	12	12	8
	3.7	12	<12	<1	<4
Maintenance interval[c], x1000 hrs	2	0.8-1	2-5	50-100	2-5
Typical wall-plug efficiency[c] (55), %	12	3-5	8-12	25-35	25-35

a Commercially available.
b The top figures are for the maximum output powers that were available at the end of 2005; the bottom figures for the same type of laser, but configured for optimum operation at 1kW. For more information on beam quality, the reader is referred to Section 6.4.
c Manufacturer's claim.

Halfway through the EngD work described in this report, two additional high-power fibre-delivered laser sources became available commercially, which showed potential for deep-penetration laser welding of aluminium and its alloys, i.e., the Yb-fibre laser and the Yb-YAG disc laser. A review of the salient features of both these lasers is also given in Table 2, with further information on the Yb-fibre laser and its use for the welding of aluminium described in EngD Submissions 5 and 6 (31,45). Their welding performance for aluminium and its alloys in comparison with the LP Nd:YAG laser was the subject of a separate study, described in EngD Submission 8 (47) and summarised in Section 6.

4.3. LASER WELDING OF ALUMINIUM – POTENTIAL CONCERNS

Whereas the high thermal conductivity and linear coefficient of thermal expansion of aluminium and its alloys can result in lack of fusion or excessive distortion when using conventional fusion welding processes, this is not the case for laser welding. The thermal conductivity of pure aluminium is 209 W/mK (at 0°C) (62), six times higher than that of steel (48-49,63), and requires an intense heat source, such as the laser, for welding. Its linear coefficient of thermal expansion is 23 x 10^{-6} K^{-1} (62), i.e., twice that of steel, and its volume change on solidification of 6.7% (62), i.e., 6% more than steel, make the material more prone to distortion compared with steel. A fast, low heat input process, such as the laser, is therefore preferred to minimise the thermal distortion. However, although the thermal properties of aluminium and its alloys are not a particular concern for laser welding, other material characteristics require attention as they can affect the laser weld quality. In principle, the same basic rules of metallurgy that apply for conventional fusion welding of aluminium, apply to laser welding. Any differences originate from the welding mode, i.e., keyhole versus conduction-limited. What follows is an overview of the material and process considerations when welding aluminium and its alloys using lasers. For more detailed information on the general fusion welding aspects, the reader is referred to other publications, including such publications as (48), (49), (61) and (63).

4.3.1. Affinity with Oxygen

Aluminium has a high affinity with oxygen, which results in a thin, continuous oxide layer forming on all aluminium surfaces (48,61,64). The oxide layer, nominally between 2.5 to 20nm in thickness (48,64) (re)forms "immediately" and grows at a decreasing rate (64). The melting point of this Al_2O_3 layer is 2050°C, more than three times higher than the melting point of the alloy underneath, which lies between 565 and 648°C depending on alloy composition (48,61, 63-65). For the arc processes, this requires special measures, such as AC current or an aggressive flux, to remove the layer prior to or during welding (48,50,61,64-65). Although the high power densities used for laser keyhole welding are capable of locally evaporating this layer, its removal prior to welding is good practice to avoid weld imperfections associated with this oxide film (50). Whereas the oxide is evaporated locally at the keyhole, the oxide adjacent to the joint line can get mixed into the weld pool. This promotes oxide inclusions, or lack of fusion or penetration, resulting from changes in the melt pool flow (59), as further discussed in Section 4.6.1. Surface contaminants such as oil, grease, moisture or other foreign bodies can reside in/on the porous oxide layer, resulting in imperfections, particularly weld metal porosity. The importance of cleaning and oxide removal prior to laser welding and their effect on the occurrence of porosity, are further discussed in Section 4.6.1.

Because of this high affinity with oxygen, the aluminium melt pool needs to be shielded from the oxidising atmosphere during fusion welding. An inert shielding gas is used for this, with pure argon, pure helium, a mixture of argon with helium, or nitrogen all being used in practice

(48,50,61,64). Typically, inert shielding gas is supplied either coaxially or behind the laser at an angle, referred to as *side-jet shielding* (59). A second function of the shielding gas, when laser keyhole welding of aluminium, is that of plasma/plume suppression, which is discussed further in Sections 4.3.5 and 4.5.2. Both functions of shielding and plasma/plume suppression and their influence on weld metal porosity in aluminium are further discussed in Section 4.6.2.

4.3.2. Loss of Strength

The *weld metal* in a welded joint is that part of the *parent material* that has been melted. It has an as-cast structure, with its properties dependent on its composition, quality and grain size (61). The composition of the weld metal depends on the parent materials to be joined, the filler material added, if any, and the ratio of mixing, i.e., *dilution*, between the two. The best weld metal properties are achieved by choosing the correct filler material, by welding with a low level of imperfections and by welding as fast as possible to minimise grain growth. The *heat-affected zone* (*HAZ*) is the area surrounding the weld, which experiences the heating and cooling cycle from the welding, without melting. For a given alloy, its size depends mainly on the heat input of the welding process and the thermal conductivity of the alloy.

In the case of aluminium alloys, the HAZ will experience a loss of strength, further also referred to as *thermal damage*. For the 2000-series aluminium alloys, loss of strength in the HAZ occurs through dissolution of the strengthening precipitates, whereas this occurs because of coarsening of the precipitates in the 6000 and 7000-series aluminium alloys (66-67). Some of this strength can be recovered in the HAZ and the weld metal, depending on the composition, by natural ageing after welding or a post-weld heat treatment. Compared with any of the arc processes, laser welding allows faster welding speeds to fully penetrate a given material thickness. The rapid heating and cooling during laser welding limits the grain growth in the weld metal, which benefits its strength. The high speed results in smaller welds and a smaller HAZ on either side of the weld, which reduces the loss of strength in the HAZ, as the time for dissolution or coarsening of the strengthening precipitates is reduced (51,66-67). Notwithstanding this, losses in strength of as much as 25 to 30% compared with the parent material are not uncommon when laser welding aluminium alloys (15,68).

In addition to this, loss of strength can also occur through excessive evaporation of low-boiling point constituents when laser keyhole welding of aluminium alloys. This results in a loss of strength, because, in case of aluminium alloys, these elements, such as magnesium or zinc, have specifically been added to increase the strength of the alloy (25,34-35,69-71). In the case of Mg-containing aluminium alloys, for example, a quasi-linear dependence exists between Mg-content and yield strength (36,72). The boiling temperature of magnesium and zinc is 1090°C and 907°C, respectively, compared with 2467°C for (pure) aluminium (73). The rate at which strengthening elements disappear from the weld pool during laser keyhole welding depends on a range of factors, including welding conditions (power and speed),

material composition and thickness (69,74). In case of laser keyhole welding, magnesium losses can be as low as 5% and as high as 20% (69,74), with even higher losses (up to 25%,) in case of conduction-limited welding (35). The losses are uniform through the weld pool, which is indicative of strong mixing inside the molten pool (36,74), thereby favouring low surface-to-volume ratio welds, explaining why less magnesium is lost in laser keyhole welds compared with laser conduction-limited welds (36,75). Loss of strength through evaporation of low-boiling point alloying elements, affects all aerospace aluminium alloys, particularly the 6000 and 7000-series alloys, as their principal strengthening alloy element, i.e., magnesium and zinc, respectively, evaporates from the weld pool. This depletion of strengthening elements can be minimised by introducing a filler material with high levels of the alloying element in question. The evaporation of low-boiling point constituents and its effect on porosity in aluminium laser welds is further discussed in Section 4.5.1.

4.3.3. Hot Cracking

Hot cracking in aluminium alloys can occur in the weld metal, i.e., *solidification* or *centre-line* cracking, or in the HAZ, i.e., *liquation* cracking (48,61,63,65,67,76-77). Particularly those alloys containing copper, magnesium and/or lithium are sensitive to this type of cracking, which include the aerospace alloys in the 2000, 6000 and 7000 series (48). Aluminium alloys have a melting/freezing range instead of a melting/freezing point, because of the alloying elements added to pure aluminium to obtain specific material properties. In liquid aluminium, solidification initiates in those areas of liquid with a high melting/freezing point. These islands progressively grow, forming grains, pushing lower melting/freezing point alloy compositions ahead and eventually end up along the boundaries of neighbouring grains. As the metal cools, it contracts, and the shrinkage stresses associated with this, have to be accommodated by the remaining liquid, i.e., this low melting/freezing point film between the grain boundaries. Depending on the strength of this low melting/freezing point film, cracking will occur along the grain boundaries (61).

When the weld starts to solidify, grains grow from the fusion line, i.e., where the HAZ begins, towards the centre of the weld. As such, a low melting/freezing point thin film is pushed towards the weld centre, where both solidifying fronts meet, resulting in *solidification* or *centre-line* cracking if its strength is not enough to withstand the shrinkage stresses. At the same time, during welding, the material in the HAZ, typically within the width of a few grains (67), can reach temperatures so high that low melting/freezing point constituents along the grain boundaries melt. Particularly if the melting/freezing point of the grain boundary phases is lower than that of the weld metal, on cooling, these will not be able to withstand the stresses, resulting in *liquation* cracks along the grain boundaries in the HAZ (77).

The tendency for hot cracking can be minimised by adding a grain refiner, such as scandium (78,79), as welding stresses are absorbed by a larger grain boundary area (61), to either the

parent material or the filler wire; by selecting a joint geometry that produces a lower aspect ratio weld (61); by welding faster (i.e., increasing the cooling rate and reducing the freezing range) (61); or by minimising the shrinkage stresses (61). In case of solidification cracking, a ductile filler wire can be added to absorb the shrinkage stresses (65,76-77,80).

4.3.4. Porosity

Porosity is a problem confined within the weld metal (61). The most common source of porosity in (conduction-limited) fusion-welded aluminium is gas, and hydrogen in particular, dissolved in the molten metal, becoming entrapped as the weld pool solidifies (34,37,53,61,70,72,81-83). *Gas-induced porosity*, further discussed in Section 4.4, is typically spherical in shape, because of an even gas build-up inside the pore (35,72), and smaller than keyhole-induced porosity (72). Gas-induced porosity resulting from hydrogen is further also referred to as *hydrogen (-induced)* or *fine porosity*. In the case of laser welding, porosity can also originate from instabilities of the keyhole, entrapping shielding gas, metal vapour and/or atmospheric gases in the process (25,27,34,53,72,81). *Keyhole-induced porosity*, further discussed in Section 4.5, can be spherical or irregular in shape depending on where in the weld pool it solidifies (27,72) and is typically larger than hydrogen porosity (27,53,72,82). For the purpose of this report, distinction is made between irregularly shaped keyhole-induced porosity found in the keyhole path, on the weld centreline, near the keyhole root, further referred to as *cavities*, and the spherically shaped keyhole-induced porosity found throughout the weld depth and larger than 0.5mm in diameter, further referred to as *coarse porosity*.

4.3.5. Plasma/Plume Effects

As referred to on page 15, keyhole welding relies on the metal vapour inside the keyhole to transfer the incident laser power into the aluminium as heat. However, in some instances, this metal vapour exits the keyhole, forming a cloud above the weld pool, further referred to as a *plasma* or *plume*, as discussed further in Section 4.5.2, This metal vapour cloud can absorb and/or scatter part of the laser energy passing through it, resulting in less laser energy entering the keyhole, leading to keyhole fluctuations and possible collapse (50). To ensure a stable keyhole and maximum welding performance, vapour cloud formation above the weld pool should be avoided, or, once formed, efficiently removed during welding. The latter can be accomplished by using a standard shielding gas arrangement (Section 4.3.1), or, through the use of a dedicated inert gas stream aimed at the vapour plume (50). The efficiency of such an arrangement depends on the inert gas used, its flow rate and positioning with respect of the vapour cloud above the weld pool (50). This, as well as the phenomenon of plasma/plume formation and its effect on porosity in aluminium laser welds is discussed further in Sections 4.5.2 and 4.6.2.

4.4. GAS-INDUCED POROSITY

When welding aluminium, gas entrapped in the weld metal may remain as bubbles in the weld metal when there is insufficient time to escape prior to solidification (84). In the case of conventional fusion welding, hydrogen accounts for 90% of all such gas pores (85), with the remainder resulting from shielding gas entrapment (59,71). As shielding gas mainly enters the weld through the keyhole, this porosity type is further discussed in Section 4.5.

A fusion weld in aluminium generally contains hydrogen-induced pores, because of the high solubility of hydrogen in liquid aluminium compared with solid aluminium. As shown in Fig.9, the hydrogen solubility in pure aluminium drops a factor of 20, from 0.7cm^3/100g to 0.036cm^3/100g, upon solidification (61,86). This large difference in hydrogen-solubility between the molten and the solid state of aluminium means that during rapid cooling, time is limited for all this hydrogen to escape, entrapping some hydrogen as pores in the weld metal.

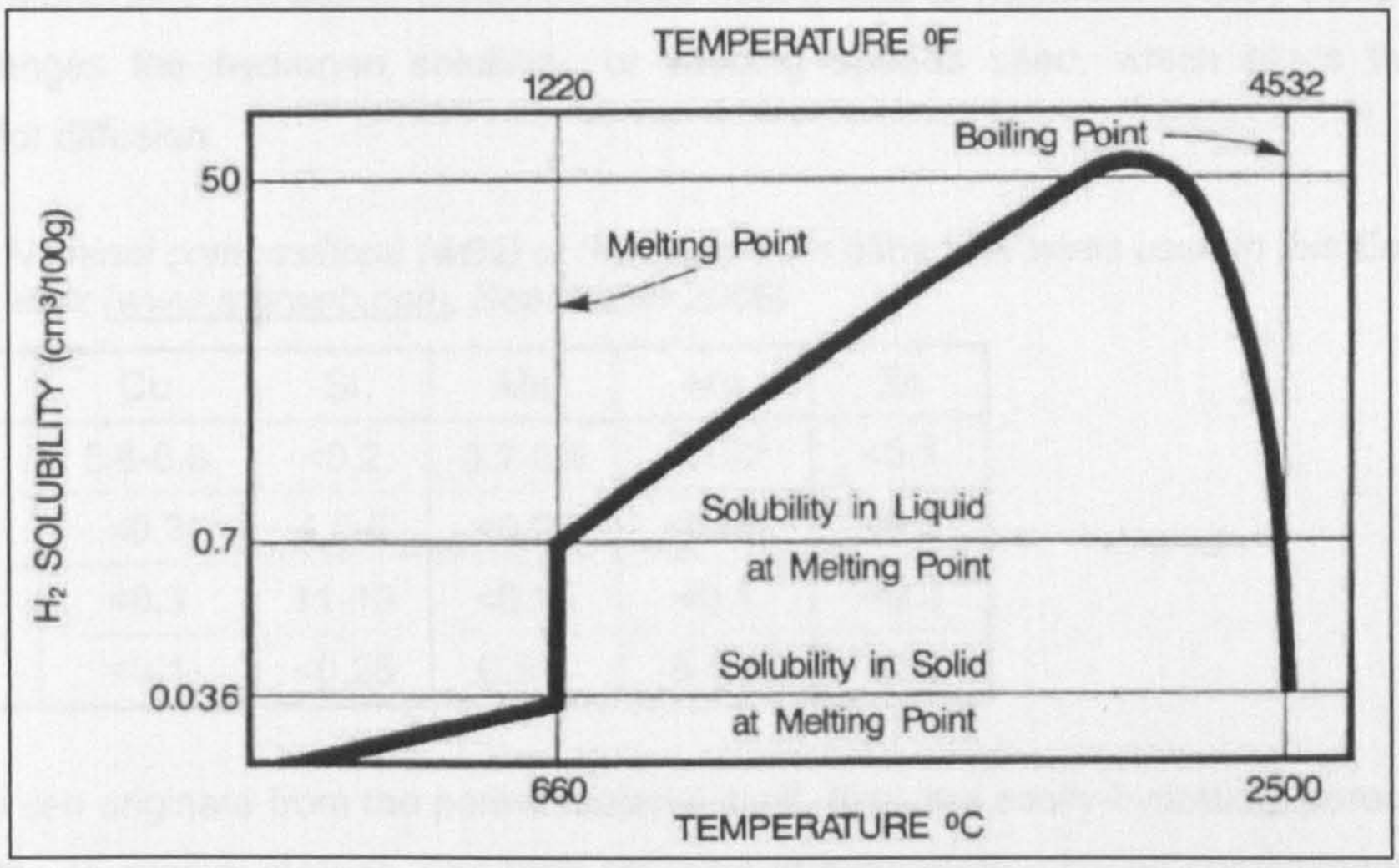

Fig.9 Solubility of hydrogen in pure aluminium (61,86)

Hydrogen pores in aluminium welds nucleate, i.e., initiate, heterogeneously at imperfections or minute inclusions in the weld, after which the pores grow by diffusion (36). Gas bubbles in general, escape through natural buoyancy or forced convection (37,86). In the presence of alloying elements, the solubility of hydrogen in the liquid and/or solid state changes (61). Magnesium, lithium and titanium, for instance, raise the hydrogen solubility in liquid aluminium, whereas the opposite is true for copper, silicon, iron and zinc (61,87). Silicon-containing filler wires, such as the 4043 and 4047 filler wire with 4.5-6% and 11-13% Si, respectively (Table 3), are recommended for welding 5000 and 6000-series aluminium alloys (48).

As for other fusion processes, hydrogen (or OH) is considered by many as the principal source of fine porosity in laser-welded aluminium (34,53,61,72,82,88-90). The temperatures

achieved during laser keyhole welding of aluminium are high compared with any of the arc welding processes, as the material is evaporated rather than melted. The evaporation and melting temperatures of pure aluminium are 2467°C and 648°C, respectively, with higher hydrogen solubility at higher temperatures (Fig.9). This increases the likelihood of fine porosity in case of laser keyhole welding (53,88). However, laser welding is carried out at faster speeds than conventional arc welding, which increases the cooling rate and results in less time for diffusion, i.e., for the hydrogen bubbles to grow (36,72). For arc welding of aluminium, hydrogen porosity can be controlled by keeping the weld hydrogen content below an alloy-dependent threshold level (91). This level increases with increasing cooling rate (35), which favours laser welding, as a higher concentration of hydrogen is required to produce porosity. According to Pastor *et al.* (36), hydrogen pores in laser-welded aluminium cannot grow beyond 0.2mm in diameter, because of the high cooling rate of laser welding. However, disagreement exists in the literature on the exact maximum size of hydrogen pores that can be found in laser-welded aluminium, ranging from 0.2mm (36,82) to 0.3 (72,92), 0.4mm (93) or even 0.5mm (94). The author attributes these differences to variations in alloy composition, which changes the hydrogen solubility, or welding speeds used, which alters the time available for diffusion.

Table 3 Nominal compositions (wt%) of the aluminium alloy filler wires used in this EngD work (www.matweb.com, September 2006)

	Cu	Si	Mn	Mg	Zn
2319	5.8-6.8	<0.2	0.2-0.4	<0.02	<0.1
4043	<0.3	4.5-6	<0.05	<0.05	<0.5
4047	<0.3	11-13	<0.15	<0.1	<0.2
5556A	<0.1	<0.25	0.6-1	5-5.5	<0.2

Hydrogen can originate from the parent material itself, from the easily-hydrating, porous oxide layer on the aluminium surface, and from moisture or hydrocarbon-based contaminants, such as oil and grease, on the material surface (35,61,95). Hydrogen can also originate from moisture or contaminants, such as drawing lubricant, present on the filler wire, or from moisture in the shielding gas (35,61,95). The latter can result from the shielding gas itself, or, more likely, from its delivery, through deficient connections, leaks or moisture-ingress through the tube wall during long periods of non-usage (61,95). Minimising any or all of these sources of hydrogen reduces the level of hydrogen porosity in laser-welded aluminium, as discussed in Sections 4.6.1 and 4.6.2. The author demonstrates in EngD Submission 2 (42), which is summarised in Section 5, that the level of porosity in laser-welded thin-section aerospace aluminium can be kept consistently below the stringent limits set by current aerospace standards, through the rigorous application of some of these measures.

In case of laser welding, some researchers claim that hydrogen only plays a marginal role in pore formation, due to the high welding speeds and cooling rates associated with laser

welding (35,36). Pastor *et al.* (36) conclude that hydrogen pores in laser-welded aluminium only exist on a micrometre-scale, based on a comparison with cast aluminium, where, at cooling rates of between 1 and 10°C/s, the hydrogen pore size is typically between 1 and 10µm. In contrast, Kutsuna and Yan (85) calculated cooling rates as high as 1400°C/s during the welding of 5083 aluminium using a 2kW CO_2 laser at a welding speed of 1m/min, by measuring the time for the weld to cool down from 700 to 400°C. However, the author comments that the casting of aluminium is a static process, during which the atmosphere above the casting can be strictly controlled. Such control is more difficult to achieve during a fast-moving process, such as laser welding. Moreover, when laser welding aluminium, hydrogen can not only originate from the base material, but also from the filler material (if any) or the shielding gas or its delivery (27,35,61). As such, the hydrogen content in case of laser welding can be much higher, which increases the risk of hydrogen porosity, with the possibility of larger pores, compared with the casting process.

An analysis of the pore content found in CO_2 laser welds made in 5083 alloy carried out by Masumoto *et al.* (90), revealed the presence of hydrogen. However, Simidzu *et al.* (73) measured "significant" amounts of shielding gas, but "no appreciable" level of hydrogen in pores found in partially penetrating Nd:YAG laser spot welds produced in the same (5083) alloy. The author found no evidence in the literature to support the assumption that this difference could be the result of the difference in laser source used, i.e., CO_2 versus Nd:YAG. However, the difference in geometry and welding mode, i.e., continuous versus spot welding, are more plausible reasons for this difference. In case of fully penetrating butt welds, any shielding gas that is drawn into the keyhole, because of its variable nature (see Section 4.5.1), can escape through the exit of the keyhole on the underside of the sample. This is not the case for the partially penetrating spot welds produced by Simidzu et al (73). Moreover, these spot welds were produced using 12kW of Nd:YAG laser power irradiating the material for only 5ms. Hydrogen bubbles will not have had the time to nucleate and grow to a size that is readily detected, by radiography for instance, in this short timescale. Similar to the findings by Simidzu *et al.* (73), Seto *et al.* (37) found that 90% of the pore content in partially penetrating CO_2 laser welded 5083 aluminium comprised of shielding gas

A study by Rapp *et al.* (96) revealed no evidence of the influence of cleaning (which is further discussed in Section 4.6.1) on the level of gas-induced porosity found in CO_2 laser welds produced in 5mm thickness 6082 aluminium alloy, concluding that gas-induced porosity did not originate from hydrogen. This was in contrast with MIG welds produced in the same alloy. However, the author comments that all welds in this research were carried out at a welding speed of 3m/min, and higher, i.e., at least six times faster than the typical MIG welding speed. The cooling rate therefore was higher, limiting the time for hydrogen pore nucleation and growth. Moreover, it was not clear from this study by Rapp *et al.* (96), which diameter pores that were found in the welds, were considered in the analysis. Because of the high welding speeds used, hydrogen-induced pores as large as 0.2mm may have been present in the weld,

but not considered, because they were deemed too small or simply because they were not detected because of the low sensitivity of the radiograph. The conclusion by Rapp *et al.* (96) therefore, that surface preparation is not important when laser welding aluminium is not justified.

Based on the above observations, the importance of hydrogen when laser welding aluminium needs to be viewed in the context of the application, including material thickness, whether the weld is fully or partially penetrating, and considering the welding conditions used, including welding speed and laser power. Its importance should also be weighed up against other factors that determine the final laser weld quality, including the presence of keyhole-induced porosity (Section 4.5). Efforts to remove all possible sources of hydrogen from the samples, filler wire and shielding gas are futile if the joint or process is prone to the formation of keyhole-induced porosity. For instance, the introduction of moisture in the helium shielding gas during Nd:YAG laser welding of 1.5mm thickness 5182 and 5754 aluminium, increased the level of porosity, but was considered not significant compared with the coarse porosity in these welds carried out at high speeds (35,36).

4.5. KEYHOLE-INDUCED POROSITY

The keyhole is an inherently unstable structure, even in the absence of motion through a material (34,59). Tsukamoto *et al.* (97) described how when CO_2 laser welding steel, the cylindrical keyhole deformed radially when the depth of the keyhole was larger than the laser spot diameter. This deformation occurred as necking and swelling of the keyhole through its depth, with the laser beam impinging where necking occurred, resulting in volatile local evaporation and a fluctuating plasma/plume and keyhole as a result. The same was observed by Seto *et al.* (37), who used high-speed video and real-time radiography to monitor partially penetrating CO_2 laser welds in 5083 and 5182 aluminium alloy, revealing a keyhole subjected to a repetitive process of violent expansion and contraction. High-speed video taken by Matsunawa *et al.* (53) during pulsed Nd:YAG laser welding of 5083 aluminium with the beam focused in a 0.7mm diameter spot, showed the keyhole diameter fluctuating between 0.1 and 0.7mm, at a frequency between 2000 and 2850Hz. This fluctuating behaviour was also observed during continuous wave (CW) CO_2 laser welding, albeit at a (unspecified) lower frequency by Matsunawa *et al.* (53), and during CW Nd:YAG laser welding of 2024 alloy, by Hu and Richardson (98), at a frequency faster than could be recorded with the 7100 frames per second (fps) high-speed camera used.

To understand this inherent instability, a closer look at the keyhole is required. In Section 4.2 on page 15, the keyhole was described as a cylinder filled with metal vapour surrounded by thin walls of liquid material. Real-time digital radiography and high-speed filming by Seto *et al.* (37), revealed a wave-shaped layer of molten aluminium at the leading edge of the keyhole

progressing downward to the keyhole tip, as shown Fig.10. A similar structure had also earlier been observed by Arata (99) during electron beam welding.

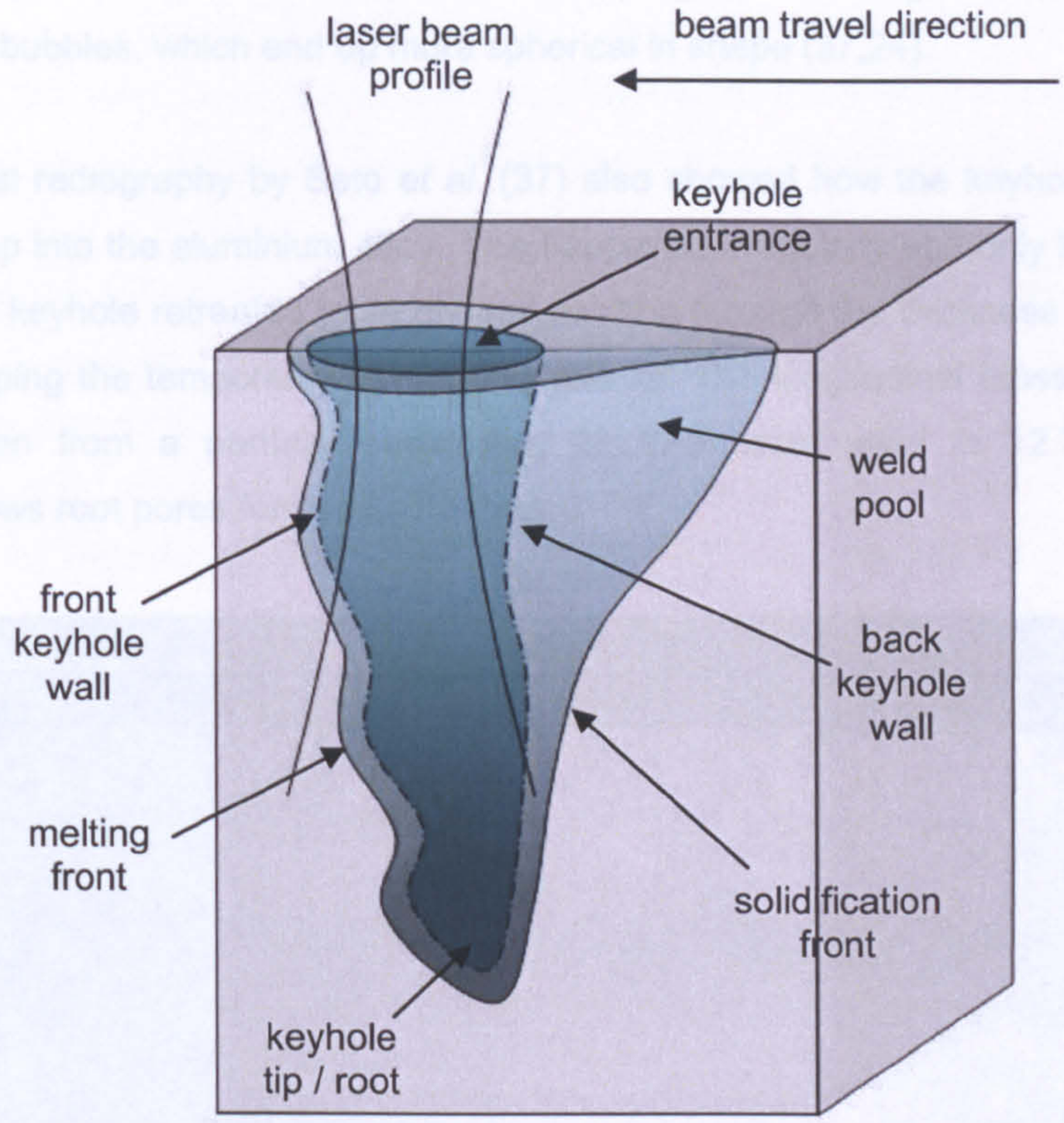

Fig.10 Wave-shaped front (liquid) edge of a laser keyhole (37)

Seto *et al.* (37) observed that vaporisation did not occur uniformly through the keyhole, but locally, and at a constantly changing position, which was assumed to be a direct result of the wave-like structure observed at the keyhole front. At those point(s) of this structure protruding into the keyhole directly in the path of the incoming beam, high power densities are created, resulting in instantaneous evaporation of the liquid at these locations, sending a stream of vapour towards the back wall of the keyhole resulting in a depression (37). The author comments that this force of evaporation is directed directly into the keyhole, but also in the liquid side and back walls of the keyhole, with the front of the keyhole largely unaffected by it, because of the unwelded (solid) material. Depending on the dynamic pressure with which this happens, the depression in the keyhole back wall can collapse on itself, forming a pore in the weld metal surrounding it. In the process, metal vapour will become entrapped, as well as shielding gas and/or atmospheric gases, as confirmed by the results of a pore content analysis (37,53,88). The author comments that this local evaporation and the resulting dynamic pressure can also result in the back wall oscillating and touching the front or side walls of the keyhole, causing it to collapse. This becomes more pronounced for intense evaporations or in case of a small diameter keyhole, as was observed by Hu and Richardson (98). The shape of the keyhole-induced porosity formed in this way is either spherical or

elongated, depending on where along the keyhole it is formed and where in the weld pool it solidifies (37,53). Pores entrapped near the bottom of the weld on the solidification interface, elongate upwards in the opposite direction to the welding direction, whereas the solidification of pores positioned in the middle or top of the weld progresses through the solidification zone enveloping the bubbles, which end up more spherical in shape (37,24).

Real-time digital radiography by Seto *et al.* (37) also showed how the keyhole intermittently penetrated deep into the aluminium alloy. This happened irregularly and only for a short time, after which the keyhole retreated to its original position through the thickness of the material, thereby entrapping the temporarily formed keyhole tip. The longitudinal cross-section shown in *Fig.11*, taken from a partially penetrating Nd:YAG laser weld in 12.7mm thickness aluminium, shows root pores formed in this way.

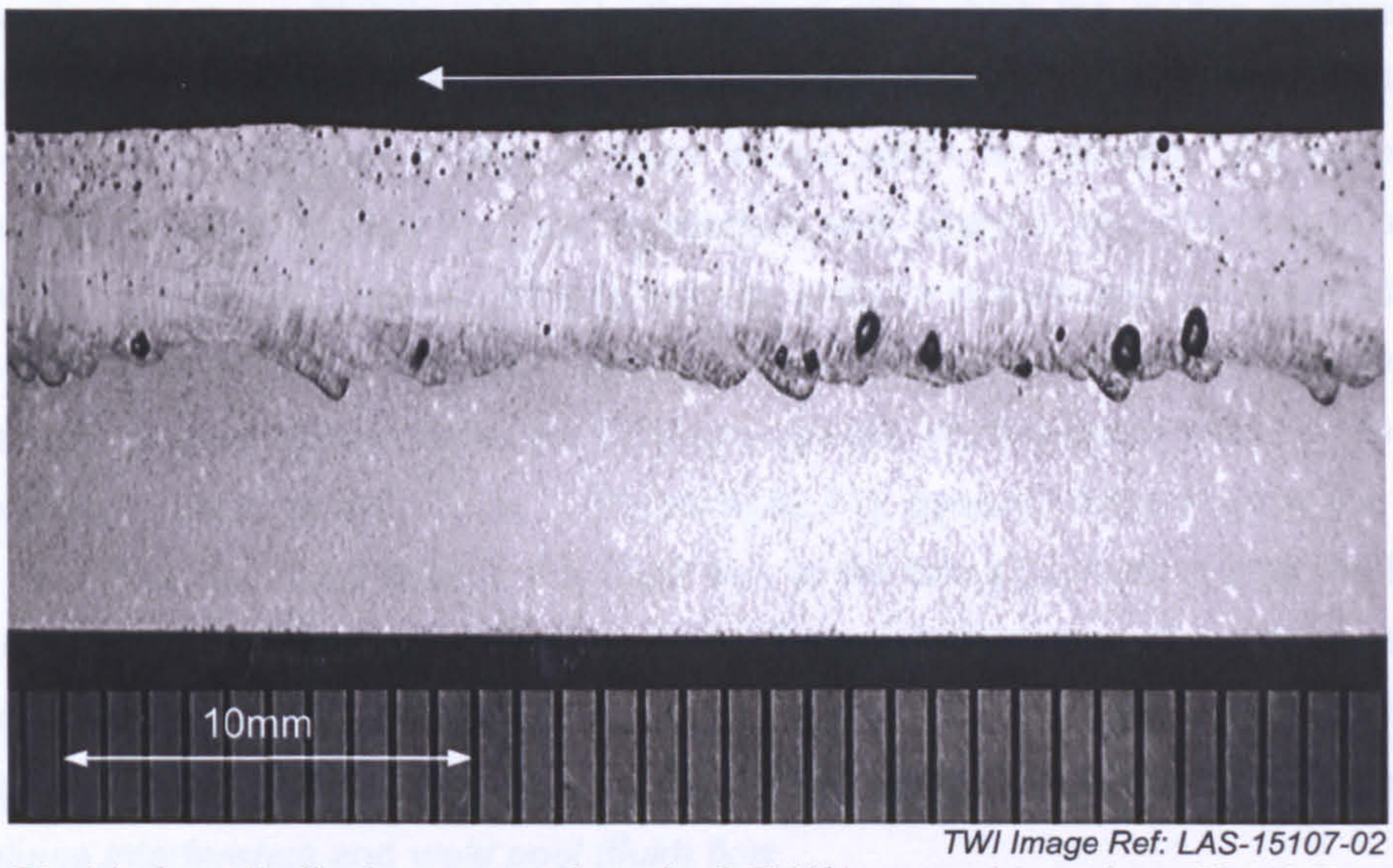

TWI Image Ref: LAS-15107-02

Fig.11 Longitudinal cross-section of a 3.5kW laser weld produced in 12.7mm thickness aluminium at a welding speed of 1m/min

According to Seto *et al.* (37), Matsunawa (53), and Haboudou *et al.* (72), such instabilities at the keyhole root are typical for partially-penetrating laser welds in aluminium, and disappear as soon as the keyhole penetrates the material thickness. Tsukamoto *et al.* (97) attributed this "spiking" phenomenon, to the radial deformation of the keyhole, i.e., necking and swelling, with the incident laser energy absorbed at a location of necking along the keyhole. This results in less of the incident power reaching the keyhole root, resulting in a local keyhole collapse. The author comments that even with a less idealised keyhole geometry, this theory remains true, in that local evaporation at protrusions along the keyhole front wall will absorb the incident laser energy, resulting in heavy local evaporations, depriving the keyhole further down from the required laser energy to sustain the keyhole. Moreover, as the surface tension is highest at the tip of the keyhole (because of the smallest radius of the keyhole at that location) the keyhole collapses preferentially at its root, forming root porosity.

Real-time radiographic evidence by Mueller (100) during CO_2 laser welding of aluminium showed that the keyhole tip in partially-penetrating welds was inclined away from the welding direction. This inclination at the keyhole tip was confirmed by Seto *et al.* (37), as well as by simulations of laser welding in glass by Duley (59), and was found to be speed-dependent (59). This inclination means that no direct optical path exists between the entrance of the keyhole and its root, with Fresnel absorption and reflection, as described in Section 4.2 on page 15, the principal mechanism for the incident laser power to reach the tip of the keyhole.

The inherent instability of the keyhole is closely associated with the vapour pressure, which is important in both its formation and behaviour, as discussed in Section 4.2. The vapour pressure is the dominant force holding the keyhole open, acting against the surface tension, which is the dominant force trying to close it (35,59). This simplified model of equilibrium to achieve a stable keyhole is true for a stationary or slow moving keyhole, with the hydrodynamic pressure, which is related to the speed with which the molten material flows around the keyhole, becoming significant only at "higher" speeds according to both Duley (59) and Forsman (101). A change in any of these forces, which are all alloy and temperature dependent (35), is a move away from the equilibrium, with keyhole instabilities as a possible consequence. As such, the factors affecting keyhole stability include welding speed (59,101), fluctuations in laser output power (59), irregularities in the absorption of the incident laser power (through plasma/plume effects, for example) (55,59), volatile evaporation of low boiling point constituents, such as Mg, Zn or Li (25,34-35,69,71), dynamic instabilities in the vapour flow (59), and dynamic instabilities in the liquid flow of the thin liquid wall around the keyhole or in the weld pool at the rear of the keyhole (59). All these factors, except welding speed and laser power, are associated with the material composition, and are further discussed in the subsequent sections, grouped into three categories, i.e., *evaporation of volatile elements*, *plasma/plume interference* and *weld pool (fluid) flow*.

4.5.1. Evaporation of Volatile Elements

Thermodynamic calculations by Dausinger *et al.* (27) show that elements, such as Mg and Zn, with low boiling point temperatures, i.e., 1090 and 907°C, respectively, lower the vaporisation temperature of an aluminium alloy. This means that, for a given laser power density, evaporation in the alloys with such elements starts earlier than for pure aluminium, which has an evaporation temperature of 2467°C, and that the evaporation pressure of these alloys will be higher (102). Keyhole observations by Rapp *et al.* (74) have shown that these low boiling point, also referred to as *volatile*, constituents evaporate readily from the laser weld, which was also the case during electron beam welding of aluminium observed by Arata (99). As mentioned earlier (Section 4.3.2) these magnesium losses can be as low as 5% and as high as 20%. The pressure associated with this evaporation can result in the keyhole collapsing, and entrapping metal vapour and shielding gas in the process, as discussed in Section 4.5 (page 26). Upon solidification, the metal vapour condenses on the inside walls of the pore,

with the shielding gas retained inside, as confirmed by various studies on both CO_2 and Nd:YAG laser welds produced in 5083 aluminium alloy (24,37,72,82). These pores are typically irregular, polyhedral, in shape (85), with their levels increasing with increasing concentration of alloying elements (72).

Because these volatile elements lower the evaporation temperature of the alloy, the threshold intensity for laser keyhole welding is lowered (102), which, for a given laser power, results in deeper penetration (102,103). For this reason, a better welding performance is claimed for aluminium alloys with a high Mg concentration, compared with those alloys with less or no Mg (73,74,103). The author notes that improved performance refers to an improved depth of penetration, or faster welding speed for a given aluminium thickness, but not weld quality.

4.5.2. Plasma/Plume Interference

As mentioned in Section 4.5.2, it is possible for the metal vapour to exit the keyhole, because of changing pressures inside the keyhole, which result, for instance, from intense localised evaporations along the front keyhole wall. High-speed video by Matsunawa *et al.* (53) during pulsed Nd:YAG laser welding of 5083 aluminium, showed a fluctuating vapour cloud periodically being ejected from the keyhole, with the keyhole fluctuating in a synchronised manner. If such a vapour cloud exists over an extended length of time, the amount of incident power that enters the keyhole will vary, because of absorption or scattering of the incident power affecting the keyhole stability (as explained further on page 31). A nailhead-shaped weld cross-section is indicative of the presence of this vapour cloud, with the wide top of the profile being the result of radiation from the vapour cloud heating the top surface around the keyhole through conduction (50). A means of removing this vapour cloud above the weld pool is through the use of a jet of inert shielding gas, as further detailed in Section 4.6.2.

Greses (56-58) determined through spectrography that the vapour above the keyhole was ionised when welding steel using 4kW of CO_2 laser power, but not ionised using the same Nd:YAG laser power. Ionised and non-ionised metal vapour is further referred to as *plasma* and *plume*, respectively. A practical implication of this difference is that when welding steel using a CO_2 laser, helium is recommended to minimise the formation of plasma, because its 24.46eV ionisation potential is higher than that of argon, i.e., 15.68eV, as shown in Table 4 (55). Helium's high thermal conductivity also readily removes heat from the plasma, lowering its temperature and (electron) density, resulting in less loss of incident laser energy (50,98).

Aluminium vapour ionises more readily than steel vapour (50) and higher power densities are required for keyhole welding of aluminium (compared with steel), because its threshold power density is higher (104). Notwithstanding this, spectroscopic measurements during Nd:YAG laser welding of pure aluminium revealed that the plume mainly consisted of hot vapours, in contrast with an ionised plasma when welded with a CO_2 laser (56,105-106). In what follows,

no distinction is made between the two for the laser welding of aluminium, with the aluminium vapour cloud above the laser keyhole further referred to as the *plasma/plume*.

Table 4 Properties of argon, helium, nitrogen and oxygen (56)

	Atomic mass	Thermal conductivity⁎, W/mK	Density, kg/m^3	Ionisation potential, eV	Typical cost, per bottle╬
Ar	39.9480	0.01772	1.78	15.759	100%
He	4.0026	0.152	0.18	24.587	300%
N_2	14.0067	0.02598	1.25	14.534	90%
O_2	15.9994	0.02674	1.43	13.618	25%

⁎ at 273K and 1 atmosphere pressure
╬ approximated cost, using the cost of a bottle of argon as reference (100%)

High-speed video images taken by Matsunawa *et al.* (107) of the plasma/plume exiting the keyhole during CO_2 laser welding of 5083 aluminium alloy using argon shielding, revealed a two-part plasma/plume, comprising a metallic component, formed by metal vapour, and a shielding gas component, resulting from the interaction between the plasma/plume and the shielding gas. The direction and size of the metallic plasma/plume varied with the keyhole behaviour during welding, forming in the opposite direction to welding at high speeds, and almost perpendicular to the workpiece surface at low speeds, because of the difference in inclination of the keyhole front wall, where evaporation occurs, as shown in Fig.12 (108). At a low welding speed, the front keyhole wall was virtually perpendicular to the material surface, with an increasing inclination (relative to the perpendicular) as the welding speed increased. The shielding gas component remained perpendicular to the material surface under all welding conditions, but varied in intensity with changing conditions of laser power and speed (55,107). Based on the images taken during Nd:YAG laser welding of 5083 aluminium, the speed at which the plasma/plume was ejected from the keyhole opening was recorded to be as high as 270m/s during pulsed welding (53, 55).

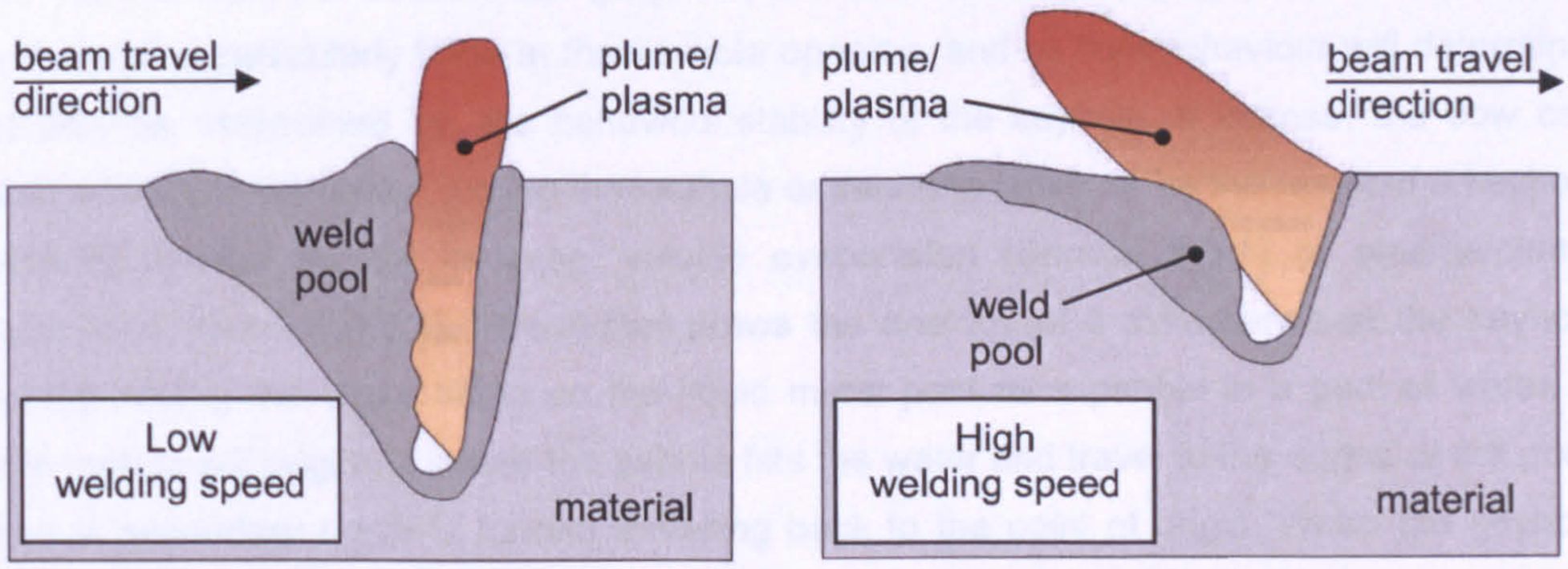

Fig.12 Change in keyhole front-wall inclination and plume/plasma with welding speed (108)

Irrespective of whether the vapour is ionised or not, the presence of such a vapour above the keyhole for a prolonged period of time affects the total laser power that enters the keyhole. This impacts on the keyhole stability, and therefore, the presence of porosity in laser-welded

aluminium. This reduction in power entering the keyhole is the result of either absorption of the beam through inverse Bremsstrahlung, explained earlier in Section 4.2, or, dissipation of the laser energy through Rayleigh or Mie scattering (34,55,90). *Rayleigh scattering* refers to the loss of power through the beam impinging on particulate material that is expelled from the keyhole, whereas *Mie scattering* is the result of a change in beam focus, because of (large) differences in the refractive index caused by steep temperature gradients in the vapour. The losses through absorption become smaller when welding with a shorter wavelength, whereas the losses through scattering increase (57,58). This means that, in case of an Nd:YAG laser, the absorption losses are smaller than for a CO_2 laser, but that more losses occur through scattering. In case of steel, it was demonstrated that the effect of the former was larger than that of the latter, meaning that the presence of a plume during Nd:YAG laser welding affects the welding performance less than the plasma formed during CO_2 laser welding (58). Notwithstanding this, the attenuation of an incident laser beam during Nd:YAG laser welding of steel was still measured to be as high as 40% (58). The fact that the plasma/plume affects the stability of the keyhole was demonstrated by high-speed video images taken by Matsunawa *et al.* (53) during pulsed Nd:YAG laser welding of 5083 alloy, showing a plasma/plume above the keyhole fluctuating in a similar manner as the keyhole itself. Based on this evidence, the author concurs with the conclusions that this fluctuation of the keyhole is the direct result of the absorption/scattering of the incident laser power by the fluctuating plasma/plume. The speed with which the vapour exits the keyhole is also a contributory factor, as it creates a localised low pressure above the keyhole (55), thereby increasing the likelihood of keyhole instabilities.

4.5.3. Fluid Flow within the Weld Pool

The molten material flow near the keyhole entrance impacts on the keyhole behaviour (37,55,82). As the keyhole moves through the material, it is surrounded by a thin layer of liquid material at the front and sides, and a large volume of liquid material, the weld pool, at back, as mentioned in Section 4.2 (page 15) and shown in Fig.10 (page 26). The volume of liquid metal is particularly large at the keyhole opening, and its flow/behaviour will determine, and also be determined by, the behaviour/stability of the keyhole. If intense, the flow can cause a keyhole instability, forcing the keyhole entrance to close, or be the result of a keyhole instability caused by, for instance, volatile evaporation (Section 4.5.1) or plasma/plume interference (Section 4.5.2). The author draws the analogy of a disturbance at the keyhole opening having the same effect on the liquid metal pool as a pebble in a pool of water. A ripple motion will originate where the pebble hits the water and travel to the edges of the pool, where a secondary ripple is formed travelling back to the point of origin. When the keyhole momentarily becomes unstable, because of the pressure variation caused by evaporation of volatile elements, for instance, a ripple motion will form in the weld pool in the form of a surface wave. This surface wave will travel away from the keyhole towards the already solidified material at the edges of the weld pool and bounce back towards the keyhole. The

reflected (surface wave) motion will force the keyhole to close, but is counteracted by the vapour pressure. Whether this will lead to the keyhole entrance to close depends on the forces acting against this, most notably the vapour pressure, and on the intensity of the flow, which in turns depends on the viscosity of the molten material and on the magnitude of the instability that caused it. This liquid motion and the tendency of the reflected wave to close the keyhole were observed from high-speed video images taken by Matsunawa *et al.* (53) during CO_2 laser welding of 5083 aluminium, with "large" weld pool ripples observed giving rise to "large" porosity, and attributed to the evaporation of Mg and Zn. The same observations were made by Hu and Richardson (98) during Nd:YAG laser welding of 3.2mm thickness 2024, who described a wave-like motion of the weld pool surface between the keyhole and the solidified material, caused by plasma/plume fluctuations resulting from localised evaporation along the keyhole front wall.

In work done in Japan by Seto *et al.* (37), welding was carried out over tin (Sn) wire that was embedded in holes in the surface of 5083 and 5182 aluminium to visualise the weld pool shape upon solidification using on-line digital radiography. Some still images taken from this are displayed in Fig.13. The captured images revealed two distinct flow patterns, one at the weld pool surface and directed towards the back of the weld pool, and the second directed upwards at the rear of the molten pool originating at the keyhole tip.

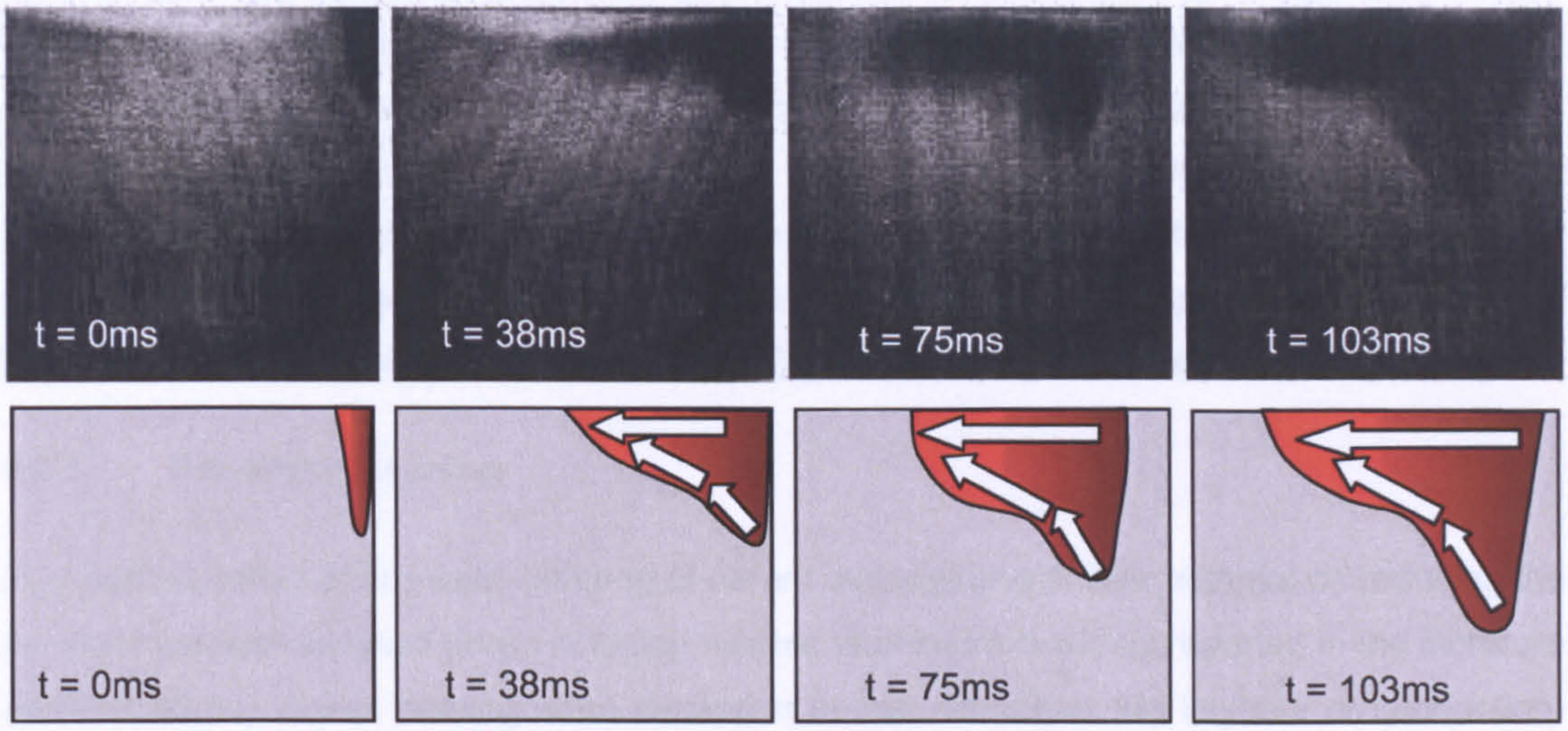

Fig.13 Formation of an aluminium laser weld pool visualised by welding over tin embedded in the sample using on-line digital radiography (37)

The same researchers also carried out welds on samples with tungsten (W) particles entrapped between the two abutting faces, to visualise the path that material particles and pores follow during laser welding. Tungsten was chosen because of its high melting temperature, resulting in the particles not melting during the welding of aluminium, and because of the difference in density with aluminium, allowing easy detection through radiography. From the results, depicted in Fig.14, Seto *et al.* (37) concluded that pores in an aluminium weld pool did not rise to the (weld pool) surface under their own buoyancy, but

were transported from the keyhole tip inside the molten pool towards the upper part at the rear of the molten pool, by an intense molten metal flow.

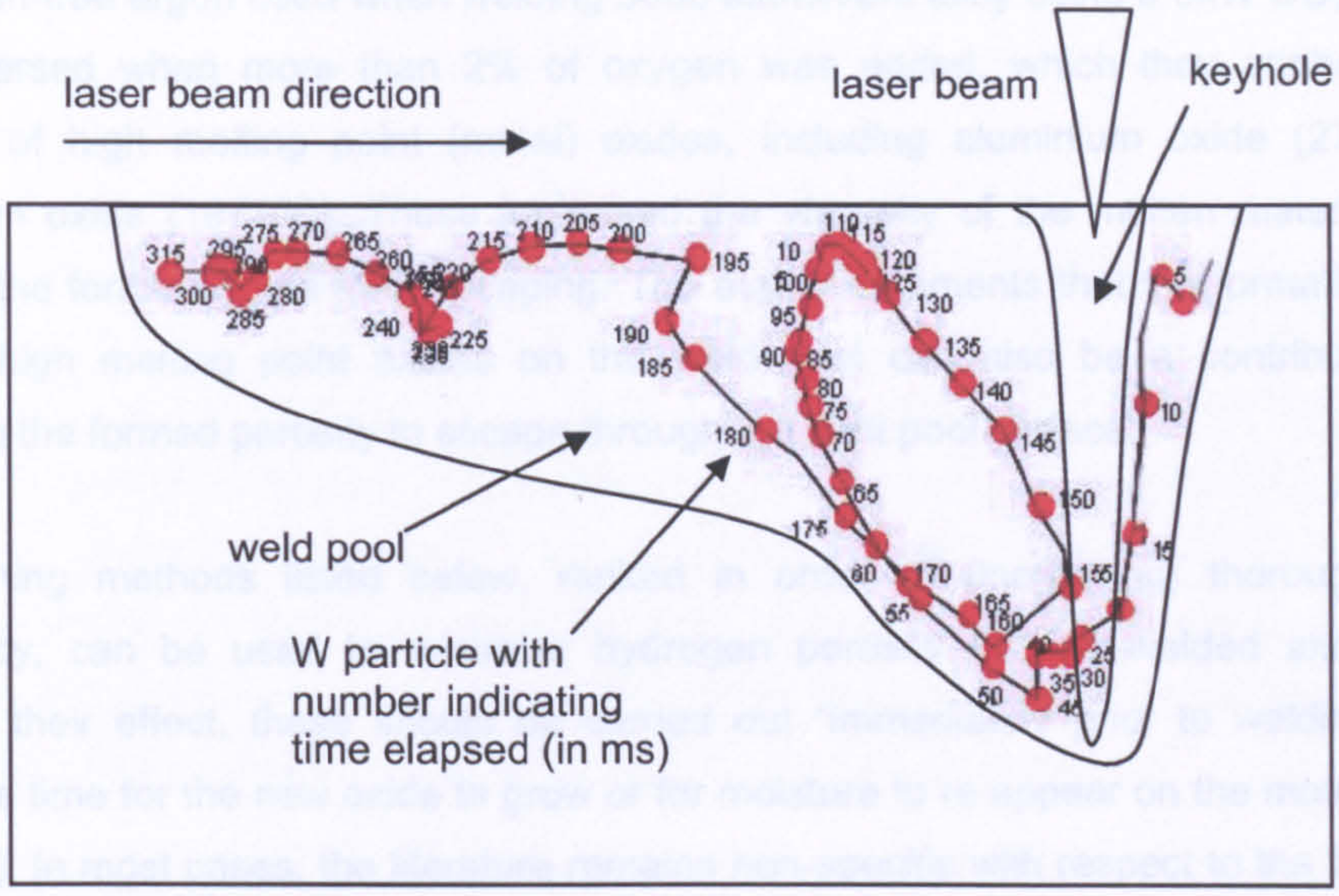

Fig.14 Movement of a pore in an aluminium laser weld visualised by welding over tungsten particles embedded in the sample, and tracked using on-line digital radiography (37)

4.6. REMEDYING POROSITY

The literature reports on various means to reduce porosity in laser-welded aluminium, with each of these addressing one, or more, of the principal causes discussed in Sections 4.4 and 4.5, i.e., hydrogen entrapment, shielding gas entrapment, volatile evaporation, plasma/plume formation and weld pool motion. Full details of each of these porosity-reduction measures are given in EngD Submission 1 (41), with a selection discussed in the following Sections. The selection includes those measures considered the most practical in application, with each of these further investigated in the experimental EngD work, detailed in Sections 5 to 7.

4.6.1. Pre-Weld Cleaning

The positive effect of pre-weld cleaning of parent material and/or filler material on reducing the level of hydrogen-induced pores in fusion-welded aluminium is widely reported in the literature (5,48,61,63,84). Laser welding is no exception in that, for either the keyhole or conduction-limited mode, cleaning can be effective in reducing the occurrence of fine porosity (27,34,49,50,53,72,82,86,92-93,109).

Although Haboudou *et al.* (72) state that the effect of cleaning, whether applied to parent or filler material or both, only extends to fine porosity and does not affect keyhole-induced porosity, the author comments that when not removed, the oxide layer influences the level of oxygen in the weld pool. Oxygen, as well as silicon and sulphur, changes the surface tension and thermal gradient of the molten material surrounding the keyhole. This affects the Marangoni (weld pool) flow, as explained in Section 4.2 (page 15) and impacts on the keyhole

behaviour. Takahashi *et al.* (34,93) describe how the total volume of both fine and coarse weld metal porosity halved when adding 0.5% oxygen to the argon shielding gas, compared with oxygen-free argon used when welding 5083 aluminium alloy using a 3kW CO_2 laser. This effect reversed when more than 2% of oxygen was added, which they attributed to the formation of high melting point (metal) oxides, including aluminium oxide (2777°C) and magnesium oxide (1977°C). These increased the viscosity of the molten material, thereby impeding the formed pores from escaping. The author comments that the formation of a film of these high melting point oxides on the weld pool can also be a contributory factor, preventing the formed porosity to escape through the melt pool surface.

The cleaning methods listed below, ranked in order of (increasing) thoroughness and consistency, can be used to minimise hydrogen porosity in laser-welded aluminium. To maximise their effect, these should be carried out "immediately prior to welding", thereby limiting the time for the new oxide to grow or for moisture to re-appear on the material surface (36,63,93). In most cases, the literature remains non-specific with respect to the time allowed between cleaning and welding to minimise the occurrence of weld metal porosity, although some refer to a maximum of four hours (61,95).

i. *Solvent degrease* – This method removes contaminants, including moisture and remnants of oil or grease, from the surface (86). Although applicable on its own, it is typically used in combination with (and following) a mechanical, chemical or laser cleaning operation (see below), with its effect maximised when carried out "immediately prior to laser welding "(86).

ii. *Mechanical cleaning* – This method removes surface contaminants, as well as the surface oxide. Katayama *et al.* (82) demonstrated the effect of different mechanical cleaning operations, including scraping, grinding and sanding (linishing) with abrasive paper, on a range of 5000 and 6000-series aluminium alloys, welded using a CO_2 laser. Pastor *et al.* (36) showed this effect to be less pronounced at higher welding speeds, because of the high cooling rates limiting the hydrogen diffusion time, i.e., the growth rate of the hydrogen bubbles. Katayama *et al.* (82) concluded that cleaning with a stainless steel brush was also effective in reducing the number of hydrogen pores, which contradicted work by Takahashi and Sato (93), who claimed that the scouring channels formed locations for water, oxygen and "other substances" to reside. The author comments that the latter is true, only if laser welding is not carried out immediately after wire-brush cleaning. For any of the mechanical cleaning operations to be effective, it is to be carried out within a "few" hours prior to welding, according to the Aluminium Association (86), and a surface layer of at least between 0.05 and 0.25mm in thickness has to be removed, according to Takahashi and Sato (93).

iii. *Chemical cleaning* – This cleaning method removes both surface contaminants and the surface oxide layer. An etching solution, such as concentrated NaOH (49,95), is applied

to the material, which reacts with and removes the surface contaminants and the hydrated oxide layer. Chemical cleaning is further also referred to as *chemical etching*. As for the mechanical cleaning, chemical cleaning is only effective in reducing the level of hydrogen porosity, when between 0.05 and 0.25mm of material is removed (93), typically within a "few" hours prior to welding (86).

iv. *Laser cleaning* – As with the mechanical and chemical cleaning operations, this method of cleaning removes both the surface contaminants and the oxide layer, through the absorption of the laser energy by these surface compounds. (72,109). Haboudou et al (72) demonstrated the use of pulsed Nd:YAG laser power for cleaning 5083 alloy prior to welding, whilst Vollertsen *et al.* (109) demonstrated the same using CO_2 laser power. In this research, the same CO_2 laser was used for both pre-weld cleaning and welding of a range of thin-section, automotive 5000 and 6000-series aluminium alloys, by diverting part of the output power ahead of the laser beam during welding.

4.6.2. Shielding Gas and its Delivery

4.6.2.1. Gas Selection

To protect the solidifying aluminium from oxidation, an inert shielding gas is applied as close as possible to the surface to be welded at a flow rate that excludes air (and moisture) from entering the weld region, as discussed in Section 4.3.1.

Helium is preferred as inert shielding gas when welding aluminium using a CO_2 laser, because of its high ionisation potential and thermal conductivity (Table 4, page 30). This results in less plasma/plume being formed and a lower plasma/plume temperature and density compared with argon, minimising its effect on keyhole stability (49,50,55,59,98). In the case of Nd:YAG laser welding of aluminium, both argon and helium can be used, with the high atomic mass of argon more effective in displacing the plasma/plume formed at the Nd:YAG wavelength (49,56), whereas helium improves process stability, because its higher heat conductivity and ionisation potential lowers the vapour pressure (98). Notwithstanding these pros and cons for both argon and helium, argon-helium mixtures are most commonly used in high-volume applications using either CO_2 or Nd:YAG lasers (49). A mixture is preferred over pure helium, because of the high cost of helium, which, per bottle is around three times more expensive than argon (Table 4 on page 30).

Katayama *et al.* (82,103) showed that, when producing partially penetrating CO_2 laser welds in 5052, 5083, 5182 and 6061 aluminium alloy, helium produced less hydrogen porosity than argon, but only when welding at speeds lower than 4.5m/min. This welding speed of 4.5m/min was also experimentally determined by Pastor *et al.* (36) for the welding of "thin-section" (automotive) 5182 and 5754 aluminium alloy. At the higher welding speeds, Takahashi et al (34) recommended the use of argon when CO_2 laser welding, because of the formation of an

argon plasma. Despite its negative impact on keyhole stability, the presence of a small amount of plasma just above the keyhole entrance offers stability at higher welding speeds, because the coupling of the laser energy with the material is improved (34). Takahashi et al (34,93) demonstrated that additions of argon of up to 40% improved the keyhole stability when CO_2 laser welding 5083 aluminium at speeds of 1.5m/min.

Nitrogen also produces lower levels of hydrogen porosity compared with argon, but increases the likelihood of undercut and produces an under-bead appearance that is more irregular compared with that achieved using argon or helium (82,75). Seto *et al.* (37) also demonstrated that nitrogen was capable of minimising the plasma/plume formation above the keyhole, thereby calming the weld pool motion, when used as shielding gas during CO_2 laser welding of 5083 and 5182 aluminium. On-line radiography of the keyhole behaviour during laser welding with nitrogen revealed a narrow keyhole with only a "small" number of pores forming at the keyhole tip. High-speed camera observations showed a plasma periodically forming above the weld pool, obstructing some of the incident laser power into the keyhole (110,111). This had a similar effect on porosity as the use of pulsed or modulated laser power, in that a gradual reduction of laser power prevented sudden collapses of the keyhole and the formation of coarse porosity at the keyhole root (112,53). Matsunawa *et al.* (53) also observed that the nitrogen reacted with the metal vapour to form aluminium nitrides. These deposited as a thin film on the metal surface, slowing down the weld pool motion and stabilising the keyhole. Seto *et al.* (37) commented that in the event of a pore forming through keyhole collapse, the nitrogen shielding gas entrapped inside formed aluminium nitrides with the entrapped vapour. These appear as metallic bubbles in the weld pool and condense inside the pool during cooling without leaving pores in the weld. Although beneficial from the point of view of porosity, the author comments that the effect of nitrides on microstructure and properties of the joint requires further investigation.

4.6.2.2. Shielding Gas Flow Rate

A minimum flow rate of inert shielding gas is required to exclude air (and moisture) from the weld region, with a maximum flow rate not to be exceeded in order to avoid turbulence at the welding point (85). Based on partial-penetration CO_2 laser welds in 5182 aluminium, Takahashi *et al.* (34) observed the highest level of porosity at an argon flow rate of 40 litre/min. The level of porosity dropped with decreasing flow rates (as low as 20 litre/min), which the authors explained by the reduction of the dynamic pressure exerted by the gas, resulting in less turbulence at the nozzle tip and thus less air entrapment. Flow rates higher than 40 litre/min, up to 50 litre/min, also resulted in lower porosity levels, which was attributed to an increased dynamic pressure of the shielding gas enlarging the keyhole entrance. This theory was not substantiated at the time, but work by Fabbro *et al.* in 2006 (108), has since demonstrated, using high-speed camera images, the potential of a gas stream jet directed towards the keyhole entrance to prevent it collapsing.

4.6.2.3. The Significance of Moisture at the Point of Use

Moisture in the shielding gas at the point of use, i.e., at the workpiece, is to be avoided, because it results in the occurrence of hydrogen-induced porosity. This was demonstrated by Pastor *et al.* (35,36) by introducing moisture in the helium shielding gas during Nd:YAG laser welding of 1.5mm thickness 5182 and 5754.

Moisture at the point of use can result from the shielding gas itself, or from the gas delivery. However, the latter is more likely because commercial shielding gases nowadays typically contain (very) low levels of moisture and impurities. Takahashi *et al.* (34) demonstrated that an inert shielding gas was *only* effective in minimising hydrogen porosity, when it contained "little" moisture at the point of use, i.e., a dewpoint of -50°C or less, and an oxygen level lower than 300ppm. Commercially available industrial grade argon has a purity of 99.99% and is supplied with a dewpoint of -60°C or less, whereas high-purity argon has a purity of 99.9995% and is supplied with a dewpoint of -70°C or less (34). These dewpoints equate to moisture contents of 10.5 and 2.5ppm, respectively (95).

Moisture can enter the shielding gas delivery system through improperly fitted connections or damaged gas lines, as condensation formed in the gas lines during extended period of non-usage, or by permeating through the gas line walls (61,86,95). Moisture ingress through the gas line walls occurs for all non-metallic gas line materials, over time, even if these are classed as non-porous (95). The preferred non-metallic gas lines materials in terms of resistance to moisture ingress are Teflon and polyethylene, with a preference for the latter because of its low oxygen permeability (95). No moisture ingress occurs through stainless steel gas lines, but because of their expense and limited flexibility, justification for use in production is often more difficult.

To avoid porosity problems caused by moisture ingress and build-up during periods of non-activity, purging the gas lines prior to welding is good practice. A purge of at least 10 to 15 minutes is recommended when TIG or MIG welding aluminium after a period of non-activity, to minimise the moisture content to "acceptable" levels (95). For laser welding, purging times of as little as a few seconds, in case of "dry gas lines" (34), to as much as one hour, in the case of high-quality aluminium welds, like for aerospace applications (95), have been reported. A non-quantified "low" level of weld metal porosity was achieved in 5182 aluminium welded using a CO_2 laser after purging for one minute using industrial grade shielding gas. By purging the gas lines for at least 20 seconds, compared with between 0 and 5 seconds, the occurrence of 0.5mm diameter pores (and smaller) was suppressed in partial penetration CO_2 laser welds in 5052, 5083, 5182 and 6061 (82).

Based on the author's work, described here in Section 5, further work at TWI has since shown that it is the (dry) condition of the shielding gas delivery and the purging time in particular,

rather than the moisture content of the shielding gas itself, that ensure low-porosity laser welds in aluminium (130-131). Porosity levels in accordance with two international standards were achieved in 3.2mm thickness aluminium, when the level of moisture at the point of use was 20ppm or below. This was accomplished by purging the lines with shielding gas prior to welding, for up to 30 minutes in some cases. It was also shown that moisture levels increased from 20ppm to between 140 and 170ppm, irrespective of initial shielding gas moisture content, within 2 hours of non-activity (130-131). Based on these results, the author comments that the exact purge time depends on a variety of factors including dewpoint (and purity) of the gas, the material and condition of the gas lines, the environmental conditions and time of non-activity. No consensus exists in the literature on the purge times to be used when laser welding aluminium, with *trial-and-error* methods being used in most cases. To reduce the number of trials, the author suggests the use of a moisture meter, which measures the dewpoint at the point of use, i.e., at the workpiece. Look-up tables can be acquired from gas companies to cross-reference the measured dewpoint to the level of moisture.

Although the moisture in the shielding gas at the point of use affects the occurrence of hydrogen-induced porosity, Pastor *et al.* (35,36) reported that it did not affect the occurrence of keyhole-induced porosity. The introduction of moisture in helium shielding gas during Nd:YAG laser welding of 1.5mm thickness 5182 and 5754 increased the level of porosity, but was not considered significant compared with the coarse porosity found in the welds when welding at speeds faster than 3.5m/min (35,36). According to Pastor *et al.* (35,36), coarse porosity was not the result of moisture in the shielding gas, but of instabilities of the keyhole during laser welding, as discussed in Section 4.5.2.

4.6.3. Controlling Heat Input

The level of porosity in laser-welded aluminium varies with the heat input, which is determined by the welding speed and laser power. Welding speed and laser power influence the level of both hydrogen and keyhole porosity, as follows.

Both a low welding speed and a high welding speed can result in a lower level of fine porosity. Seto *et al.* (37) report that if the welding speed is below that of the hydrogen pore velocity in the weld pool, as determined by real-time radiography of a CO_2 laser keyhole in 5083 and 5182 alloy, there is sufficient time for the pores to float up and escape the weld pool surface prior to it solidifying (86). Vollertsen and Thomy (114) used a welding speed of 8m/min for fully penetrating an aluminium extrusion wall thickness of 4mm using a 10kW Yb-fibre laser. This speed was lower than the maximum welding speed of 20m/min capable of full penetration, and selected to avoid, or at least minimise, the occurrence of fine porosity. If laser welding is carried out at a high welding speed, the cooling rate increases, which reduces the time available for hydrogen pores to nucleate and grow to a significant size (72,82,85).

Real-time radiography and high-speed video taken by Seto *et al.* (37) when producing partial penetration welds in 5083 and 5182 aluminium using a CO_2 laser, revealed that as the welding speed increased from 1.5 to 4.5m/min, the keyhole reduced in both width and depth. The keyhole became unstable, resulting in a non-uniform penetration and an increase in the level of porosity, resulting from bubbles getting entrapped in the solidifying weld pool because of the higher speed and cooling rate (37). At speeds higher than 4.5m/min, for a given laser power, the keyhole disappeared and welding continued in the conduction-limited mode. This resulted in shallow penetration welds with a low level of porosity, as confirmed by Pastor *et al.* (36). The author comments that, in the absence of a keyhole, these would have been hydrogen pores, small in both size and number, because of the high cooling rate during laser welding. Seto *et al.* (37) also observed that particularly at the speeds between keyhole and conduction-limited welding, the keyhole became unstable, with coarse porosity as result.

For low laser powers, the penetration is shallow and the welds small. The shallower the weld, the less time required for the formed bubbles to float up to the surface (86). Takahashi and Sato (93) observed no coarse porosity in partial penetration CO_2 laser welds in 5083 and 5182 aluminium alloy that were shallower than 4.5mm. Work by Katayama *et al.* (82) revealed low levels of porosity in CO_2 laser welds in 5052, 5083, 5182 and 6061 aluminium when the penetration was less than 3.0mm. In contrast, as the laser power is increased, the weld pool deepens, giving less time for gas pores to float up to the surface (34).

As the laser power is increased, the power density increases for a given laser spot size. This results in a higher rate of evaporation, which increases likelihood of keyhole instabilities (37,93). Whereas a certain power density is required to initiate and maintain the keyhole during laser welding (Section 4.2, page 17), the stability of the keyhole also depends on the value of the available power density above this threshold (26,36). Yoshida *et al.* (115) observed that during the CO_2 laser welding of steel, the level of porosity increased as the laser power was raised. Variations in the metal vapour pressure and the molten metal flow (through the material thickness) associated with the increase in laser power, were considered the main causes of this porosity. Takahashi and Sato (93) observed coarse pores, larger than 1mm in diameter, when producing both full and partial penetration welds in 6mm thickness 5083 alloy using 4kW of CO_2 laser power, which resulted from keyhole instabilities. Their level increased as the keyhole deepened, which was attributed to the higher laser power used and the higher vapour pressure associated with this. Coarse porosity was not observed when producing fully penetrating welds using 3kW of power (93). However, the author comments that, in addition to the lower laser power used, the welding speed would also have been lower to achieve full penetration in the 6mm thickness 5083 aluminium alloy. The lower welding speed reduces the risk of keyhole instabilities occurring, as explained in Section 4.6.3.

4.6.4. Selecting the Laser Spot Size

When the laser spot diameter is changed, the power density will change accordingly, for a given laser power. The above comments, in Section 4.6.3, related to the effect of power density on keyhole stability when changing the laser power, are also applicable for a change in laser spot (for a given laser power), in that the keyhole becomes more unstable as the laser spot diameter is reduced (increased power density). This is the case for both steel (115) and aluminium (26,36).

High-speed video of the laser keyhole during Nd:YAG laser welding of 3.2mm thickness 2024 aluminium, revealed keyhole fluctuations faster than a camera with a frame rate of 7200 per second could record (98). Although not quantified, the keyhole fluctuations were more pronounced when using a 0.45mm spot size, compared with a 0.6mm spot size. Hu and Richardson (98) concluded that this resulted from the higher surface tension forces produced by the smaller keyhole radius. However, the author comments that the increased power density (because of the smaller spot size) also increases the vapour pressure inside the keyhole, which counteracts this higher tension force. In turn, the higher vapour pressure results in more intense local evaporations and a more violent motion of the molten pool, both of which impact negatively on the stability of the keyhole. This theory is supported by high-speed video evidence from the weld pool motion recorded by Hu and Richardson (98). The author also remarks that the smaller the keyhole, the easier it is for the front, back or sidewalls of the keyhole to touch, with the shape and position of the keyhole capillary continuously varying because of localised evaporation of the material.

4.6.5. Defocusing the Beam

Defocusing refers to the positioning of the laser beam spot above or below the material surface. For the purpose of this review, a negative defocus refers to a laser beam focused below the material surface. Defocusing results in a reduction in power density at the material surface. As the defocus increases, the keyhole becomes unstable and disappears.

Pastor *et al.* (35,36) observed keyhole instabilities during Nd:YAG laser welding of 5182 and 5754 alloys, when positioning the focus lower than –1mm and higher than +0.5mm. Keyhole welding changed to conduction-limited welding for a defocus larger than –1.75mm and +1.5mm, with the level of porosity lowest for the conduction-limited welds, "low" in case of stable keyhole conditions and highest when the keyhole became unstable. A relatively higher level of porosity was observed in those welds produced with a negative defocus (up to –1mm) compared with those produced with a positive defocus (up to +0.5mm). Pastor *et al.* (35,36) concluded this to be the result of an increased depth of penetration in case of a negative defocus, formed through the higher power density available at the depressed weld pool. The same observation of a higher level of porosity resulting from a negative defocus was made by

Kim *et al.* (116) when Nd:YAG spot welded 6061 aluminium, and by Haboudou *et al.* (72) when producing partially penetrating Nd:YAG laser welds in 5083 aluminium, who contributed a lower level of porosity for a positive defocus to the widening of the weld. The author comments that, in addition to this, the negative defocus creates a higher vapour pressure, and vapour temperature, which increases the occurrence of coarse porosity. Takahashi *et al.* (34) reported the same observations, but only when using helium as shielding gas, with the opposite true in case of argon. The earlier mentioned studies by Pastor *et al.* (35,36), Kim *et al.* (116) and Haboudou *et al.* (72) all reported on welds produced with an Nd:YAG laser, and using helium as shielding gas. The opposite was reported by Takahashi *et al.* (34), who used a CO_2 laser to weld 5182 aluminium and argon as shielding gas, and contributed to the formation of a plasma above the weld pool, absorbing part of the incident laser energy, thereby increasing the likelihood of keyhole instabilities (see Section 4.6.2).

4.6.6. Enlarging the Keyhole

A small keyhole is more prone to collapse than a large keyhole (Section 4.6.4). Enlarging the keyhole is therefore a means of reducing the level of keyhole-induced porosity, and can be achieved, for instance, by a twin-spot optic, or the hybrid laser-arc process.

Having two beam foci working in the same weld pool, elongates and stabilises the keyhole, and improves the weld quality, as demonstrated for laser welding by Haboudou *et al.* (72) and Xie (117) for the laser welding of aluminium. The technique particularly affects the occurrence of keyhole-induced porosity, although the level of gas-induced porosity is also affected, because of the slower cooling rate associated with the technique, which increases the time available for formed bubbles to escape the solidifying weld pool (26,27,92). The technique can be applied by using two separate laser beams, or, more common in practice, by using a twin-spot laser welding optic separating a single laser beam into two separate foci. Commercially available twin-spot optics allow spot separation, power density per spot and spot orientation (with respect to the weld direction) to be altered.

By enlarging the keyhole, the surface tension force reduces (because of the larger radius) which facilitates the keyhole to stay open (72), improving its stability and the outflow of metal vapour (27,53,92), as confirmed by high-speed video images taken by Sakamoto *et al.* (118) during the CO_2 laser welding of steel. However, by splitting the laser power into two separate foci, the depth of penetration, for a given welding speed, reduces compared with a single-spot laser weld using the same power. As discussed in Section 4.6.3, the level of porosity decreases with decreasing weld depth. Therefore, to achieve a given depth of penetration with the twin-spot technique, the welding speed needs to be lowered compared with the single-spot technique. Again, as discussed in Section 4.6.3, the slower the welding speed, the lower the cooling rate and the longer the time available for formed bubbles to escape the solidifying weld pool. The author comments that the effect of a twin-spot technique on the

level of weld metal porosity in laser-welded aluminium is therefore difficult to dissociate from the effect of weld depth on weld metal porosity and from that of welding speed. For instance, Haboudou *et al.* (72) reported only half the volume of pores in partial penetration welds in 5083 aluminium alloy produced with the twin-spot technique compared with single-spot laser welding. The welds were produced using an Nd:YAG laser and at the same welding speed of 5m/min. This raises the question if the reduction in porosity was the result of the twin-spot technique or by the reduction in penetration. Haboudou *et al.* (72) also reported a six-fold reduction in porosity by increasing the spot separation from 0.3 to 0.9mm, with each of the laser foci 0.45mm in diameter (72). However, the author comments that the onset of conduction-limited welding is more likely for the larger process separation, with conduction-limited welds exhibiting lower levels of porosity, compared with keyhole laser welds. This could not be confirmed, as no cross-sections were provided in the publication by Haboudou *et al.* (72).

In a similar way, the weld pool can be enlarged by focusing a laser beam and an electric arc in the same weld pool. This stabilises the keyhole, reducing the tendency for keyhole instabilities to occur when laser welding aluminium (119-123). For more information on hybrid laser-arc welding, the reader is referred to the literature, including (119) to (122), and the author's own work (123).

5. THIN-SECTION TRIALS

Trials were carried out to assess the effect of parent and filler material cleaning prior to welding, the use of a twin-spot laser energy distribution (compared with single-spot) and the moisture content in shielding gas and its delivery system, on the presence of fine porosity in Nd:YAG laser-welded 3.2mm thickness 2024 AlCuMg aluminium alloy. The alloy was selected because of its common use for fuselage skin and lower wing structures (49), and its thickness in line with current fuselage structures, comprising aluminium sheet typically between 2 and 3mm in thickness. The European standard BS EN 13919-2, related to the laser welding of aluminium, and the American standard AWS D17.1, related to fusion welding of aerospace materials, were used as benchmark weld quality comparators for this application. Full details of the thin-section welding trials and the results are given in EngD Submission 2 (42).

5.1. MATERIAL

The thin-section trials were carried out on 2024 aluminium alloy, of which the nominal composition is given in Table 1 (page 12). This heat-treatable AlCuMg alloy was selected because of its frequent use for high-strength structural applications in airframe manufacture (48,65). The material used was 3.2mm in thickness and supplied in the T3-temper condition, i.e., solution heat-treated, cold worked and naturally aged. A limited number of trials were also carried out on 3.2mm thickness 6056 aluminium alloy (Table 1), because this heat-treatable AlSi1MgCuMn material is one of the alloys currently considered by the aerospace industry sector to replace the more conventional, but less weldable, 2024 aluminium alloy for structural airframe applications (Section 4.1). The material was cold band-sawn to 150mm wide by between 250 and 400mm long samples. A minimum of 0.25mm was subsequently (dry) machined off the long edges using a single-cut edge, high-speed steel cutting tool, to ensure a zero joint gap along the weld length. In addition to this *primary cleaning operation*, carried out upon receipt of the material, the material was subjected to a *secondary cleaning operation,* which was carried out immediately prior to welding. Details of the *secondary cleaning operation* are given further in Section 5.4.

5.2. EQUIPMENT

All thin-section welding trials were carried out using one of two LP Nd:YAG lasers. At the onset of the trials, a 4kW *prototype* LP Nd:YAG laser was used, transmitting its power through a 600µm diameter, single optical fibre into a processing head equipped with an optical lens combination producing a 0.6mm diameter spot size. During the experimental programme, this laser was replaced with a commercially available 3kW system, which was used with an identical set-up, except for a processing head focusing the beam into a 0.45mm spot diameter and capable of producing both a single-spot and a twin-spot laser energy distribution. At the same output power of up to 3kW, and same spot diameter, no difference in performance was observed between the two lasers, as determined experimentally (42).

5.3. EXPERIMENTAL SET-UP

All thin-section trials were carried out with the laser focused on the material surface, unless otherwise stated, using the maximum output power of the laser. This was 3.1kW for the 4kW beta-site and 2.85kW for the commercial 3kW LP Nd:YAG laser, as measured at the workpiece using an OPHIR power meter, which is a calorimetric device. Further in this document, unless otherwise stated, when laser power is mentioned, this refers to the laser power as measured at the workpiece, i.e., the actual laser power used for welding.

The protection of the processing head, clamping of the samples, set-up of the filler wire and set-up of the top and under-bead shielding, were based on the author's own (124) and TWI's past experience (12,49) when laser welding aluminium, as detailed below.

- For all welds, an optical glass cover slide was used in combination with an airknife to reduce the risk of smoke and/or spatter damaging the focussing optics.

- All thin-section welding trials were carried out in the flat (PA) position by moving the processing head, mounted on a 6-axis articulated robot arm, over the stationary workpiece. The samples were mounted in a sandwich-type jig, as shown in Fig.15 and Fig.16, comprising steel top clamping bars and a heavy-section steel backing plate with a copper insert, in which a 10mm deep slot was machined to shield the underside of the weld bead. The samples were clamped as close to the weld line as possible to avoid problems with sample misalignment and weld distortion, without compromising the joint access.

- A 1.2mm diameter 2319 (Table 3) filler wire was introduced into the leading edge of the weld pool, between 1.0 and 1.5mm ahead of the laser-workpiece impingement point, through a Planetics Saturn 501 wire feed unit at an angle of between 35 and 50° with the horizontal. This filler wire was selected, in line with recommendations from the Aluminium Association (48), as it provides high weld strength and ductility after heat treatment.

- Industrial grade helium was used to shield both top and underside of the weld (125). The top-bead shielding was delivered from a gas cylinder, through 2m long, 4mm ID polyurethane tubing, to a coaxial, Fig.15, or a side-jet shielding nozzle, Fig.16.

Both these arrangements are common practice when laser welding, as discussed in Section 4.3.1. The 20mm exit diameter of the coaxial shielding nozzle was positioned 10mm above the workpiece, whereas the 10mm exit diameter of the side-jet nozzle was positioned behind the laser at an angle of 30° to the laser axis and an axial stand-off distance of 15mm with the workpiece. The under-bead shielding was supplied through a 10mm deep channel in the jigging arrangement. The flow rates were set to give oxidation-free welds, determined visually, at 30 litres/min for the top-bead and 5 litre/min for the under-bead shielding. The shielding gas

line was purged for at least five seconds prior to each weld and for at least two minutes when welding had been interrupted for longer than 1 hour. Additional trials were carried out with a higher purity, lower dewpoint helium and nitrogen, and using different gas line lengths and purging times (see Section 5.6.6).

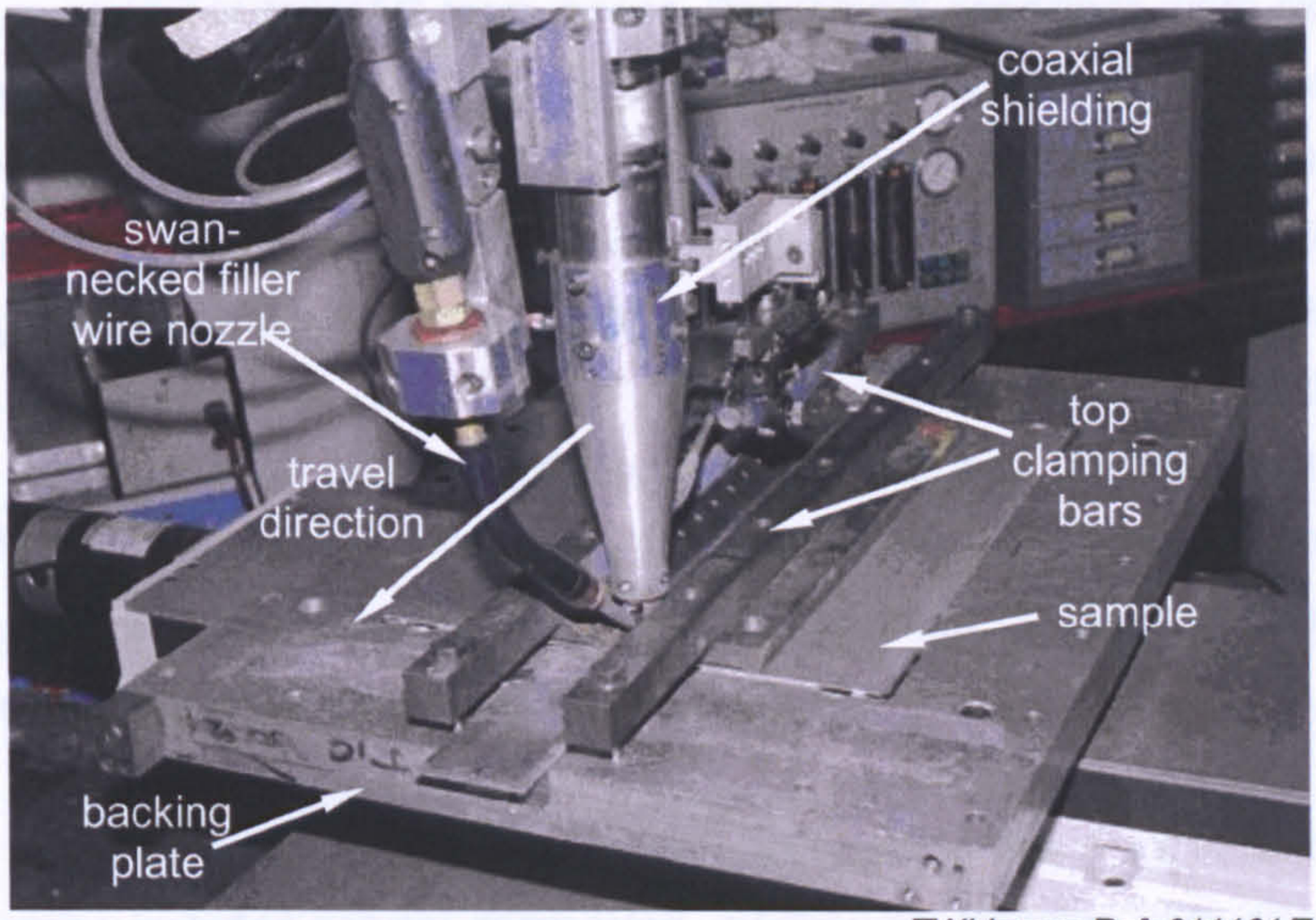

TWI Image Ref: 011161/7

Fig.15 Thin-section welding set-up including coaxial shielding nozzle, wire feed and jigging arrangement

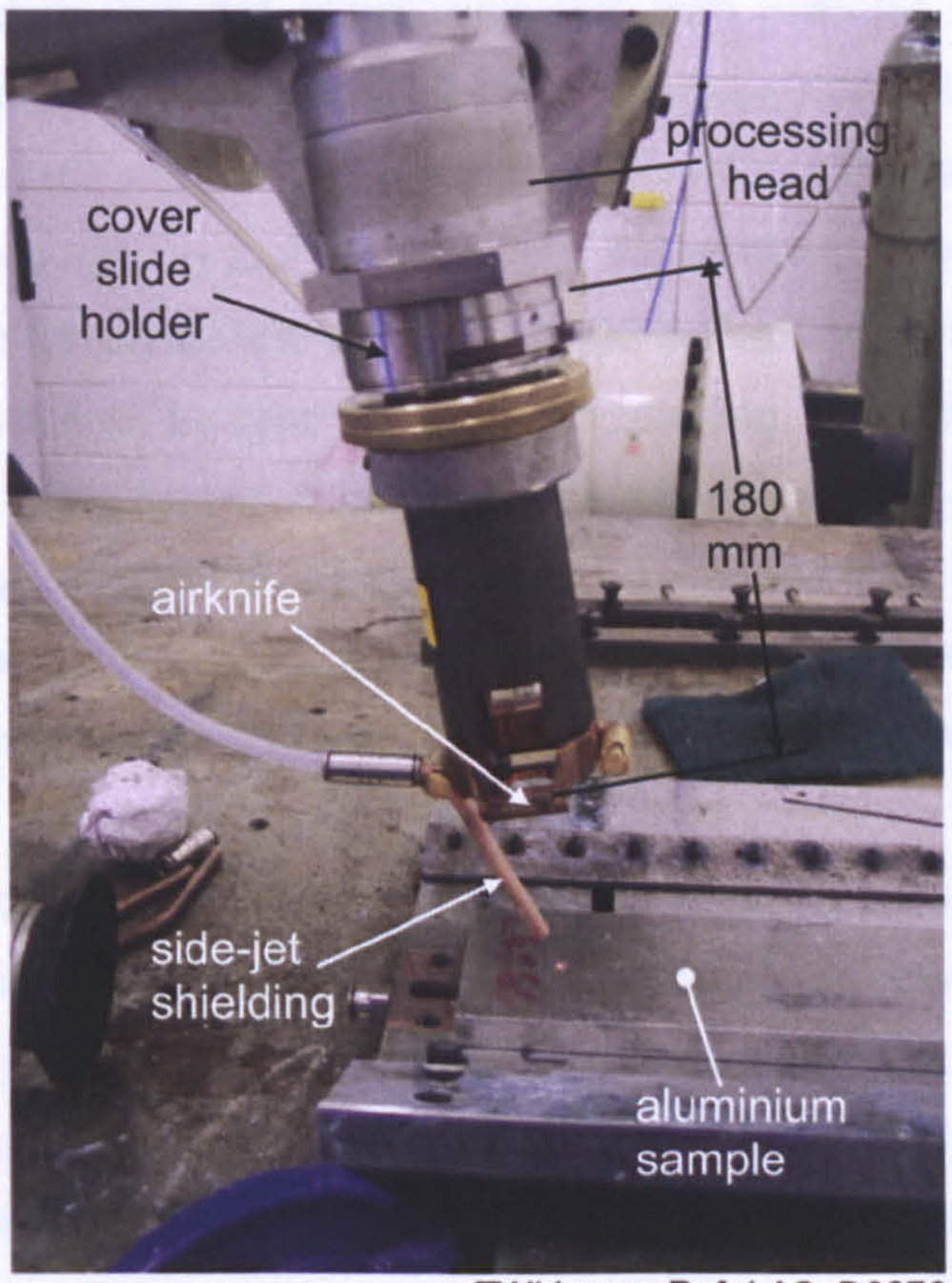

TWI Image Ref: LAS_D0376

Fig.16 Processing head, angled 10° from the vertical, with air knife and side-jet shielding

5.4. SCOPE OF WORK

Initial welds were produced using a range of conditions of welding speed, wire feed speed (WFS) and laser focus position, to ascertain if fully penetrating, crack-free welds with acceptable visual weld bead appearance could be produced in 3.2mm thickness 2024 alloy using the maximum available Nd:YAG laser power. Benchmark conditions were established from these, with welding speeds selected as high as possible to minimise the thermal damage caused by laser welding (Section 4.3.2), with further work then aimed at assessing the effects of (secondary) parent material cleaning, filler wire cleaning, laser beam energy distribution and gas shielding conditions on the presence of weld metal porosity. Particular attention in these trials was on reducing the occurrence of hydrogen-induced porosity, with the above factors selected based on their reported influence on fine porosity, as described in EngD Submission 1 (41) and summarised in Section 4.6. The effect of spot size on the presence of fine porosity was also assessed, but not the effect of heat input or defocusing because of potential problems with back-reflection (Section 4.2, page 14).

The (secondary) parent material cleaning operations assessed in this work in terms of their effect on fine porosity, included solvent degreasing, mechanical cleaning (including linishing, abrading, scraping and dry-machining) and chemical etching, as described in Section 4.6.1. The mechanical and chemical cleaning operations were followed by a solvent degreasing immediately prior to welding. Solvent degreasing was with acetone applied with a lint-free cloth, linishing using a belt sander with a P120 grit-size silicon carbide paper, abrading using a ScotchBrite® abrasive pad, and scraping and dry-machining using a single-cut edge, high-strength steel scraping and cutting tool, respectively. All cleaning operations were applied to the long sample edges to be joined and to both top and bottom surface of the samples, up to 10mm away from the joint line. In case of the dry-machining and chemi-etching, it was not always possible to clean the samples immediately before welding, as multiple samples were prepared simultaneously. To avoid contamination and moisture pick-up between dry-machining / chemi-etching and welding, the samples were stored in a desiccating cabinet. If welding could not be carried out within 48 hours, the sample cleaning was repeated.

To determine the effect of the filler wire, and contaminants on its surface in particular, on the occurrence of fine porosity, a series of welds was completed using filler wire that was subjected to an abrading or a chemi-etching cleaning operation prior to welding. Some laser welds were also produced without filler wire, although this would not be used in practice, as metallurgically such a weld would be prone to cracking. The filler wire cleaning was carried out immediately prior to welding and in the same way as described (above) for the parent material.

To investigate the effect of moisture content in the shielding gas and its delivery on the presence of weld metal porosity, laser welds were produced using high-*grade* helium. This

differed from industrial-grade helium in that it was 99.9995% pure (instead of 99.999%), with a moisture and oxygen content, as quoted by the supplier, five and two times lower, respectively, i.e., nominally 1ppm instead of 5ppm moisture and 0.5ppm instead of 1ppm oxygen. The high-grade helium was fed through a *dry* shielding gas delivery system, developed by the author based on recommendations from the literature (Section 4.6.2). This comprised the shortest polyurethane tubing length possible, i.e., 1.5m, between gas cylinder and shielding nozzle, and a gas line that was acclimatised to laboratory conditions for several hours prior to welding to avoid formation of condensation in the tubing. All welding trials using this high-grade helium and dry shielding delivery were carried out subsequently, without interruptions of more than one hour, and after purging the gas delivery system for at least two minutes with 30 litres/min of high-grade helium prior to each weld. This is more than 3150 times the volumetric capacity of the 1.5m long, 4mm ID gas lines used.

To investigate the influence of a twin-spot energy profile on the presence of fine porosity, welds were completed using a twin-spot laser energy profile with a 0.27mm spot separation and a 50/50 laser energy distribution. The spot separation and energy distribution were selected based on earlier work at TWI, demonstrating low levels of fine porosity in partially penetrating bead-on-plate runs in 2024 aluminium (126).

5.5. WELD ANALYSIS

All thin-section welds produced were inspected visually for external imperfections, such as surface breaking porosity and undercut, in accordance with BS EN 13919-2 (38). Metallographic sections were taken from representative welds in accordance with BS EN 1321 (127,128), transverse to the weld at positions with a weld bead appearance representative of the entire weld length. Following grinding and polishing, the sections were etched with a Keller's reagent, an aqueous solution of 1vol% HF, 1.5%vol HCl and 2.5 vol% HNO_3, to reveal the weld bead shape and HAZ. Radiographic examination as per BS EN 1435 (127,129) was used to confirm the internal quality of the welds. This included checking for cracks in the weld metal and HAZ. It is noteworthy that the sensitivity of this technique did not allow detection of micro-cracks in the HAZ.

Particular attention in this work (as in the thick-section trials in Section 7) was on achieving an acceptable level of weld metal porosity, with analysis of the welds mainly restricted to the results of a visual inspection and radiographic examination, including pore counting, as detailed below. The limited cross-sections that were taken as part of these trials did not reveal micro-cracking. However, given the levels of weldability associated with the types of aluminium alloys used in this work, the author recommends that additional testing, including fatigue and crack-growth testing, is carried out before applying the procedures developed here in a production application, to ensure full fitness-for-purpose of the welded joints.

A pore count was carried out from the radiographs to quantify the level of fine porosity. To minimise discrepancies, a single operator carried out all pore counts. A magnifying glass (magnification x10) with graticule was used to measure the pores sizes in a 100mm representative section of the weld, i.e., how many pores were found in this section to be of a diameter between 0 and 0.1mm, how many of a diameter between 0.1 and 0.2, etc. The measured levels were compared with those specified for the *stringent* weld quality class in BS EN 13919-2 (38) and AWS D17.1:2001 (39). BS EN 13919-2 was selected because the standard deals with the laser welding of aluminium and AWS D17.1 because it is specific to fusion welding for aerospace applications. A third (confidential) standard, ABP 2-4102 (40), which is specific to laser welding of aluminium and currently in use in the UK aerospace industry, was also used. The values in Table 5, Table 6 and Table 7 summarise the three acceptance criteria for weld metal porosity that need to be fulfilled to achieve a given weld quality category, i.e., *moderate*, *intermediate* or *stringent*, in accordance with BS EN 13919, AWS D17.1 and ABP 2-4102.

Table 5 Limits for porosity-related weld imperfections for the stringent, intermediate and moderate weld quality class, as defined in EN 13919-2 (38)

Limits for porosity-related weld imperfections per weld quality class, as defined in BS EN 13919-2		CRITERION 1 *Maximum dimension of a single pore*, mm			CRITERION 2 *Minimum distance between individual pores*, mm			CRITERION 3 *Maximum value for the total projected pore area*, mm^2		
		limit†	thin limit ⋕	thick limit ☼	limit †	thin limit ⋕	thick limit ☼	limit†	thin limit ⋕	thick limit ☼
porosity and gas pores	stringent	<0.3*T	1.0	2.4	-	-	-	<3%◊	9.6	24
	intermediate	<0.4*T	1.3	3.2	-	-	-	<6%◊	19.2	48
	moderate	<0.5*T	1.6	4.0	-	-	-	<10%◊	38.4	96
localised (clustered & linear) porosity	stringent	<0.3*T	1.0	2.4	<½T	1.6	1.6	<2%◊	6.4	16
	intermediate	<0.4*T	1.3	3.2	<½T	1.6	1.6	<5%◊	16	40
	moderate	<0.5*T	1.6	4.0	<¼T	0.8	0.8	<15%◊	48	120

† limit as specified in BS EN 13919-2 for a 100mm weld length
⋕ limit calculated for a thickness T of 3.2mm, i.e., the thickness of samples used in the thin-section trials
☼ limit calculated for a thickness T of 8mm, i.e., the thickness of samples used in the thick-section trials
◊ as a percentage of the weld area for a 100mm long section of weld

These criteria relate to the diameter of the largest pore (criterion 1), the minimum distance between adjacent pores (criterion 2) and the projected pore area, for BS EN 13919, or pore length, for AWS D17.1 and ABP 2-4102, per given area and length of weld, respectively (criterion 3). The percentage values for projected pore area, i.e., criterion 3 of BS EN 13919 (Table 5), are in relation to a 100mm long weld. For the total pore lengths, i.e., criterion 3 of AWS D17.1 (Table 6) and ABP 2-4102 (Table 7), the pore numbers that were counted for a 100mm long section of weld, were proportionally reduced to the equivalent pore length for a 76mm (3") and 50mm length of weld length, as defined in AWS D17.1 and ABP 2-4102,

respectively. These are further referred to as the *normalised pore area* and *normalised pore lengths*. All thin-section welds produced, passed the second criterion (*minimum distance between adjacent pores*), with all the pores isolated and randomly distributed along the weld length. For that reason, only the first and third criteria, i.e., maximum (single) pore diameter and projected pore area / maximum pore length, are discussed further.

Table 6 Limits for porosity-related weld imperfections for the stringent, intermediate and moderate weld quality class, as defined by AWS D17.1 (39)

Limits for porosity-related weld imperfections per weld quality class, as defined in AWS D17.1		CRITERION 1 *Maximum dimension of a single pore,* mm			CRITERION 2 (*pore distance*, mm)	CRITERION 3 *Maximum value for the total projected pore length,* mm		
		limit†	thin limit‡	thick limit☼	limit†	limit†	thin limit‡	thick limit☼
Sub-surface porosity	stringent	<0.33*T or <1.5	1.1	1.5	<4*Ø◊	<1.33*T or <6	4.3	7.9
	intermediate	<0.5*T or <2.3	1.6	2.3	<2*Ø◊	<2*T or <9	6.4	11.8
	moderate	-	-	-	-	-		-
Surface-breaking porosity	stringent	<0.25*T or <0.76	0.76	0.76	<8*Ø◊	<1*T or <3	3.2	3.9
	intermediate	<0.33*T or <1.5	1.1	1.5	<4*Ø◊	<1.33*T or <6	4.3	7.9
	moderate	<0.5*T or <2.8	1.6	2.8	<2*Ø◊	<2*T or <9	6.4	11.8

† limit as specified in AWS D17.1 for a 76mm (3") weld length
‡ limit calculated for a thickness T of 3.2mm, i.e., the thickness of samples used in the thin-section trials, and proportionally increased from 76mm (3") to 100mm
☼ limit calculated for a thickness T of 8mm, i.e., the thickness of samples used in the thick-section trials, and proportionally increased from 76mm (3") to 100mm
◊ largest pore diameter

Table 7 Limits for porosity-related weld imperfections, as defined ABP 2-4102 (38)

Maximum diameter (D) of pores	0.8mm	Randomly dispersed, isolated pores are acceptable, provided that they appear round bottomed and their depth does not exceed their diameter.
Number of max. diameter pores	6	A large number of smaller diameter pores are acceptable, provided that the spacing ration is maintained and the total area does not exceed the equivalent standard.
Minimum distance between max. diameter pores	10xD	The sum of the diameter of all pores in any length of weld shall not exceed 6.0mm.

5.6. RESULTS AND DISCUSSION

5.6.1. Establishing Process Conditions

A series of welds was produced under various conditions of welding speed, wire feed speed and focus. The results demonstrated that a welding speed of between 1.25 and 1.6m/min produced full penetration in 3.2mm thickness 2024 aluminium alloy using 3.1kW of Nd:YAG laser power. Combined with a wire feed speed (WFS) of 1.25m/min, top and under-bead weld profiles were acceptable, visually, in accordance with the stringent quality class of standard BS EN 13919-2. This weld quality was achieved with the beam focus positioned on or 1mm below the material surface. The top and under-bead appearances of such a weld produced using 3.1kW of laser power at a speed of 1.4m/min and a defocus of -1mm is given in Fig.17.

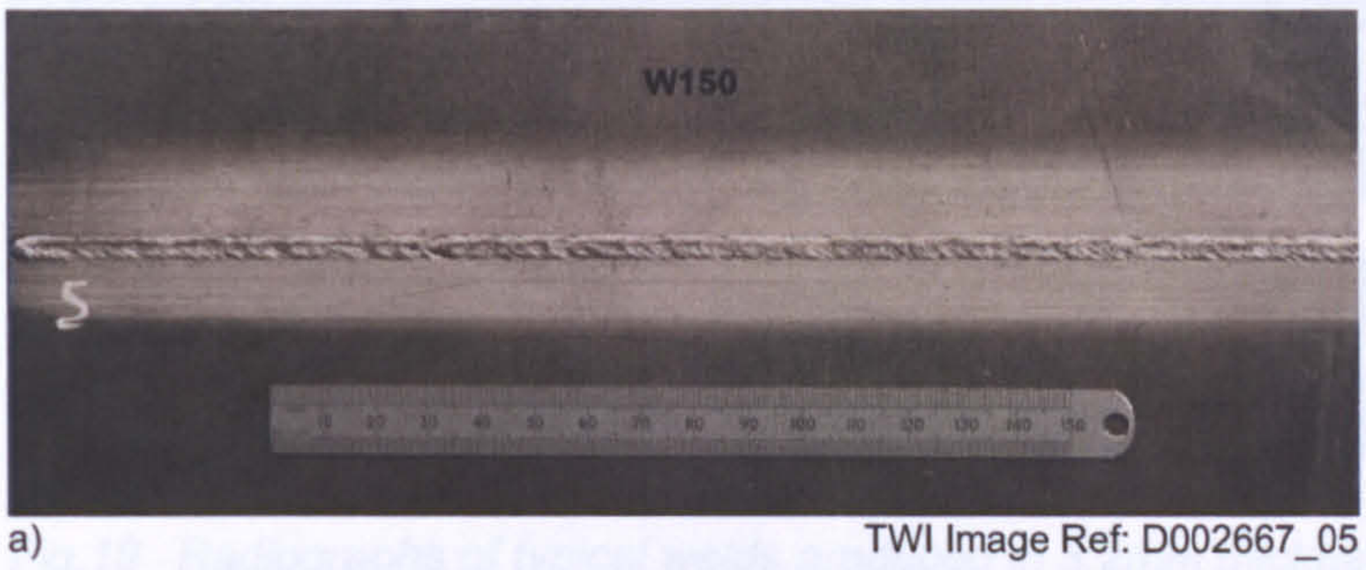

a) TWI Image Ref: D002667_05 b) TWI Image Ref: D002667_11

c) TWI Image Ref: D002667_06 d) TWI Image Ref: D002667_12

Fig.17 A typical weld produced in 3.2mm thickness 2024 alloy, using 3.1kW of laser power, Ø0.6mm laser spot, defocus -1mm, welding speed 1.4m/min, WFS 1.25m/min:

a) weld top-bead profile
b) detail of weld top-bead profile
c) weld under-bead profile
d) detail of weld under-bead profile

Defocusing the laser further (below the material surface) resulted in intermittent penetration and loss of penetration for a defocus of -2mm and -3mm, respectively. This change in penetration was attributed to the reduction in power density when defocusing, increasing the likelihood of keyhole instability and resulting coarse porosity / cavities (Section 4.6.5). The power density at focus used here, with 3.1kW of laser power focused into a 0.6mm spot, was 1.1×10^6 W/cm^2, which is below the (alloy-dependent) threshold power density required to initiate keyhole welding when using an Nd:YAG laser (Section 4.2, page 17). When defocusing 1mm below the material surface, the spot size at the material surface increases to 0.85mm, i.e., an increase of 42%, which reduces the laser energy density by a factor of two. A focus position 2mm and 3mm below the material surface equals a laser energy density 3.3 and 5 times lower than the value at focus.

Despite the acceptable visual appearance and the absence of (macro) cracks, a significant number of coarse pores were observed in these welds, as shown by the radiograph in Fig.18a. These pores were all round in shape, denoting the presence of a gas, i.e., hydrogen, shielding gas and/or oxygen or nitrogen (from air entrapment) (Section 4.3.4). Analysis of the pore content was not carried out, but the size of the porosity observed, i.e., as large as half the material thickness, i.e., 1.6mm, indicates shielding gas entrapment rather than pores formed through diffusion of hydrogen (Section 4.4, page 23). The author remarks that shielding gas entrapment can occur after a keyhole instability, potentially caused by evaporation of Mg, of which between 1.2 and 1.8% of Mg is present in the 2024 alloy (Table 1). However, welds carried out on samples that were abraded prior to welding, see Section 5.4, revealed no coarse porosity, with the radiograph of such a weld shown in Fig.18b.

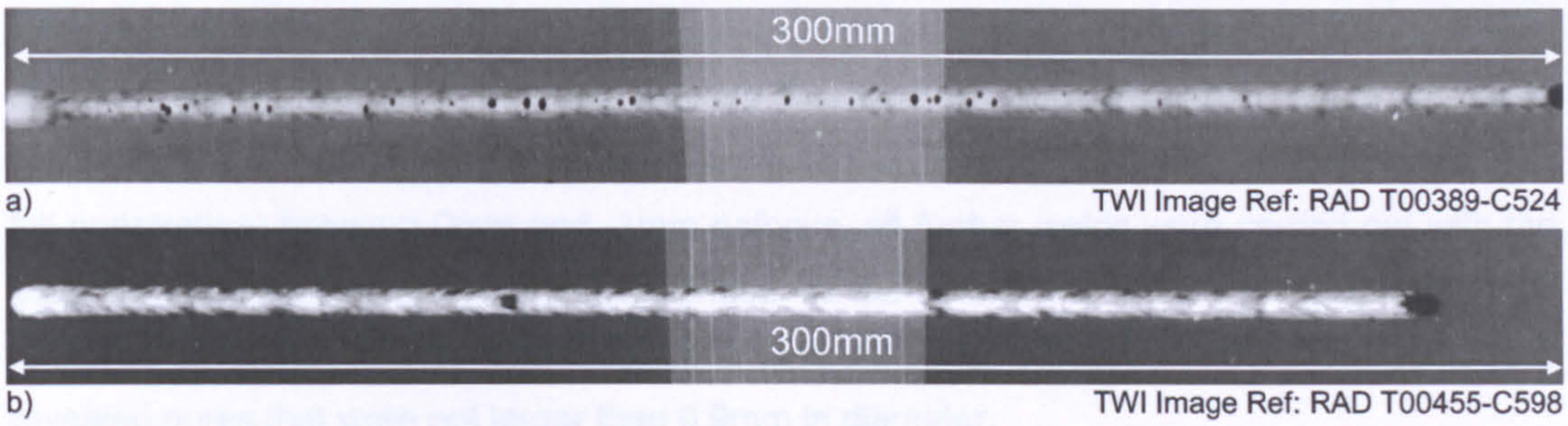

Fig.18 Radiographs of typical welds produced in 3.2mm thickness 2024 alloy, using 3.1kW of power focused in a Ø0.6mm spot positioned 1mm below the material surface, and:
a) 1.4m/min welding speed and 1.25m/min wire feed speed, no cleaning
b) 1.25m/min welding speed and 1.25m/min wire feed speed, abraded

The cross-sections taken from these welds, produced on as-received and abraded samples, are shown in Fig.19a and b, respectively. From these can be observed that the overall width of the welds produced on the abraded samples was larger.

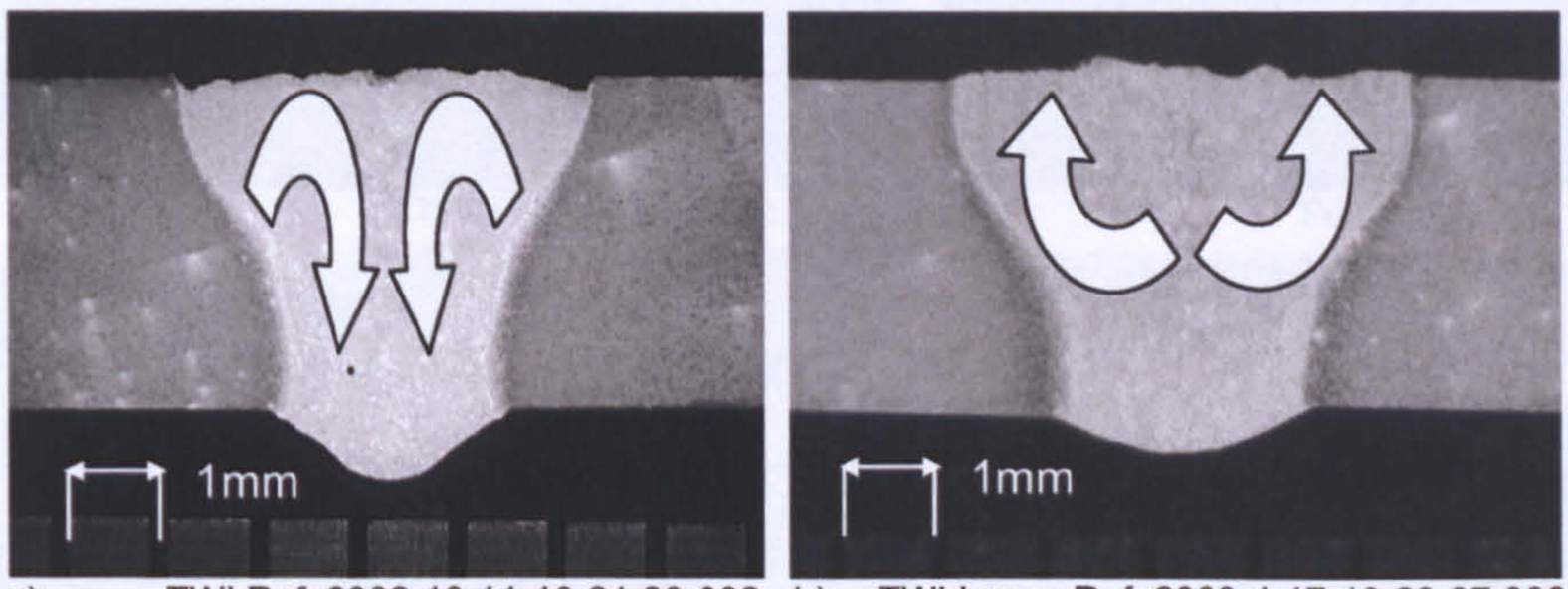

Fig.19 Cross-sections of typical welds, with the white arrows indicating the molten metal flow, produced in 3.2mm thickness 2024 alloy using 3.1kW of laser power, Ø0.6mm spot size, defocus –1mm, and:
a) 1.4m/min welding speed and 1.25m/min wire feed speed, no cleaning
b) 1.25m/min welding speed and 1.25m/min wire feed speed, abraded

Contributory factors to this change in weld width include the (10%) reduction in welding speed and the parent material cleaning. The effect (on the level of fine porosity) of a slower

welding speed is as described in Section 4.6.3, with the effect of parent material cleaning related to a change in molten metal flow (as described in Section 4.6.1). For instance, by removing the surface oxide layer by abrading prior to welding, the weld pool oxygen content decreases. This affects the molten metal flow as shown in Fig.19a and b and widens the weld top-bead. As the weld widens, the degassing improves, i.e., entrapped pores can escape the weld pool. Based on these initial observations, the effect of parent material cleaning on the presence of fine porosity, was further investigated (Section 5.6.2).

5.6.2. The Effect of Parent Material Cleaning

The influence of parent material cleaning on weld metal porosity, both fine and coarse, was further evaluated by repeating the earlier established processing conditions (Section 5.6.1), using the lower welding speed of 1.25m/min, on samples that were cleaned by either linishing, scraping, dry-machining or chemi-etching. No filler wire cleaning was carried out at this stage in the work. With negligible difference in terms of visual weld quality and welding speed (for full penetration) between 0mm and -1mm defocus, all further welds were carried out with the laser focus positioned on the material surface. At the time of the trials, the maximum output power of the prototype laser had dropped to 3kW. All welds produced under these conditions revealed pores that were not larger than 0.9mm in diameter.

Typical top-bead appearances of welds that were linished and welds that were dry-machined prior to welding are shown in Fig.20 and Fig.21, respectively.

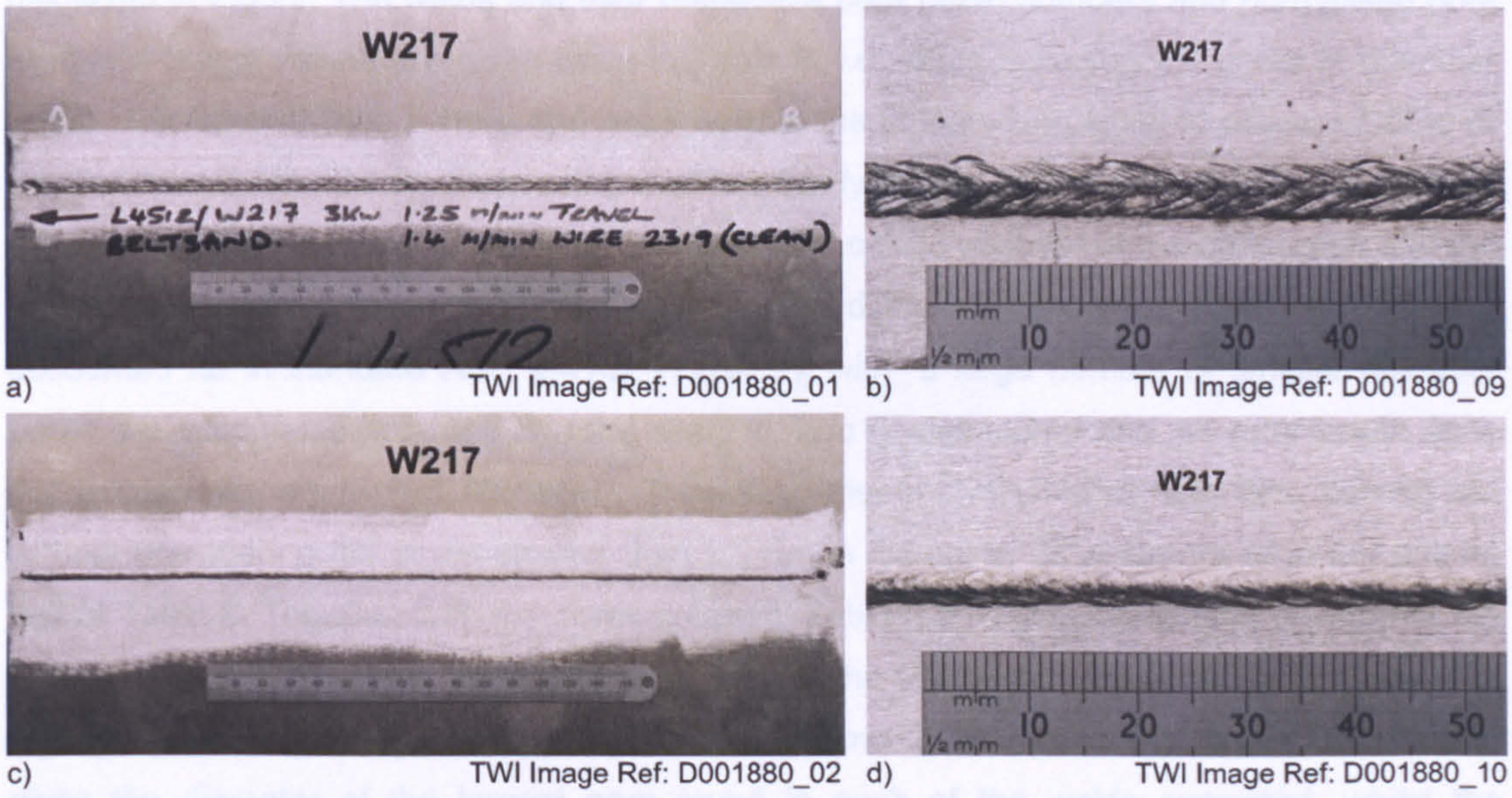

a) TWI Image Ref: D001880_01 b) TWI Image Ref: D001880_09

c) TWI Image Ref: D001880_02 d) TWI Image Ref: D001880_10

Fig.20 Weld bead appearance of a weld produced on linished samples in 3.2mm thickness 2024 aluminium alloy, using 3kW of laser power, Ø0.6mm spot size, focus 0mm, 1.25m/min welding speed, 1.4m/min WFS:

a) weld top-bead profile
b) detail of weld top-bead profile
c) weld under-bead profile
d) detail of weld under-bead profile

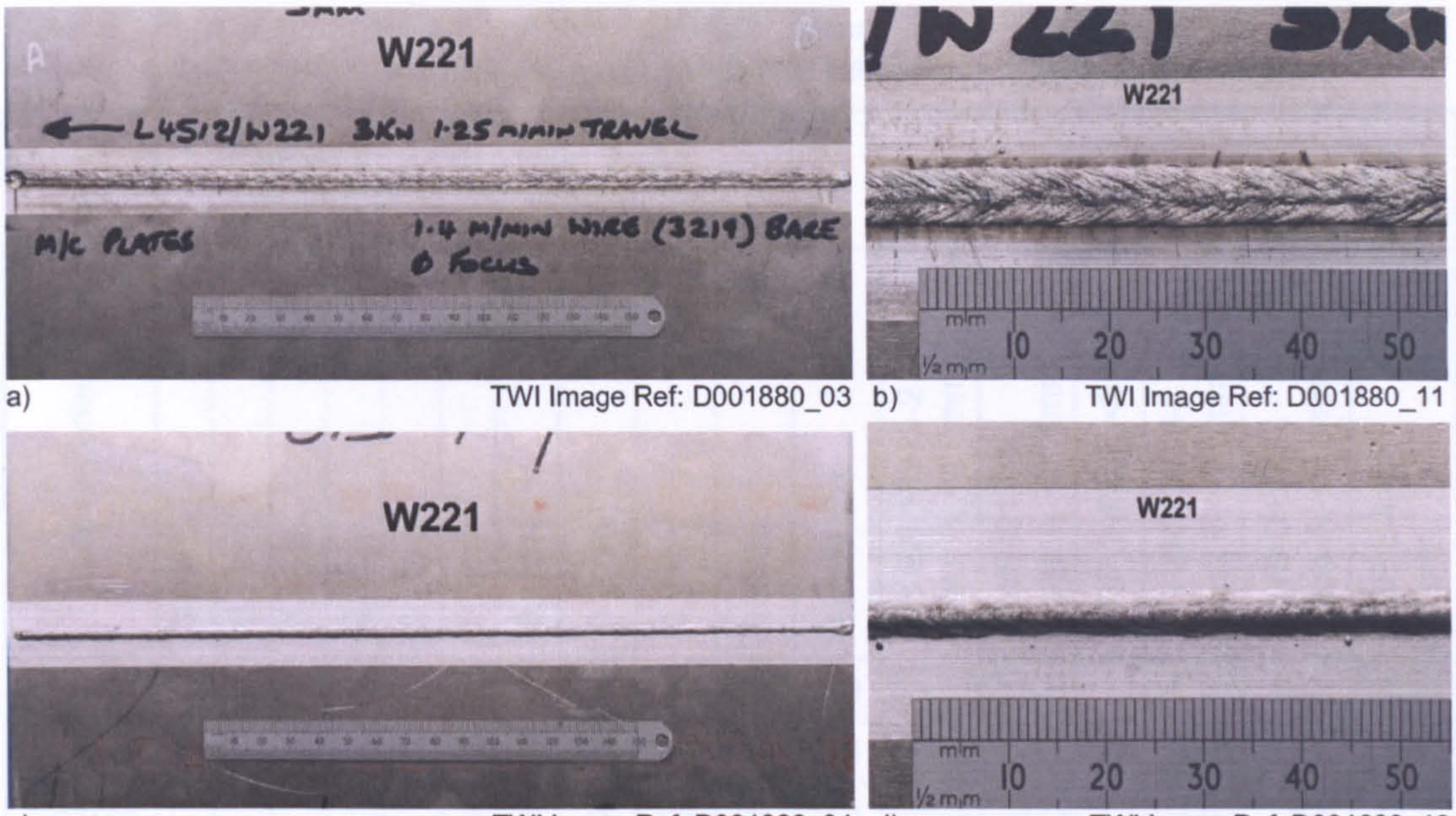

a) TWI Image Ref: D001880_03 b) TWI Image Ref: D001880_11

c) TWI Image Ref: D001880_04 d) TWI Image Ref: D001880_12

Fig.21 Weld bead appearance of a weld produced on dry-machined samples in 3.2mm thickness 2024 aluminium alloy, using 3.0kW of laser power, Ø0.6mm spot size, focus 0mm, 1.25m/min welding speed, 1.4m/min WFS:

a) weld top-bead profile
b) detail of weld top-bead profile
c) weld under-bead profile
d) detail of weld under-bead profile

Radiographic examination of a random selection of welds, representative of the different cleaning methods used, revealed an internal weld quality similar to the one shown in Fig.18b, with the pore count results of each of these welds summarised in Table 8 and graphically displayed in Fig.22. The welds and their respective pore (size) numbers and normalised pore area and length values are given twice in Table 8, i.e., once including the pores in diameter equal to or smaller than 0.1mm and once without them. Detecting isolated pores equal to or smaller than 0.1mm in diameter using a x10 magnifying glass was difficult and inconsistent. Whether such a pore was detected or not depended on the contrast of the radiograph and the individual inspector assessing the radiographs. The difficulty in detecting such small pores is accounted for in standard ABP 2-4102 (Table 7), with "*a large number of smaller diameter pores are acceptable provided that the spacing ratio is maintained and the total length does not exceed the equivalent standard*". Therefore, the analysis below was also carried out without considering the pores smaller than 0.1mm in diameter, as summarised in the bottom half of Table 8. Together with the pores counted, Table 8 also gives indication of whether the welds passed or failed the first and third criterion of the standards considered, with those cells highlighted in grey denoting a pass. The first column '*Actual size, mm*' under '*Criterion 1*' gives the diameter of the largest pore found in each of the welds examined, whilst the remainder three columns indicate a pass or fail of the first criterion for the three standards. The first column under '*Criterion 3*' gives, for each weld, the equivalent pore area per 100mm weld length (BS EN 13919-2), whilst the second and third column give the equivalent pore length per 76mm (3") and 50mm weld length (AWS D17.1 and ABP 2-4102, respectively).

Table 8 Pore count results for the different parent material cleaning methods, with normalised pore area and length values, as per BS EN 13919-2 and AWS D17.1

Base material preparation *	Pores in 100mm weld length (non-localised and sub-surface)										Criterion 1				Criterion 3		
	1.0mm	0.9mm	0.8mm	0.7mm	0.6mm	0.5mm	0.4mm	0.3mm	0.2mm	0.1mm	Actual size	BS EN 13919-2 class B, <1.0mm	AWS D17.1, class A, < 1.1mm	ABP 2-4102, <0.8mm	BS EN 13919-2 class B, <9.6mm^2	AWS D17.1 class A, <4.3mm	ABP 2-4102 <6mm
LI+DG		1		1			1	6	22	36	0.9	✓	✓		2.5	9.0	5.9
SC+DG							2	15	30	40	0.4	✓	✓	✓	2.6	11.7	7.7
MA+DG						3	7	8	64	52	0.5	✓	✓	✓	4.5	18.8	12.4
CE+DG							5	4	32	65	0.4	✓	✓	✓	2.4	12.3	8.1
LI+DG		1		1			1	6	22		0.9	✓	✓		2.3	6.2	4.1
SC+DG							2	15	30		0.4	✓	✓	✓	2.3	8.6	5.7
MA+DG						3	7	8	64		0.5	✓	✓	✓	4.0	14.9	9.8
CE+DG							5	4	32		0.4	✓	✓	✓	1.9	7.3	4.8

* DG = acetone degrease, LI = linish, SB = abrasive pad, SC = scrape, MA = machine, CE = chemi-etch
The cells highlighted in grey indicate a 'pass' for the criterion and standard in question

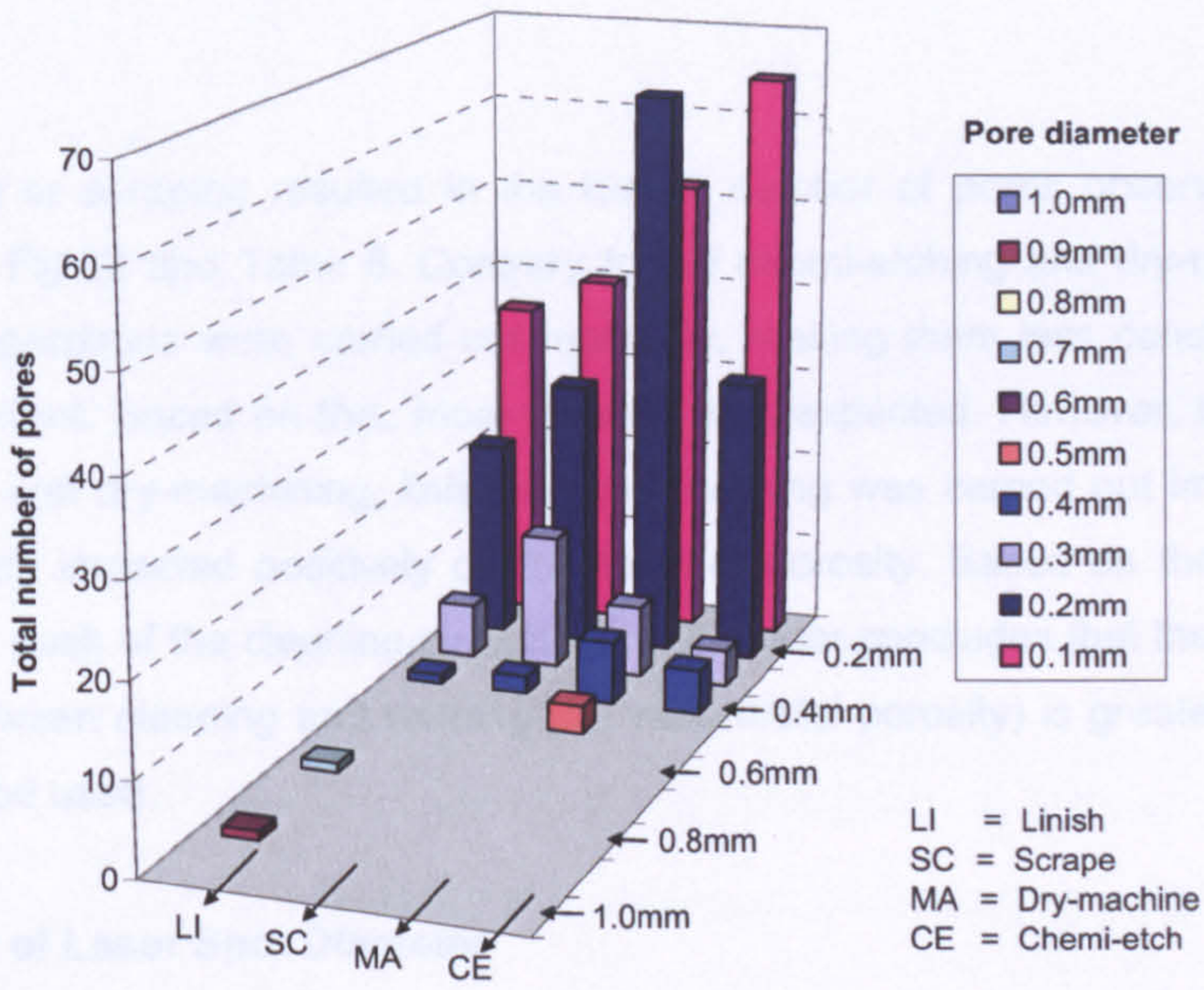

Fig.22 Pore count results for the different parent material cleaning methods

Similar numbers of pores of different sizes were found in the welds produced using the various parent material cleaning conditions, Table 8, particularly for those samples that were abraded, linished and chemi-etched. Notwithstanding one 0.7mm and one 0.9mm diameter

pore found in the linished weld, depicted in Fig.22, the normalised pore area/length of the linished weld in Table 8, with or without the smallest pores, was the lowest of the four welds. However, the 0.9mm diameter pore resulted in the linished weld failing the first criterion of ABP 2-4102, with all other welds passing the first criterion of all three standards. The 0.9mm diameter pore in question was the only one of that size found, with the maximum pore diameter in the rest of the samples welded under these conditions smaller than 0.7mm in diameter. The origin of the 0.9mm diameter pore was not determined.

All welds in Fig.22 and Table 8 passed the third criterion of BS EN 13919-2, but failed that of AWS D17.1, with or without taking into account the smallest pores. Without considering these smaller pores, all welds, except those on the dry-machined samples, passed the third criterion of the ABP 2-4102 standard. Moreover, the dry-machined samples contained the most pores, resulting in the highest *normalised* pore area/length of the four cleaning methods examined (Table 8). Particularly the number of pores in diameter between 0.1 and 0.2mm was higher for the dry-machined welds that for the other cleaning operations. The author attributes the 'poor' performance of the dry-machined samples to the fact that dry-machining was not in all cases carried out immediately prior to welding. Up to 12 samples were dry-machined in a single operation, contrary to a maximum of 6 samples in case of the chemi-etching operation, leaving some of the dry-machined samples in the desiccating cabinet for a longer period of time, although limited up to 48 hours, as stated in Section 5.4. Repeated opening and closing of the desiccating cabinet to remove samples to be welded, pushes the cabinet's moisture level up, despite the use of silica gel, which increases the likelihood of fine porosity in the welds.

Cleaning by linishing or scraping resulted in the lowest number of pores observed in the welds, as seen from Fig.22 and Table 8. Contrary to the chemi-etching and dry-machining, these two cleaning operations were carried out manually, making them less consistent and more operator-dependent. Based on this, more porosity was expected. However, in contrast to the chemi-etching and dry-machining, linishing and scraping was carried out immediately prior to welding, which impacted positively on the level of porosity. Based on the levels of porosity observed for each of the cleaning operations, the author concludes that the impact of the time elapsed between cleaning and welding (on weld metal porosity) is greater than the actual cleaning method used.

5.6.3. The Effect of Laser Spot Diameter

All welds produced from this point onwards were welded with a newly acquired commercial 3kW LP Nd:YAG laser, see Section 5.2, using the maximum available laser output power of 2.85kW (measured at the workpiece) focused in a 0.45mm diameter spot, unless otherwise stated. This power and spot size equated to a power density of 1.8×10^6 W/cm^2, more than 50% higher than that used for the aforementioned trials (Sections 5.6.1 and 5.6.2), and higher

than the $1.5x10^6$ W/cm^2 threshold power density required to initiate Nd:YAG laser keyhole welding in aluminium (Section 4.2, page 17). This resulted in full penetration in the 3.2mm thickness 2024 alloy at a welding speed of 1.75m/min, 40% higher than the 1.25m/min welding speed used in earlier trials. Although the higher welding speed produced full penetration and visually acceptable weld profiles, radiographic examination of the welds revealed a total pore area up to 4 times larger compared with the earlier welds, which were produced using 3kW of laser power focused in a 0.6mm spot size (and the same parent material conditions).

Nine (coarse) pores as large as 1.0mm in diameter were found in one of the welds produced under these conditions. The size of these pores excludes hydrogen as a possible cause (see Section 4.4, page 23). The author concludes that the coarse pores resulted from the higher welding speed (compared with earlier welds), based on the fact that keyhole stability deteriorates with increasing welding speed (Section 4.6.3). The higher welding speed also increases the cooling rate, allowing less time for (coarse) porosity to escape the solidifying weld pool. The difference in cross-sectional weld profile between the two different processing conditions used for the two different lasers, is demonstrated in Fig.23a and b, with the cross-sectional area reducing 43% from 13.7mm^2 (using 3kW of laser power focused in a 0.6mm diameter spot size at a welding speed of 1.5m/min) to 7.8mm^2 (using 2.85kW of laser power focused in a 0.45mm diameter spot size at a welding speed of 1.75m/min).

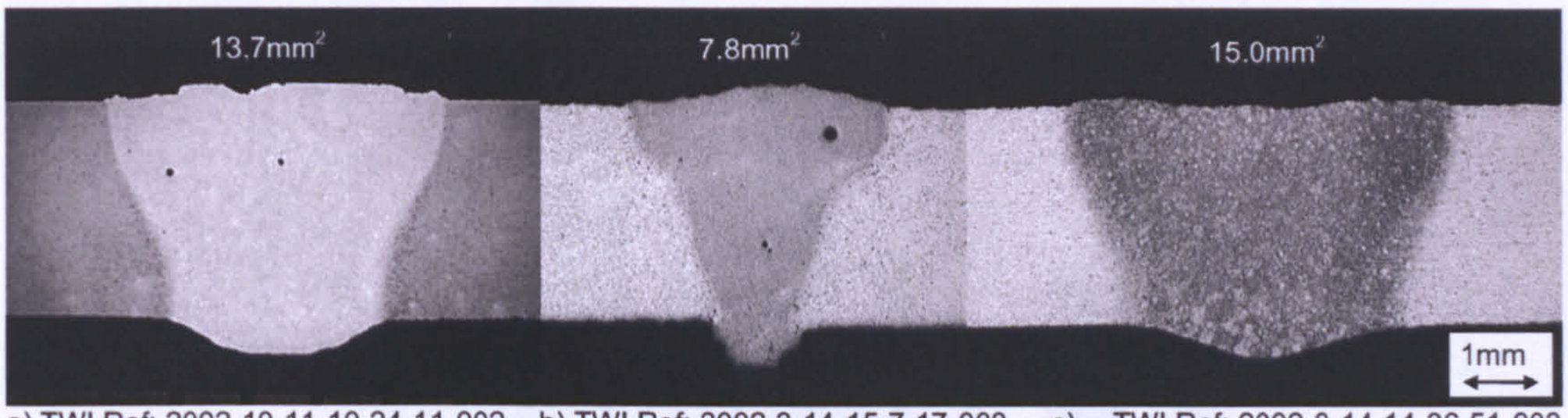

a) TWI Ref: 2002-10-11-10-24-11-002 b) TWI Ref: 2002-3-14-15-7-17-003 c) TWI Ref: 2002-3-14-14-36-51-003

Fig.23 Cross-sections of welds produced using:

a) 3.0kW laser power, Ø0.6mm (single) spot, defocus -1mm, 1.5m/min travel speed, 2.0m/min WFS, linished and degreased material
b) 2.85kW laser power, Ø0.45mm (single) spot, defocus 0mm, 1.75m/min travel speed 1.2m/min WFS, linished and degreased material
c) 2.85kW laser power, Ø0.45mm twin-spot (0.27mm separation, 50/50 energy distribution), defocus 0mm, 0.75m/min travel speed, 1.2m/min WFS, linished and degreased material

The proof that the increase in the (coarse) porosity observed was related to the welding speed rather than the decrease in spot size was in bead-on-plate runs produced using the prototype laser at 3kW of laser power focused in a 0.6mm spot. The welding speed was increased from the 1.25m/min (as in Section 5.6.2) until penetration in the 3.2mm thickness 2024 aluminium alloy was lost, which occurred at 1.6m/min. A welding speed of 1.5m/min, i.e., 20% higher than 1.25m/min, continued to produce full penetration welds, but with a narrower, more

irregular, under-bead. The normalised pore area/length of such a weld was 44mm^2 and 47mm, respectively, compared with 14mm^2 and 17mm, respectively, for the welds carried out at 1.25m/min welding speed.

5.6.4. The Effect of Twin-Spot Energy Distribution

The cross-sections in Fig.23 show the effect of a twin-spot energy distribution on the cross-sectional area. The twin-spot weld, Fig.23c, is 2.3 times wider mid-thickness than its single-spot equivalent, Fig.23b, i.e., 4.4mm instead of 1.9mm. The cross-sectional weld profile produced with the twin-spot technique (spot diameters 0.45mm, 0.27mm spot separation) is similar to that produced using the single-spot technique with a 0.6mm diameter spot, with the cross-sectional area and the mid-thickness width 10% and 19% higher, respectively, i.e., 15.0mm^2 and 4.4mm compared with 13.7mm^2 and 3.7mm.

The effect of the twin-spot technique on the occurrence of fine porosity can be seen from the pore count results and normalised pore area/length values summarised in Table 9 and from the pore count results graphically depicted in Fig.24.

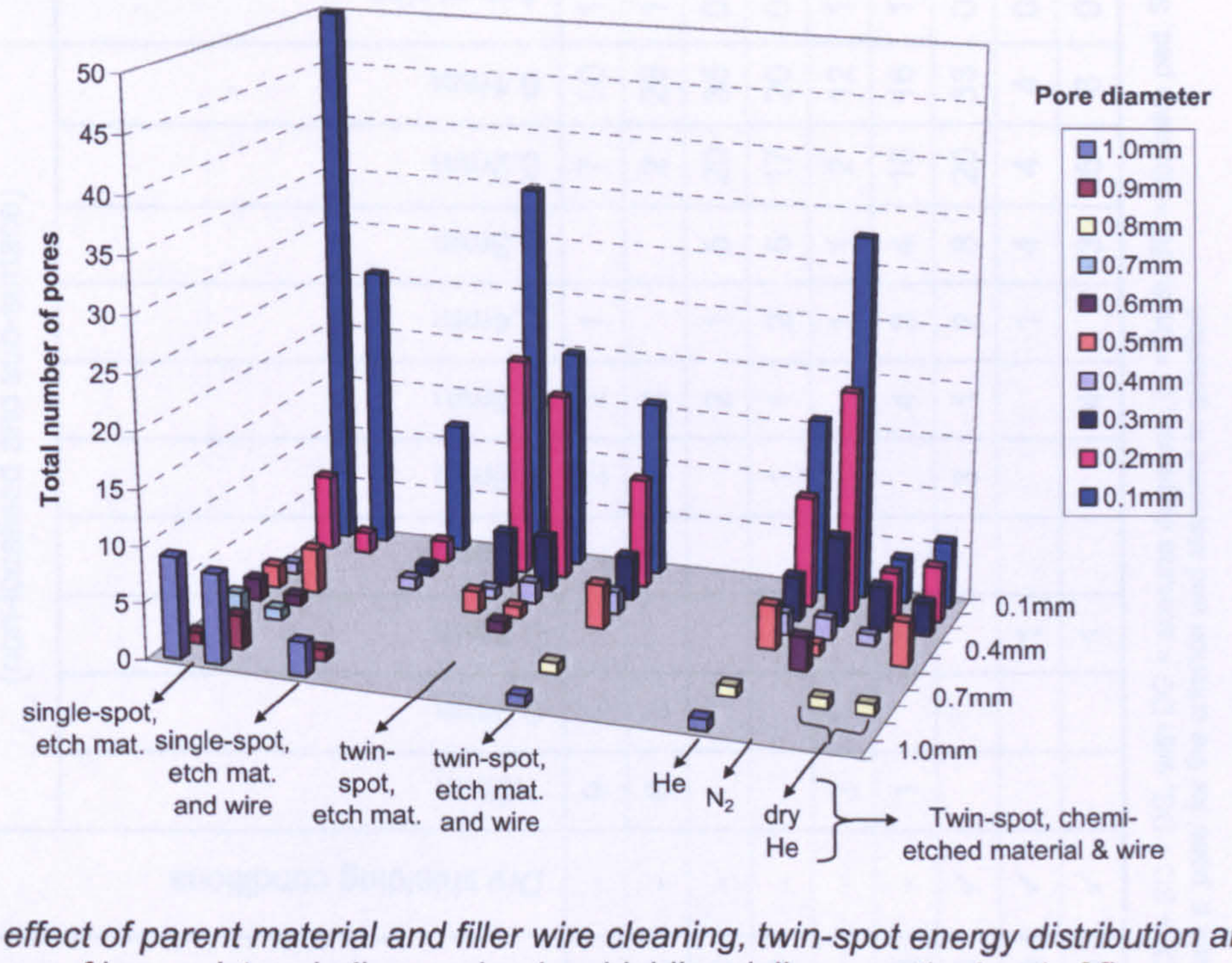

Fig.24 The effect of parent material and filler wire cleaning, twin-spot energy distribution and the use of low-moisture helium and a dry shielding delivery on the level of fine porosity in laser-welded 3.2mm thickness 2024 aluminium alloy

Table 9 Pore count results summarising the effect of filler material cleaning, twin-spot energy distribution and the use of high-purity helium and a dry shielding delivery on the level of fine porosity in laser-welded 3.2mm thickness 2024 aluminium

Filler wire preparation	Spot distance, mm	Intensity distribution between spots, %/%	*Dry* shielding conditions	Pores in 100mm weld length (non-localised and sub-surface)										Criterion 1				Criterion 3			
				1.0mm	0.9mm	0.8mm	0.7mm	0.6mm	0.5mm	0.4mm	0.3mm	0.2mm	0.1mm	Actual size	BS EN 13919-2 class B, <1.0mm	AWS D17.1, class A, < 1.1mm	ABP 2-4102, <0.8mm	BS EN 13919-2 class B, <9.6mm2	AWS D17.1 class A, <4.3mm	ABP 2-4102 with 'small' pores, <6mm	ABP 2-4102 without 'small' pores, <6mm
LI + DG	-	-	-	9	1		2	2	2	1		7	50	1.0		✓		10.2	15.5	10.2	7.7
LI + DG	-	-	-	8	3		1	1	4			2	26	1.0		✓		9.9	13.0	8.5	7.2
LI + DG	0.27	60/40	-						2	1	5	20	35	0.5	✓	✓	✓	1.8	7.9	5.2	3.5
LI + DG	0.27	50/50	-					1	1	2	5	17	20	0.6	✓	✓	✓	1.8	6.7	4.4	3.4
CE+ DG	-	-	-	3	1					1	1	2	12	1.0		✓		3.3	4.7	3.1	2.5
CE+ DG	0.27	50/50	-	1		1			4	2	4	10	16	1.0		✓		3.0	7.2	4.7	3.9
CE+ DG	0.27	50/50	✓					3	1	2	8	20	33	0.6	✓	✓	✓	2.7	9.8	6.4	4.8
CE+ DG	0.27	50/50	✓			1				1	4	4	4	0.8	✓	✓	✓	1.1	2.7	1.8	1.6
CE+ DG	0.27	50/50	✓			1			4		3	5	6	0.8	✓	✓	✓	1.7	4.0	2.7	2.4

All samples were cleaned using CE + SC + DG, with DG = acetone degrease, LI = linish, SB = abrasive pad, SC = scrape, MA = machine, CE = chemi-etch.
The cells highlighted in grey indicate a 'pass' for the criterion and standard in question

The twin-spot welds passed the first criterion of all three standards, passed the third criterion of BS EN 13919-2 and ABP 2-4102, but failed that of AWS D17.1. Whereas coarse pores were observed for those welds produced using the single-spot technique, no pores larger than 0.5mm in diameter were present in the welds produced with the twin-spot technique. Welds were completed using the same laser power of 2.85kW (combined in the case of the twin-spot) and spot size (Ø0.45mm), but in case of the twin-spot technique, with a lower welding speed of 1.0m/min, to allow full penetration to be maintained.

Additional welds were also produced on 3.2mm thickness 6056 alloy, using identical conditions as those established for single and twin-spot welding of 3.2mm thickness 2024 alloy. The results are shown in Fig.25 and Table 10, with three (identical) welds produced using a single-spot energy profile and two with a twin-spot energy profile, confirming the effect of the twin-spot technique (compared with single-spot) on the presence of porosity, and particularly the occurrence of coarse pores. Applying the twin-spot technique reduced the normalised pore area/length (including the pores in diameter smaller than 0.1mm) on average by 33% and 23%, respectively, for the 6056 alloy material. Moreover, only three pores larger than 0.5mm in diameter were observed in the single-spot welds completed in this alloy, compared with the large number, see Table 8, found in the 2024 alloy welds completed under identical welding conditions.

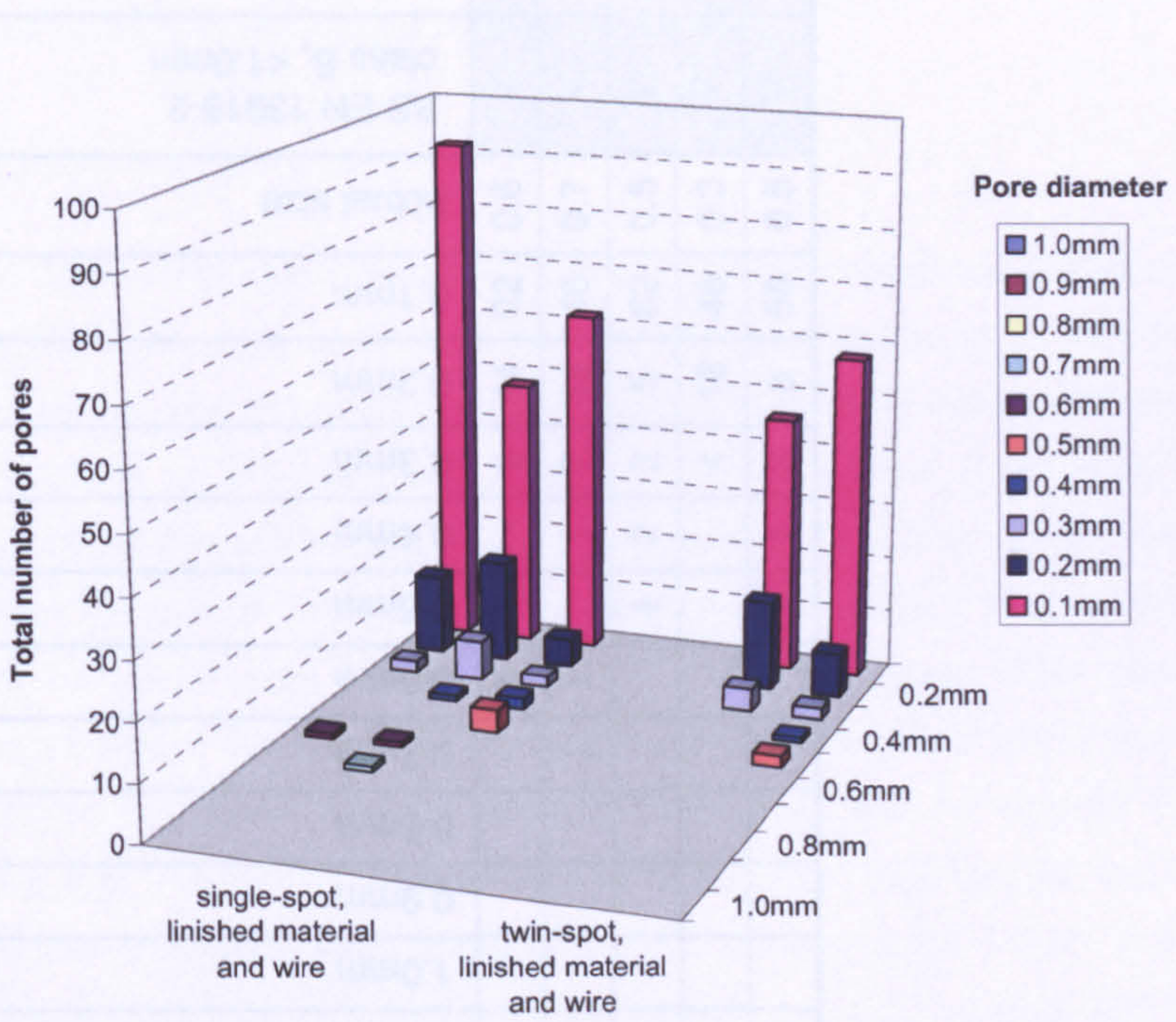

Fig.25 Pore counts of welds produced on 6056 alloy samples, using 2.85kW of laser power, Ø0.45mm single and twin-spot (0.27mm separation, 50/50 energy distribution), defocus 0mm, 1.75m/min (single-spot) and 1.0m/min (twin-spot) welding speed, linished and degreased parent material and filler wire

Table 10 Summary of pore counts of welds produced on 6056 aluminium samples.

Spot distance, mm	Intensity distribution between spots %/%	Travel speed, m/min	Pores in 100mm weld length (non-localised and sub-surface)										Criterion 1				Criterion 3			
			1.0mm	0.9mm	0.8mm	0.7mm	0.6mm	0.5mm	0.4mm	0.3mm	0.2mm	0.1mm	Actual size	BS EN 13919-2 class B, <1.0mm	AWS D17.1, class A, < 1.1mm	ABP 2-4102, <0.8mm	BS EN 13919-2 class B, =<9.6mm2	AWS D17.1 class A, =<4.3mm	ABP 2-4102 =<6mm	ABP 2-4102 without 'small' pores, =<6mm
-	-	1.75					1			2	14	92	0.6	✓	✓	✓	1.6	10.1	6.6	2.0
-	-	1.75				1	1		1	7	18	48	0.7	✓	✓	✓	2.2	9.3	6.1	3.7
-	-	1.75						4	2	2	5	62	0.5	✓	✓	✓	1.8	8.1	5.3	2.2
0.36	50/50	1.00								4	16	46	0.3	✓	✓	✓	1.1	6.9	4.5	2.2
0.36	60/40	1.00						2	1	2	8	58	0.5	✓	✓	✓	1.4	7.2	4.7	1.8

As mentioned in Section 4.6.6, the keyhole opening is enlarged by using a twin-spot compared with a single-spot technique. This results in a reduction of the surface tension (larger radius), making it easier for the keyhole to stay open. The author comments that, although this in itself minimises the level of coarse porosity/cavities found in the weld, it is the reduction in welding speed in particular, associated with the change from a single to a twin-spot energy profile (at a given power), that is the overriding factor here. The twin-spot welds were carried out at a welding speed of 1.0m/min, compared with the single-spot welds carried out at a welding speed of 1.75m/min for both the 2024 and the 6056 alloy samples (Table 10). By splitting a given laser power into two separate foci, the welding speed has to be reduced to maintain a given depth of penetration (118). This reduction in speed results in an enlarged cross-sectional area, as shown in Fig.23, and in a reduction of the cooling rate (72), both of which are more favourable conditions for entrapped pores to escape the solidifying weld pool. No excessive formation of plasma/plume above the keyhole, which can lead to keyhole instabilities, was observed during the twin-spot welding trials carried out at 1m/min.

Alloy composition was also found to influence the occurrence of coarse porosity, which the author attributes to the presence of the low-boiling point constituent Mg. This is based on the fact that for identical welding conditions, using the single-spot energy profile, no coarse porosity was observed in the 6056 alloy, Fig.25, contrary to the welds produced in the 2024 alloy, as shown in Fig.24. The 6056 alloy contains between 0.6 and 1.2 wt% Mg, compared with between 1.2 and 1.8 wt% in case of the 2024 aluminium alloy.

5.6.5. The Effect of Filler Wire Cleaning

Although recognised that chemi-etch cleaning of the filler wire is impractical in production, it was applied to the filler wire prior to welding to investigate the influence of filler material cleaning on the presence of fine porosity. Chemi-etching was compared with a (standard) light abrasive cleaning followed by a solvent degreasing, which is deemed more practical in a production environment and would be possible to incorporate in the wire feeder. The pore count results shown in Fig.24 and Table 9 demonstrate that chemi-etching the filler wire prior to welding reduced the laser weld metal porosity in 3.2mm thickness 2024 aluminium, compared with parent material cleaning only. Although coarse porosity was still observed, the welds produced with the chemi-etch cleaned filler wire passed, as was the case for the twin-spot welds (Section 5.6.4), the third criterion of BS EN 13919-2 and ABP 2-4102, but not that of AWS D17.1, with the normalised pore length of 4.7mm still above the 4.3mm limit of the stringent weld quality in AWS D17.1 (Table 9). From Table 9 can also be observed that the use of a chemi-etched filler wire in combination with the twin-spot technique did not further reduce the level of weld metal porosity. These results underline the importance of filler material cleaning prior to welding to achieve a low level of fine porosity when laser welding 3.2mm thickness 2024 aluminium using a single-spot energy distribution

5.6.6. The Effect of Shielding Gas Condition

All experience obtained up to this point with regards to the effect of parent material surface contaminants, filler wire surface contaminants and laser energy distribution, on the presence of fine and coarse weld metal porosity (Sections 5.6.1 to 5.6.5), was applied for a final series of welding trials, in which the effect of shielding gas and its delivery on the presence of fine porosity was investigated. Welding was carried out on 3.2mm thickness 2024 aluminium samples using the twin-spot laser technique, at a welding speed of 0.8m/min (which produced full penetration) with the samples and filler wire chemi-etched immediately prior to welding. High-grade helium was used and supplied through a *dry* shielding delivery, as described in Section 5.4. The pore count results in Fig.24 and Table 9 show that this shielding set-up enabled laser welds to be completed in 3.2mm thickness 2024 aluminium alloy, with a weld metal porosity level in accordance with the stringent weld quality class defined in BS EN 13919-2, ABP-4102 and the most stringent AWS D17.1 standard. The normalised pore length of these welds was on average 4.0mm, i.e., below the 4.3mm limit set for the stringent weld quality limit in AWS D17.1. Subsequent work based on the author's experience has since shown that the use of a dry shielding delivery and purging time are the dominant factors in this set-up to minimise fine porosity in laser welded 3.2mm thickness 2024 aluminium (130-131). Moisture levels as low as 20ppm result in low porosity levels in accordance with the standards, and can be achieved by purging the lines with shielding gas up to 30 minutes prior to welding. The purging time is dependent on the material and length of the shielding line, standing time and initial shielding gas moisture content. Moisture levels increased from 20ppm to between 140 and 170ppm, irrespective of initial shielding gas moisture content, within 2 hours of non-activity (130-131).

5.7. CONCLUSIONS

A welding procedure was developed for producing fully penetrating, square-edge butt welds in 3.2mm thickness 2024 aluminium alloy using 3kW CW lamp-pumped Nd:YAG laser power. By minimising the moisture content in the shielding gas and its delivery, rigorous parent and filler material cleaning prior to welding and the use of a twin-spot energy distribution, a level of weld metal porosity was achieved consistently, that was lower than that defined for the stringent quality class in BS EN 13919-1:1997 and AWS D17.1:2001. The measures required to achieve this level of weld metal porosity were as follows:

- The use of a low dew-point (-98°C) helium shielding gas, delivered through a short, 1.5m long, polyamide gas line, containing a minimum of moisture. This was achieved in this work, through storage at elevated temperature for 24 hours, acclimatisation for 2 hours prior to welding and purging for at least 2 minutes prior to welding.
- Removing the surface oxide layer from the edges to be welded and from the top and bottom of the samples near the fusion line, using linishing, scraping, dry-machining or

chemi-etching. The effect of pre-weld cleaning (on weld metal porosity) is largely determined by the time elapsed between cleaning and welding. Cleaning immediately prior to welding is recommended, as it minimises the time for oxide growth and moisture pick-up.

- Removing surface contaminants from the filler wire by mechanical or chemical means, immediately prior to welding.
- The use of a twin-spot laser energy profile with a 0.27mm spot separation and a 50/50 energy distribution.

6. PERFORMANCE COMPARISON TRIALS

With only 6 to 8mm thickness aluminium that can be penetrated in a single pass using a fibre-delivered Nd:YAG laser, there was a requirement to investigate the potential of the new Yb-fibre lasers for the welding of thicker section aluminium, as these lasers are capable of emitting a similar wavelength laser beam at higher output powers compared with Nd:YAG lasers. The performance of such an Yb-fibre laser at an output power of 7kW for the welding of thick-section aluminium is further described in Section 7. However, prior to using this laser at its maximum output power, the author initiated a study in which this new Yb-fibre laser was used at an output power of (only) 4kW and compared, in terms of welding performance on aluminium, with a lamp-pumped (LP) Nd:YAG laser at the same output power. A common problem with performance comparisons of this kind, is that newly obtained data (in this case, for the Yb-fibre laser) is often compared with historical data (in this case, for the LP Nd:YAG laser), which may have been obtained using different material grades or thicknesses, different spot sizes or even different power levels. This makes it difficult to draw concise comparative conclusions on the performances of the different lasers, which is why for these trials, a set of experiments was designed to be carried out using both the Yb-fibre laser and the LP Nd:YAG laser under *identical* processing conditions. That is, welding was performed on the same material, i.e., 5083 aluminium; using the same output power of 4kW at the workpiece (as measured using the same power meter); using the same spot diameter (i.e., as close to 0.4mm as possible with available focussing optics); using the same welding jig (to minimise the heat sink variations) and the same helium shielding arrangement for shielding both the top and under side of the welds. The details of this work and its results are described in EngD Submission 8 (47) and summarised in this Section.

6.1. MATERIAL

All trials in this part of the work were carried out on 5083 aluminium alloy, Table 1 (page 12). This AlMg4.5Mn0.7 alloy is part of the 5000-series aluminium alloys, which offer the highest strength of the non heat-treatable alloys and are readily weldable (48,61,63). The 5083 alloy is commonly used for structural applications, specifically in the field of transportation, which explains its frequent use in research work (Section 4.1) and is the reason why it was selected for the performance comparison trials. All material used was supplied in a standard O-temper, i.e., fully annealed, in sheets of 5 and 10mm in thickness. The material was cold band-sawn to 75mm wide by 300mm long samples, which were machined to give a tapered profile such that the thickness along the 300mm length varied continuously from 1 to 5mm and from 4 to 10mm, as shown in Fig.26.

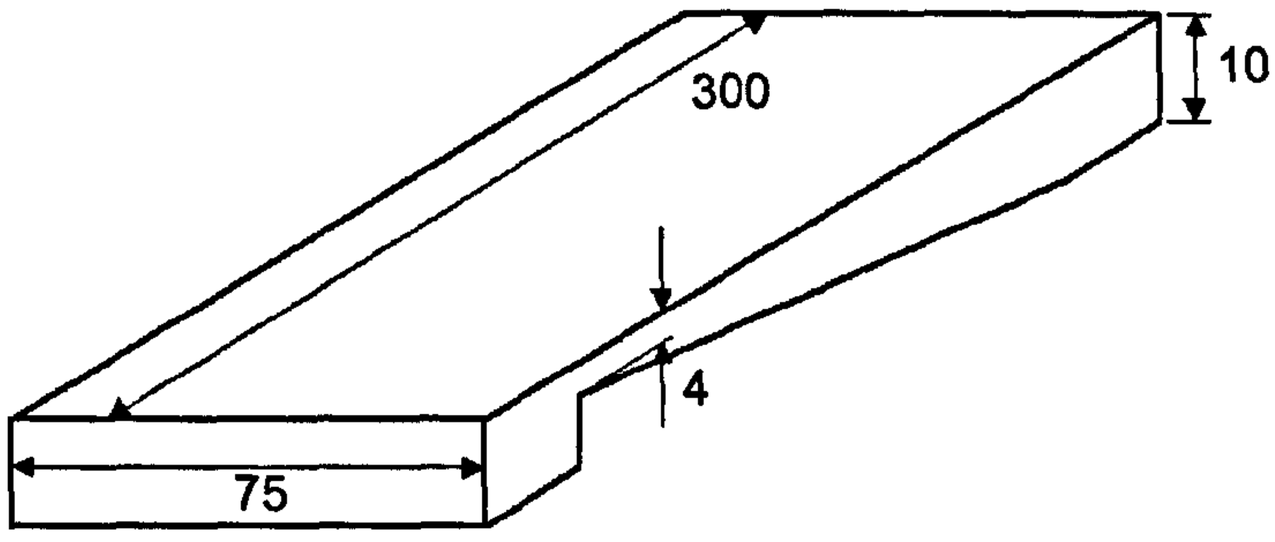

Fig.26 Tapered sample used for the performance comparison welding trials

6.2. EQUIPMENT

The primary aim of the trials was to compare the performance of 4kW of Yb-fibre laser power with that of 4kW of LP Nd:YAG laser power for the welding of aluminium. For a given output power, the Yb-fibre laser is available with a better beam quality than the Nd:YAG laser, which means that what is actually assessed here, is the effect of laser beam quality, expressed as Beam Parameter Product (BPP), on the welding performance on aluminium. More information on beam quality (or BPP) and its (practical) impact on welding in terms of stand-off distance between the process head and the workpiece, laser spot size and power density, is given in Section 6.4, with the reader referred to EngD Submission 5 (31), for additional details on Yb-fibre laser technology, the advantages and disadvantages, and its use for materials processing.

Laser technology developed at a fast pace between 2003 and 2005, with the commercialisation of the (high-power) Yb-YAG disc laser and the further improvement of laser beam quality (and output power) for the Yb-fibre lasers. For these reasons, the comparison exercise was expanded to include, in addition to the 4kW LP Nd:YAG laser and the 7kW Yb-fibre laser (YLR-7000), a 4kW Yb-YAG disc laser and a 5kW Yb-fibre laser (YLR-5000). These two laser sources were chosen because of the available BPP of 7 and 4mm.mrad, respectively, adding to the 23mm.mrad and the 18mm.mrad available from the 4kW LP Nd:YAG laser and the 7kW Yb-fibre laser, respectively.

To investigate the effect of beam quality on welding performance, the beam delivery optics for each of the lasers were chosen to produce laser spot size diameters as close to 0.4mm as possible, which is a spot size often used for industrial welding applications, thereby ensuring that in each case the same laser power density was used at the workpiece. To assess the effect of spot size and power density on welding performance, beam delivery optics were also selected to produce a smaller spots size for the laser sources with the highest beam quality, i.e., 0.14mm and 0.2mm for the YLR-5000 and Yb:YAG respectively, and a larger spot size for the source with the lowest beam quality, i.e., 0.61mm for the LP Nd:YAG. The laser sources and beam delivery optics used in these trials are summarised in Table 11.

Table 11 Characteristics of the laser sources and beam delivery optics used in the performance comparison trials

	LP Nd:YAG		Yb-fibre	Yb-fibre		Yb:YAG disc	
Delivery fibre diameter, mm	0.6		0.3	0.1		0.2	
Collimating lens focal length, mm	200		120	120		150	200
Focusing lens focal length, mm	200	150	160	500	160	280	200
Nominal beam waist, mm	0.60	0.45	0.40	0.42	0.13	0.37	0.20
Measured beam waist (86% pts), mm	0.61	0.44	0.39	0.40	0.14	0.34	0.20
Beam parameter product*, mm.mrad	23	22	18	4	4	7	7
Rayleigh length*, mm	4.0	2.5	2.1	9.9	1.2	4.0	1.1
Laser power at workpiece, kW	4	4	4	4	4	4	4
Power density (at beam waist for 4000W), kW/mm^2	13.7	26.6	33.8	31.5	264.4	45.1	134.2
Beam brightness (at beam waist, for 4000W), $x10^5$ W/mm^2.steradian	2.79	3.04	5.96	54.25	46.60	18.01	27.34

* Derived from beam caustic (measured) data

The beam waist diameters given in Table 11 were measured using both a Prometec and a Primes laser beam analyser, with measured values for both within ±3% of each other, as determined experimentally (47). The minimum beam waist diameters, beam parameter products, and Rayleigh lengths listed in Table 11 are those calculated by the beam analyser software using 86% intensity values. The Rayleigh length of a laser beam is the distance from the beam waist along its propagation direction where the cross-sectional area of the beam increases a factor of two (132).

6.3. SET-UP

All performance comparison trials were carried out with the beam focused on the material surface, unless otherwise stated. An Ophir 8kW power meter with an accuracy of ±5%, as claimed by the manufacturer, was used with each of the lasers, to adjust and measure a laser power of 4kW in the focused beam at the workpiece, notwithstanding some of the lasers used were capable of operating at higher output powers. The protection of the processing head, clamping of the samples and set-up of the top and under-bead shielding was achieved in the same way as for the thin-section trials (see Section 5.3), with specific details given below. No filler wire was added.

- The axial stand-off distance of the shielding tube with the workpiece was 10mm, with flow rates set at 8 and 5 litre/min for the top and underside, respectively, to give an oxidation-

free appearance, as determined visually. The gas line was purged using shielding gas for at least five minutes at the start of each day and at least one minute prior to each weld.

- The samples were clamped with the machined side facing down. Immediately prior to welding, the samples were brushed with a clean stainless steel wire and degreased with acetone.

6.4. SCOPE OF THE WORK

With the seven combinations of laser and beam delivery optics, as detailed in Table 11, melt runs were carried out, under *identical* processing conditions (including laser power, material, spot size, clamping and shielding), on tapered samples at welding speeds between 0.5 and 15m/min. Melt runs were produced with the tapered side facing down, so that the focus position in relation to the material surface remained unchanged when moving the laser from the thick end of the tapered sample to the thin end. The thickness of the tapered sample was measured at those points at which full penetration was achieved. The averages of at least two of these thickness values per welding speed were used to construct the welding performance graphs, which relate the welding speed to the material thickness that can be penetrated (for a given power), for each of the seven laser – beam delivery optics listed in Table 11.

Beam quality is a measure of how "tightly" a laser beam can be focused (52). The beam quality is defined as *the ratio of the beam width and divergence angle product of the real beam to that expected for a perfect beam*, and remains unchanged along a beam passing through perfect optics (132-134). For CO_2 lasers, the beam quality is usually expressed using the term M^2, a dimensionless quantity, with an M^2 of 1 representing a 'perfect' beam with a Gaussian distribution, also referred to as the *diffraction-limited beam quality* (132-134). The term beam parameter product (BPP) refers to the beam quality for solid-state laser sources and is defined as the product of the beam width with the divergence angle of the real beam, expressed in mm times milliradians (mm.mrad). In this report, beam quality is quoted in terms of half beam diameter and half divergence angle, in line with the EN ISO standard for laser beam propagation (133). Because of the high beam quality of newly developed fibre-delivered lasers, both M^2 and BPP are now commonly used, with a low M^2 or BPP value signifying a higher/better beam quality. The relationship between M^2 and BPP is shown in Equation 1.

$$M^2 = \frac{BPP_{real\ beam}}{BPP_{perfect\ beam}} \qquad \text{[Equation 1]}$$

with $BPP_{perfect\ beam} = \frac{\lambda}{\pi} = 3.4$ for a CO_2 laser;

and $BPP_{perfect\ beam} = \frac{\lambda}{\pi} = 0.34$ for an Nd:YAG laser (132),

where λ = wavelength in mm.

The practical implications of a better/higher beam quality are shown schematically in Fig.27. One consequence of a higher laser beam quality is that the beam can be focussed into a smaller diameter optical (delivery) fibre. This translates, for a focusing optic of given diameter, Fig.27a, into a better focusability of the laser beam into a smaller spot size, or a smaller focussing optic diameter for the same spot size, Fig.27b. Or, for a given spot size and focusing optic diameter, Fig.27c, a higher beam quality will result in a greater depth of focus at focus, allow greater working distances between focusing lens and workpiece, i.e., a larger stand-off distance, as well as produce a higher brightness (defined as the ratio of the power density in the beam waist and the included solid angle formed by the focusing beam cone). A larger stand-off distance provides the practical advantage of minimising spatter damaging the focussing optics.

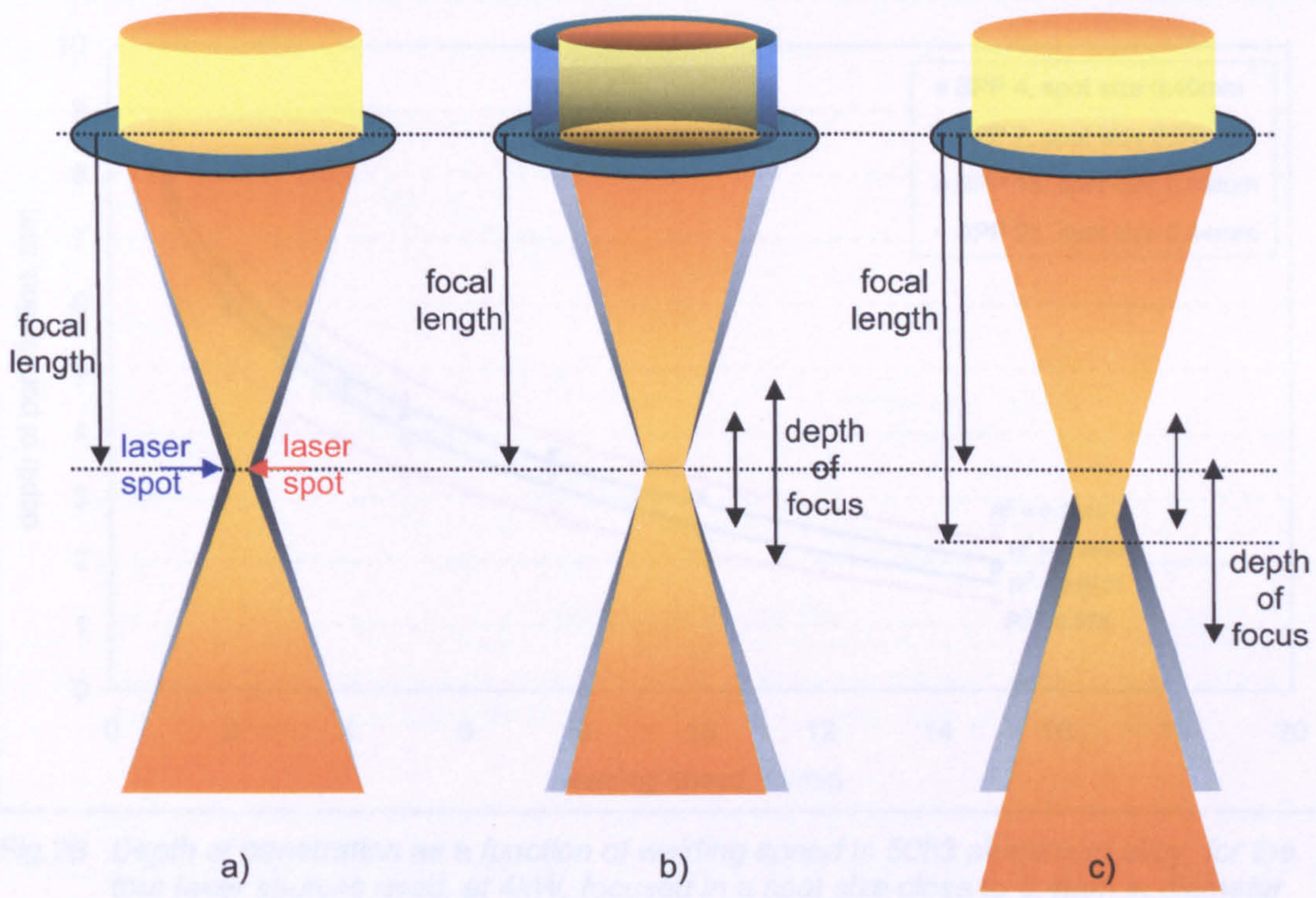

Fig.27 Practical implications of an improvement in laser beam quality (in yellow)

6.5. WELD ANALYSIS

The thickness of the tapered sample was measured at those points at which full penetration was achieved and these thickness values were used to construct the welding performance graphs, as discussed in Section 6.4. Metallographic sections were taken and prepared in the same way as for the thin-section trials (Section 5.5).

6.6. RESULTS AND DISCUSSION

The performance curves in Fig.28 show the depth of penetration against the welding speed obtained using the four available laser sources focused in a spot size close to 0.4mm in diameter. The four curves thus represent the performance of the four different beam qualities, i.e., BPPs, and all show a similar trend at both low and high welding speeds. The closer the *coefficient of determination* (i.e., R^2 values, next to each of the curves in Fig.28) is to unity, the better the (logarithmic) trend line fits the data points. The points used to construct the performance curves are average values of two, and in some cases three, measurements of depth of penetration. The consistency of the measured values is given by the error bars in Fig.28, which in all cases was lower than 4% of the values shown in Fig.28.

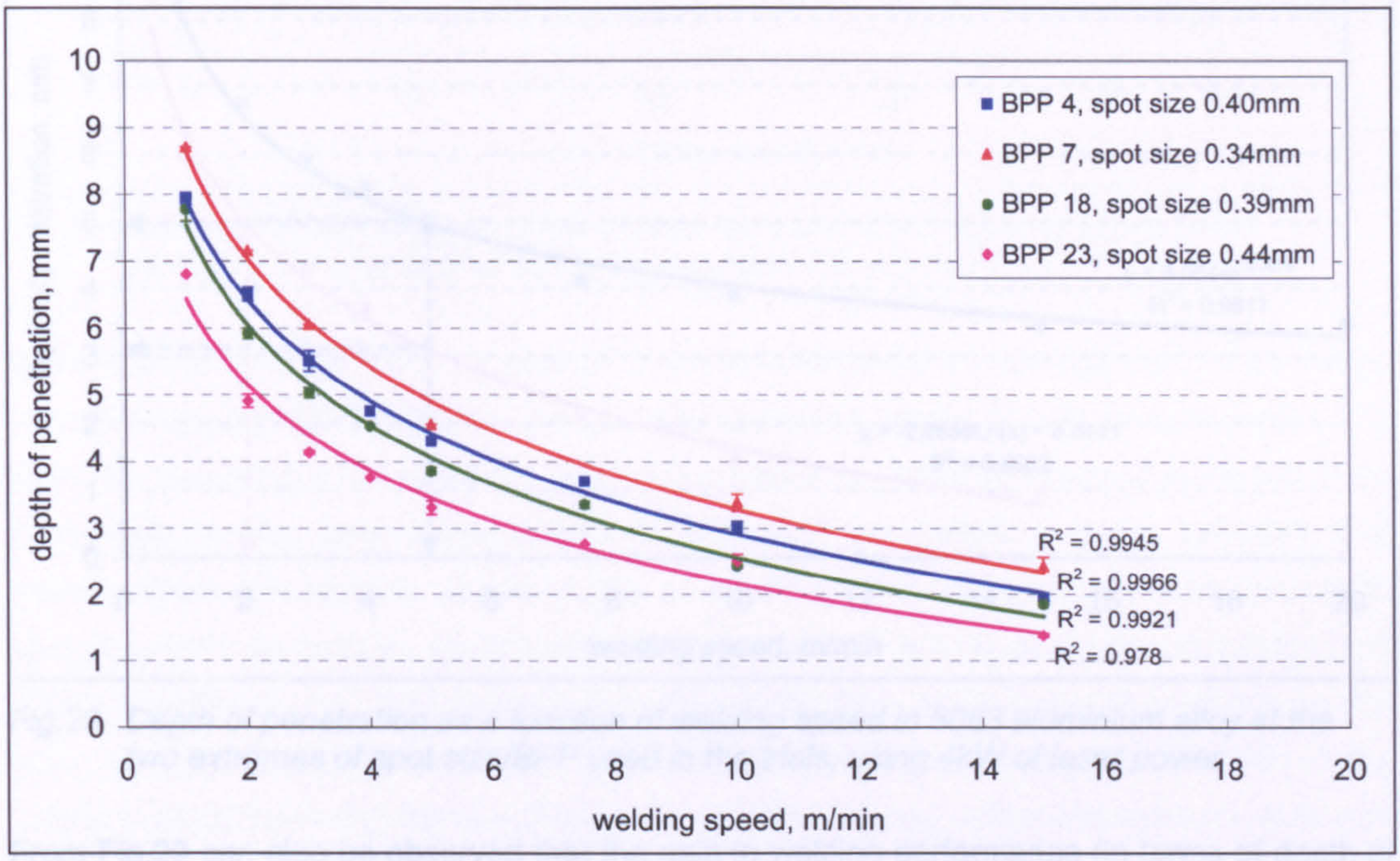

Fig.28 Depth of penetration as a function of welding speed in 5083 aluminium alloy, for the four laser sources used, at 4kW, focused in a spot size close to 0.4mm in diameter

The lowest welding performance in terms of depth of penetration, for a given welding speed at a laser power of 4kW, was recorded for the 23mm.mrad LP Nd:YAG laser, followed by that of the 18mm.mrad Yb-fibre laser and that of the 4mm.mrad Yb-fibre laser. Based on these three curves, an increasing welding performance for aluminium can be concluded with an increasing laser beam quality (decreasing BPP). However, the performance curve recorded for the 7mm.mrad Yb-YAG disc laser was higher than that of the 4mm.mrad Yb-fibre laser. Considering the consistency in measurements recorded for these two laser systems, which on average was between 2 and 3% of the values shown in Fig.28, the average difference of 12% between the 7mm.mrad and the 4mm.mrad curves cannot be assumed negligible. This improved welding performance (depth of penetration) is the result of a 38% increase in power density, because of the smaller spot size used, i.e. 0.34mm compared with 0.40mm.

The curves in Fig.29 show the depth of penetration against the welding speed for the two extremes of BBP / spot size used in these trials. The advantage of a smaller spot / smaller BPP in terms of achieving a larger depth of penetration is obvious from the two curves. For example, at a welding speed of 5m/min, the 4mm.mrad Yb-fibre laser focused in a 0.14mm spot offered a 60% increase in depth of penetration, from 3mm to 5mm, over that achieved using the 23mm.mrad LP Nd:YAG focused in a 0.61mm spot. Or, for a given depth of penetration of 5mm, the 4mm.mrad Yb-fibre provided a 2.5-fold increase in welding speed, over that achieved using the 23mm.mrad LP Nd:YAG laser.

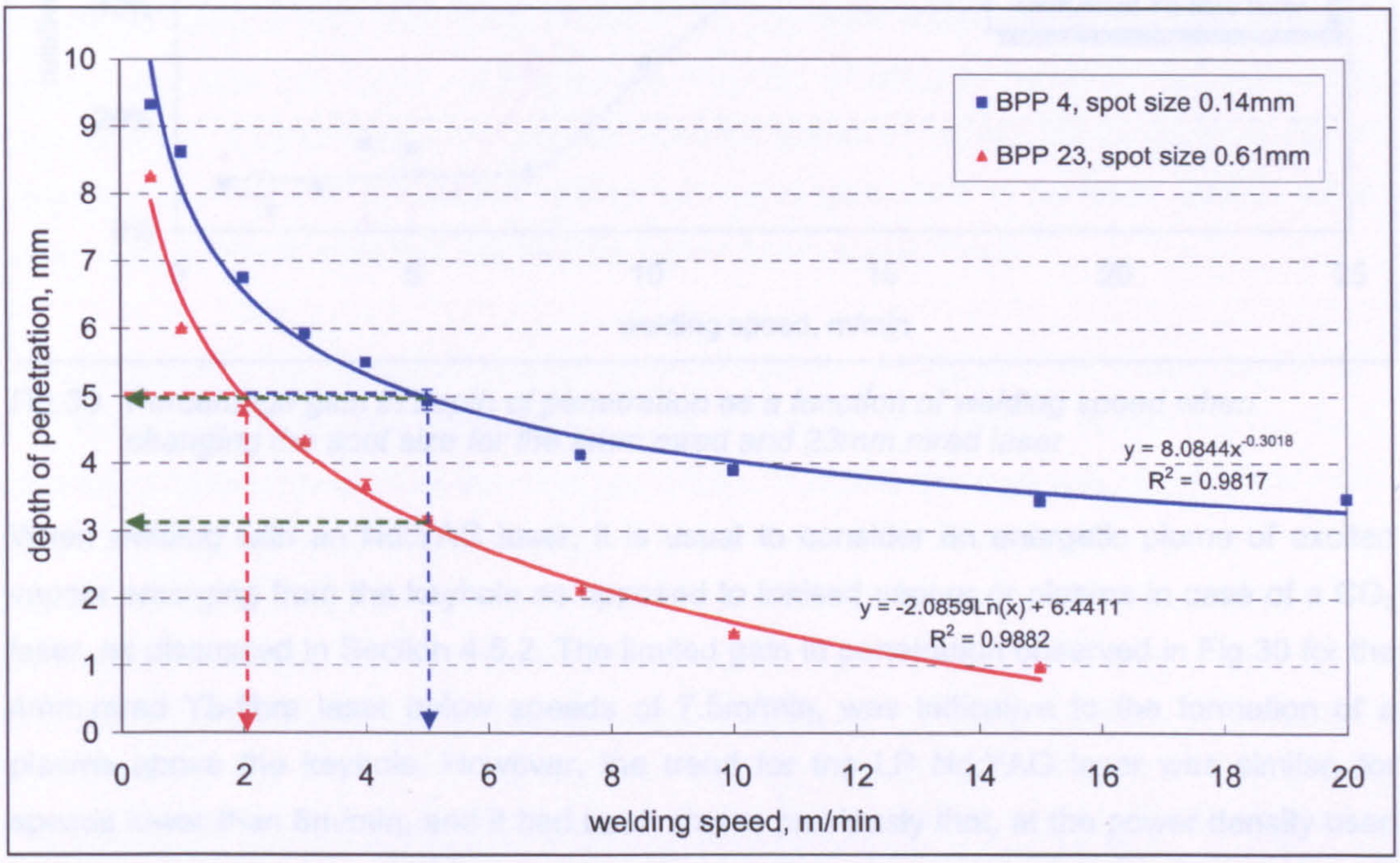

Fig.29 Depth of penetration as a function of welding speed in 5083 aluminium alloy at the two extremes of spot size/BPP used in the trials, using 4kW of laser power

From Fig.29 can also be observed that the gain in welding performance (in terms of depth of penetration) between the two extremes of BBP / spot size used in these experiments, increased as the welding speed increased, with a gain of 45% and 95% at a welding speed of 1m/min and 7.5m/min, respectively. The relative increase in depth of penetration, as a function of welding speed, when changing from a 0.4mm to a 0.14mm spot size, for the 4mm.mrad Yb-fibre laser, and from a 0.61mm to a 0.44mm spot size for the 23mm.mrad LP Nd:YAG laser, is shown in Fig.30. For the 4mm.mrad Yb-fibre laser, the gain in penetration was limited to less than 10% for welding speeds lower than 7.5m/min, but increased sharply, and linearly, above this speed. For the 23mm.mrad LP Nd:YAG laser, the same trend was observed, albeit with the inflection point at a lower welding speed of around 6m/min.

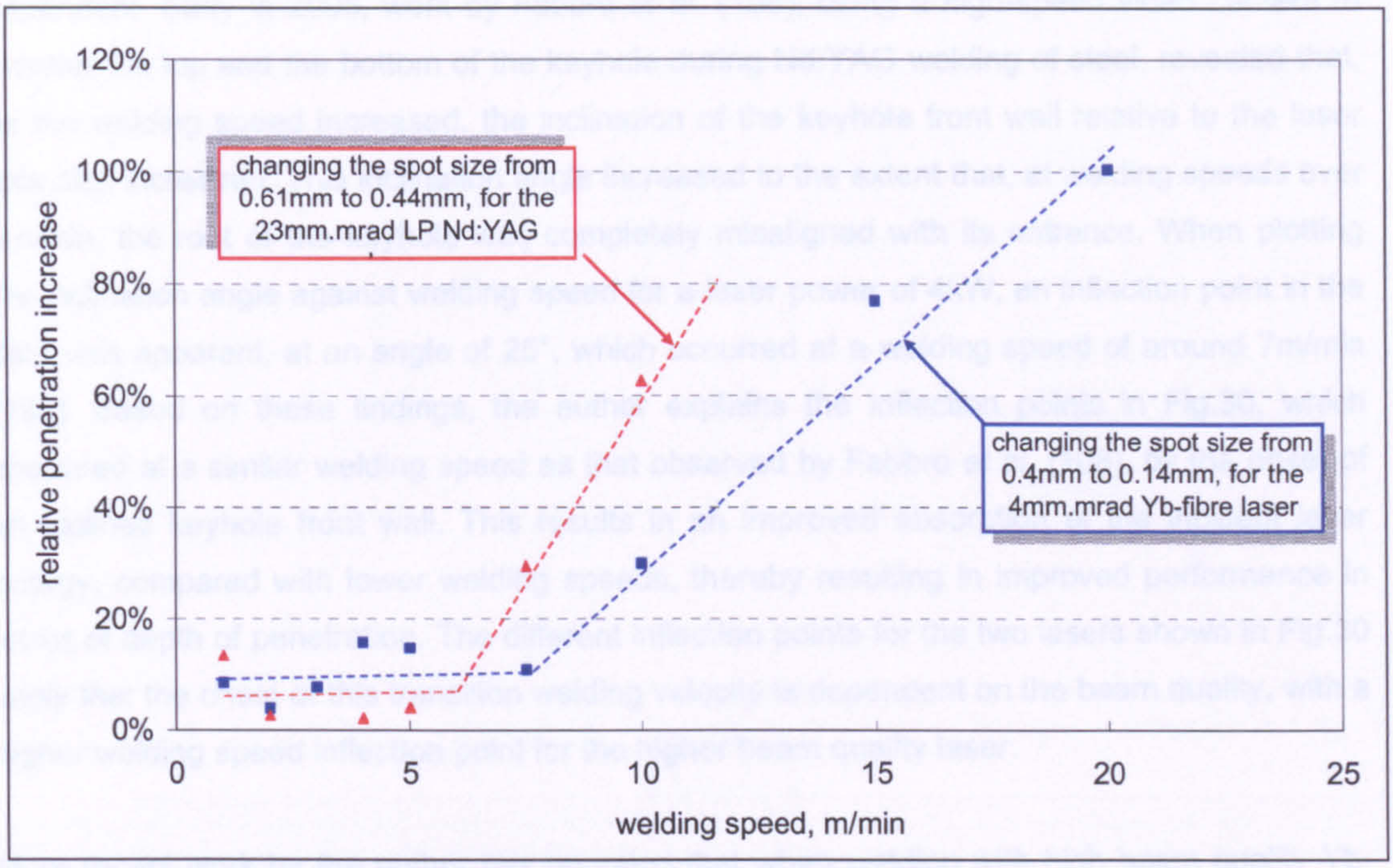

Fig.30 Percentage gain in depth of penetration as a function of welding speed when changing the spot size for the 4mm.mrad and 23mm.mrad laser

When welding with an Nd:YAG laser, it is usual to consider an energetic plume of excited vapour emerging from the keyhole as opposed to ionised vapour or plasma in case of a CO_2 laser, as discussed in Section 4.5.2. The limited gain in penetration observed in Fig.30 for the 4mm.mrad Yb-fibre laser below speeds of 7.5m/min, was indicative to the formation of a plasma above the keyhole. However, the trend for the LP Nd:YAG laser was similar, for speeds lower than 6m/min, and it had been shown previously that, at the power density used in this experiment, i.e., 4kW focused in a 0.4mm diameter spot, a plasma was not present when welding with an Nd:YAG laser (56-58). This was observed for steel, but also during pulsed Nd:YAG laser welding of a 5000-series aluminium alloy, with measurements of plasma temperatures and densities revealing a plume, not a plasma (56). Based on this, the author questions if the presence of a plasma above the keyhole at this power density, could be the reason for the sharp increases observed in Fig.30 for both lasers. In contrast, spectrometry of vapour emission during the laser welding of a 5000-series aluminium using a 2mm.mrad Yb-fibre laser at 4kW, revealed a plasma, which was not present when using a 25mm.mrad LP Nd:YAG laser at the same power (135). However, the author comments that this comparison was irrelevant, as the spot size in case of the Nd:YAG laser was four times larger than that used with the Yb-fibre laser, i.e., 0.5mm instead of 125µm. Based on this and his own findings, the author recommends further spectroscopic studies of the vapour emission to confirm the presence/absence of a plasma above the keyhole when welding with high-brightness (Nd:YAG wavelength) lasers at various power densities.

As mentioned in Section 4.5 (page 28), earlier research had shown that during laser welding, the keyhole tip inclined away from the welding direction and that this inclination was speed-

dependent. Early in 2006, work by Fabbro *et al.* (108), using a high-speed video camera to monitor the top and the bottom of the keyhole during Nd:YAG welding of steel, revealed that, as the welding speed increased, the inclination of the keyhole front wall relative to the laser axis also increased. This inclination angle increased to the extent that, at welding speeds over 8m/min, the root of the keyhole was completely misaligned with its entrance. When plotting the inclination angle against welding speed for a laser power of 4kW, an inflection point in the data was apparent, at an angle of 25°, which occurred at a welding speed of around 7m/min (108). Based on these findings, the author explains the inflection points in Fig.30, which appeared at a similar welding speed as that observed by Fabbro *et al.* (108), by the onset of an inclined keyhole front wall. This results in an improved absorption of the incident laser energy, compared with lower welding speeds, thereby resulting in improved performance in terms of depth of penetration. The different inflection points for the two lasers shown in Fig.30 imply that the onset of this transition welding velocity is dependent on the beam quality, with a higher welding speed inflection point for the higher beam quality laser.

More recent work by the author has revealed that when welding with high beam quality Yb-fibre laser beams, *thermal convection* occurs in the air immediately above and up to a distance of 300mm away from the weld pool (136). This phenomenon was observed for both steel and aluminium at welding speeds below 8m/min and compromised the welding performance. The author considers that the thermal convection causes (Mie) scattering of the incident laser energy, which results in a reduced depth of penetration. Similar observations have since been reported by other researchers, with the possibility of dispersing this region of thermal convection above the weld pool by applying a low-pressure curtain of inert gas to improve the welding performance (135). This is a new phenomenon in laser processing which results from the superior laser beam quality that up to now could not be achieved for fibre-delivered lasers. Further investigation into this phenomenon and how to eliminate it efficiently to maximise welding performance in a production environment is required.

A significant welding speed dependence is observed from Fig.31, which shows the depth of penetration obtained for all seven combinations of BPP / spot size used, plotted against the inverse of the spot size, for three different welding speeds of 1, 5 and 15m/min. The inverse of the spot size was used to allow integer numbers in the X-axis of the plot. Up to a value of $3mm^{-1}$, the data points show a linear behaviour, with a steeper slope as the welding speed reduces, and a significant change in the slope of these curves, for all three welding speeds, beyond this ($3mm^{-1}$) point. In this work, at a welding speed of 1m/min, no additional gain in depth of penetration was observed for a spot size smaller than 0.33mm in diameter, i.e., 1/spot of $3mm^{-1}$. A similar trend was observed for 5 and 15m/min, with the inflection points still clear at $3mm^{-1}$, but with small increases in depth of penetration recorded at these welding speeds beyond this point. This means that, under the processing conditions used here, little or no gain in depth of penetration was achieved by focussing the 4kW laser power into a spot smaller than 0.33mm in diameter.

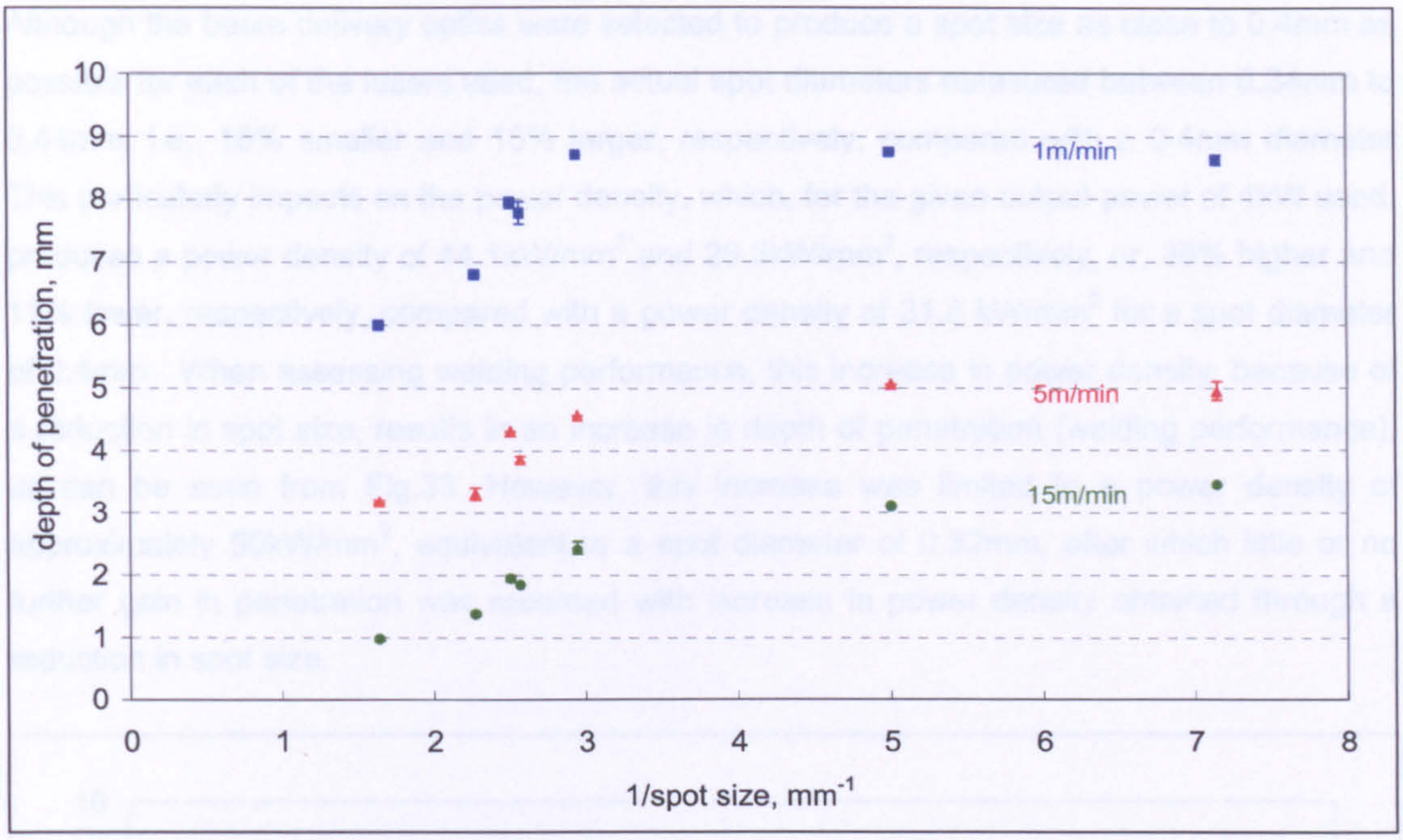

Fig.31 Depth of penetration achieved in 5083 aluminium alloy using 4kW of laser power vs. the inverse of the spot size, for a welding speed of 1, 5 and 15m/min

This is in line with findings by Weberpals *et al.* (137) who observed an inflection point at around 0.2mm (spot diameter) when welding steel and aluminium using a 4kW Yb-YAG disc laser focused in various spot sizes at welding speeds of 5 and 10m/min. Weberpals *et al.* (137) concluded that the change in divergence angle of the focused beam of the Yb-YAG disc laser was the reason for this abrupt change in welding performance. However, the results of this work could not confirm this explicitly, with no clear relationship obvious when plotting depth of penetration against divergence angle, Fig.32, but a declining trend apparent.

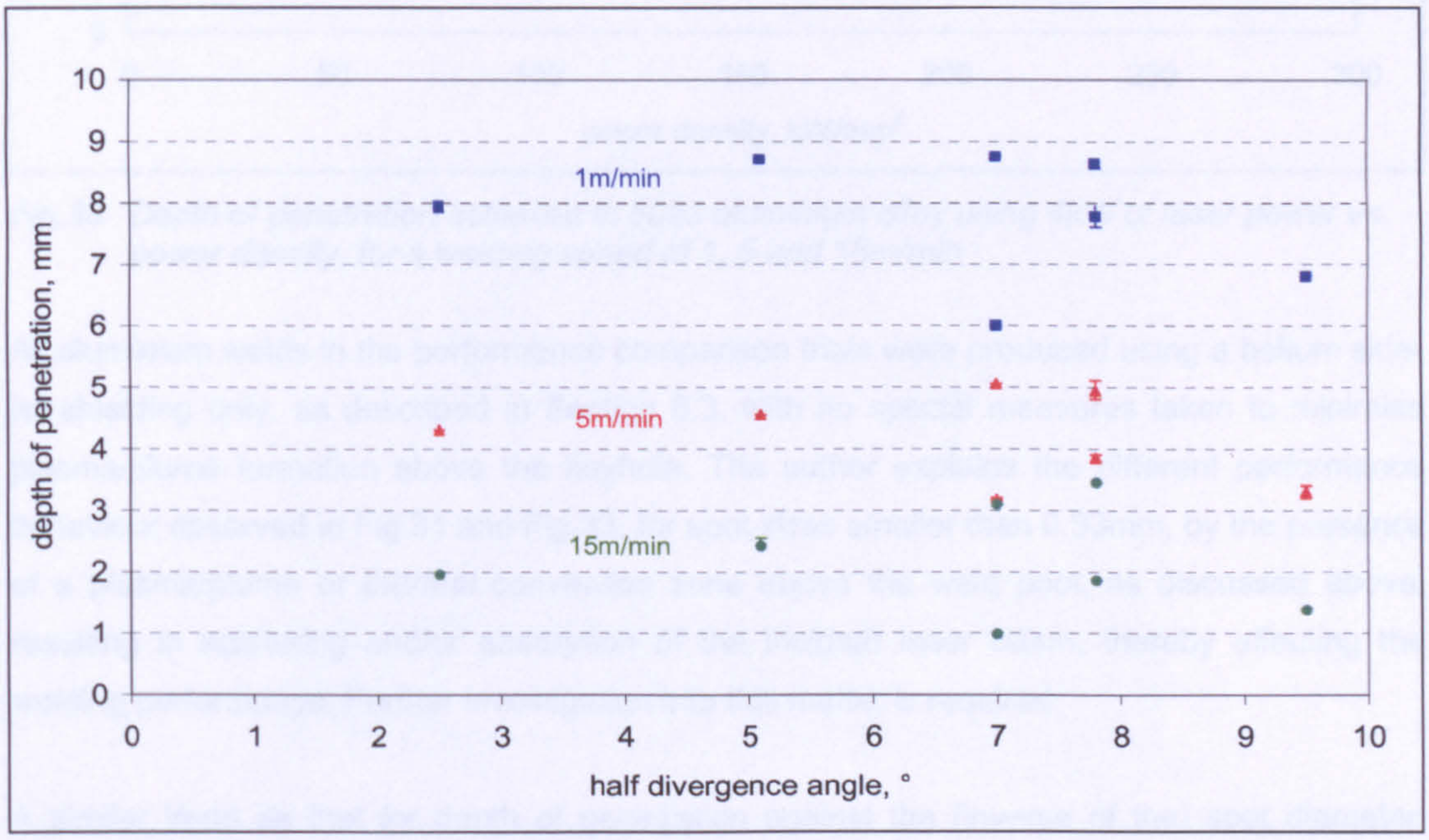

Fig.32 Depth of penetration achieved in 5083 aluminium alloy using 4kW of laser power vs. the half divergence angle of the beam, for a welding speed of 1, 5 and 15m/min

Although the beam delivery optics were selected to produce a spot size as close to 0.4mm as possible for each of the lasers used, the actual spot diameters measured between 0.34mm to 0.44mm, i.e., 15% smaller and 10% larger, respectively, compared with a 0.4mm diameter This particularly impacts on the power density, which, for the given output power of 4kW used, produces a power density of 44.1kW/mm^2 and 26.3kW/mm^2, respectively, or, 38% higher and 17% lower, respectively, compared with a power density of 31.8 kW/mm^2 for a spot diameter of 0.4mm. When assessing welding performance, this increase in power density, because of a reduction in spot size, results in an increase in depth of penetration (welding performance), as can be seen from Fig.33. However, this increase was limited to a power density of approximately 50kW/mm^2, equivalent to a spot diameter of 0.32mm, after which little or no further gain in penetration was recorded with increase in power density obtained through a reduction in spot size.

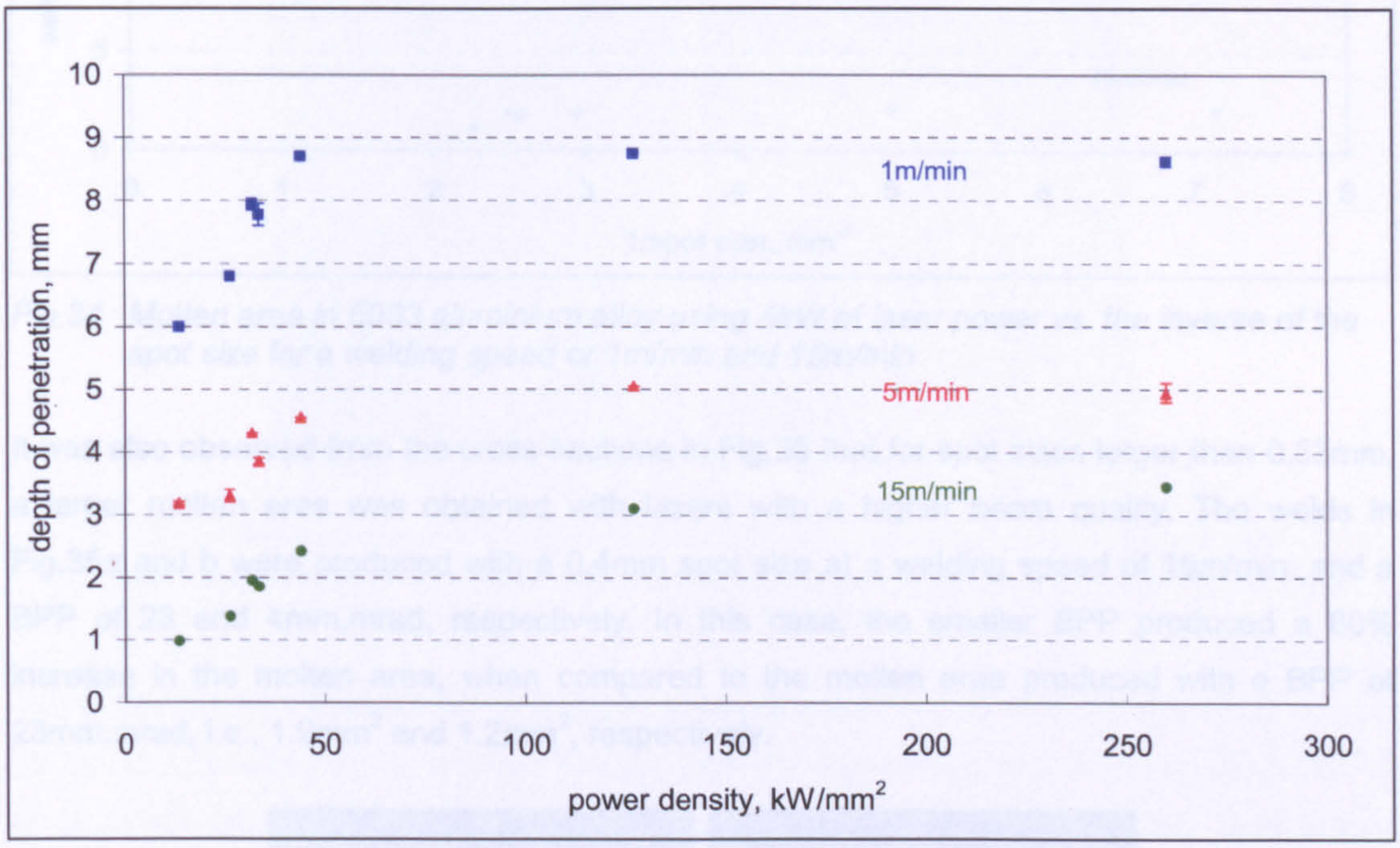

Fig.33 Depth of penetration achieved in 5083 aluminium alloy using 4kW of laser power vs. power density, for a welding speed of 1, 5 and 15m/min

All aluminium welds in the performance comparison trials were produced using a helium side-jet shielding only, as described in Section 6.3, with no special measures taken to minimise plasma/plume formation above the keyhole. The author explains the different performance behaviour observed in Fig.31 and Fig.33, for spot sizes smaller than 0.33mm, by the presence of a plasma/plume or *thermal convection* zone above the weld pool, as discussed above, resulting in scattering and/or absorption of the incident laser beam, thereby affecting the welding performance. Further investigation into this matter is required.

A similar trend as that for depth of penetration against the (inverse of the) spot diameter, Fig.31, and power density, Fig.33, can be observed when plotting the molten area of the welds against the inverse of the spot diameter, as shown in Fig.34 for a welding speed of 1

and 15m/min. The molten area of the welds was measured from the cross-sections using AutoCAD software. For spot sizes larger than 0.33mm, the molten area increased linearly with a decreasing spot size.

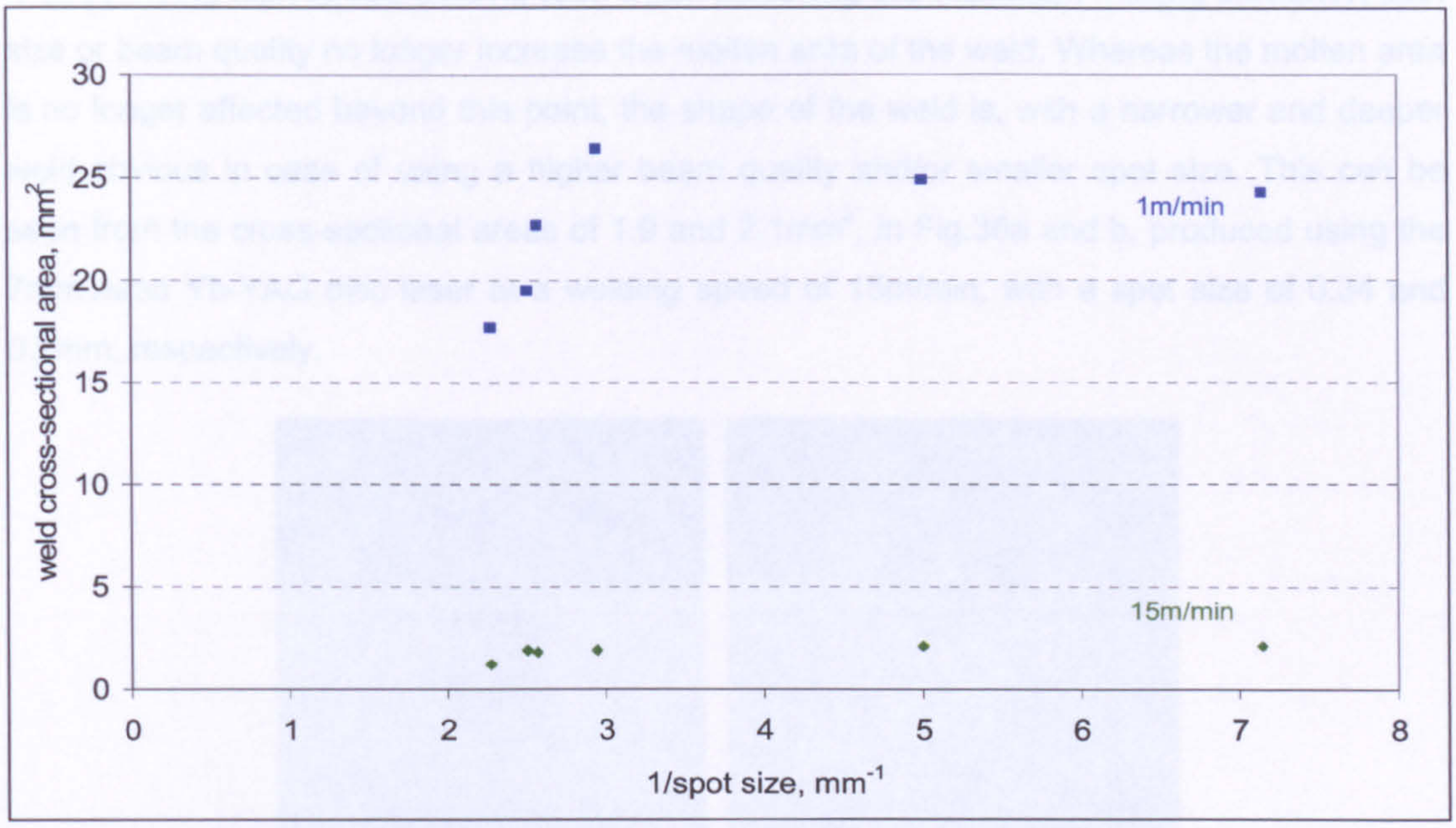

Fig.34 Molten area in 5083 aluminium alloy using 4kW of laser power vs. the inverse of the spot size for a welding speed or 1m/min and 15m/min

It was also observed from the cross-sections in Fig.35 that for spot sizes larger than 0.33mm, a larger molten area was obtained with lasers with a higher beam quality. The welds in Fig.35a and b were produced with a 0.4mm spot size at a welding speed of 15m/min, and a BPP of 23 and 4mm.mrad, respectively. In this case, the smaller BPP produced a 60% increase in the molten area, when compared to the molten area produced with a BPP of 23mm.mrad, i.e., 1.9mm^2 and 1.2mm^2, respectively.

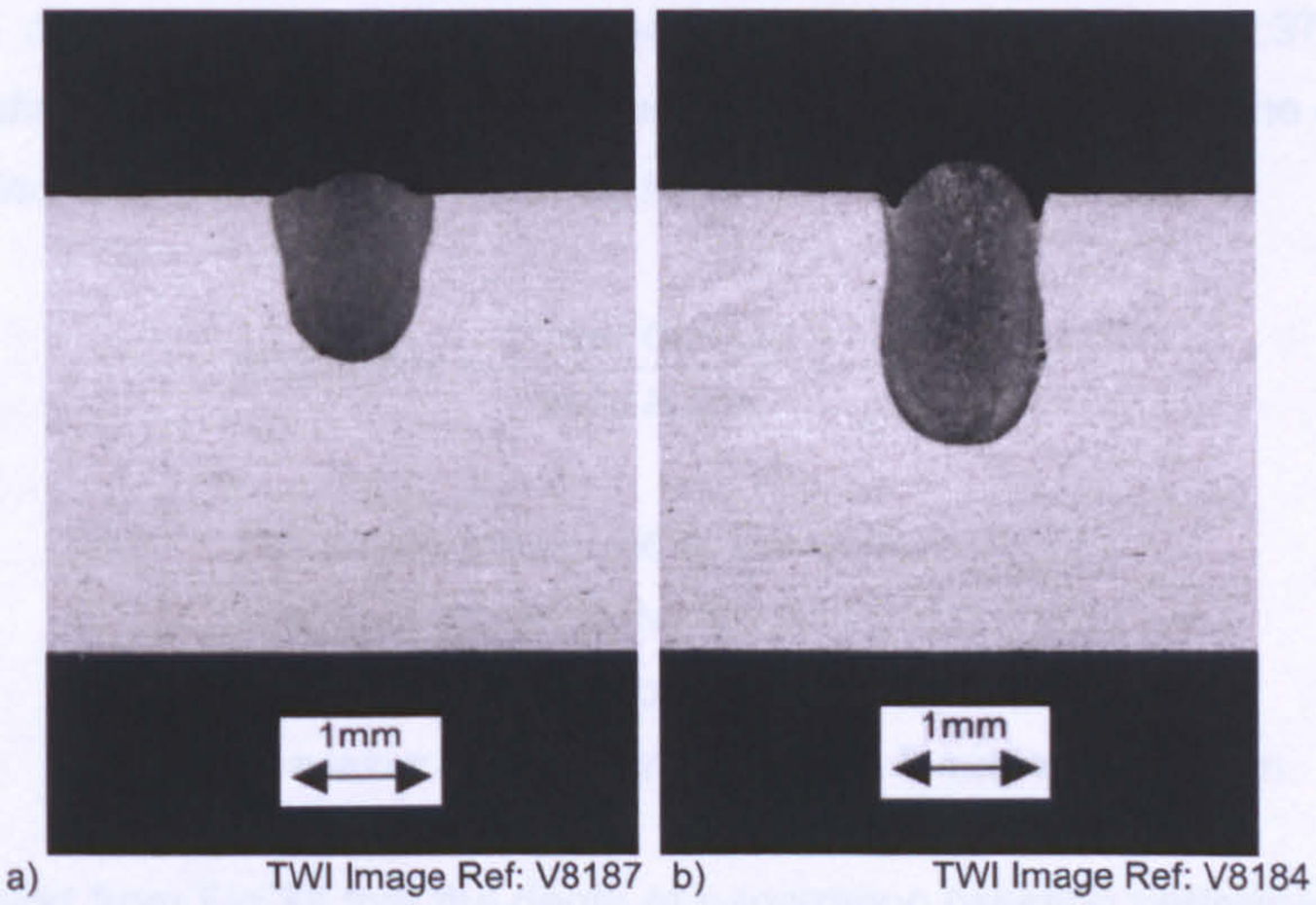

a) TWI Image Ref: V8187 b) TWI Image Ref: V8184

Fig.35 Cross-sections of two welds made in 5083 aluminium alloy using 4kW of laser power focused in a laser spot of 0.4mm in diameter at a welding speed of 15m/min, using a laser with BPP of 23mm.mrad (a) and 4 mm.mrad (b)

However, the molten area did not increase further for spot sizes smaller than 0.33mm, Fig.34, indicating that the maximum melting efficiency was achieved. It was shown by Rykalin, and later by Swift-Hook and Gick, that a theoretical maximum of 48% of the absorbed laser energy is used during high-speed welding (56). Upon achieving this maximum melting efficiency, spot size or beam quality no longer increase the molten area of the weld. Whereas the molten area is no longer affected beyond this point, the shape of the weld is, with a narrower and deeper weld obvious in case of using a higher beam quality and/or smaller spot size. This can be seen from the cross-sectional areas of 1.9 and 2.1mm^2, in Fig.36a and b, produced using the 7mm.mrad Yb-YAG disc laser at a welding speed of 15m/min, with a spot size of 0.34 and 0.2mm, respectively.

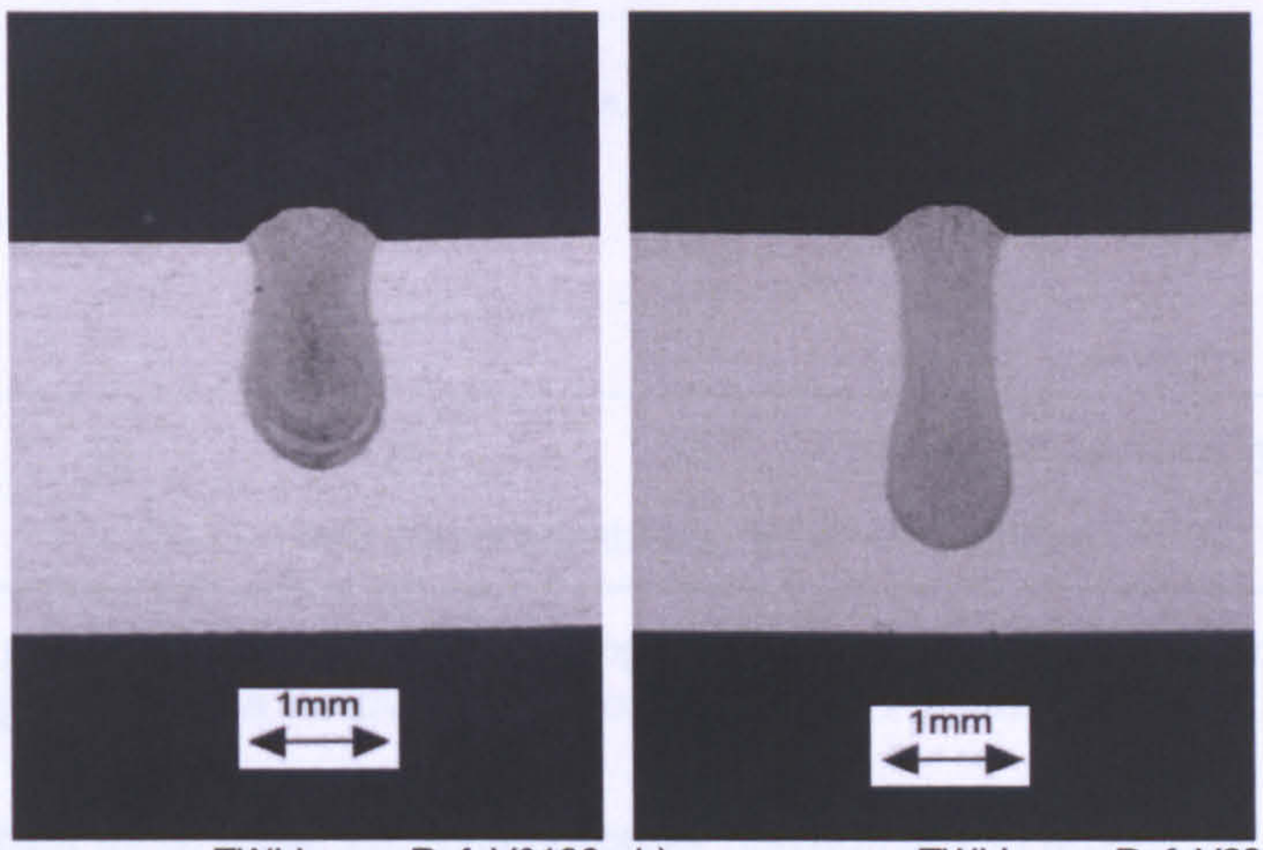

a) TWI Image Ref: V8193 b) TWI Image Ref: V8394

Fig.36 Cross-sections of two welds made in 5083 aluminium alloy using a 7mm.mrad Yb-YAG disc laser at a laser power of 4kW at a welding speed of 15m/min, using a spot size of 0.34mm (a) and 0.2mm (b) in diameter

The welding performance data for each of the seven combinations of BPP / spot size, against the *beam brightness* of the focused beams used, for the welding of aluminium using 4kW of laser power at a welding speed of 1, 5 and 15m/min, is shown in Fig.37. *Laser beam brightness* is defined as the available power density per solid angle in the cone of the focusing beam, i.e., the *included solid angle*, measured in W/mm^2.sterad (Equation 2).

$$\text{Brightness} = \frac{\text{power density}}{\text{solid angle}} = \frac{P.F^2.4}{\pi^2.\omega_0^2.D^2} \qquad \text{[Equation 2]}$$

with P = power measured at the workpiece, W
F = focal length of the focussing lens, mm
ω_0 = laser beam spot radius, mm
D = laser beam aperture (at the focusing lens), mm

It can be observed from Fig.37 that the depth of penetration (welding performance) increases with increasing laser beam brightness, for all three welding speeds, but that the degree in

performance increase drops as brightness increases, and even reverses for the highest brightness laser system used in these trials.

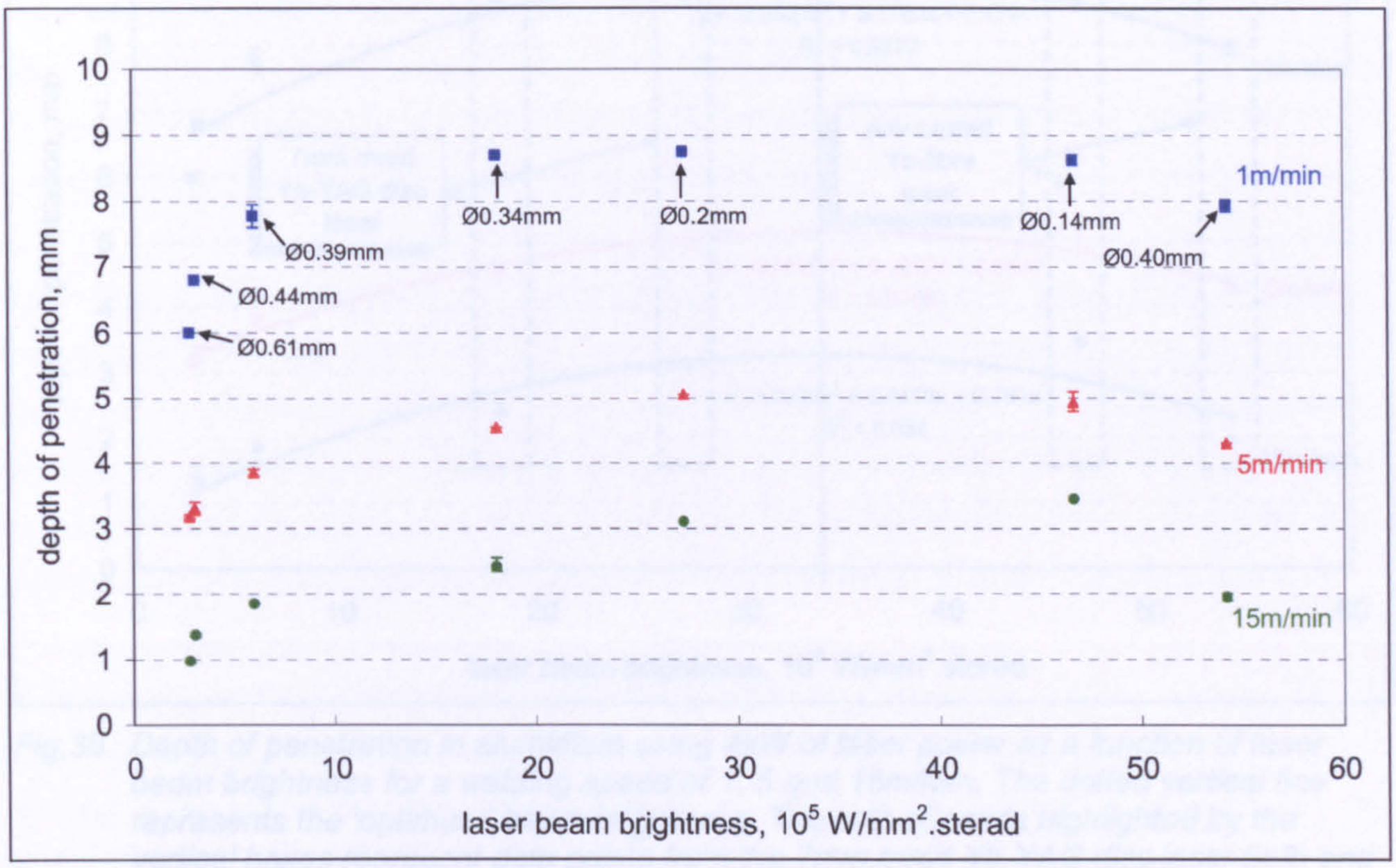

Fig.37 Depth of penetration in aluminium using 4kW of laser power as a function of laser beam brightness for a welding speed of 1, 5 and 15m/min.

When fitting the best trend lines, i.e. second-order polynomials in MS Excel, through the data points, as in Fig.38, it can be observed that the depth of penetration increases up to a brightness of $33x10^5$ W/mm^2.sterad, after which the depth of penetration decreases, regardless of welding speed. This level is further referred to as the *optimum beam brightness* for welding aluminium using a laser power of 4kW at a welding speed between 1 and 15m/min, beyond which the welding performance (in terms of depth of penetration) cannot be improved upon by changing laser source (beam quality) and/or focussing optics.

It is noteworthy, that the same decline in welding performance (depth of penetration) for the higher values of beam brightness, as seen in Fig.37 and Fig.38 for aluminium, was also observed from the results of a similar set of welding experiments carried out on steel. This work is not reported here, but for the welding of steel, an *optimum beam brightness* was observed that varied slightly for the different welding speeds investigated, between 32 and $38x10^5$W/mm^2.sterad.

However, the author points out that the behaviour in Fig.37 and Fig.38 is currently based only on one set of data points, and suggests further trials to confirm whether the depth of penetration for the higher beam brightness values reduces, or remains constant. Moreover, it could be argued that the coefficients of determination (R^2-value) for the best-fitting trend lines in Fig.38 are relatively low for 1m/min and 15m/min welding speed.

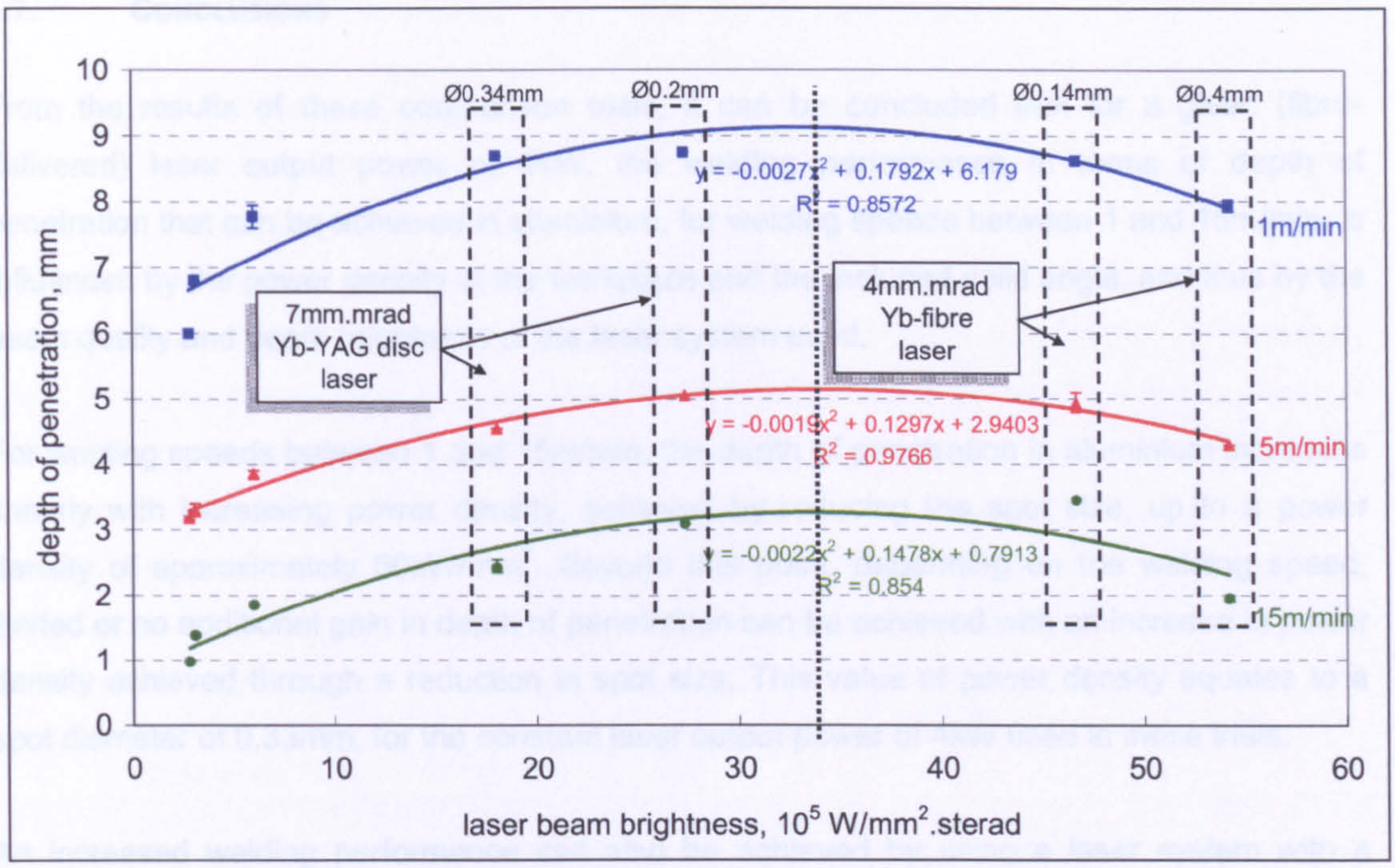

Fig.38 Depth of penetration in aluminium using 4kW of laser power as a function of laser beam brightness for a welding speed of 1, 5 and 15m/min. The dotted vertical line represents the 'optimum' beam brightness. The sets of points highlighted by the vertical boxes represent data points from the 7mm.mrad Yb-YAG disc laser (left) and the 4mm.mrad Yb-fibre laser (right), both at a spot size of 0.4mm.

Notwithstanding this, when comparing the data points in Fig.33 with those in Fig.37, the fact remains that the trends of the brightness curves (Fig.37) are different from the power density curves (Fig.33). As brightness incorporates power density (Equation 2 on page 76), the author concludes that the included solid angle, as well as the power density, has an effect on the welding performance.

The included solid angle determines the power density immediately above the weld pool and for the smaller included solid angles, i.e., those systems with the higher beam brightness values produced using the larger focal length focussing lenses, this power density above the weld pool may reach values sufficiently high to create a plasma, which obstructs the laser power from entering the keyhole by either reflection or absorption. More recent trials by the author, not reported here, support this conclusion. However, further work should focus on repeating the above trials, using identical power density values, to quantify the (individual) influence of included solid angle on welding performance. This could be accomplished, for instance, by changing the beam delivery optics to ones that produce a spot diameter of 0.4mm precisely, which, in practice, is difficult and/or expensive to realise. An easier approach is to change the laser output power for the beam delivery optics used in the above trials. However, in this case, a difference in keyhole and weld pool geometry, and beam interaction time with the material, resulting from the difference in spot diameter, albeit small, should also be considered.

6.7. CONCLUSIONS

From the results of these comparison trials, it can be concluded that for a given (fibre-delivered) laser output power of 4kW, the welding performance in terms of depth of penetration that can be achieved in aluminium, for welding speeds between 1 and 15m/min, is influenced by the power density at the workpiece and the included solid angle, and thus by the beam quality and beam brightness of the laser system used.

For welding speeds between 1 and 15m/min, the depth of penetration in aluminium increases linearly with increasing power density, achieved by reducing the spot size, up to a power density of approximately 50kW/mm^2. Beyond this point, depending on the welding speed, limited or no additional gain in depth of penetration can be achieved with an increase in power density achieved through a reduction in spot size. This value of power density equates to a spot diameter of 0.33mm, for the constant laser output power of 4kW used in these trials.

An increased welding performance can also be achieved by using a laser system with a higher beam quality, although such an increase is not linear. High beam quality lasers allow the use of long focal length focussing optics, which give small included solid angles. In combination with power density, the solid angle determines the beam brightness of a laser system. For welding speeds ranging from 1 to 15m/min, the welding performance (in terms of penetration) in aluminium increases with increasing laser beam brightness, up to a maximum performance at a brightness of around 33×10^5W/mm^2.sterad. Beyond this 'optimum' brightness, which is independent of welding speed and material, the degree in performance increase drops as brightness increases, and even reverses in case of the higher beam brightness values.

Being the first of its kind for fibre-delivered lasers, this research requires further work to investigate some of the phenomena reported here. In particular, the changes of welding performance associated with power densities higher than 50kW/mm^2 (obtained by spot diameters smaller than 0.33mm) and beam brightnesses beyond the reported 'optimum' value. Particular focus hereby should be on a study of the absorption/scattering of the laser energy by a plasma suspected to form above the weld pool during laser welding, the presence of this plasma in relation to the power density and included solid angle of the focusing system used, the behaviour of the keyhole (and the inclination of the keyhole front wall in particular) and the thermal disturbances observed at up to 300mm above the weld pool.

7. THICK-SECTION TRIALS

In the final part of this EngD research work, thick-section trials were carried out on a 12.7mm thickness aluminium alloy that was developed specifically for the manufacture of upper wing structures. In this thickness of aluminium, the keyhole behaviour can become unstable, resulting in cavities and coarse porosity in the weld (see Section 4.5). Trials were carried out to assess the effect of alloy composition, oxide removal, welding process (i.e., autogenous laser versus hybrid laser-MIG), laser spot diameter and welding speed, on the occurrence of such keyhole-induced porosity. Additional trials aimed at reducing the total level of weld metal porosity, including fine porosity (Section 4.4), for both autogenous laser and hybrid laser-MIG welding, by using the knowledge gained from the thin-section trials (Section 5). Full details of the thick-section trials are described in EngD Submission 7 (46) and summarised in the following sections.

7.1. MATERIAL

The thick-section welding trials were performed on a proprietary 7000-series Al-Zn-Mg-Cu aluminium alloy supplied in a proprietary temper, further referred to as the *7xxx aluminium alloy*. The alloy was specifically developed for use in compression-dominated aircraft components, such as upper wing structures, providing advantages over conventionally used 7150 (Table 1) alloy in terms of compressive and tensile strengths, whilst offering similar fracture toughness and corrosion resistant properties (46). The material is highly formable, with a higher resistance to stress corrosion cracking and reduced manufacturing cost compared with the 7075 alloy (4). The alloy was selected because it is currently being considered for the manufacture of aluminium wing structures (46). A limited number of trials was also carried out on 12.7mm thickness 2024 and 2519 aluminium alloy (Table 1), supplied in the annealed condition, to investigate the influence of alloy composition on laser weld quality, and on the presence of cavities and coarse porosity in particular. All material was cold band-sawn into samples 75mm wide and 300mm long.

7.2. EQUIPMENT

Both the autogenous laser and the hybrid Yb-fibre laser-MIG trials were carried out using a 7kW Yb-fibre laser (YLR-7000). The reader is referred to Section 4.6.6 for more information about hybrid laser-arc welding. The laser power was transmitted from the YLR-7000 laser source, via a 300µm diameter, single optical fibre, into the processing head. Two processing heads were used, producing a laser spot diameter of 0.6mm and 0.4mm. For a more detailed description of the YLR-7000 Yb-fibre laser and its beam delivery used for these trials, the reader is referred to EngD Submissions 5 (31) and 6 (45).

For the hybrid Yb-fibre laser-MIG welding trials, an ESAB AristoMIG 450 synergic MIG welding set was used, equipped with a standard PSF 410MW MIG torch and an AristoFeed

30 (MA6) wire feeder and controller. The set-up and conditions used, i.e., the MIG arc trailing the laser, a 2mm process separation between the laser and MIG wire impingement point (on the material surface) and a 16mm contact-tip-to-workpiece distance, were chosen, based on the author's prior experience with hybrid laser-MIG/MAG welding (123,138), to provide improved process stability over a hybrid configuration with the MIG arc leading, or with the laser and MIG wire positioned in the same point on the material surface. Further in this document, unless otherwise stated, when hybrid welding is mentioned, this refers to hybrid Yb-fibre laser-MIG welding.

7.3. SET-UP

All thick-section trials were carried out with the beam focused on the material surface, using 7kW of laser power (measured at the workpiece). This level of laser power was selected to fully penetrate the 12.7mm thickness samples, in a single pass, at the highest welding speed possible. The high speed was essential to minimise the heat input and therefore thermal damage, which is inevitable when fusion welding heat-treatable alloys, such as the 7xxx alloy (see Section 4.3.2).

The protection of the processing head and the clamping of the samples were achieved in the same way as for the thin-section and performance comparison trials (see Section 5.3). Further details of the set-up for the thick-section trials, were as follows.

- For the hybrid welding trials, a 1.2mm diameter 5556A filler wire was used (Table 1). This high-strength wire was selected, because it is one of the commercially available wires recommended for use when fusion welding 7000-series alloys (48).
- Industrial grade argon and helium were both evaluated to shield the top and underside of the weld bead (125). As observed in earlier trials, detailed in EngD Submission 6 (45), a coaxial shielding arrangement was not effective in preventing spatter from damaging the cover slide/focussing optics when using 7kW in laser power for welding 12.7mm thickness aluminium. Top-bead shielding was supplied through a side-jet shielding arrangement positioned behind the laser beam at an angle of 30° with the laser axis (42,59). This comprised either a 4mm internal diameter copper tube, as used for the thin-section trials, shown in Fig.16 on page 45, or a 16mm internal diameter PSF 410 MW MIG shroud, Fig.39. The exact position of the side-jet shielding arrangement with respect to the material surface and the shielding gas flow rates were varied to maximise the weld pool support (see further in Section 7.6.1). The under-bead shielding was supplied through a 10mm deep channel in the jigging arrangement.

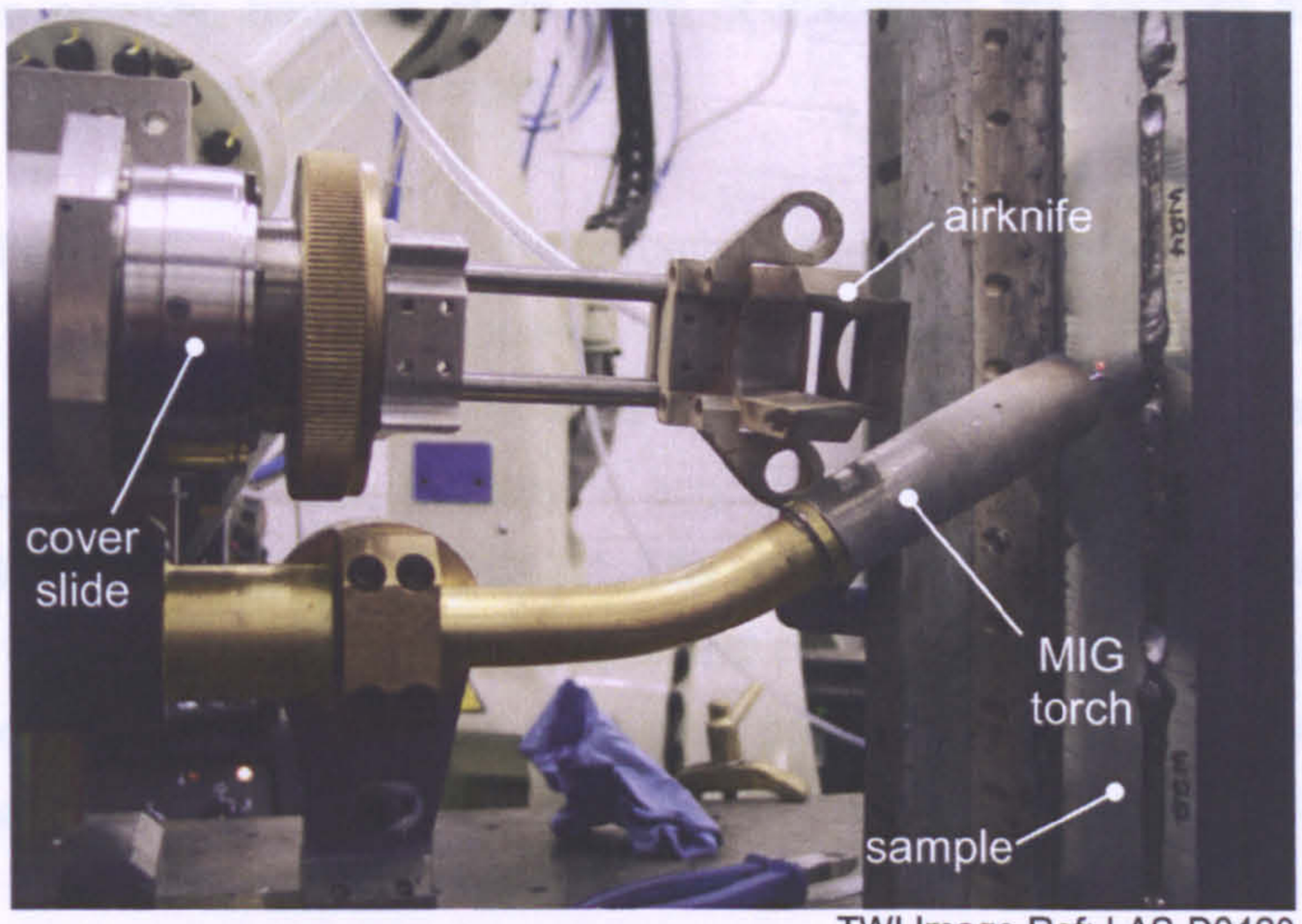

TWI Image Ref: LAS-D0420

Fig.39 Welding arrangement with the laser processing head and MIG torch for welding in the vertical-up (PF) welding position

- All samples were degreased with acetone immediately prior to welding. Further cleaning operations used in addition to the degreasing operation are further discussed below in Section 7.1.

7.4. SCOPE OF WORK

The thick-section trials were carried out in four stages. The first stage was to ascertain whether fully penetrating, single-pass laser welds with acceptable visual appearance could be produced in the 7xxx aluminium using 7kW of Yb-fibre laser power. Autogenous laser welds were carried out using different top-bead shielding arrangements, different welding positions (flat, or PA, horizontal-vertical, or PC and vertical-up, or PF) and different orientations of the laser with respect to the welding direction.

In the second stage, the process tolerance was established for both autogenous laser and hybrid welding, in terms of the minimum and maximum welding speed producing full penetration. The welding position, orientation of the laser in relation to the welding direction, and position and type of top-bead shielding was selected based the outcome of the first stage trials. The MIG shielding shroud, gas type and flow rate, WFS and MIG droplet transfer mode, were all investigated to obtain good visual appearance of both top and underside of the welds.

In the third stage trials, the process conditions for both autogenous laser and hybrid welding were varied, within the process tolerance established in the second stage, to consistently eliminate keyhole-induced porosity (i.e., cavities and coarse porosity, as discussed in Section 4.5). The influence of alloy composition, surface oxide, laser spot size and welding speed on the occurrence of keyhole-induced porosity was investigated. Besides autogenous laser welding, the hybrid process was also investigated in terms of its influence on the presence of

cavities and coarse porosity, because of its claim of stabilising the keyhole and thereby resulting in a lower level of weld metal porosity (119).

In the final stage of the thick-section trials, the porosity-reduction measures established in the thin-section trials (Section 5.4) were applied to those autogenous and hybrid welding conditions capable of producing welds that were free of keyhole-induced cavities, with the objective of achieving a level of fine porosity in accordance with the stringent weld quality class defined in BS EN 13919-2 and AWS D17.1. The porosity-reduction measures comprised the removal of the surface oxides from top, bottom and edge of all samples by dry-machining immediately prior to welding, and, shielding of the weld pool using a high-grade, low-dewpoint helium shielding gas delivered through *dry* gas lines which were purged at least 2 minutes prior to welding.

Finally, the welds produced using both processes were compared in terms of level of weld metal porosity and in terms of resulting joint properties, i.e., hardness and tensile strength, as detailed in Section 7.5.

7.5. WELD ANALYSIS

All thick-section welds were inspected visually for the presence of surface-breaking imperfections, such as porosity, cracks, excessive underfill and undercut. The visual appearance also provided valuable information on the stability of the welding process and (hence) the internal weld quality. From the third stage trials onwards, the weld quality was assessed after machining off either side of the welded joint, leaving only the central 8mm of the weld. This would also be done in production to eliminate distortion of the structures (which would be several metres long) and remove potential crack-initiators from the weld surface. All thick-section welds produced were subjected to a radiographic examination, with a selection cross-sectioned, to assess the internal weld quality, as described in Section 5.5.

Hardness measurements, tensile testing and pore count analyses were carried out for those laser and hybrid welds produced in the fourth stage trials, of which the welding conditions produced a total weld metal porosity level lower than the limit set for the stringent weld quality class of both BS EN 13919-2 and AWS D17.1. Details of the hardness measurements, tensile testing and pore count analyses, were as follows:

- Hardness measurements were taken on the (8mm) transverse samples prepared for metallography, mid-thickness and after a proprietary post-weld heat-treatment, using a micro-hardness machine, with a 300g load.

- Tensile testing was carried out, after a proprietary post-weld heat treatment, in accordance with BS EN 10002-1 (139). Three samples were taken from representative

sections across the weld (a), three along the weld in the centre of the weld metal (b) and three along the weld in the HAZ (c), as shown in Fig.40. The tensile test pieces were 52mm in length, 8mm in width (taken through-thickness) and 1.9mm in thickness. Tensile testing was carried out at ambient temperature and the 0.2% proof strength ($R_{p,0.2}$), the tensile stress (R_m), and the percentage elongation at fracture (El) recorded.

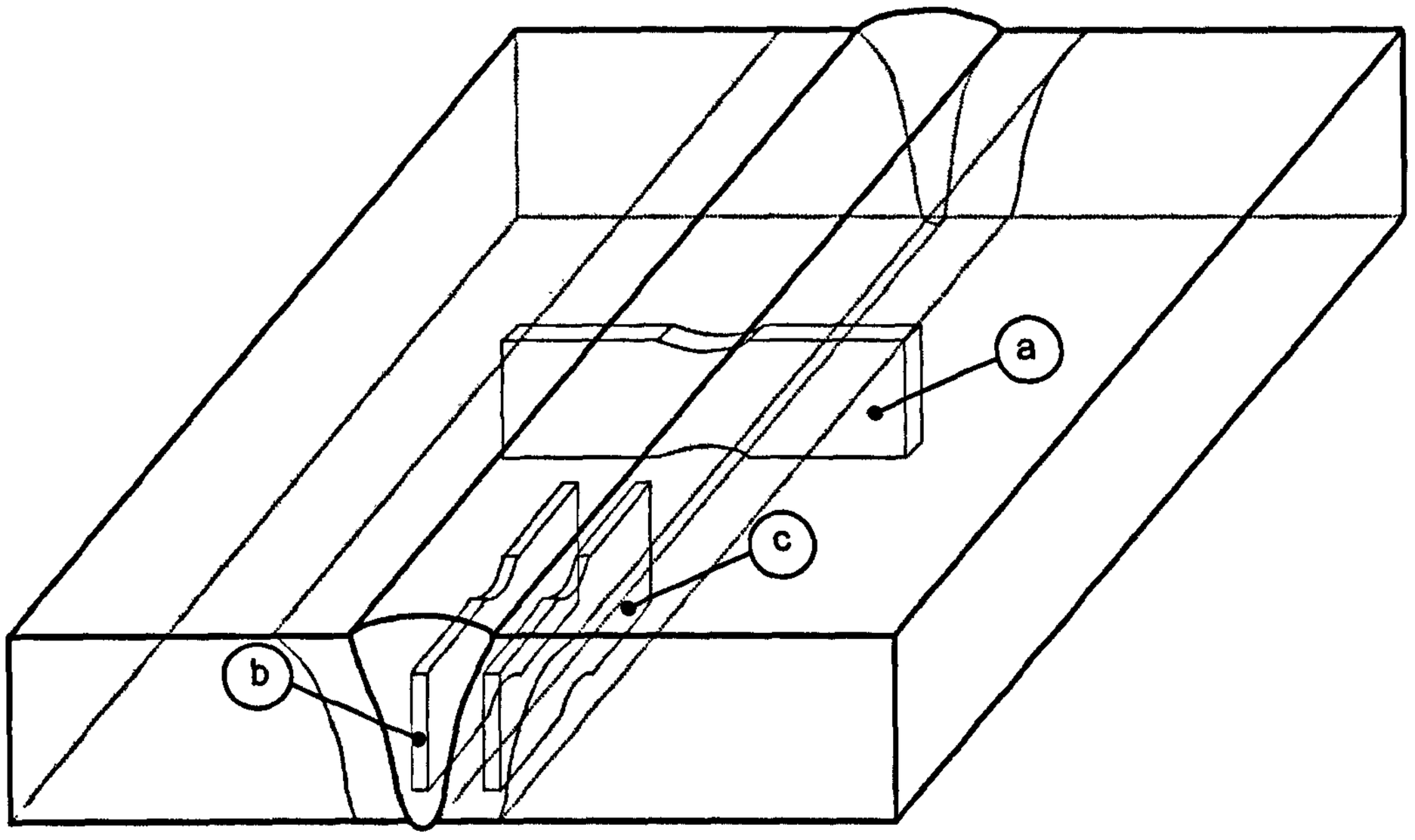

Fig.40 Schematic showing locations where tensile samples were taken.

- The pore counts were carried out in the same way as for the thin-section trials, described in Section 5.5, using the radiographs taken from welds that had the top and bottom machined off, leaving only the centre 8mm. The counts were performed over the entire weld length, excluding 25mm at the start and 25mm at the end of the weld, and the pore number proportionally reduced to a 100mm weld length, in accordance with BS EN 13919-2. The pore length values summarised in Table 6, have been proportionally increased from the 76mm (3") weld length, as specified in AWS D17.1, to a 100mm weld length, as specified in BS EN 13919-2, for the purpose of comparison between the two standards.

7.6. RESULTS AND DISCUSSION

7.6.1. Stage I - Initial Process Optimisation

Welding the 7xxx alloy in the PA (flat) position was abandoned, because of problems with burn-through when using 7kW of Yb-fibre laser power focused in either the 0.4mm or the 0.6mm spot size. Burn-through, which occurs because the surface tension of the large molten weld pool is unable to resist the hydrostatic forces, was not unexpected as it had also been observed by the author when laser welding 12.7mm thickness C-Mn steel in the flat position (140) and considering the fact that the surface tension force for pure aluminium is 0.915N/m, compared with 1.835 N/m for iron (141). To counter burn-though and to enhance control of the

molten material flow when fully penetrating the 12.7mm thickness aluminium, the remainder of the thick-section welding trials was carried in the horizontal-vertical, PC, Fig.41a, and the vertical upward, PF, Fig.41b, welding position. Welding in the vertical downward, PG, welding position was not pursued, as the molten material flow tended to interfere with the laser beam.

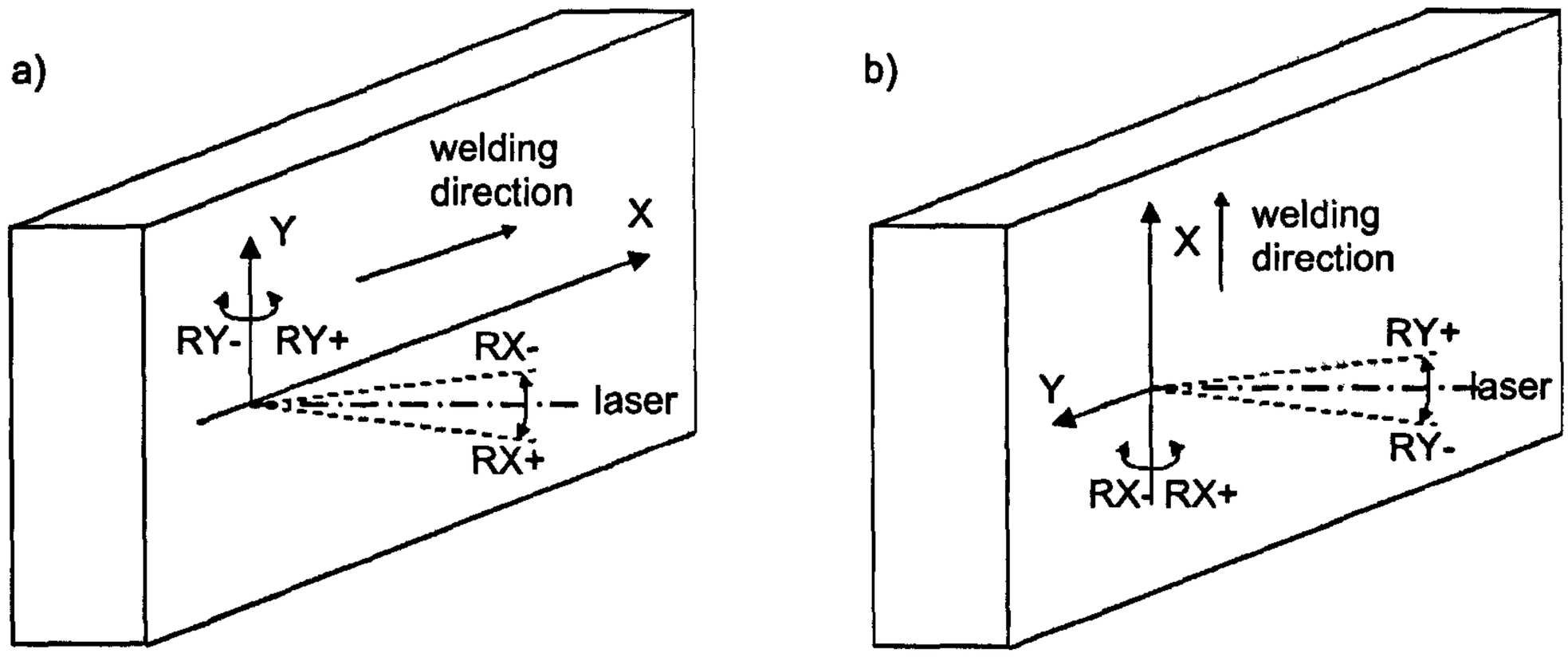

Fig.41 Out-of-position welding with possible orientations of the processing head:
a) horizontal-vertical (PC) position
b) vertical-up (PF) position

Notwithstanding the fact that the laser power density for both the 0.6mm and 0.4mm spot size was higher than the threshold intensity of $1.5x10^6 W/cm^2$ for laser keyhole welding of aluminium with the Nd:YAG wavelength, a laser angle 10° away from the perpendicular direction to the material surface was used for all thick-section welding trials to avoid problems with initial back-reflection (Section 4.2, page 14). The direction of the 10° relative to the welding direction was varied in an effort to maximise weld pool support, and, for both the PC and PF welding position, a laser pointing downward orientation was preferred to counter sagging of the weld pool (which destabilised the keyhole). This is the orientation RX(–) and RY(+) in the PC and PF welding position, respectively (Fig.41).

Using the 4mm ID, copper nozzle side-jet shielding arrangement, fully penetrating melt runs were produced at a maximum welding speed of 0.65 and 0.75m/min, using 7kW of Yb-fibre laser power focused in a 0.6mm and 0.4mm spot diameter, respectively. However, weld bead profiles and appearances were irregular and oxidised, and radiography revealed the presence of keyhole-induced porosity. This could not be improved upon, by changing the shielding gas conditions, in terms of position with respect to beam impingement point, stand-off distance and/or flow rate, as described in a EngD Submissions 6 (45) and 7 (46). To confirm the author's thinking that this was the result of air entrapment through turbulent flow (61), a larger shielding nozzle was used for subsequent trials to create a laminar flow at high flow rates. As hybrid welding would also be assessed as part of these trials, and to prevent time-consuming set-up changes between the autogenous laser and hybrid welding set-up, inert shielding gas for subsequent thick-section trials was supplied through a standard, 16mm ID MIG shroud.

Using this MIG shroud side-jet shielding arrangement, oxidation-free weld top-bead appearances with a regular surface ripple were achieved using 7kW of Yb-fibre laser power for welding both 6.35 and 12.7mm thickness aluminium. This shielding arrangement was suitable for welding in both the PC and PF welding position, at welding speeds ranging between 0.5 and 3m/min, using either helium or argon as shielding gas. The laser orientation (with respect to the welding direction), welding speed and type of shielding gas used, determined the shielding gas flow rate to be selected so as to produce oxidation-free weld top-beads, as described in EngD Submission 6 (45). Although both helium and argon were capable of producing fully penetrating melt runs with acceptable weld bead appearances, the stability of the process was better when using helium. It is claimed (see Section 4.6.2) that this is the result of the higher heat conductivity and higher ionisation potential of helium, compared with argon, creating a lower (keyhole) vapour pressure. However, if a lower vapour pressure results from using helium as shielding gas, this would also reduce the ability of the keyhole to withstand any pressure changes inside the keyhole (55). Helium, when used for arc welding, creates a hotter weld pool and allows degassing of the weld pool (61). According to the author, the helium plume/plasma created during laser welding heats up the material at the surface, in the same way, through conduction, but more so than an argon plasma. This results in an enlarged laser weld pool, preventing the top of the keyhole from closing, with better keyhole stability as result. A larger weld pool was confirmed in the case of welding with helium, from a comparison of the weld end crater of two welds in 12.7mm thickness 7xxx aluminium, i.e., one produced with argon as shielding gas and the other with helium, as discussed in an EngD Submission 7 (46).

Using the MIG shroud shielding arrangement, full penetration was maintained consistently along a 300mm weld length in the 7xxx alloy, at a welding speed of 0.65 and 0.83m/min for the PC and the PF welding position, respectively, using 7kW of Yb-fibre laser power focused into a 0.4mm spot diameter. When using the larger spot size of 0.6mm, the welding speed for full penetration dropped to 0.5 and 0.65m/min, respectively. At the lower of these welding speeds, the tendency for the weld top-bead to sag increased, because of the large volume of molten material created at these speeds.

The welds shown in Fig.42 and Fig.43 show the typical weld bead profiles of fully penetrating melt runs produced using 7kW of Yb-fibre laser power, focused in a 0.6mm spot, at a welding speed of 0.5m/min in the PC and PF position, respectively. The molten area for the weld carried out in the PF position measured less than that of the PC position weld, i.e., 50mm^2 and 60mm^2, respectively. From this can be concluded that more lateral heat transfer occurred when welding in the PC position, melting a larger cross-sectional area of material. The heat remained constrained in a smaller area when welding in the PF position, which explains the higher maximum speed for full penetration for the PF position compared with the PC position. This higher speed is advantageous when welding heat-treatable alloys, such as the 7xxx aluminium, as a higher welding speed reduces the thermal damage (see Section 4.3.2). The

exact reason for this speed difference between the PC and PF welding position requires further investigation, but the author suggests that the difference in the shielding gas flow direction (in relation to the weld pool) and the amount of thinning of the leading edge of the keyhole wall, may have contributed to this. The shielding gas extracts heat from the melt pool, thereby affecting its temperature, cooling rate and overall behaviour. When welding in the PF position, the leading edge of the keyhole wall thins, because of gravity, improving the heat flow into the cold material in front of the keyhole.

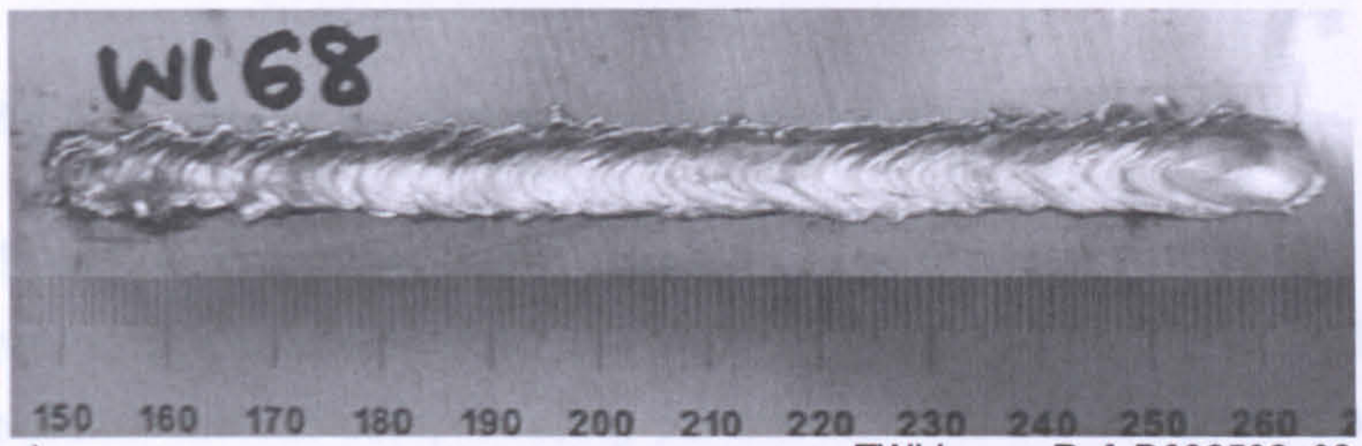

a) TWI Image Ref: D006532_03

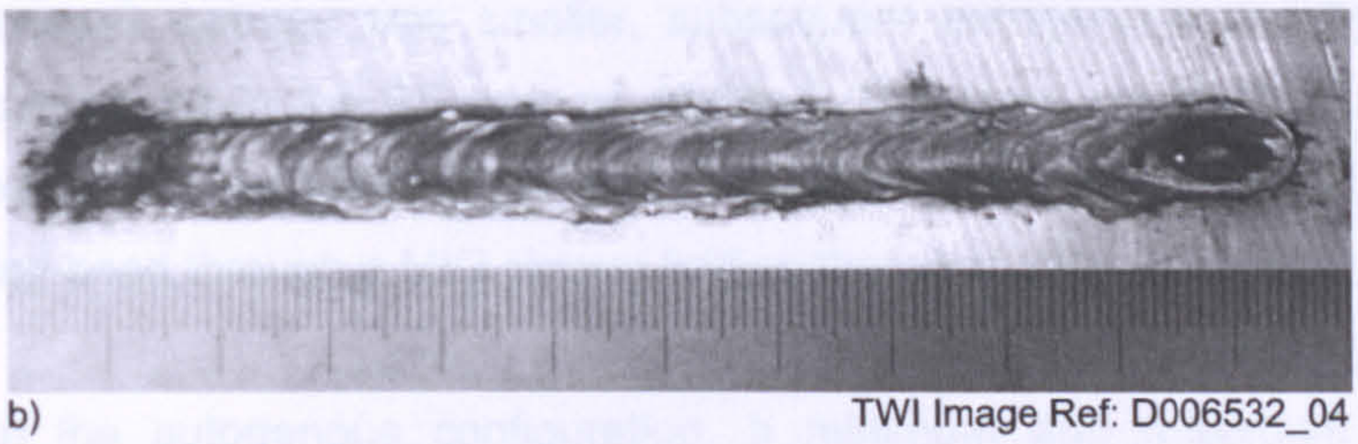

b) TWI Image Ref: D006532_04

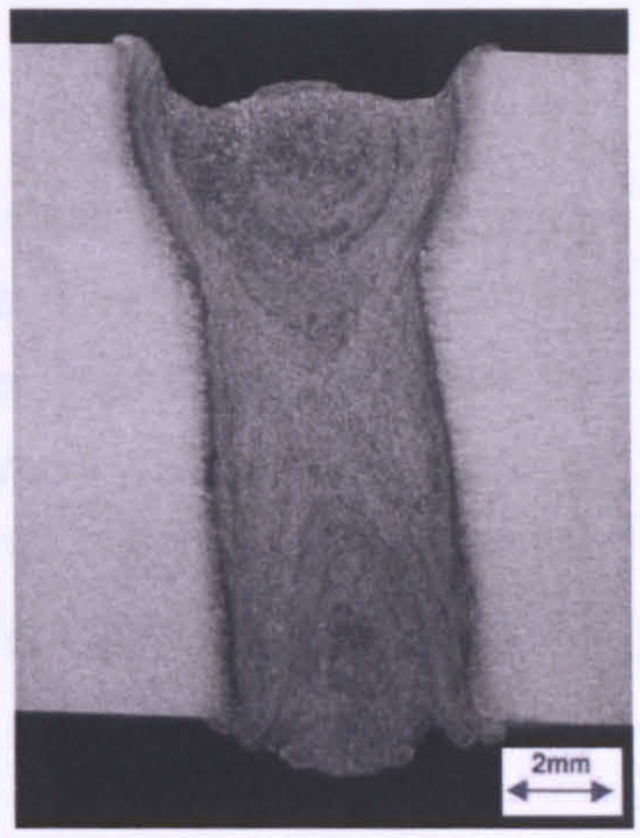

c) TWI Image Ref: V9403

Fig.42 A fully penetrating melt run produced in the PC welding position in 12.7mm thickness 7xxx aluminium using 7kW of Yb-fibre laser power focused in a 0.6mm spot at a welding speed of 0.5/min:

a) weld top-bead appearance
b) weld under-bead appearance
c) weld cross section

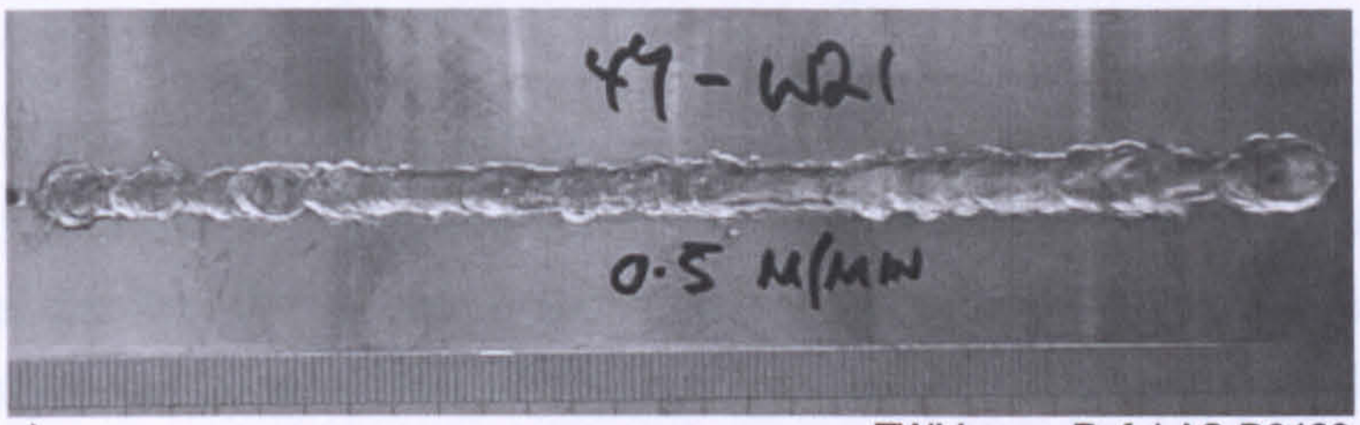

a) TWI Image Ref: LAS-D0428

b) TWI Image Ref: LAS-D0429

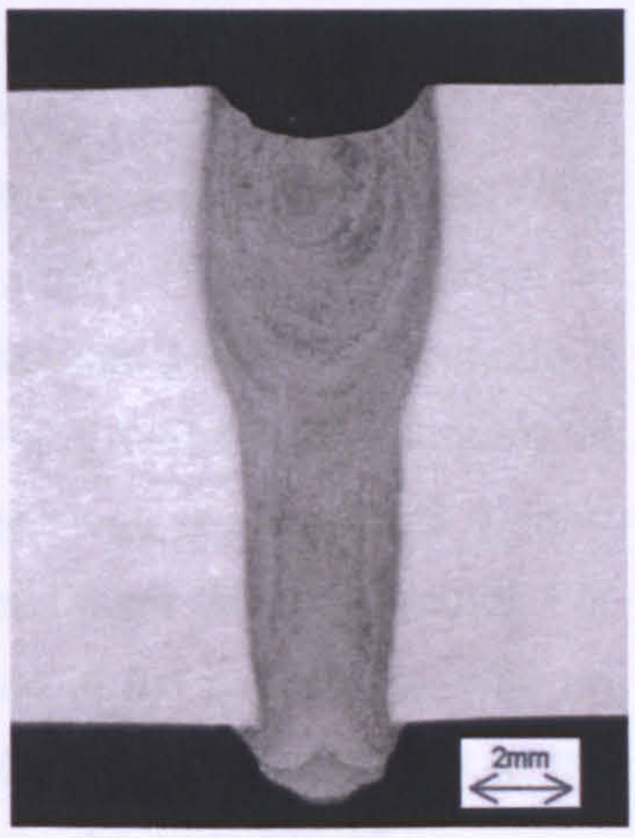

c) TWI Image Ref: V7698

Fig.43 A fully penetrating melt run produced in the PF welding position in 12.7mm thickness 7xxx aluminium using 7kW of Yb-fibre laser power focused in a 0.6mm spot at a welding speed of 0.5/min:

a) weld top-bead appearance
b) weld under-bead appearance
c) weld cross section

At a welding speed of 0.5m/min, the welds carried out in the PC position were more sensitive to the formation of keyhole-induced porosity than their PF position equivalents. In the PC welding position, the hydrodynamic force of the liquid aluminium weld pool acts with the surface tension forces against the vapour pressure to close the keyhole. In the PF welding position, this is not the case as the weld pool lies underneath the keyhole. Moreover, the process stability was better in the PF position, because of the gravitational forces acting against any surface ripple motion bouncing of the solidified material back towards the keyhole, as detailed in EngD Submission 7 (46) and summarised in Section 4.5.3.

7.6.2. Stage II – Reference Welding Conditions

Based on the observations that melt runs produced in the PC welding position were more prone to keyhole-induced porosity, that higher welding speeds were achieved in the PF position without compromising penetration and visual appearance, and that, as a result, the thermal damage was smaller, subsequent autogenous and hybrid welding trials were all carried out in the PF welding position. The laser was rotated 10° pointing downward, i.e., away from the welding direction (RY+10°), Fig.41, with industrial grade helium supplied to the top-bead through a MIG shroud trailing the laser 30°.

In the autogenous configuration, a minimum and maximum welding speed of 0.5 and 0.83m/min, respectively, produced full penetration in 12.7mm thickness 7xxx aluminium using 7kW of Yb-fibre laser power focused into a 0.4mm spot diameter. These speeds were 0.5 and 0.65m/min, respectively, when welding with the same power focused in a 0.6mm spot diameter. Typical weld bead profiles achieved at the maximum welding speeds for both the 0.6 and 0.4mm spot size are shown in Fig.44.

In the hybrid configuration, acceptable weld bead profiles were achieved using 30 and 10litre/min of helium as top and under-bead shielding, and a pulsed synergic setting at a WFS of 6m/min WFS. This resulted in an average arc energy of 2.65kW (105A, 25V) used in combination with 7kW of Yb-fibre laser power. The pulsed setting was preferred, because it resulted in fewer spatters than the synergic spray condition. For a laser spot diameter of 0.4mm and 0.6mm, the maximum welding speed for full penetration was similar, i.e., 0.92 and 0.94m/min, 11% and 45% faster, respectively, than the autogenous laser welding results. For both spot sizes, a welding speed as low as 0.5m/min still resulted in full penetration with an acceptable weld bead appearance. Typical weld bead profiles of melt runs carried out at the maximum welding speeds for both the 0.6 and 0.4mm spot size are shown in Fig.45.

The faster welding speeds possible when using the hybrid configuration, compared with autogenous laser welding, resulted from the additional arc energy and the reported *synergic* interaction between the two processes (120-123). The latter essentially means that the hybrid process is a more efficient process compared with the sum of its two (process) components,

in that it requires less energy to melt a given volume of metal. For welding the 6.35mm thickness Al-Zn-Mg-Cu alloy, the hybrid process was demonstrated to have a melting efficiency that was 11% higher than that of the sum of the (autogenous) laser and MIG process, for a given heat input, as detailed in EngD Submission 7 (46). This synergy and a more fundamental understanding of hybrid laser-arc processing is the subject of a further study by the author (138) and by others (142-146).

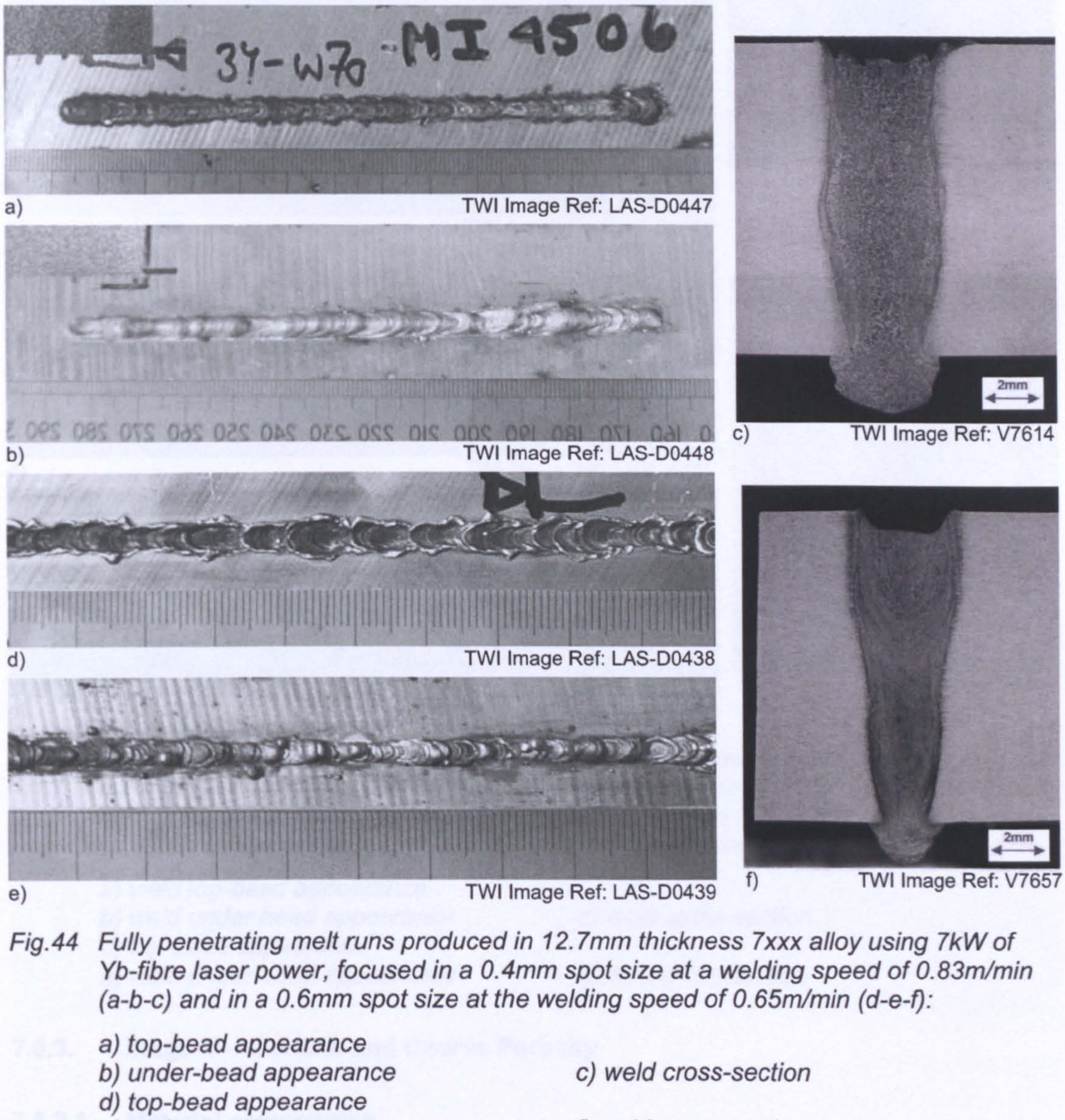

a) TWI Image Ref: LAS-D0447

b) TWI Image Ref: LAS-D0448

c) TWI Image Ref: V7614

d) TWI Image Ref: LAS-D0438

e) TWI Image Ref: LAS-D0439

f) TWI Image Ref: V7657

Fig.44 Fully penetrating melt runs produced in 12.7mm thickness 7xxx alloy using 7kW of Yb-fibre laser power, focused in a 0.4mm spot size at a welding speed of 0.83m/min (a-b-c) and in a 0.6mm spot size at the welding speed of 0.65m/min (d-e-f):

a) top-bead appearance
b) under-bead appearance
c) weld cross-section
d) top-bead appearance
e) under-bead appearance
f) weld cross-section.

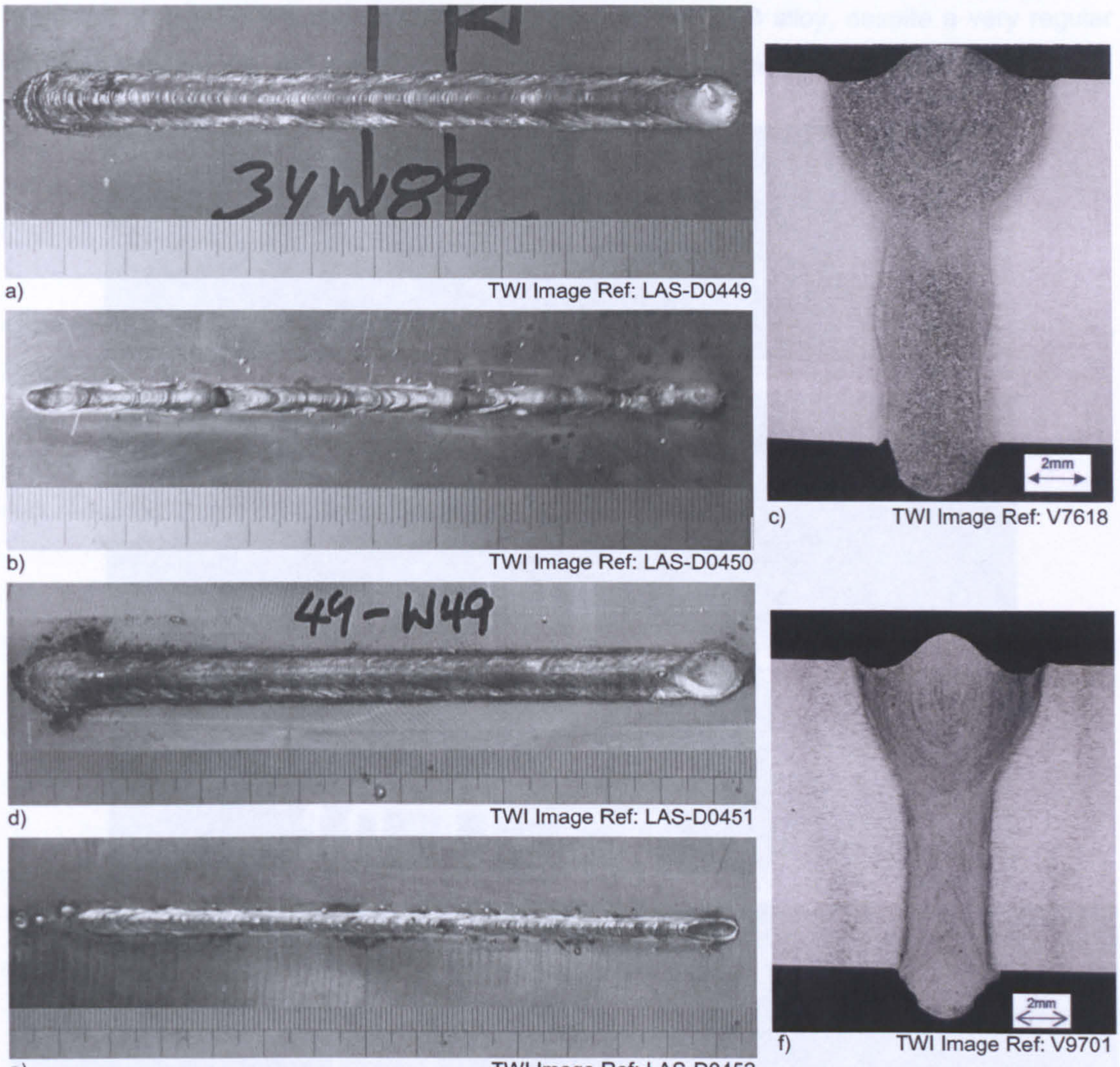

a) TWI Image Ref: LAS-D0449

b) TWI Image Ref: LAS-D0450

c) TWI Image Ref: V7618

d) TWI Image Ref: LAS-D0451

e) TWI Image Ref: LAS-D0452

f) TWI Image Ref: V9701

Fig.45 Fully penetrating melt runs produced in 12.7mm thickness 7xxx alloy using hybrid laser-MIG welding, using 2.65kW of MIG arc power (6m/min WFS) with 7kW of Yb-fibre laser power, at a welding speed of 0.92m/min when focused in a 0.4mm spot size (a-b-c) and a welding speed of 0.94m/min for a 0.6mm spot size (d-e-f):

a) weld top-bead appearance
b) weld under-bead appearance
c) weld cross-section
d) top-bead appearance
e) weld under-bead appearance
f) weld cross-section

7.6.3. Stage III – Cavities and Coarse Porosity

7.6.3.1. Material composition

Fully penetrating welds produced using 7kW of Yb-fibre laser power under identical welding conditions in three different aluminium alloys, 7xxx, 2024 and 2519, of the same (12.7mm) thickness, contained different levels of keyhole-induced porosity. The welding conditions used for the three alloys were those established for producing fully penetrating autogenous laser welds in the 12.7mm thickness 7xxx aluminium using 7kW of laser power focused in a 0.6mm spot (Section 7.6.2).

The level of keyhole-induced porosity was highest in the 2519 alloy, despite a very regular top-bead appearance, and lowest in the 7xxx alloy, as seen from the radiographs in Fig.46.

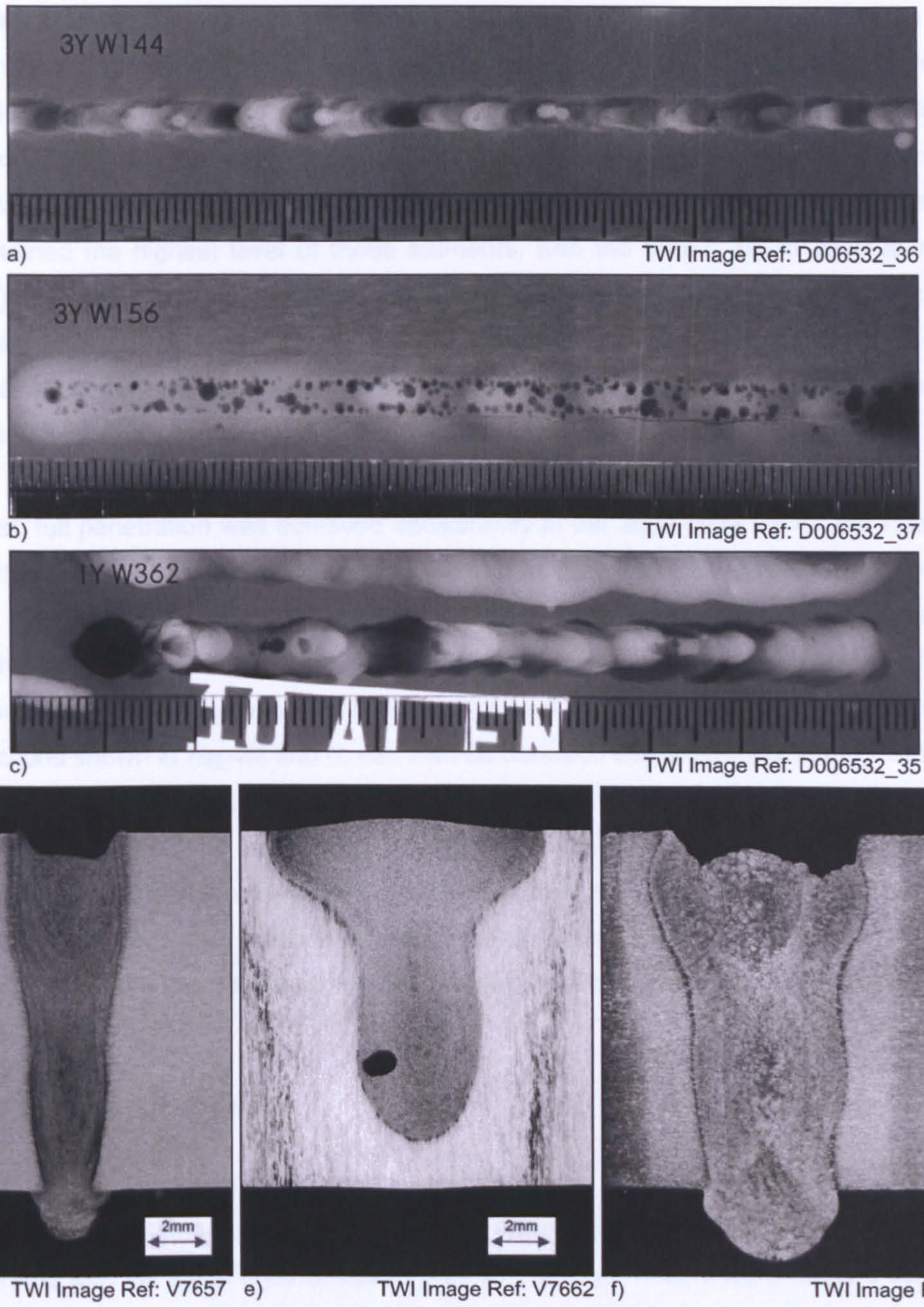

a) TWI Image Ref: D006532_36

b) TWI Image Ref: D006532_37

c) TWI Image Ref: D006532_35

d) TWI Image Ref: V7657 e) TWI Image Ref: V7662 f) TWI Image Ref: V6457

Fig.46 Fully penetrating melt runs produced in the PF welding position using 7kW of Yb-fibre laser power focused in a 0.6mm spot size at a welding speed of 0.65m/min, in 12.7mm thickness:

a) 7xxx alloy, radiograph
b) 2519 alloy, radiograph
c) 2024 alloy, radiograph
d) 7xxx alloy, weld cross-section
e) 2519 alloy, cross-section with typical pore
f) 2024 alloy, weld cross-section

Despite the same welding conditions being used for all three alloys, excessive plasma/plume formation was observed from the CCTV images (and concluded from the typical nail head cross-section in Fig.46e) only when laser welding the 2519 alloy samples, but not when welding the 2024 or the 7xxx alloy. The author concludes that the presence of the

plume/plasma affected the keyhole stability, produced a large number of keyhole-induced porosity, but also resulted in conductive heating of the top of the molten pool, producing the regular weld bead appearance observed. Both these effects were described earlier in Section 4.5.2. In addition, the presence of the plume/plasma resulted in intermittent penetration with a high quantity of spherical coarse pores positioned along the fusion boundaries on either side of the weld in this alloy, as observed in Fig.46e. If keyhole instability had been the result of the evaporation of volatile elements, such as Mg and Zn, then most of the keyhole-induced porosity would have been expected in the 7xxx alloy, as, out of the three alloys examined, this alloy contained the highest level of these elements, with the lowest in the 2519 aluminium (Table 1). By reducing the welding speed to 0.6m/min, full penetration was achieved consistently in the 2519 alloy, but this did not reduce the level of porosity observed in the weld. The effect of welding speed on the presence of keyhole-induced porosity in laser-welded aluminium is further detailed in Section 7.6.3.5.

In contrast, full penetration was achieved consistently in the 2024 alloy, as for the 7xxx alloy, but the 2024 alloy weld contained a higher level of keyhole-induced porosity compared with the 7xxx alloy weld. The silicon content in 2024 is five times higher than in the 7xxx alloy. Silicon changes the fluid flow of the molten material surrounding the keyhole (see Section 4.6.1), thereby making it more fluid (62,87) and more prone to keyhole instabilities. From the cross-sections shown in Fig.46f and d, can also be deduced that in terms of finding 'optimised' conditions when laser welding 2024 alloy of this thickness, this would involve a higher welding speed, to reduce the total weld area, as well as underfill and excessive penetration in particular, compared with what was achieved for the 7xxx alloy. An increase in welding speed would further increase the number of cavities and coarse pores, as discussed further in Section 7.6.3.5. From this can be concluded that the level of keyhole-induced porosity is alloy-dependent.

7.6.3.2. Surface oxide layer

The influence of the oxide layer on the occurrence of coarse weld metal porosity was demonstrated by welding 6.35mm and 12.7mm thickness samples both in the as-received condition and with the oxide layer removed prior to welding. Welds were produced using 7kW of laser power focused into a 0.4mm spot diameter, at a welding speed of 2.8 and 0.83m/min respectively, both without and with the oxide removed from the joint (edge, top and bottom) by dry-machining immediately prior to welding. For both thicknesses, less keyhole-induced porosity was observed in those welds produced on the samples from which the oxide layer was removed, despite statements in the literature that 'cleaning does not affect keyhole-induced porosity' (Section 4.6.1). Without removing the oxide layer prior to welding, oxygen (from the oxide layer) will mix in with the weld metal and change the molten material flow (see Section 4.6.1). The author concludes that, depending on the level of oxygen that enters the weld pool, this contributes to the level of keyhole-induced porosity found in the as-received

laser welds. This conclusion is based on the findings that a small amount of oxygen, up to 0.5% in 5083 alloy, can reduce coarse (and fine) porosity, whereas levels of 2% or higher, result in metal oxides that change the weld pool viscosity or form an oxide skin on the weld pool, affecting keyhole stability (Section 4.6.1).

7.6.3.3. Autogenous laser or hybrid laser-MIG

Despite being more complex than autogenous laser welding, because of the larger number of process variables, the hybrid process has a number of specific advantages over autogenous laser welding when used for the manufacture of (thick-section) aluminium wing structures. The increase in welding speed can reduce the heat input and minimises the extent of the thermal damage in heat-treatable alloys, such as the 7xxx alloy. The hybrid process also tolerates larger joint gaps, compared with autogenous, relaxing the fit-up requirements for welding metre-long wing structures in production, whilst the MIG arc inherently introduces a filler wire into the weld pool, of which the composition can be tailored to suit the joint's properties, e.g., hardness, tensile, corrosion and/or fatigue strength. Finally, and of particular interest for this work (and application), the process is capable of stabilising the process through the enlargement of the keyhole (see Section 4.6.6). Work by other researchers has shown that the hybrid laser-MIG process, using either a CO_2 or Nd:YAG laser, is capable of reducing, but not eliminating, the level of coarse porosity in 6000-series aluminium (119), in Li-containing aerospace alloy 2519 (29) and in thin-section 5000 and 6000-series automotive aluminium (147). The purpose of this part of the work was to ascertain if this was also the case when using an Yb-fibre laser for the welding of 12.7mm thickness 7xxx aluminium alloy.

As established earlier (Section 7.6.2), compared with autogenous laser welding, the hybrid configuration allows 11% and 45% faster welding speeds when focusing the laser power in a 0.4 and a 0.6mm spot diameter, respectively. At the maximum speed for full penetration, coarse pores were observed in the hybrid welds, but in number lower than for the equivalent autogenous laser welds. For representative welds produced using the 0.4mm spot size, 13 and 5 coarse pores were observed, for a 100mm weld length, when using autogenous and hybrid welding, respectively. In case of a 0.6mm spot size, these numbers reduced to 5 and 4, respectively. By introducing a MIG arc, the weld pool at the top of the keyhole is enlarged, thereby dampening the weld pool motion (Section 4.5.3). This, in turn, stabilised the keyhole, with a lower number of keyhole-induced pores as a result. Evidence of this dampening effect is in the small and well-defined top-bead surface ripples observed for the hybrid welds, Fig.45a and d, compared with their autogenous counterparts, in Fig.44a and d. These results demonstrate that hybrid welding using 7kW of Yb-fibre laser power at the maximum speed for full penetration was capable of reducing, but not eliminating coarse porosity, in the 7xxx alloy. To eliminate coarse porosity consistently, it was necessary to reduce the welding speed, as discussed further in Section 7.6.3.5.

7.6.3.4. Laser spot size

The level of the coarse porosity was higher when welding with the smaller 0.4mm laser spot size compared with the 0.6mm spot size, for both autogenous laser and hybrid welding of the 7xxx alloy. An increase in coarse porosity when focusing the power into a smaller spot size had also been observed from the thin-section trials, when laser welding 3.2mm thickness 2024 alloy (see Section 5.6.3). The smaller spot size creates a smaller keyhole, which increases the surface tension forces, as the keyhole radius is smaller, and destabilises the keyhole (Section 4.6.4). Moreover, a smaller spot size, for a given laser power, results in a higher power density and thus a higher vapour pressure inside the keyhole. This increases the rate of evaporation, and the likelihood of keyhole instabilities (Section 4.6.4). Because of the availability of a higher laser power density, faster welding speeds can be achieved for a given depth of penetration. As the welding speed increases, the stability of the keyhole deteriorates, with the pores formed also having less time to escape the weld pool prior to solidifying, because of the higher cooling rate (Section 4.6.3). The effect of welding speed on keyhole-induced porosity is further discussed in Section 7.6.3.5. Because of the increased tendency of coarse pore formation when laser welding with the smaller spot size, further welding trials were carried out with a laser spot diameter of 0.6mm.

7.6.3.5. Welding speed

When comparing the radiographs of the welds made at the minimum and maximum speeds for full penetration in the 7xxx alloy, using either the autogenous laser or hybrid process and a 0.4mm or 0.6mm spot size, no keyhole-induced porosity was observed in any of the welds produced at the minimum speed for full penetration. In contrast, in all welds produced at the maximum speeds for full penetration, keyhole-induced porosity was observed. The effect of welding speed on the level of porosity observed in hybrid welds produced in the 7xxx alloy is shown in Fig.47, with four keyhole-induced pores observed at the maximum welding speed (for full penetration) of 0.94m/min, one at 0.8m/min and none at the lower welding speeds of 0.6 and 0.5m/min.

By increasing the welding speed from the minimum welding speed for full penetration in increments of 0.05m/min, the maximum speed for full penetration at which no keyhole-induced porosity was observed, was determined for both the autogenous laser and hybrid process. This speed, further referred to as the *keyhole porosity-free welding speed*, was determined to be 0.55 and 0.75m/min for autogenous laser and hybrid welding, respectively, when welding the 7xxx alloy using 7kW of Yb-fibre laser power focused in a 0.6mm spot diameter. This effect can be explained by the fact that, as the welding speed is reduced, the weld pool is enlarged, the weld pool motion dampened and the keyhole stability improved, reducing the likelihood of keyhole-induced porosity. Moreover, the cooling rate drops with a reduction in welding speed, thereby giving more time for any pores that have formed to

escape the weld pool. This includes hydrogen pores that may have formed, explaining why the overall level of weld metal porosity found in these welds was low. An excessive formation of plasma/plume above the weld pool, and resulting instabilities or loss of penetration, was not observed at these lower speeds for the (300mm) length of welds produced.

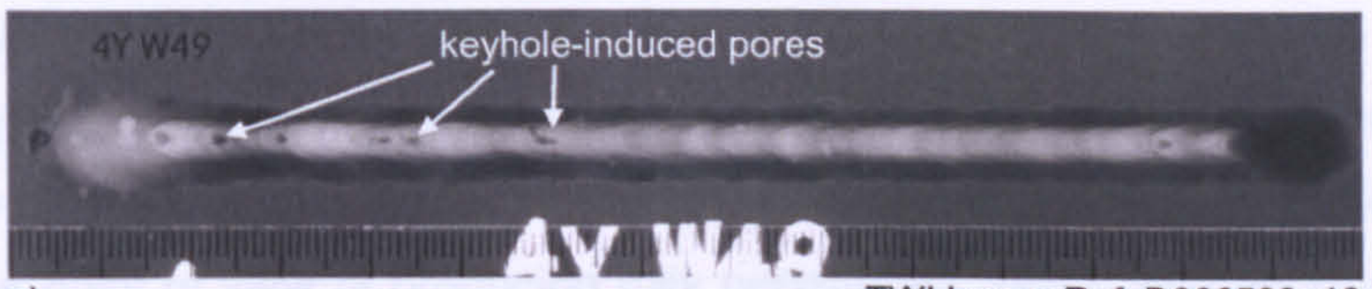

a) TWI Image Ref: D006532_19

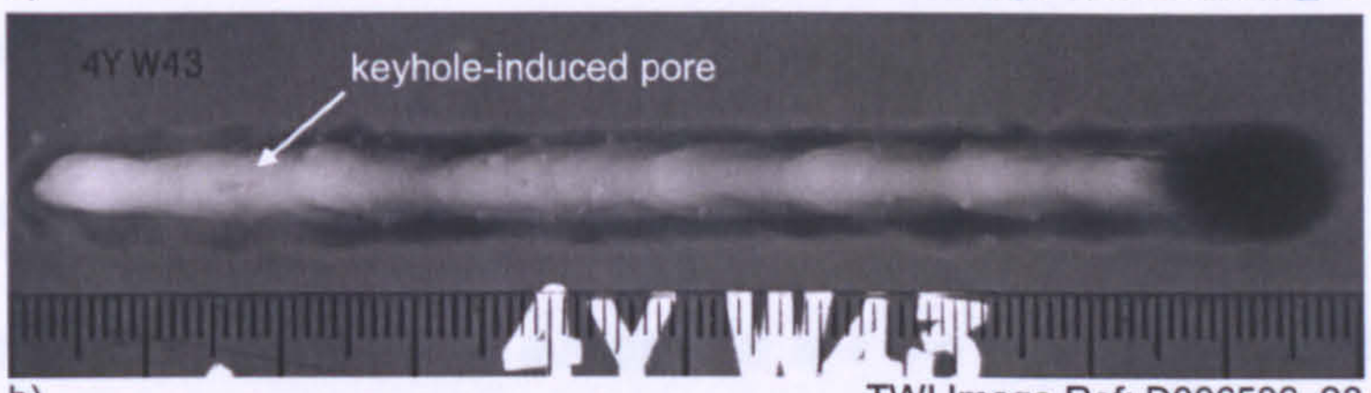

b) TWI Image Ref: D006532_28

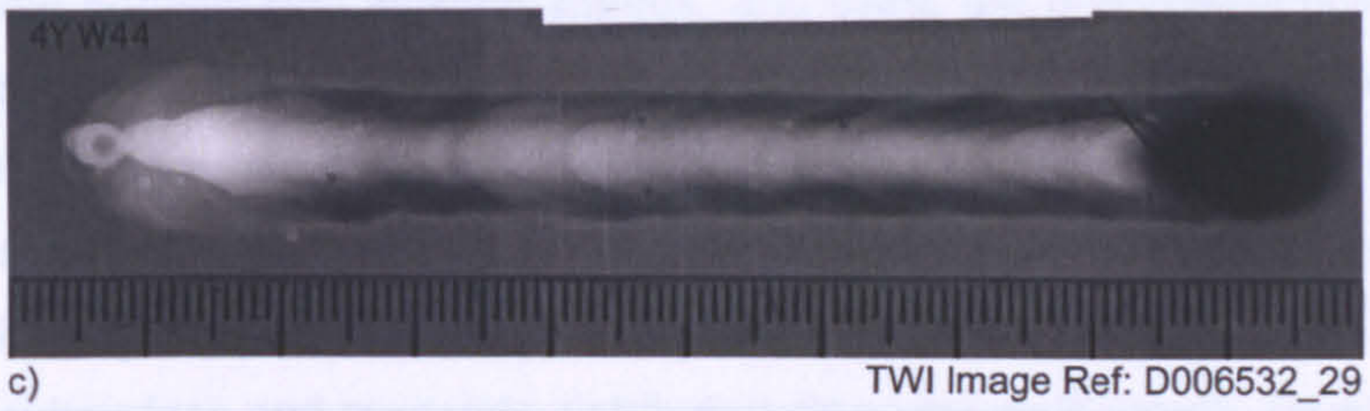

c) TWI Image Ref: D006532_29

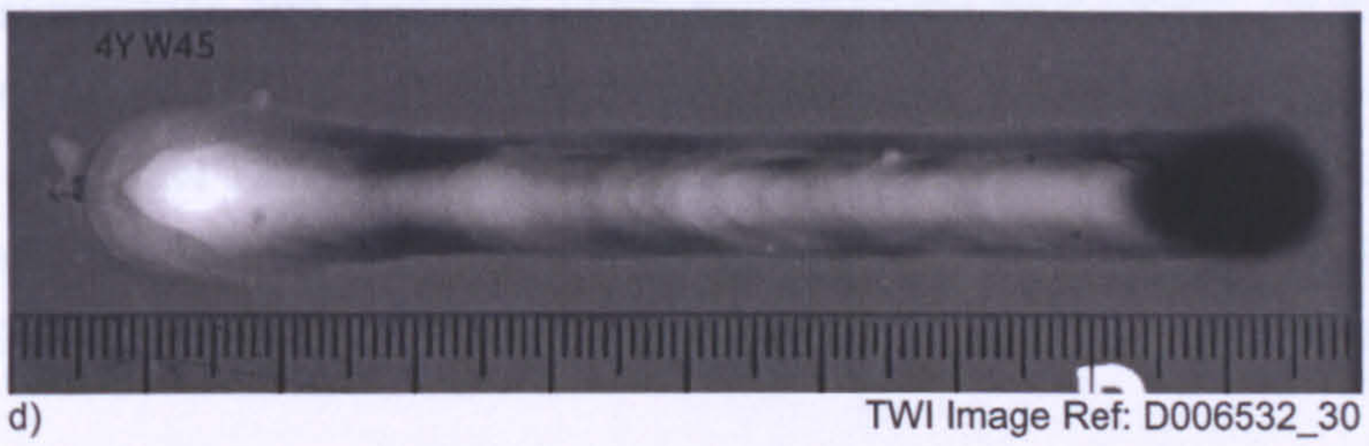

d) TWI Image Ref: D006532_30

Fig.47 Radiographs of fully penetrating melt runs produced in 12.7mm thickness 7xxx alloy using hybrid laser-MIG, with 2.65kW of MIG arc power and 7kW of Yb-fibre laser power focused in a 0.6mm spot, and at a:

a) maximum welding speed for full penetration, 0.94m/min
b) welding speed of 0.8m/min
c) welding speed of 0.6m/min
d) minimum welding speed for full penetration, 0.5m/min

Based on the above observation that keyhole-induced porosity was eliminated consistently by lowering the welding speed, an earlier decision which favoured PF position welding over welding in the PC position, was revisited. This is because, from a practical point of view for the (production) welding of aircraft wing structures, welding in the horizontal-vertical (PC) position would be preferred over the vertical-up (PF) position, as welding the metre-long sections would require a purpose-built (tall) building in case of the latter. Autogenous laser welding trials were repeated in the PC position, using 7kW of laser power focused into a 0.6mm spot size, to determine the minimum and maximum welding speed at which full penetration and a good visual weld appearance was attained in the 7xxx alloy. Welding speeds of 0.35 and 0.5m/min, respectively, were determined, compared with 0.5 and

0.65m/min, respectively, when welding in the PF position. The radiographs of typical welds produced in the PC position at the lower welding speed, revealed no keyhole-induced pores, with several observed for those carried out at the maximum welding speed (for full penetration). As the maximum speed for full penetration, was already lower than the keyhole porosity-free welding speed determined for the PF welding position, the keyhole porosity-free welding speed for the PC welding position was not determined, as it would be lower still. A lower welding speed means a higher heat input, which adversely affects the thermal damage in the 7xxx alloy (Section 4.3.2). PF position welding therefore remained the preferred welding position from the point of view of producing fully penetrating welds, with no keyhole-induced pores and a minimal heat input.

7.6.4. Stage IV – Fine Porosity

The results of the pore counts of four autogenous and two hybrid welds produced at their respective keyhole porosity-free welding speeds, and using the porosity-reduction measures described in Section 7.4, are summarised in Table 12. The values in italic are average values. The table contains values less than unity, because the pore counts were carried out for the full weld lengths, discarding the first and last 25mm of each weld and then proportionally reduced to a 100mm weld length, as specified in BS EN 13919-2 (Sections 5.5 and 7.5). For all welds, the pores were subsurface and randomly distributed along the weld length. Clustered or linear porosity was not observed in any of the welds, so criterion 2 on "*minimum distance between adjacent pores*" of BS EN 13919-2 (Table 5) and AWS D17.1 (Table 6) was not considered. In what follows therefore, only criteria 1 and 3, i.e., maximum pore diameter and accumulated pore area (BS EN 13919-2) or accumulated pore length (AWS D17.1), were considered.

The actual values for maximum pore diameter and pore area and pore length calculated from the pore count results (using a weld thickness of 8mm, i.e., the thickness of the joint in service) are given in Table 12. For calculating the pore area and length, the maximum pore diameter for each pore class was used. For instance, 1.6mm was used in the calculation of pore area/length, for the number of pores found to be in diameter between 1.4 and 1.6mm, and 0.6mm for the number of pores found with a diameter between 0.5 and 0.6mm. For an 8mm thickness weld to pass the stringent weld quality class in accordance with BS EN 13919-2, the maximum pore area per 100mm weld and the maximum pore diameter had to be less than 24mm^2 and 2.4mm, respectively (Table 5, page 48). For that same weld to pass the stringent weld quality class in accordance with AWS D17.1, the maximum pore length per 100mm weld and the maximum pore diameter had to be less than 7.9mm and 1.5mm, respectively (Table 6, page 49). The total pore area, per 100mm of weld length, for each of the autogenous and hybrid welds remained below the 24mm^2 limit specified in BS EN 13919-2, with a maximum of 3.1 and 2.1mm^2 for one autogenous laser and one hybrid weld, respectively.

Table 12 Pore count results for four autogenous laser and two hybrid laser-MIG welds carried out at their respective keyhole porosity-free welding speeds of 0.55 and 0.75m/min.

Weld ID	Total weld length, mm	Number of pores per 100mm weld length (non-localised and sub-surface)													*total calculated pore area per 100mm weld, in mm²* ✚	*total calculated pore length per 100mm weld, in mm* ✲
		Ø1.8-2.0mm	Ø1.6-1.8mm	Ø1.4-1.6mm	Ø1.2-1.4mm	Ø1.0-1.2mm	Ø0.9-1.0mm	Ø0.8-0.9mm	Ø0.7-0.8mm	Ø0.6-0.7mm	Ø0.5-0.6mm	Ø0.4-0.5mm	Ø0.3-0.4mm	Ø0.2-0.3mm	<Ø0.2mm	
8YW4	254			0.4			0.4			0.8	1.6	1.2	3.9	2.8	6.7	3.0	6.9
8YW5	251					0.4					0.8	2.0	2.0	1.6	9.2	1.7	5.1
8YW20	256							0.4	0.4		1.6	1.2	0.8	5.1	4.3	1.7	4.9
8YW21	251					1.2			0.8		0.8	1.2	4.0	4.0	4.8	3.1	6.9
autogenous laser				*0.1*		*0.4*	*0.1*	*0.1*	*0.3*	*0.2*	*1.2*	*1.4*	*2.7*	*3.4*	*6.2*	*2.4*	*5.9*
5YW3	233				0.4					0.4		1.3	2.1	4.7	12.4	2.1	6.3
5YW4	233								0.4		1.7	1.3	1.7	5.6	14.2	2.0	7.2
hybrid laser-MIG					*0.2*				*0.2*	*0.2*	*0.9*	*1.3*	*1.9*	*5.2*	*13.3*	*2.0*	*6.8*

✚ the maximum level allowed for the stringent weld quality class B in BS EN 13919-2 is 24.0mm²
✲ the maximum level allowed for the stringent weld quality class A in AWS D17.1 is 7.9mm

The total pore length, per 100mm of weld length, also remained below the 7.9mm limit as specified in AWS D17.1, with a maximum of 6.9 and 7.2mm for two autogenous laser and one hybrid weld, respectively. All welds also passed the maximum pore diameter criterion of both standards, with the largest pore found in autogenous laser weld 8YW4 (Table 12) 1.5mm in diameter, i.e., the limit set for the stringent weld quality in AWS D17.1.

The average values of the numbers of different pore sizes from all the pore counts taken from the autogenous and hybrid laser-MIG welds given in Table 12, in italic, are shown graphically Fig.48. Although the values for pore area and pore length in Table 12 are similar, differences can be observed between the pore counts carried out for the autogenous laser and the hybrid welds. For the hybrid welds, a larger number of pores smaller than 0.4mm in diameter can be observed, with the majority of pores smaller than 0.7mm in diameter. In case of the autogenous laser welds, the pores were generally larger in diameter, but with the majority smaller than 1.2mm in diameter. The author concludes that this results from the enlarged weld pool created by the hybrid process, which stabilises the keyhole and results in a lower number of large diameter keyhole-induced pores. Moreover, in contrast to autogenous laser welding, where hydrogen originates from the parent material or the shielding gas, the filler wire is another source of hydrogen when welding with the hybrid process. The high cooling rate of the process minimises the hydrogen diffusion time, which results in a large number of small diameter, i.e., less than 0.4mm, fine pores in the welds.

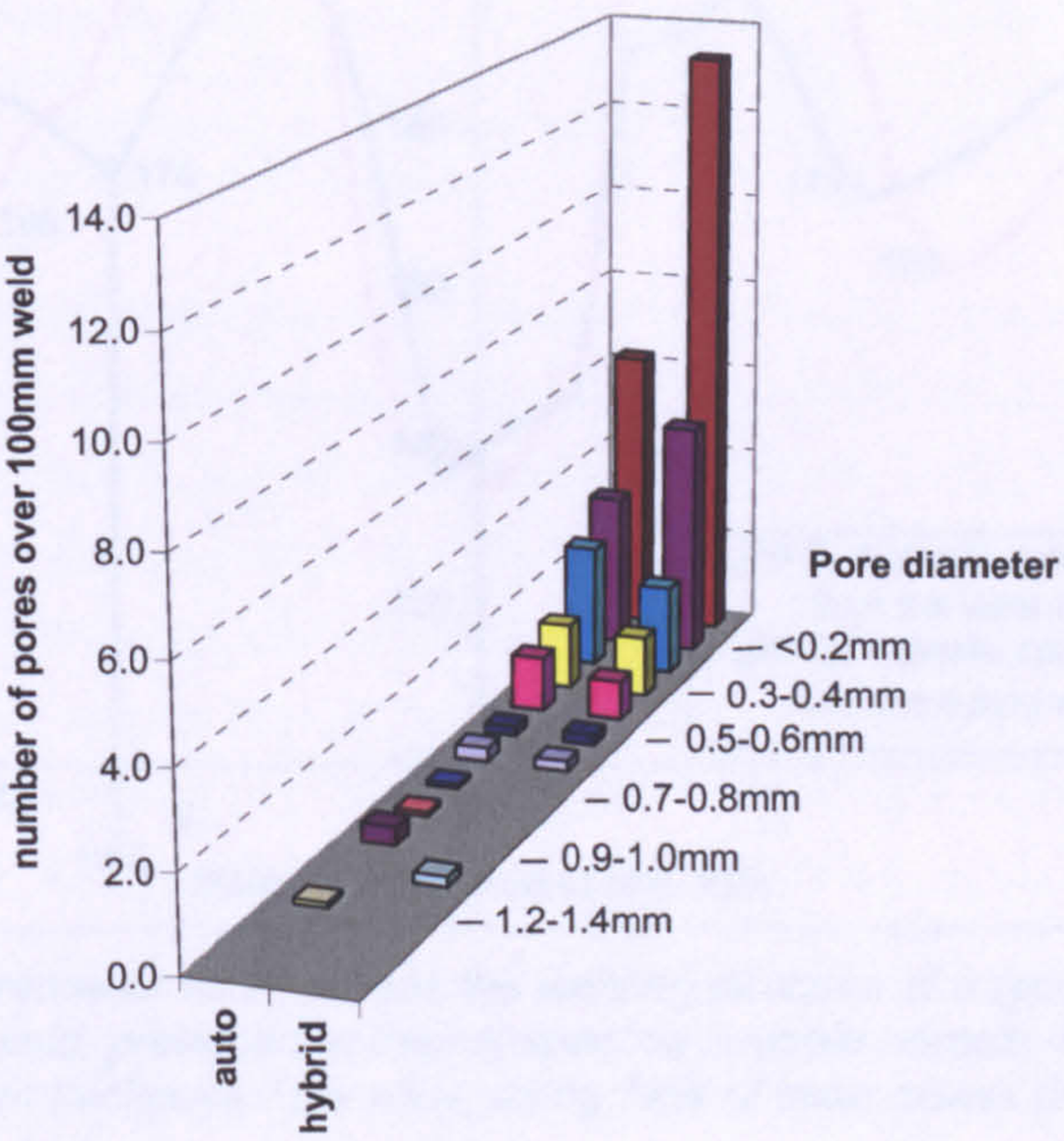

Fig.48 The average values of the pore count results for four autogenous laser and two hybrid laser-MIG welds carried out at their respective keyhole porosity-free welding speeds of 0.55 and 0.75m/min.

7.6.5. Process comparison

Cross-weld hardness scans of typical welds carried out using autogenous laser and hybrid at their respective keyhole porosity-free welding speeds are shown in Fig.49. For both processes, the lowest hardness value was along the weld centre line, position W_L and W_H, with no difference in hardness evident between the processes. This indicates that the 5556A filler wire used when hybrid laser-MIG welding did not contribute to the strength of the weld metal. A second degradation in hardness was observed for both processes, on either side of the weld, in the HAZ, position HAZ_L and HAZ_H, which is typical for a fusion weld in a heat-treatable aluminium alloy. In this position away from the weld centreline, the strength of material deteriorates because of the elevated temperatures causing the strengthening precipitates in the 7xxx alloy to growth (48). The smaller the heat input, the less pronounced the hardness drop (48), as demonstrated by the hardness scans for the hybrid welds produced at 0.5 and 0.94m/min, and 0.75m/min, Fig.50. These are the minimum and maximum welding speeds for full penetration and the keyhole porosity-free welding speed, as established for hybrid welding in the 7xxx alloy, using 7kW of Yb-fibre laser power focused in a 0.6mm spot diameter.

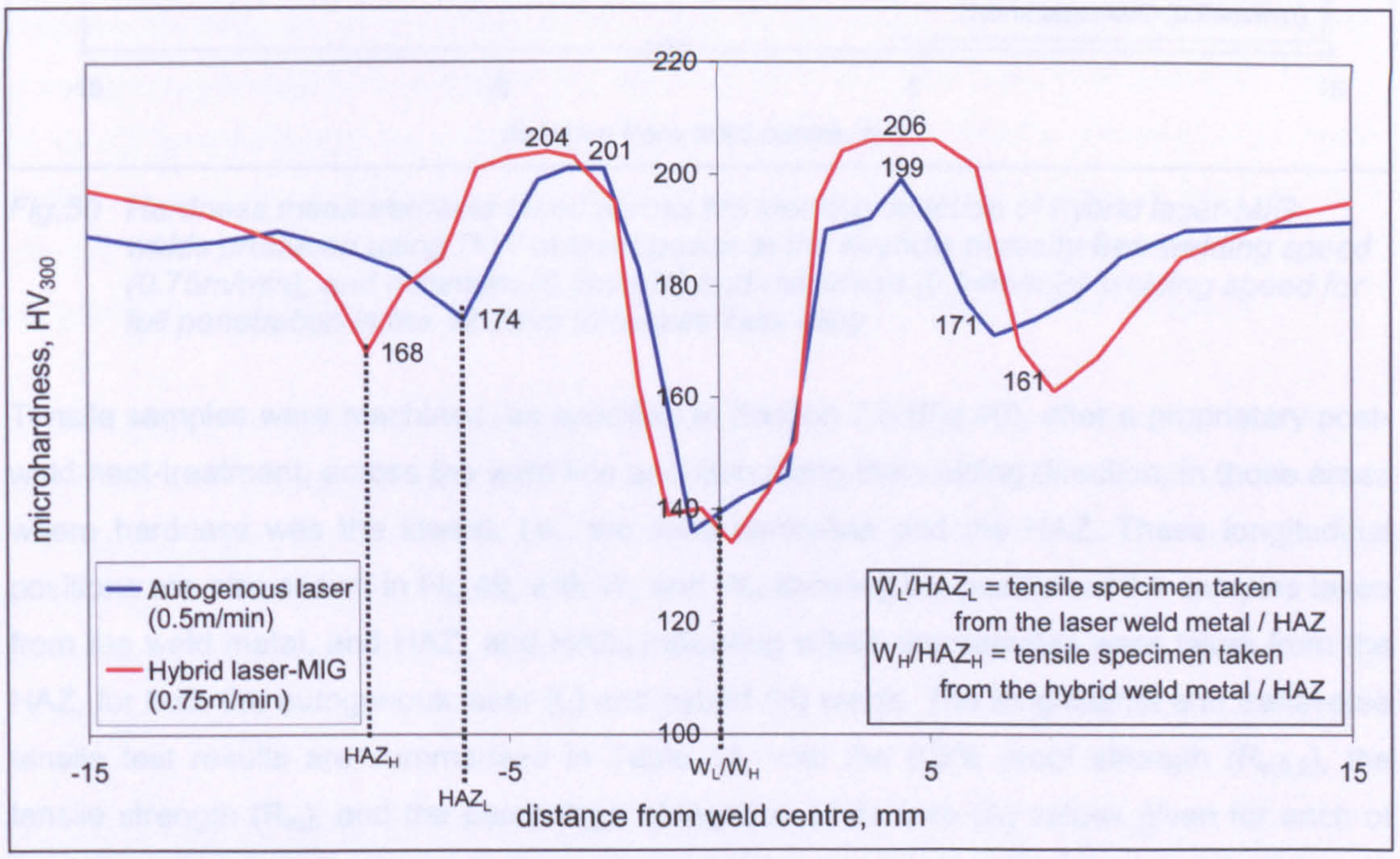

Fig.49 Hardness measurements taken across the welding direction of a typical autogenous laser and hybrid weld, produced at their respective keyhole porosity-free welding speeds, in 12.7mm thickness 7xxx alloy, using 7kW of laser power (in a 0.6mm spot)

Despite the higher welding speed used, a lower (average) HAZ hardness value was recorded for the hybrid welds compared with the autogenous laser welds, Fig.49. However, it is noteworthy that the percentage difference between the average values was less than 5%. From Fig.49 can also be seen that the location of the second hardness degradation (in the HAZ) was further removed from the weld centreline for the hybrid welds than for the

autogenous laser welds, i.e., 8mm instead of 6mm, despite the same weld width (at mid-thickness) for both processes. The larger HAZ for the hybrid welds resulted from the higher energy used, with 2.65kW of MIG energy used combined with 7kW of Yb-fibre laser power, and the process synergy, resulting in an 11% higher melting efficiency for the hybrid process compared with autogenous laser welding (see Section 7.6.2).

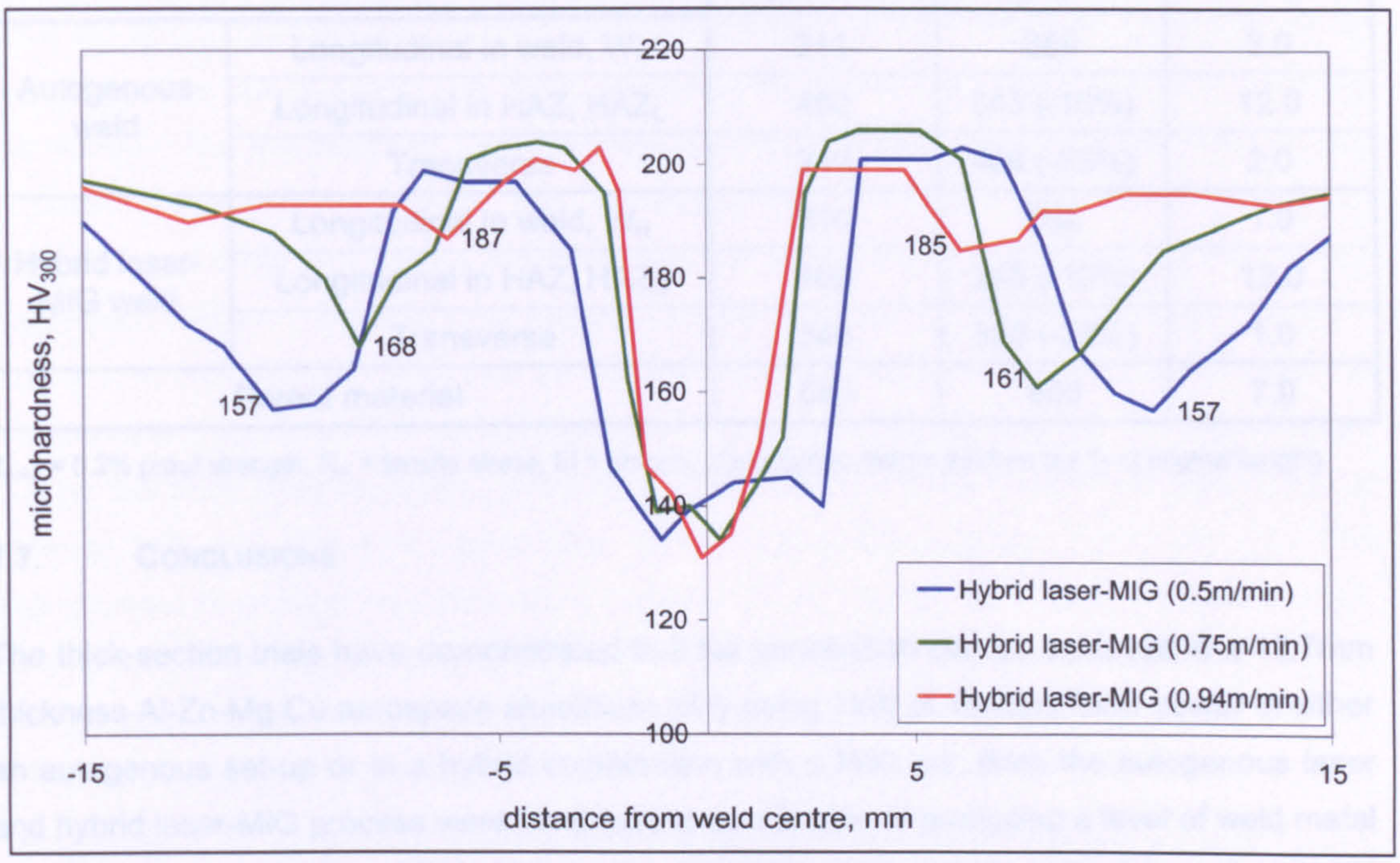

Fig.50 Hardness measurements taken across the welding direction of hybrid laser-MIG welds produced using 7kW of laser power at the keyhole porosity-free welding speed (0.75m/min), and minimum (0.5m/min) and maximum (0.94m/min) welding speed for full penetration in the 12.7mm thickness 7xxx alloy

Tensile samples were machined, as specified in Section 7.5 (Fig.40), after a proprietary post-weld heat-treatment, across the weld line and also along the welding direction, in those areas where hardness was the lowest, i.e., the weld centreline and the HAZ. These longitudinal positions are also shown in Fig.49, with W_L and W_H showing the position of the samples taken from the weld metal, and HAZ_L and HAZ_H indicating where the samples were taken from the HAZ, for both the autogenous laser (L) and hybrid (H) welds. The longitudinal and transverse tensile test results are summarised in Table 13, with the 0.2% proof strength ($R_{p,0.2}$), the tensile strength (R_m), and the percentage elongation at fracture (A) values given for each of the aforementioned positions. In line with the lowest hardness values recorded in the weld metal, the lowest weld proof and tensile strength was found in the weld, as recorded in the longitudinal direction, which were lower than those taken from the HAZ or the parent material. The weld metal therefore governed the transverse tensile strength recorded for both the autogenous laser and the hybrid welds. When comparing the processes, no difference was observed between the HAZ tensile strength values. For the weld metal, the proof stress was also similar, but a lower tensile strength, i.e., 5% lower, and an elongation value three times lower, were recorded for the hybrid welds compared with the autogenous laser welds. From

this can be concluded that the 5556A filler wire used for the hybrid welding did not improve the strength or ductility of the joint.

Table 13 Transverse and longitudinal tensile test results of welds produced in 12.7mm thickness 7xxx alloy using autogenous laser and hybrid laser-MIG welding at their respective keyhole porosity-free welding speeds of 0.55 and 0.75m/min.

		$R_{p,0.2}$, MPa	R_m, MPa	El, %
Autogenous weld	Longitudinal in weld, W_L	311	380	3.0
	Longitudinal in HAZ, HAZ_L	462	543 (-10%)	12.0
	Transverse	349	408 (-33%)	2.0
Hybrid laser-MIG weld	Longitudinal in weld, W_H	314	362	1.0
	Longitudinal in HAZ, HAZ_H	468	545 (-10%)	12.0
	Transverse	348	388 (-35%)	1.0
Parent material		580	605	7.0

$R_{p,0.2}$ = 0.2% proof strength, R_m = tensile stress, El = amount of elongation before fracture (as % of original length)

7.7. CONCLUSIONS

The thick-section trials have demonstrated that full penetration can be achieved in a 12.7mm thickness Al-Zn-Mg-Cu aerospace aluminium alloy using 7kW of Yb-fibre laser power in either an autogenous set-up or in a hybrid combination with a MIG arc. Both the autogenous laser and hybrid laser-MIG process were confirmed to be capable of producing a level of weld metal porosity in accordance with the most stringent weld quality class defined in both BS EN 13919-2 and AWS D17.1, by considering shielding gas supply and material surface preparation prior to welding, and selecting an appropriate spot size and welding speed.

To consistently eliminate the occurrence of keyhole-induced porosity, welding had to be carried out at a welding speed lower than the maximum capable of achieving full penetration. This welding speed varied with alloy composition, welding process (i.e., autogenous or hybrid laser-MIG) and laser spot diameter used. The occurrence of keyhole-induced porosity was also reduced by removing the surface oxide prior to welding and selecting a larger laser spot diameter, in this case 0.6mm instead of 0.4mm.

By dry-machining top and bottom surface of the samples close to the joint line, and the edges to be welded, less than one hour prior to welding, and by the use of a low-moisture shielding gas delivery, a total level of weld metal porosity in accordance with the stringent weld quality class defined in BS EN 13919-2 and AWS D17.1 was achieved. The low-moisture shielding gas delivery comprised a short, 1.5m long, polyamide gas line, stored at an elevated temperature for 24 hours, acclimatised to laboratory conditions for at least 2 hours prior to welding and purged with shielding gas at least 2 minutes prior to welding.

8. OVERALL CONCLUSIONS

This EngD work has demonstrated that, using 3kW of lamp-pumped (LP) Nd:YAG laser power, fully penetrating, square-edge butt joints can be produced in 3.2mm thickness 2024 aluminium alloy, containing a level of weld metal porosity that is consistently lower than the limits specified for a *stringent weld quality* in BS EN 13919-2 and AWS D17.1:2001. This was achieved by mechanically (or chemically) cleaning parent and filler material immediately prior to welding, the use of a twin-spot laser energy profile and a low moisture-content shielding gas delivery. The availability of higher average output powers at near-infrared wavelength and a better beam quality, through the introduction of Yb-fibre lasers, allows aluminium thicknesses of 8mm, the limit for conventional Nd:YAG lasers, and above, to be welded in a single pass. When comparing the welding performance of an Yb-fibre laser with a beam quality of 4mm.mrad, with that of an LP Nd:YAG laser with a beam quality of 23mm.mrad , at a given output power of 4kW and 0.4mm diameter spot, a 2.5-fold increase in welding speed can be achieved in 6mm (5083) aluminium alloy, or an increase in depth of penetration of between 25% and 45% in the same alloy for welding speeds between 1 and 15m/min. This improvement in welding performance, together with an Yb-fibre laser output power of 7kW, allowed full penetration to be achieved, in a single pass, in a 12.7mm thickness Al-Zn-Mg-Cu aerospace aluminium alloy, of proprietary composition, using the laser autogenously and in a hybrid configuration with a MIG arc. Both the autogenous laser and hybrid laser-MIG process were capable of producing welds containing a level of weld metal porosity that was consistently below the limits specified for a stringent weld quality in both BS EN 13919-2 and AWS D17.1, by strict control of shielding gas supply and material surface preparation prior to welding, for a given laser spot size and welding speed.

In terms of the stringer-to-skin aluminium fuselage panels that are currently welded, at Airbus, using CO_2 lasers, this study has shown that fibre-delivered Nd:YAG lasers can also be used, producing a weld quality in terms of porosity, that is acceptable to current aerospace industry standards. For an equal output power, the Nd:YAG laser has the advantage over the CO_2 laser in that its wavelength is more efficiently absorbed by aluminium and its alloys, thereby resulting in an improved process stability and allowing a higher productivity. However, to compete with the higher output powers that are commercially available for CO_2 lasers, Yb-fibre lasers offer an alternative to the Nd:YAG laser, with, as demonstrated in this EngD work, when used at the same output power of 4kW, a 60% increase in welding speed achievable for the typical (aluminium) stringer thickness of 3mm, compared with a LP Nd:YAG laser. This increase in welding speed achievable with Yb-fibre lasers could help Airbus to realise its forecast for a cost-saving of between 20 and 25% over its riveted panels. With a wavelength that is more easily absorbed by aluminium alloys than the CO_2 laser wavelength, the Yb-fibre laser also offers flexibility in production, because of fibre-delivery instead of the use of mirrors, a power efficiency of at least three times that of CO_2 lasers, and a footprint at least three times smaller.

In terms of using laser welding for the manufacture of thick-section aluminium wing structures, this study has shown the potential of the new, high-power Yb-fibre lasers in producing laser welds with a minimum of weld metal porosity in line with current industry standards. Although the welding speed of 0.55 and 0.75m/min for autogenous laser welding and hybrid laser-MIG welding, respectively, falls short of the (Airbus) estimated welding speed of 1m/min, these processing speeds still constitute a five and seven-fold improvement over the current riveting speed of 0.11m/min. This means that the 248 metres of stringer incorporated in a typical aluminium wing structure can be welded in 7.5 and 5.5 hours in case of autogenous laser and hybrid laser-MIG, respectively, compared with 37.6 hours currently needed for the riveting process.

The following findings and conclusions can also be drawn from this EngD work.

- In accordance with standard practice when laser welding aluminium alloys, inert shielding gas can be supplied either coaxially or through a side-jet shielding arrangement. Whereas both are suitable for the welding of 3.2mm thickness 2024 alloy using 3kW of (fibre-delivered) laser power, a coaxial shielding arrangement is not effective in preventing spatter from damaging the cover slide/focussing optic when using 7kW of (fibre-delivered) laser power to weld 12.7mm thickness alloy. Under these conditions, a side-jet shielding arrangement can be applied, comprising a standard MIG shroud positioned behind the laser at an angle of 30° with the laser beam axis. This arrangement is effective in shielding the top-bead when laser welding 6.35mm and 12.7mm thickness Al-Zn-Mg-Cu alloy, at welding speeds between 0.5 and 3m/min. Both argon and helium are suitable for top and under-bead shielding, with helium preferred because of a better process stability, based on the visual weld bead appearance.

- Whereas the laser welding of 3.2mm thickness 2024 aluminium alloy using 3kW of fibre-delivered laser power can be carried out in the flat position, out-of-position welding is required for the 12.7mm thickness Al-Zn-Mg-Cu alloy to prevent problems with burn-through. The horizontal-vertical (PC) and the vertical-up (PF) welding positions are both capable of producing fully penetrating welds in the 12.7mm thickness alloy, with the latter preferred, because of the higher welding speeds, i.e., lower heat input and less thermal damage in the heat-treated alloy, and the smaller weld beads achievable (for a given welding speed) compared with the PC welding position.

- In addition to the weld pool support provided by the PF (and PC) welding position, support of the large molten pool of aluminium is also achieved by angling the laser in the opposite direction to the direction of welding. In this work, additional weld pool support was provided by a 10° angle of the laser pointing downward, when welding in the vertical-up (PF) position.

- For the purpose of this research, two types of keyhole-induced porosity were considered, i.e., cavities, which are irregular in shape and typically found in the root of the weld, and coarse pores, which are spherical in shape and in diameter larger than 0.5mm. A third type of porosity, i.e., hydrogen or fine porosity, is also spherical in shape, but in diameter smaller than 0.5mm and not the result of a keyhole instability, but entrapment of hydrogen. No cavities were observed in the laser welds produced in the 3.2mm thickness alloy, but coarse pores were observed in those (fully penetrating) welds completed at the higher welding speeds. Both cavities and coarse pores were observed in the laser welds in the 12.7mm thickness alloy. However, it was demonstrated for both thicknesses of material that reducing the welding speed impacts on the presence of keyhole-induced porosity, to the degree that this porosity can be consistently eliminated. For a given laser output power, full penetration can be achieved for a range of welding speeds, with the faster welding speeds resulting in a lower heat input and less thermal damage. However, from the point of view of avoiding keyhole-induced porosity, a lower welding speed is preferred. By controlling the welding speed, the number of keyhole-induced pores in the laser-welded Al-Zn-Mg-Cu alloy can be consistently reduced to zero. This effect was demonstrated on both 6.35mm and 12.7mm thickness material, in both the PC and PF welding position, for both a 0.4mm and a 0.6mm spot size and for both autogenous laser and hybrid laser-MIG welding. The number of fine pores also reduces as welding is carried out at a lower welding speed, as demonstrated for the laser welds in both the 3.2mm thickness 2024 and the 12.7mm thickness Al-Zn-Mg-Cu aluminium alloys.

- The high melting temperature, tenacious oxide present on the surface of all aluminium alloys, affects the occurrence of both fine and keyhole-induced porosity. The presence of the oxide layer influences the level of oxygen in the weld metal, which in turn impacts on the viscosity and degassing of the weld, and on the stability of the keyhole. This EngD work has demonstrated, that by removing the oxide prior to welding, from the top and bottom surface of the samples and from the edges to be welded, the number of hydrogen pores, cavities and coarse pores in the aluminium laser welds can be reduced. However, in the case of the 12.7mm thickness Al-Zn-Mg-Cu aluminium alloy, removal of this oxide layer alone is not sufficient to eliminate cavities or to reduce the number and size of the coarse pores sufficiently to a level acceptable to the stringent weld quality defined in BS EN 13919-2 or AWS D17.1.

- A laser spot diameter of 0.6mm results in less cavities and coarse porosity than a 0.4mm diameter spot, as was demonstrated for laser welds produced in both the 3.2mm thickness 2024 alloy and the 12.7mm thickness Al-Zn-Mg-Cu alloy. This results from the higher welding speed achievable with the smaller spot size (for a given power), the increase in surface tension (acting on the keyhole) and laser keyhole walls that are in closer proximity to each other, in case of the smaller spot size. For a given laser power

and beam quality, a smaller spot size produces a higher power density, and allows thicker sections of aluminium alloy to be welded in a single pass, for a given speed, or a faster welding speed to penetrate a given thickness of alloy. However, the welding performance does not improve further when decreasing the spot size below 0.3mm in diameter.

- Alloy composition influences the occurrence of keyhole-induced porosity. Cavities and coarse porosity are often attributed to the evaporation of low boiling-point, or volatile, constituents, resulting in keyhole instabilities. However, in 12.7mm thickness aluminium alloy samples welded under identical conditions, the cavity and coarse porosity content was lowest in laser welds in the Al-Zn-Mg-Cu alloy, followed by those in the 2024 alloy, another aerospace aluminium frequently used in the aerospace industry, and highest in the 2519 alloy, an aluminium alloy used in the manufacture of armoured vehicles. This was despite the fact that the Al-Zn-Mg-Cu alloy has the highest content of low boiling-point constituents, such Zn and Mg, and 2519 the lowest. However, alloying elements such as silicon also affect the melt pool fluidity and molten material flow in thick-section aluminium laser welds. Based on the different levels of keyhole-induced porosity observed in the three 12.7mm thickness alloys investigated, the author concludes that the latter dictates the keyhole stability, although further work is required to quantify this.

- In a hybrid configuration with a MIG arc, 7kW of Yb-fibre laser power is capable of producing fully penetrating welds in 12.7mm thickness Al-Zn-Mg-Cu alloy without keyhole-induced porosity. This was achieved by using a standard synergic MIG set operating in the pulsed mode and a laser-leading hybrid configuration, with the MIG wire positioned 2mm behind and at a 30° angle with the laser, and a MIG wire feed speed of 6m/min. The top and under-bead profiles of these hybrid welds display a well-defined surface ripple. Although the hybrid process introduces additional heat, the total heat input can be equal or less than for autogenous laser welding, because of the higher welding speeds that can be achieved with the hybrid process. For a similar heat input, the melting efficiency of the hybrid laser-MIG process was demonstrated, on a 6.35mm thickness Al-Zn-Mg-Cu alloy, to be 11% better than that of the sum of the (autogenous) laser and MIG process.

- The commercially available 5556A filler wire used for the hybrid laser-MIG welding trials on the 12.7mm thickness Al-Zn-Mg-Cu aluminium alloy does not improve the hardness or tensile strength values that can be achieved using the autogenous laser process. In fact, for welds carried out at a speed producing full penetration without keyhole-induced pores, the tensile strength ($R_{p,0.2}$ and R_m) and the elongation at fracture (El) values for the hybrid laser-MIG welds are lower than those of the autogenous laser welds.

- The level of hydrogen porosity in laser-welded aluminium can be lowered by the use of a shielding gas delivery system containing a minimum level of moisture. This can be achieved by the use of gas lines that prohibit moisture ingress during periods of inactivity, and/or by purge times long enough so that the moisture content in the gas line levels off to a minimum value. Additional measures to reduce the level of fine porosity include the removal of the porous oxide layer (and contaminants) from the material surface, the removal of contaminants from the filler material and the use of a twin-spot energy profile. Linishing, scraping, dry-machining or chemi-etching can be used for the surface oxide removal. Based on the levels of fine porosity observed for each of the cleaning operations investigated, the author concludes that the impact of the time elapsed between cleaning and subsequent welding (on weld metal porosity) is greater than the actual cleaning method used, and suggests a time of less than one hour. A drop in welding speed is associated with the use of a twin-spot laser energy profile (in case the laser power is split, rather than doubled up), which makes it difficult to separate the individual effects of using a twin-spot profile and a lower welding speed on the presence of fine weld metal porosity.

- A stringent weld quality in terms of porosity in accordance with BS EN 13919-2 and AWS D17.1 can be achieved consistently in 3.2mm thickness 2024 aluminium alloy, using 3kW of Nd:YAG laser power, and the following conditions:

  ⇒ a low dew-point helium shielding gas, delivered through a short, 1.5m long, polyamide gas line, that is free of moisture, through storage at elevated temperature for 24 hours, acclimatisation for 2 hours prior to welding and purging for at least 2 minutes prior to welding;
  ⇒ chemi-etching the samples no longer than 1 hour prior to welding;
  ⇒ chemi-etching the filler wire no longer than 1 hour prior to welding;
  ⇒ a twin-spot laser energy profile with a 0.27mm spot separation and a 50/50 energy distribution.

- A stringent weld quality in terms of porosity in accordance with BS EN 13919-2 and AWS D17.1 can be achieved consistently in 12.7mm thickness Al-Zn-Mg-Cu aluminium alloy, when autogenous laser and hybrid laser-MIG welding using a 7kW Yb-fibre laser, and the following conditions:

  ⇒ a low dew-point helium shielding gas, with less than 3ppm moisture, delivered through a short, 1.5m long, polyamide gas line, that is free of moisture, through storage at elevated temperature for 24 hours, acclimatisation for 2 hours prior to welding and purging for at least 2 minutes prior to welding;
  ⇒ dry-machining the samples no longer than 1 hour prior to welding;

- For a given (fibre-delivered) laser output power of 4kW, the welding performance in terms of depth of penetration that can be achieved in aluminium, for welding speeds between 1 and 15m/min, is influenced by the power density at the workpiece and the included solid angle, and thus by the beam quality and beam brightness of the laser system used. For those welding speeds, the depth of penetration in aluminium increases linearly with increasing power density, achieved by reducing the spot size, up to a power density of approximately 50kW/mm^2. Beyond this point, depending on the welding speed, limited or no additional gain in depth of penetration can be achieved with an increase in power density achieved through a reduction in spot size. This value of power density equates to a spot diameter of 0.33mm, for the constant laser output power of 4kW used in these trials. An increased welding performance can also be achieved by using a laser system with a higher beam quality, although such an increase is not linear. High beam quality lasers allow the use of long focal length focussing optics, which give small included solid angles. In combination with power density, the solid angle determines the beam brightness of a laser system. For welding speeds ranging from 1 to 15m/min, the welding performance (in terms of depth of penetration) in aluminium increases with increasing laser beam brightness, up to a maximum performance at a brightness of around 33×10^5W/mm^2.sterad. Beyond this 'optimum' brightness, which is independent of welding speed and material, the degree in performance increase drops as brightness increases, and even reverses in case of the higher beam brightness values.

9. SUGGESTIONS FOR FURTHER WORK

This work has demonstrated that the availability of higher output powers for fibre-delivered lasers, in the form of Yb-fibre lasers, has made it possible to weld, in a single pass, aluminium sections thicker than 8mm, which is currently the limit for conventional Nd:YAG laser technology. A good weld quality in terms of porosity can be achieved using the laser autogenously or in a hybrid configuration with a MIG arc. However, the (composition of the) filler wire used in this programme of work did not improve on the mechanical performance of the weld over and above that achievable with the autogenous laser process. Further work is recommended on the composition of filler material to be used with the hybrid laser-MIG process for the welding of aluminium, so as to maximise the mechanical properties of the joint, in particular strength and elongation (by the use of grain refiners, for instance), to suit the performance required.

An optimum laser beam brightness was demonstrated to achieve the maximum welding performance in terms of depth of penetration in aluminium (and steel), for a (fibre-delivered) laser output power of 4kW used at a welding speed between 1 and 15m/min. However, as this was obtained from only a single set of data points, further trials should be carried out to confirm whether the welding performance reduces or drops for the higher beam brightness values. Focus hereby should also be on using, as much as possible, identical power density values, to quantify the (individual) influence of included solid angle on welding performance, by changing the beam delivery optics to ones that produce a spot diameter of 0.4mm precisely, or, by changing the laser output power for a given beam delivery optic. The author also recommends repeating this investigation at different output powers, ranging between 3 and 8kW, subject to availability of different beam qualities at these particular laser output powers.

Further research is also recommended into the phenomena responsible for the change in welding performance, in terms of depth of penetration, observed when using power densities higher than 50kW/mm^2 (obtained by spot diameters smaller than 0.33mm) and laser beam brightnesses beyond the reported 'optimum' value established for both aluminium (and steel) in the performance comparison trials. Particular focus hereby should be on a study of the absorption/scattering of the laser energy by a plasma suspected to form above the weld pool during laser welding, the presence of this plasma in relation to the power density and included solid angle of the focusing system used, the behaviour of the keyhole (and the inclination of the keyhole front wall in particular) and the thermal disturbances observed at up to 300mm above the weld pool.

10. REFERENCES

1. Welding and Metal Fabrication: 'Welded aluminium aircraft structures ready for take off'. Welding and Metal Fabrication, Vol.66, No.8, September 1998, pp.16-17.

2. Zink W: 'Integral solutions for fuselage shells'. Proceedings of the 19th European Conference on Advanced Aerospace Materials - Materials for Aerospace Applications, Munich, Germany, 6-8 December 2000, pp.25-32.

3. Zink W: 'Laser welding aircraft fuselage shells'. Industrial Laser Solutions, Vol.16, No.4, April 2001, pp.7-8.

4. Liu J and Kulak M: 'A new paradigm in the design of aluminium alloys for aerospace applications'. Proceedings of the 7th International Conference on Aluminium alloys (ICAA7), Charlottesville, USA, 9-14 April 2000. Published in Materials Science Forum, 2000, Vol.331-337, pp.127-140 (www.scientific.net).

5. Altenpohl D G: 'Aluminium: Technology, Applications and Environment. A profile of a Modern Metal'. Publ: Warrendale PA 15086, USA & Minerals, Metals & Materials Society (TMS), 6th Edition, November 1997. ISBN 0-87339-406-2.

6. Dunkerton S B: 'Welding for the 21st century'. Materials World, Vol.10, No.3, March 2002, pp.18-19.

7. Liu J: 'Advanced aluminum and hybrid aerostructures for future aircraft'. Materials Science Forum, 2006, Vol.519-521, pp.1233-1238 (www.scientific.net).

8. Calder N J: 'Laser Source Optimisation for Welding Aircraft Materials'. Proceedings of the 17th International Congress on Applications of Lasers and Electro-Optics (ICALEO) 1998, Orlando, Florida, USA, 16-19 November 1998. Section A, pp.158-166.

9. Ide H: 'Progress of aluminium welding and technology in aircraft industries'. Journal of Light Metal Welding and Construction, Vol.42, No.12, December 2004, pp.585-591.

10. Vollertsen F, Schumacher J, Schneider K, Seefeld T: 'Innovative welding strategies for the manufacture of large aircraft'. Welding in the World, Vol.48, Special issue, pp.231-247.

11. Ferstl S, Heimerdinger C, Kretschmar T, Lang R, Meister H, Müller-Hummel P: 'Laserstrahlschweissen von Strukturcomponenten im Flugzeugbau bei EADS Militärflugzeuge'. Lectures of the International Symposium on Welding and Brazing in Aerospace Industry - Modern Applications and Materials for New and In-Service Parts, Berlin-Schönefeld, Germany, 12-13 May 2004, pp.25-30. DVS Berichte No.229. ISBN 3-87155-688-2.

12. Jones I A, Riches S T, Yoon J W, Wallach E R: 'Laser welding of aluminium alloys'. TWI Industrial Members Report 517/1995, October 1995.

13. Hunston H: 'Audi A2 to debut at Frankfurt'. Automotive World, September 1999, p.12.

14. Lewin T: 'A space odyssey'. Automotive World, May 2000, pp.56-60.

15. Kokkonen J, Ion J C: 'CO_2 Laser Welding of the Aluminium Aerospace Alloy AA2024'. Proceedings of the 7th Nordic Conference on Laser Advanced Materials Processing (NOLAMP) 1999, Lappeenranta, Finland, 23-25 Augustus 1999. Vol.84, pp.418-429.

16. Neye G, Heider P: 'Laser beam welding of modern Al-alloys for the aircraft industry'. Proceedings of the 5th European Conference on the Laser Treatment of Materials (ECLAT) 1994, Bremen, Germany, 26-27 September 1994, pp.108-117. DVS Berichte No.163.

17. Neye G: 'Laserstrahlschweisskonzept fur Rumpfschalen-Strukturen (Laser beam welding concept for fuselage shell structures)'. Proceedings of the Conference on Advanced Materials in Aerospace Industry - Welding, Brazing and Thermal Spraying, Berlin, Germany, 7-8 June 2000, pp.18-24. DVS Berichte No.208.

18. Rendigs K H, Winkler P J: 'Today's level and perspective prospects of metallic aircraft structures'. Proceedings of the 3rd International Conference on Welding in Aerospace Industry, Essen, Germany, 21-22 September 1993, pp.1-10. DVS Berichte No.54.

19. Palm F: 'Laser welding aluminium for fuselage structures'. Presentation for the EPIC/SPIE workshop on Laser Applications in Europe, Dresden, Germany, 23 November 2005. Presentation only.

20. Soudage et Techniques Connexes: 'L'A380 innove a tout va (The Airbus A380 innovation is all go!)'. Soudage et Techniques Connexes, Vol.58, No.5-6, May-June 2004, p.12.

21. 'Technical status of laser beam welding'. Extract from an Airbus confidential document, issued 16 May 2006. Private discussion at TWI on 25 January 2007 with R Ilyushenko, Materials and Processing Research Engineer at Airbus (Filton, UK), and R Maziarz, Structural Design Engineer at Airbus (Filton, UK).

22. Matsunawa A, Katayama S, Fujita Y: 'Laser welding of aluminium alloys - Defects formation mechanisms and their suppression methods'. Proceedings of the 7th International Conference on Joints in Aluminium (INALCO) 1998, Cambridge, England, 15-17 April 1998, pp.65-76.

23. Matsunawa A, Katayama S, Nishizawa K: "Defects reduction in laser spot welding by pulse shaping'. Proceedings of the *Welding, Joining, Coating and Surface Modification of Advanced Materials* Pre-Assembly Symposium of the.47th Annual Assembly JIW, Dalian, China, 1-3 September 1994. Vol.1, pp.1-6.

24. Katayama S, Yoshida D, Yokoya S, Matsunawa A: 'Development of tornado nozzle for reduction in porosity during laser welding of aluminium alloy. Proceedings of the 20th International Congress on Applications of Lasers and Electro-Optics (ICALEO) 2001, Jacksonville, Florida, USA, 15-18 October 2001. Laser Micro-fabrication Conference, Section C.

25. Martukanitz R P: 'Laser processing of aluminum and its alloys'. Course presented at 18th International Congress on Applications of Lasers and Electro-Optics (ICALEO) 1999, San Diego, California, USA, 15-18 November 1999.

26. Dausinger F, Rapp J, Beck M, Faisst F, Hack R, Hũgel H: 'Welding of aluminium - a challenging opportunity for laser technology'. Journal of Laser Applications, Vol.8, No.6, December 1996, pp.285-290.

27. Dausinger F, Rapp J, Hohenberger B, Hugel H: 'Laser beam welding of aluminium: State of the art and recent developments'. Proceedings of the International Body Engineering Conference (IBEC) 1997, Stuttgart, Germany, 30 September – 2 October 1997. Advanced Technologies & Process, Vol.33, pp.38-46.

28. Boisselier D, Lenoir R: Weldability and manufacture of YAG laser welds on aluminum alloys'. Proceedings of the European Symposium on Assessment of Power Beam Welds, Geesthacht, Germany, 4-5 February 1999.

29. Lang R, Kullick M, Muller-Hummel P: 'Laserstrahlschweissen von hochfesten Flugzeugstrukturen aus AlLi2195 (Laser beam welding of high strength AlLi2195 aircraft structures)'. Proceedings of the Conference on Advanced Materials in Aerospace Industry - Welding, Brazing and Thermal Spraying, Berlin, Germany, 7-8 June 2000, pp. 25-29. DVS Berichte No.208.

30. Mueller-Hummel P, Ferstl S, Sengotta M, Lang R: 'Laser beam welding of high stressed complex aircraft structural parts'. Proceedings of the 1st International Symposium on High-Power Laser Macro-processing, Osaka, Japan, 27-31 May 2002. SPIE Vol.4831, pp.438-441.

31. Verhaeghe G: 'Fibre lasers for materials processing – A technology review'. EngD Submission 5, February 2006.

32. Bransden A S, Endres T: 'High power laser processing of aluminium alloys'. Proceedings of the 3rd European Conference on the Laser Treatment of Materials (ECLAT) 1992, Gottingen, Germany, 12-15 October 1992, pp.117-123.

33. Katayama S, Matsunawa A, Kojima K, Kuroda S: 'CO_2 laser weldability of aluminium alloys. Report 4: Effect of welding defects on mechanical properties, deformation and fracture of laser welds'. Welding International, Vol.14, No.1, 2000, pp.12-18.

34. Takahashi K, Mehmetli B, Sato S: 'Influence of shielding gas and laser irradiation conditions on porosity formation in CO_2-laser welding of aluminium alloy'. Journal of Light Metal Welding and Construction, Vol.35, No.9, September 1997, pp.409-416.

35. Pastor M, Zhao H, Debroy T: 'Pore formation during continuous wave Nd:YAG laser welding of aluminium for automotive applications'. Welding International, Vol.15, No.4, April 2001, pp.275-281.

36. Pastor M, Zhao H, Martukanitz R P, Debroy T: 'Porosity, Underfill and Magnesium loss during continuous wave Nd:YAG laser welding of thin plates of aluminum alloys 5182 and 5754'. Welding Journal, Vol.78, No.6, June 1999, pp.207s–216s.

37. Seto N, Katayama S, Matsunawa A: 'Porosity formation mechanism and suppression procedure in laser welding of aluminium alloys'. Welding International, Vol.15, No.3, 2001, pp.191-202.

38. BS EN 13919-2:2001: 'Welding – Electron and laser beam welded joints – Guidance on quality levels for imperfections'.

39. AWS D17.1:2001 'Specification for fusion welding for aerospace applications'.

40. ABP 2-4102 (Appendix C) 'Acceptance standards for aluminium and aluminium alloys'. Internal British Aerospace Plc standard, Issue 3, Jan 1996.

41. Verhaeghe G: 'The technical challenges when laser welding aluminium and the difficulties with porosity – A review of the literature'. EngD Submission 1, April 2007.

42. Verhaeghe G: 'Factors affecting the level of porosity in Nd:YAG laser welded thin-gauge 2024 aluminium'. EngD Submission 2, April 2004.

43. Verhaeghe G, Hilton P A, Barnes S: 'Achieving low-porosity laser welds in aerospace aluminium alloy'. Proceedings of the Aerospace Manufacturing Technology Conference (AMTC) 2003, Montreal, Quebec, Canada, 9 September 2003. SAE Transactions 2003, Vol.112, Part 1, pp. 286-294. ISSN 0096-736X. EngD Submission 3, April 2004.

44. Verhaeghe G, Hilton P A: Laser welding of low-porosity aerospace aluminium alloy'. Proceedings of the 34th International MATADOR conference, University of Manchester, Manchester, UK, July 2004. Publ: Springer-Verlag, London, UK, 2004. ISBN-10 1852338806. EngD Submission 4, April 2004.

45. Verhaeghe G: 'Welding aluminium with a high-power Yb-fibre laser – An initial performance assessment'. EngD Submission 6, March 2006.

46. Verhaeghe G: 'Achieving aerospace standard porosity requirements when welding 12.7mm thickness aluminium alloy using a high-power Yb-fibre laser'. EngD Submission 7, October 2006.

47. Verhaeghe G, Hilton P A: 'The effect of spot size and laser beam quality on welding performance when using high-power continuous wave solid-state lasers'. Proceedings of the 24th International Congress on Applications of Lasers and Electro-Optics (ICALEO) 2005, Miami, Florida, USA, 31 October – 3 November 2005. Paper 507, pp.264-271. EngD Submission 8.

48. Aluminium Association: 'Welding aluminum: Theory and Practice'. Publ: The Aluminum Association, Washington DC, 3rd edition, November 1997. ISBN 89-080539.

49. Ion J C: 'Laser beam welding of wrought aluminium alloys', Science and Technology of Welding, Vol.5, No.5, 2000, pp.265-276.

50. Migliore L: 'Laser materials processing'. Publ: Marcel Dekker Inc, New York, 1996. ISBN 0-8247-9714-0.

51. Dawes C J: 'Laser welding: A practical guide'. Publ: Abington Publishing, Cambridge, England, 1992. ISBN 1 85573 034 0.

52. Paschotta R: 'Encyclopedia of Laser Physics and Technology'. Published on www.rp-photonics.com/encyclopedia.html, 28 November 2005.

53. Matsunawa A, Kim J D, Seto N, Mizutani M, Katayama S: 'Porosity formation and solidification cracking in laser welding'. Proceedings of the Taiwan International Welding Conference (TIWC) 1998 on *Technology Advancements and New Industrial Applications in Welding*, Taipei, Taiwan, 7-9 September 1998, pp.47-56.

54. Thomy C, Seefeld T, Vollertsen F: 'Industrial potential for high power fibre laser welding'. Association of Industrial Laser Users (AILU) magazine, Issue 42, March 2006, pp.22-25.

55. Steen W: 'Laser material processing'. Publ: Springer-Verlag, London, UK, 2003. ISBN 1-85233-698-6.

56. Greses J: 'Plasma/plume effects in CO_2 and Nd:YAG laser welding'. PhD dissertation, University of Cambridge, England, March 2003.

57. Greses J, Barlow C Y, Steen W M, Hilton P A:' Spectroscopic studies of plume/plasma in different gas environments'. Proceedings of the 20th International Congress on Applications of Lasers and Electro-Optics (ICALEO) 2001, Jacksonville, Florida, US, 15-18 October 2001. Paper 808.

58. Greses J, Hilton P A, Barlow C Y, Steen W M: 'Plume attenuation under high power Nd:YAG laser welding'. Proceedings of the 21st International Congress on Applications of Lasers and Electro-Optics (ICALEO) 2002, Scottsdale, Arizona, 14-17 October 2002. Laser Materials Processing Conference. Vol.94, Section C - Sensing Monitoring and Modelling.

59. Duley W W: 'Laser welding'. Publ: John Wiley &Y Sons Inc, New York, 1999. ISBN 0-471-24679-4.

60. Berger P, Dausinger F and Hugel H: 'Laser beam welding of aluminium alloys - scaling laws and identification of parameters determining the quality of the weld'. Proceedings of the International WLT Conference on Lasers in Manufacturing (LIM) 2003, Munich, Germany, 24-26 June 2003, pp.241-246.

61. Mathers G: 'The welding of aluminium and its alloys'. Publ: Woodhead Publishing Ltd., Cambridge, England, 2002. ISBN 1-85573-567-9.

62. King F: 'Aluminium and its alloys'. Publ: Ellis Horwood Limited, Chichester, England, 1987. ISBN 0-7458-0013-0.

63. Mandal N R: 'Aluminium welding'. Publ: Woodhead Publishing Ltd., Cambridge, England, 2002. ISBN 1-85573-597-0.

64. Forsman T: 'Laser welding of aluminium'. Doctoral Thesis 2000:39. Publ: Lulea Unversity of Technology, 2000. ISSN 1402-1544.

65. Gittos M F, Scott M H: 'Selection of filler metals for arc welding aluminium alloys'. Welding Institute Research Bulletin, Vol. 28, August 1987, pp. 59-63.

66. Pfannenmueller T, Palm F: 'Properties of weldments in aluminium-magnesium-lithium alloys for future aircraft fuselage application'. Presentation at the 2nd International EWI/TWI Seminar on Joining of Aerospace Materials, 24-25 March 1999, Littleton, Colorado, USA.

67. Gittos M F: 'Welding Al-Mg-Si alloys'. Welding Institute Research Bulletin, Vol.27, July 1986, pp.231-235.

68. Lang A, Bergmann H W: 'Mechanical properties of laser welded Al-alloys'. Proceedings of the 3rd European Conference on Laser Treatment of Materials (ECLAT) 1992, Göttingen, Germany, 12-15 October 1992, pp.163-168.

69. Moon D W and Metzbower E A: 'Laser beam welding on aluminum alloy 5456'. Welding Journal, Vol.62, No.2, February 1983, pp.53s-58s.

70. Behler K, Beyer E, Schafer R: 'Laser welding of aluminium'. Proceedings of the 7th International Congress on Applications of Lasers and Electro-Optics (ICALEO) 1988, Santa Clara, California, USA, 30 October – 4 November 1988, pp.249-258.

71. Katayama S: 'Defect formation mechanism in laser welding and suppression methods'. Journal of Light Metals Welding & Construction, Vol.34, No.4, 1996, pp.199-209.

72. Haboudou A, Peyre P, Vannes A B: 'Influence of surface preparation and process parameters on the porosity generation in aluminium alloys'. Journal of laser applications, Vol.16, No.1, February 04, 2004, pp.20-24.

73. Simidzu H, Yoshino F, Katayama S, Matsunawa A: 'Pulsed Nd:YAG laser welding of aluminium alloys'. Proceedings of the Conference on Laser Advanced Materials Processing (LAMP) 1992, Niigata, Japan, 7-12 June 1992, pp.511-516.

74. Rapp J, Glumann C, Dausinger F, Hugel F: 'The effect of magnesium evaporation in laser welding of aluminium alloys'. Proceedings or the 5th International Conference on Welding and Melting by Electron and Laser Beams (CISFFEL) 1993, La Baule, France, 14-18 June 1993. Vol.1, pp.275-282. ISBN 2-7272-0160-5.

75. Katayama S, Kojima K, Matsunawa A: 'CO_2 laser weldability of aluminium alloys (3rd report): Metallurgical characteristics of laser welds'. Welding International, Vol.3, No.9, pp.683-692.

76. Scott M H and Gittos M F: 'Selection of filler metals for arc welding aluminium alloys: Part 2 - Alloys of other countries'. Welding Institute Research Bulletin, February 1988, pp.57-59.

77. Gittos M F and Scott M H: 'Cracking in the heat affected zone (HAZ) of Al-Mg-Si alloys - a review'. Welding Institute Bulletin, September/October 1990, pp.99-102.

78. Kramer L S, Tack W T, Fernandes M T: 'Scandium in aluminium alloys'. Advanced Materials and Processes, Vol.152, No.4. October 1997, pp.23-24.

79. Norman A F, Birley S S, Prangnell P B: 'Development of new high strength Al-Sc filler series aluminium aerospace alloys'. Science and Technology of Welding and Joining, Vol.8, No.4, August 2003, pp.235-245.

80. Jones, I A: 'Laser welding of aluminium'. Proceedings of the International Conference on Advances in Welding Technology (ICAWT) 1996, Columbus, Ohio, USA, 6-8 November 1996, pp.321-340.

81. Dunlop H M, Benmalek M: 'Role and characterisation of surfaces in aluminium industry'. Supplément au Journal de Physique III - Colloque C6, Vol.7, No.12, December 1997, C6-163.

82. Katayama S, Matsunawa A, Kojima K: 'CO_2 laser weldability of aluminium alloys (2nd report): Defect formation conditions and causes'. Welding International, Vol.12, No.10, 1998, pp.774-789.

83. Matsumura H, Orishashi T, Nakayama S, Koga S, Inuzuka M, Nakazawa Y, Nagatani H: "CO_2 laser welding characteristics of various aluminium alloys'. Proceedings of the Conference on Laser Advanced Materials Processing (LAMP) 1992, Niigata, Japan, 7-12 June 1992, pp.529-533.

84. Harris I D: 'A review of porosity formation and recommendation on the avoidance of porosity in TIG welding'. TWI Industrial Members Report 387/1988, December 1988.

85. Kutsuna M, Yan Q: 'Study on porosity formation in laser welds in aluminium alloys (Report 1): Effects of hydrogen and alloying elements'. Welding International, Vol.12, No.12, 1998, pp.937-949.

86. 'Aluminum and aluminum alloys'. ASM Speciality Handbook, Publ: ASM International, December 1993. ISBN 0-87170-496-X.

87. Zhao H, White D R, DebRoy T: 'Current issues and problems in laser welding of automotive aluminium alloys'. International Materials Review, Vol.44, No.6, June 1999, pp.238-265.

88. Matsunawa A, Katayama S: 'Mechanism and prevention method of imperfection in high power laser welding'. Proceedings of the Symposium on *New-Wave of Welding and Joining Research for the 21st Century*, Osaka, Japan, 22-23 March 2001. pp.97-110.

89. ASM International: 'ASM Handbook Vol.6 - Welding, Brazing and Soldering'. Publ: American Society for Metals, Ohio, USA, 1993. ISBN 0-87170-377-7.

90. Masumoto I, Kutsuna M, Suzuki J: 'Laser welding of A5083 aluminium alloy'. Proceedings of the 5th International Symposium of Japanese Welding Society (JWS), Tokyo, Japan, 17-19 April 1990. Advanced Technology in Welding, Materials Processing and Evaluation, Vol.1, Paper I-2, pp.23-28.

91. Woods R A: 'Porosity and hydrogen absorption in aluminium welds' .Welding Journal, Vol.53, No.3, March 1974, pp.97s-108s.

92. Hohenberger B, Chang C L, Schinzel C, Dausinger F, Hügel H: 'Laser welding with Nd:YAG-Multi-Beam Technique'. Proceedings of the 18th International Congress on Applications of Lasers and Electro-Optics (ICALEO) 1999, San Diego, California, USA, 15-18 November 1999. Vol.87, Section D, pp.167-176.

93. Takahashi K, Sato S: 'Porosity reduction in CO_2 laser welding of aluminium alloys - Influence of penetration, joint, oxygen gas and oxide films'. Welding International, Vol.14, No.6, June 2000, pp.439-446.

94. Ion J C: 'Laser processing of engineering material – Principles, procedure and industrial applications'. Publ: Elsevier Butterworth-Heinemann, Oxford, England, 2005. ISBN 0-7506-6079-1.

95. Vennekens R, Verstraeten B: 'Aluminium, het materiaal van de toekomst – Aflevering 1, deel 1'. Lastechniek, Vol.69, No.12, December 2003, pp.14-17.

96. Rapp J, Glumann C, Dausinger F, Hugel H: 'Lap welding of AlMg5Mn alloy plates (sheet) with CO_2 lasers'. Proceedings of the 25th International Symposium on Automotive Technology and Automation (ISATA) 1992, Florence, Italy, 1-5 June 1992. Paper 921067, pp.461-468.

97. Tsukamoto S, Kawaguchi I, Arakane G, Honda H: 'Prevention of weld defect by power modulation in high power laser welding'. Proceedings of the 4th Conference on Laser Assisted Net Shape Engineering (LANE), Erlangen, Germany, 21-24 September 2004. Vol.1 – Joining, pp.119-130.

98. Hu B, Richardson I M:' Autogenous laser keyhole welding of aluminium alloy 2024'. Journal of laser applications, Vol.17, No.2, May 2005, pp.70-80.

99. Arata Y: 'Plasma, electron and laser beam technology - Development and use in material processing'. Publ: American Society for Metals, Metals Park, 1986. ISBN 0-87170-254-1, pp.378-396.

100. Mueller R E: 'A model for predicting keyhole and fusion zone depths in blind keyhole welding'. Proceedings of the 13th International Congress on Applications of Lasers and Electro-Optics (ICALEO) 1994, Orlando, Florida, USA, 17-20 October 1994, pp.509-518.

101. Forsman T, Kaplan A F H, Powell J, Magnusson C: 'Initiation and termination phenomena in laser welding of aluminium'. Journal of laser applications, Vol.12, No.2, April 2000, pp.81-84.

102. Sakamoto H, Shibata K, Dausinger F: 'Laser welding of different aluminium alloys' Proceedings of the Proceedings of the 3rd European Conference on Laser Treatment of Materials (ECLAT) 1992, Göttingen, Germany, 12-15 October 1992, pp.125-130.

103. Matsunawa A, Katayama S, Kojima K: 'CO_2 laser weldability of aluminium alloys (1st report): Effects of welding conditions on melting characteristics'. Welding International, Vol.12, No.7, 1998, pp.519-528.

104. 'The Industrial Laser Handbook - 1992-1993 Edition'. Publ: Springer-Verlag New York Inc, USA, 1992. ISBN 0-387-97751-1.

105. Lewis G K, Cremers D A, Dixon R D: 'Laser plume temperature measurements in various gases'. Report LA-UK-88-540 (DE88006462; CONF-880922-2). Publ: Los Alamos National Laboratory, Los Alamos, USA, 1988.

106. Kim J D, Lee M H, Kim Y S, Katayama S, Matsunawa A: 'Diagnostics of plasma induced in Nd:YAG laser welding of aluminium alloy'. Proceedings of the International Welding/Joining Conference on Intelligent Technology in Welding and Joining for the 21st Century, Gyeongju, Korea, 28-30 October 2002. Monitoring and Modelling Session, paper MM1-5, pp.612-619.

107. Matsunawa A, Katayama S: 'Understanding physical mechanisms in laser welding for construction of mathematical model'. Welding in the World, Vol.46, Special Issue, July 2002, pp.27-38.

108. Fabbro R, Slimani S, Coste F, Briand F: 'Study of keyhole behaviour for full penetration Nd-YAG laser welding'. Proceedings of the 23rd International Congress on Applications of Lasers and Electro-Optics (ICALEO) 2004, San Francisco, California, USA, October 2004. Vol.97, Paper 809.

109. Vollertsen F, Thomy C, Schilf M, von Beeren J, Seefeld T: 'Improvement of weld quality in laser and friction stir welding of aluminium'. Proceedings of the 4th Conference on Laser Assisted Net Shape Engineering (LANE), Erlangen, Germany, 21-24 September 2004. Vol.1 – Joining, pp.235-246.

110. Seto N, Katayama S, Mizutani M, Matsunawa A: 'Relationship between plasma and keyhole behaviour during CO_2 laser welding'. Proceedings of SPIE Conference on High-Power Lasers in Manufacturing, Osaka, Japan, 1-5 November 1999. Vol.3888, pp.61-68.

111. Matsunawa A, Seto N, Kim J-D, Mizutani M, Katayama S: 'Dynamics of keyhole and molten pool in high power CO_2 laser welding', Proceedings of SPIE Conference on High-Power Lasers in manufacturing, Osaka, Japan, 1-5 November 1999. Vol.3888, pp.34-45.

112. Matsunawa A, Katayama S, Nishizawa K: 'Defects reduction in laser spot welding by pulse shaping'. Proceedings of the *Welding, Joining, Coating and Surface Modification of Advanced Materials* Pre-Assembly Symposium of the.47th Annual Assembly JIW, Dalian, China, 1-3 September 1994. Vol.1, pp.1-6.

113. Olivier C A, Gerritsen C H J: 'Study into the use of process gases in high power Nd:YAG laser welding of C-Mn and stainless steels'. TWI Industrial Members report 723/2000, November 2000.

114. Vollertsen F, Thomy C: 'Welding with fibre lasers from 200 to 17000W'. Proceedings of the 24th International Congress on Applications of Lasers and Electro-Optics (ICALEO) 2005, Miami, Florida, USA, 31 October – 3 November 2005, pp.254-263.

115. Yoshida Y, Fukaya Y, Minami N, Hirozane T: 'Study on the prevention of weld defects in CO_2 laser welding'. Proceedings of the 4th International IIW/IIS Conference, Tokyo, Japan, 14-15 July 1986. Paper IV-599-93, pp. 349-350.

116. Kim J S, Watanabe T, Yoshida Y: 'Effect of the beam-defocusing characteristics on porosity formation in laser welding'. Journal of Materials Science Letters, Vol.14, No.22, 1995, pp.1624-1626.

117. Xie J: 'Dual beam laser welding'. Welding Journal, Vol.81, No.10, October 2002, pp.223s-230s.

118. Sakamoto H, Iwas I, Shibata K: 'The effect of twin spot beam arrangement on energy coupling during welding. Study of twin spot Nd:YAG laser welding of aluminium alloys'. Welding International, Vol.18, No.9, September 2004, pp.677-682.

119. Shida T, Hirokawa M, Sato S: 'CO_2 laser welding of aluminium alloys – welding of aluminium alloys using CO_2 laser beam in combination with the MIG arc'. Quarterly Journal of the Japan Welding Society, Vol.15, No.1, 1997, pp.18-23.

120. Eboo M, Steen W M, Clarke J: 'Arc-augmented laser welding'. Proceedings of the 4th International Conference on Advances in Welding Processes, TWI, Cambridge, UK, 1978. Paper 17, pp.257-265.

121. Shi G, Hilton P A, Mulligan S J, Verhaeghe G: Hybrid Nd:YAG laser-MAG welding of thick section steel with adaptive control'. Association of Industrial Laser Users (AILU) magazine, Issue 38, March 2005, pp.34-37.

122. Dilthey U, Lueder F, Wieschemann A: 'Technical and economical advantages by synergies in laser arc hybrid welding'. Welding in the World, Vol.43, Supplementary Issue, July-August 1999, pp.141-152.

123. Verhaeghe G: 'Hybrid laser-arc processing from improved productivity and quality - Progress report for the Period January-June 2003'. Confidential report from the joint TWI – Institut de Soudure Group Sponsored Project, 13782/12/03, June 2003.

124. Verhaeghe G: 'High power Nd:YAG laser welding of thin gauge aluminium sheet'. TWI Confidential Report 88277/43/98, July 2000.

125. BS EN 439:1994: 'Welding consumables - shielding gases for arc welding and cutting'.

126. Lugan A: 'Feasibility of twin spot Nd:YAG laser welding of 2024 aluminium alloy'. TWI Industrial Members Report 765/2003, March 2003.

127. BS EN 288-4:1992: 'Specification and approval of welding procedures for metallic materials – Part 4. Welding procedure tests for the arc welding of aluminium and its alloys'.

128. BS EN 1321:1997: 'Destructive test on welds in metallic materials – Macroscopic and microscopic examination of welds'.

129. EN ISO 1435:1997 'Non-destructive examination of welds. Radiographic examination of welded joints'.

130. Graham H: 'The influence of shielding gas systems on porosity in Nd:YAG laser welded aluminium'. TWI Confidential Report 14714/1/04, January 2004.

131. Mercer C J: 'Brief report on moisture in helium laser welding'. Air Products Plc Confidential Report, August 2003.

132. Hilton P A: 'Fibre optic beam delivery for high-power CW Nd:YAG lasers'. TWI Confidential Report 88277/49/98, December 1998.

133. EN ISO 11145:2001 'Optics and optical instruments. Lasers and laser-related equipment. Vocabulary and symbols'.

134. EN ISO 11146:1999 'Lasers and laser related equipment – Test methods for laser beam parameters – Beam Widths, Divergence Angles and Beam Propagation Factor'.

135. Danzer W, Beyer E, Himmer T, Brenner B, Göbel G: 'Influence of plasma and shielding gas on welding processes'. Proceedings of the 2nd International Workshop on Fibre lasers, Dresden, Germany, 5-6 July 2006. Welding I session.

136. Verhaeghe G, Hilton P: 'Making the most of welding with the new generation of high-power fibre-delivered lasers'. Association of Industrial Laser Users (AILU) magazine, Issue 43, June 2006, pp.18-21.

137. Weberpals J, Russ A, Dausinger F, Hügel H: 'Influence of the focus diameter in laser welding with thin disk laser'. Proceedings of the International WLT Conference on Lasers in Manufacturing (LIM) 2005, Munich, Germany, 13-16 June 2005, pp.39-42.

138. Verhaeghe G: 'Study of the laser-arc interactions during hybrid Nd:YAG laser – MIG/MAG welding'. TWI Industrial Members Report 15077.01/2007/1313.1, May 2007.

139. EN 10002-1:2001: 'Metallic materials – Tensile testing – Part 1: Method of test at ambient temperature'.

140. Verhaeghe G: 'Initial performance assessment of Yb-fibre laser technology in power range from 4 to 7kW for the welding of structural steel'. TWI members report 822/2005, March 2005.

141. Lancaster J F: 'The Physics of Welding'. Publ: Pergamon Press, Oxford, UK, 1984. ISBN 0-08-030555-5.

142. Kutsuna M, Chen L: 'Interactions of both plasmas in CO_2 laser-MAG hybrid welding of carbon steel'. Proceedings of the 1st International Symposium on High-Power Laser Macro-processing, Osaka, Japan, 27-31 May 2002. ISBN 0-8194-4602-5, SPIE Vol.4831, pp.341-346.

143. Naito Y, Katayama S, Matsunawa A: 'Keyhole behaviour and liquid flow in molten pool during laser-arc hybrid welding'. Proceedings of the 1st International Symposium on High-Power Laser Macro-processing, Osaka, Japan, 27-31 May 2002. ISBN 0-8194-4602-5, SPIE Vol.4831, pp.357-362.

144. Gornyi, Lapota, Redozobov: 'Examination of the electrical characteristics of the arc in laser-arc welding'. Welding International, Vol.4, No.6, 1992, pp.474-476.

145. Shilf M, Thomy C, Seefeld T, Vollertsen F: 'Some aspects of arc stability in GMA-Laser-Hybrid welding'. Proceedings of the International WLT Conference on Lasers in Manufacturing (LIM) 2005, Munich, Germany, 13-16 June 2005, pp.171-175.

146. Sugino T, Tsukamoto S, Nakamura T, Arakane G: 'Fundamental study on welding phenomena in pulsed laser – GMA hybrid welding'. Proceedings of the 24th International Congress on Applications of Lasers and Electro-Optics (ICALEO) 2005, Miami, Florida, USA, 31 October – 3 November 2005. Paper 302, pp.108-116.

147. Hornig H and Duran J: 'Experiences on laser beam welding of aluminium materials at BMW', Proceedings of the 7th JWS International Symposium on *Today and Tomorrow in Science and Technology of Welding and Joining*, Kobe, Japan, 20-22 November 2001. Vol.1, Paper PL2-3, pp.445-453.